# Grafting-to and Grafting-from Proteins - Synthesis and Characterization of Protein-Polymer Conjugates on the Way to Biohybrid Membrane Materials

---

**Dissertation**

Zur Erlangung des akademischen Grades

„doctor rerum naturalium“ (Dr. rer. nat.)

in der Wissenschaftsdisziplin „Polymerchemie“

Eingereicht an der Mathematisch-Naturwissenschaftlichen Fakultät

Institut für Chemie

der Universität Potsdam

von

**M. Sc. Maria Mathieu-Gaedke**

Potsdam, Oktober 2021

Published online on the
Publication Server of the University of Potsdam:
https://doi.org/10.25932/publishup-54292
https://nbn-resolving.org/urn:nbn:de:kobv:517-opus4-542921

The following project was carried out in the research group of Prof. Dr. Alexander Böker from October 1st, 2017 to March 31st, 2021 at the Fraunhofer Institute for Applied Polymer Research IAP and the Institute of Chemistry of the University Potsdam.

**First Reviewer:** Prof. Dr. Alexander Böker

**Second Reviewer:** Prof. Dr. Heiko Möller

**Third Reviewer:** Dr. Dietmar Appelhans

Submitted: October 27th, 2021

I certify that the content presented within this report is my own original work based on the research I performed using only the means and source materials as noted therein.

This thesis was not submitted to another examination board in this or other countries. There were no unsuccessful examination processes.

_____

Potsdam-Golm - October 27th, 2021 Maria Mathieu-Gaedke

## Acknowledgements

I would like to thank **Prof. Dr. Alexander Böker** for the opportunity to work on this highly interesting topic and the possibility to be part of his research group. I thank him for his helpful input, the lots of new ideas and insights into so many interesting fields discussed in the seminar and personal meetings.

I would particularly like to thank **Prof. Dr. Heiko Möller** for taking the time to do the second examination of my thesis. Furthermore, I sincerely thank **Dr. Dietmar Appelhans** for being the third reviewer of my thesis.

Sincere thanks go to the **NMR-** and **GPC-department** at University of Potsdam for measuring my samples, especially Angela Krtitschka, Dr. M. Heydenreich, Prof. Dr. Heiko Möller, Sascha Prentzel and Prof. Dr. Helmut Schlaad.

The **Bundesministerium für Bildung und Forschung (BMBF)** is kindly acknowledged for financial support in the framework of the BMBF-Forschertandem ‘‘Chiral Membranes II’’ (Förderkennzeichen: 031B0559). I would like to thank the tandem partner from the biotechnology department of the RWTH Aachen, namely Prof. Dr. Ulrich Schwaneberg, Dr. Tayebeh Mirzaeigarakani, Dr. Marco Grull and Dr. Deepak Anand for the interesting cooperation.

Also, I would like to thank my numerous **cooperation partners** Dr. Jasmin Preis and Prof. Dr. Thorsten Hofe from PSS Polymer Standards Service GmbH, PD Dr. Ivo Nischang positioned at the Jena Center for Soft Matter (JCSM), Friedrich-Schiller-Universität Jena, and Marcus Michaelis and Prof. Dr. Heiko Möller from University of Potsdam.

I thank **my colleagues** at Fraunhofer Institute for Applied Polymer Research (IAP), in particular Sany Chea, Jo Sing Tang, Chris Gäbert, Pinar Akarsu, Stefan Reinicke and Thilo Fischer, for the nice working atmosphere, lovely lunch and lab conversations and group activities. I also thank **my office colleagues** Marc Zimmermann, Falko Rottke and Ulrike Doering.

Especially, I would like to thank my **lab colleagues** Johannes Martin, Liang Qiu, Lynn Dai, Yannic Müllers and my students Lucas Al-Shok and Daniel Bragança Viana for the support and the humorous working atmosphere, for the response to my questions, the conversations, group activities and to endure bravely my taste of music.

I would like to express particularly my gratitude to **Dr. Ulrich Glebe** and **Magnus Schwieters** for working with me on the project. It wouldn´t have been so much fun without you. Sincere thank goes to Uli for being my daily supervisor. Couldn´t have picked a better mentor for this thesis.

I am particularly grateful for **my family and my friends** (which are also part of my family), especially for my parents which always supported me on my way. I am so happy to have my dearest friends in my life, Elli Weibert, Jana Göller and Hanne Alina Balzer.

Last but not least I owe a huge hug, many kisses and want to express my love to **my husband Marius Gaedke**. I checked some alternatives to say “I couldn´t be happier” but I couldn´t pick one so here is a selection for you: I am happy as a pig in clover; I am happy as a duck in Arizona; I am happy as a clam at high tide or as happy as a clam in butter sauce - to have you in my life.

# Abbreviations

**Following abbreviations were used:**

| | |
|---|---|
| A(R)GET | Activator (re-)generated by electron transfer |
| ATRP | Atom transfer radical polymerization |
| AUC | Analytical ultracentrifugation |
| BSA | Bovine serum albumin |
| Cbh9A | Cellobiohydrolase 9a |
| CBM | Carbohydrate binding module |
| CD | Circular dichroism |
| CLM | Crosslinkable monomer |
| COSY | Correlated spectroscopy |
| CRP | Controlled radical polymerization |
| Cryo-EM | Cryogenic electron microscopy |
| CTA | Chain transfer agent |
| DLS | Dynamic light scattering |
| *E. Coli* | *Escherichia coli* |
| FDA | U.S. Food and drug administration |
| FhuA | Ferric hydroxamate uptake protein component A |
| FID | Free induction decay |
| GFC | Gel filtration chromatography |
| GFP | Green fluorescent protein |
| GISANS | Grazing-incidence small-angle neutron scattering |
| GISAXS | Grazing-incidence small-angle x-ray scattering |
| GPC | Gel permeation chromatography |
| HIM | Helium ion microscopy |
| HPLC | High performance liquid chromatography |
| HSQC | Heteronuclear single quantum coherence |
| ICAR | Initiators for continuous activator regeneration |
| ILL | Institute Laue-Langevin |
| IR | Infrared |
| LC/MS | Liquid chromatography–mass spectrometry |
| LCST | Lower critical solution temperature |
| MALDI-ToF | Matrix assisted laser desorption ionization time of flight |
| MALS | Multi angle laser light scattering |
| Mb | Myoglobin |

| | |
|---|---|
| MI | Macroinitiator |
| MS | Mass spectrometry |
| $M_W$ | Mass averaged molar mass |
| MWCO | Molecular weight cut-off |
| NMR | Nuclear magnetic resonance |
| PDB | Protein data bank |
| PET-RAFT | Photoinduced electron/energy transfer reversible addition-fragmentation chain transfer polymerization |
| PRE | Paramagnetic relaxation enhancement |
| PTH | Parathyroid hormone |
| RAFT | Reversible addition-fragmentation chain transfer |
| RDRP | Reversible-deactivation radical polymerization |
| SANS | Small-angle neutron scattering |
| SARA | Supplemental activator and reducing agent |
| SAXS | Small-angle x-ray scattering |
| SDS-PAGE | Sodium dodecyl sulfate polyacrylamide gel electrophoresis |
| SEC | Size exclusion chromatography |
| SET-LRP | Single-electron transfer living radical polymerization |
| SFG | Sum frequency generation |
| SFM | Scanning force microscopy |
| SLD | Scattering length density |
| SV | Sedimentation velocity |
| TEM | Transmission electron microscopy |
| UV–Vis | Ultraviolet–visible |
| VLP | Virus-like particle |
| WT | Wild type |
| XRR | X-ray reflectivity |

**Following abbreviations for chemical compounds were used:**

| | |
|---|---|
| ABCVA | 4,4'-Azobis(4-cyanovaleric acid) |
| AIBN | α-α'-Azobisisobutyronitrile |
| BCA | Bicinchoninic acid |
| BiBa | 2-Bromoisobutyric acid |
| Boc | *tert*-Butyloxycarbonyl |
| CoumAAm | 7-(2-Acrylamidoethoxy)-4-methylcoumarin |
| DEA | *N*,*N*-Diethylacrylamide) |
| DHB | 2,5-Dihydroxybenzoic acid |
| DMAc | Dimethylacetamide |
| DMAEMA | 2-(Dimethylamino)ethyl methacrylate |
| DMF | Dimethylformamide |
| DMIAm | 2-(Dimethyl maleinimido)-*N*-ethyl-acrylamide |
| DMMIBA | 3,4-Dimethyl maleic imidobutyl acrylate |
| DMMIBAAm | *N*-[2-(3,4-Dimethyl-2,5-dioxo-2,5-dihydro-pyrrol-1-yl)-butyl]-acrylamide |
| DMSO | Dimethyl sulfoxide |
| DSS | Sodium 3-(trimethylsilyl)propane-1-sulfonate |
| $Me_6$TREN | Tris[2-(dimethylamino)ethyl]amine |
| $MEO_2MA$ | Di(ethylene glycol) methyl ether methacrylate |
| MPD | 2-Methyl-2,4-pentanediol |
| NHS- | *N*-Hydroxysuccinimidyl |
| NIPAM | *N*-Isopropylacrylamide |
| NVCL | *N*-Vinylcaprolactam |
| OEG(m)A | Oligo ethylene glycol (meth)acrylate |
| PEG | Poly(ethylene glycol) |
| PEO | Poly(ethylene oxide) |
| PET | Polyethylene terephthalate |
| PFP- | Pentafluorophenyl |
| PMDETA | *N,N,N′,N″,N″*-Pentamethyldiethylenetriamine |
| PS | Poly(styrene) |
| SDS | Sodium dodecyl sulfate |
| Super-DHB | 9:1 Mixture of DHB and 2-hydroxy-5-methoxybenzoic acid |
| TFA | Trifluoroacetic acid |
| TMS | Tetramethylsilane |

# Zusammenfassung

Der Einbau von Proteinen in künstliche Materialien bietet eine Vielzahl an neuen Möglichkeiten. Besonders relevant ist die Nutzung der spezifischen Eigenschaften dieser Biomakromoleküle, die seit Millionen von Jahren durch die Natur perfektioniert wurden, und deren Übertragung auf ein Produkt. Dazu gehören die hohe Spezifität und Selektivität von Membranproteinen und ihre Verwendung als Poren in Biohybrid-Membranen. Eine Möglichkeit, diese Membranen herzustellen, ist der Einsatz von Protein-Polymer-Konjugaten als universelle Bausteine. Die resultierenden Biohybrid-Materialien vereinen die Eigenschaften beider Komponenten: die Funktionalität und Spezifität der Biomoleküle sowie die Stabilität und spezifischen Eigenschaften der Polymere. Für die Synthese der Konjugate stehen hauptsächlich zwei Ansätze zur Verfügung. Bei *grafting-to* wird zunächst ein endgruppenfunktionalisiertes Polymer synthetisiert und anschließend an das Protein angebunden. Dagegen wird bei *grafting-from* das Protein in einem ersten Schritt mit Initiatoren oder Kettenüberträger-Molekülen für eine Polymerisation funktionalisiert und in einem nachfolgenden Schritt das Polymer ausgehend vom Protein synthetisiert. Beide Methoden wurden genutzt, um Konjugate verschiedener Proteine mit unterschiedlichen thermoresponsiven und optional UV-verlinkbaren Polymeren zu erhalten. Ein Überblick über die verwendeten Proteine, Monomere und die beiden Konjugationsmethoden ist in Abbildung 1 gegeben. Im Rahmen der hier vorliegenden Dissertation wurden vier Teilprojekte bearbeitet, die sich entweder mit der tiefergehenden Charakterisierung von Protein-Polymer-Konjugaten oder deren Nutzung als Bausteine für Biohybrid-Membranen beschäftigten.

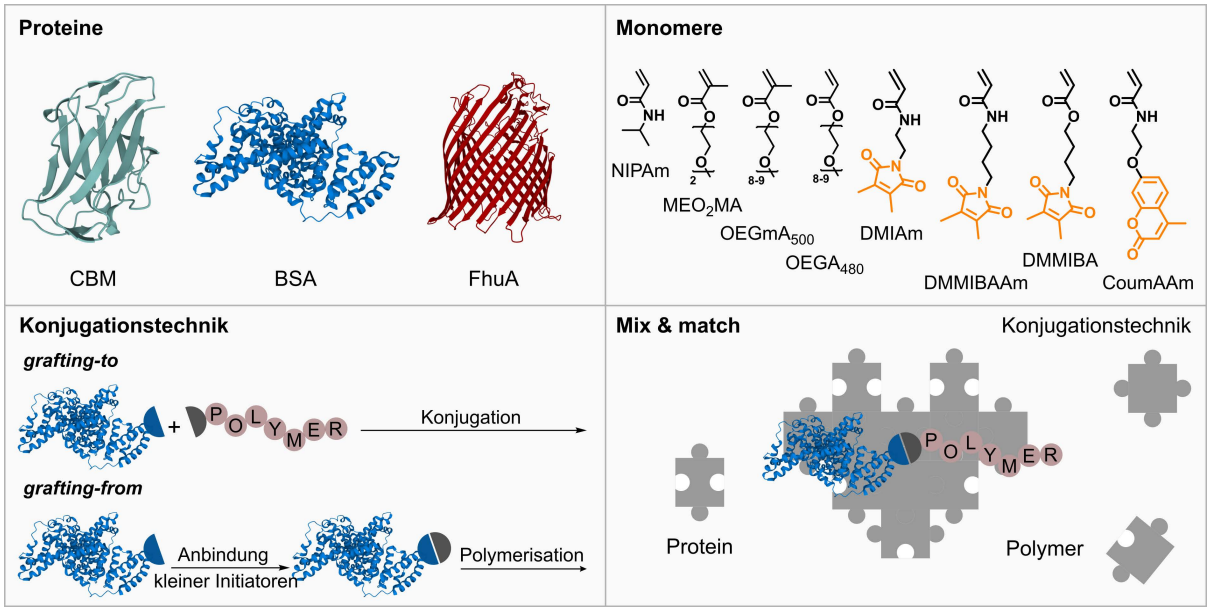


Abbildung 1: Überblick über die verwendeten Proteine, Monomere und Konjugationstechniken zur Herstellung von Protein-Polymer-Konjugaten. Die Konjugate wurden entweder mittels 2D-NMR-Spektroskopie (CBM-PNIPAm), SEC-MALS (BSA- und FhuA-PNIPAm) oder SV-AUC (BSA-PNIPAm) analysiert. Weiterhin wurden Konjugate von FhuA mit PNIPAm und UV-vernetzbaren Monomeren (orange hervorgehoben) synthetisiert und als Membran immobilisiert.

Im ersten Teilprojekt wurde der Einfluss der Konjugation auf die Proteinstruktur mittels **Protein-NMR-Spektroskopie** in Zusammenarbeit mit Prof. Dr. Heiko Möller und Marcus Michaelis von der Universität Potsdam untersucht. Viele Analysemethoden wie SDS-PAGE und CD-Spektroskopie geben Aufschluss über den Erfolg der Konjugation und die Erhaltung großer, lokal ausgebildeter Strukturelemente nach Modifizierung. Kleine strukturelle Änderungen innerhalb der 3-dimensionalen Struktur des Proteins bleiben dort meist unerkannt. NMR-Spektroskopie ist eine der wenigen Methoden, die auch solche kleinen Änderungen aufzeigen kann. Während die Verwendung dieser Methode in der Literatur nur für durch *grafting-to* PEGylierte Proteine beschrieben ist, stellt diese Arbeit die systematische Charakterisierung von Konjugaten, hergestellt durch *grafting-from* und *grafting-to*, mit NMR-Spektroskopie vor. Als Modellsystem wurde eine Mutante der Proteindomäne *carbohydrate binding module 3b* (CBM3b$^{N126W}$) der Cellobiohydrolase 9A (Cbh9A) aus *Clostridium thermocellum* mit dem thermoresponsiven Poly(*N*-Isopropylacrylamid) (PNIPAm) funktionalisiert. Die Analyse der Konjugate zeigte einen starken Einfluss der Konjugationsmethode auf die Proteinfaltung. Während Konjugate, die durch Anbindung eines vorher synthetisierten Polymers an das Protein hergestellt wurden, eine vollständige Erhaltung der Proteinfaltung zeigten, führte das Wachsen der Polymerkette von der Proteinoberfläche zu einer (teilweisen) Entfaltung von Cbh9A CBM3b$^{N126W}$. Um dieses Ergebnis zu bestätigen, wurden Konjugate durch *grafting-from* mit unterschiedlichen Polymerisationstechniken hergestellt. Bei der Cu(0)-katalysierten radikalischen Polymerisation, eine spezielle Art der *Atom Transfer Radical Polymerization* (ATRP), werden zunächst kleine Initiatorgruppen an das Protein angebunden und anschließend die Polymerisation durch ein Wechselspiel aus Aktivierung und Deaktivierung des Initiators durch verschiedene Kupfer-Spezies initiiert. Bei der photoinduzierten Polymerisation mit reversibler Additions-Fragmentierungs-Kettenübertragung (*eng. photo-induced electron/energy transfer reversible addition-fragmentation chain transfer, PET-RAFT*) wird dagegen ein sogenanntes Kettenübertragungsagenz (*eng. chain transfer agent, CTA*) angebunden. Die Polymerisation wird anschließend durch Bestrahlung mit sichtbarem Licht einer bestimmten Wellenlänge gesteuert. Abhängig von der Anzahl der angebundenen Initiatoren/CTAs und der anschließenden Polymerisation zeigte sich ein Einfluss des Funktionalisierungsgrads auf die Proteinstabilität. Die strukturelle Integrität des Proteins nahm mit zunehmendem Ausmaß der Modifizierung und angestrebten Polymerisationsgrads (analog der Kettenlänge und Masse des angebundenen Polymers) ab. Innerhalb dieser Dissertation konnte somit gezeigt werden, dass mittels NMR-Spektroskopie signifikante Unterschiede zwischen Konjugaten, hergestellt durch *grafting-from* und *grafting-to*, detektiert und Auswirkungen auf die Proteinfaltung nachgewiesen werden können.

Im nächsten Teilprojekt wurden Konjugate von Rinderserumalbumin (*eng. bovine serum albumin, BSA*) als kostengünstiges und leicht erhältliches Referenzprotein mit PNIPAm und verschiedenen verzweigten PEG-Derivaten synthetisiert. Die erhaltenen Protein-Polymer-Konjugate wurden mit einer

**Kombination aus Größenausschlusschromatographie und Mehrwinkellichtstreuung** (*eng. size exclusion chromatography multi-angle laser light scattering, SEC-MALS*) analysiert. Diese Technik ist besonders geeignet für die Bestimmung von Molmassen von komplexen Systemen, da keine externe Kalibrierung des Systems erforderlich ist. Zusammen mit meinen Kooperationspartnern Dr. Jasmin Preis und Prof. Dr. Thorsten Hofe von der Firma Polymer Standards Service (PSS) in Mainz wurden verschiedene SEC-Säulenmaterialien und Betriebsbedingungen getestet, um die Anwendbarkeit dieses Systems zur Bestimmung der absoluten Molmassen und hydrodynamischen Eigenschaften von heterogenen Konjugaten, hergestellt durch *grafting-from* und *grafting-to*, zu bewerten. Leider traten hydrophobe und unspezifische Wechselwirkungen der Konjugate mit den verwendeten Säulenmaterialien auf. Diese ließen sich auch nicht durch Änderung der Chromatographiebedingungen wie des Elutionsmittels unterbinden. Durch diese Wechselwirkungen kam es zu einer fehlerbehafteten absoluten Molmassenbestimmung, sodass die erhaltenen Werte nicht mit den zu erwarteten Molmassen, basierend auf dem theoretischen Modifizierungsgrad der Proteine, übereinstimmten. Die vielversprechendsten Ergebnisse wurden bei Konjugaten mit verzweigten PEG-Derivaten erhalten. Daher sollten sich weitere Untersuchungen auf Block-Copolymere zwischen BSA und solchen Polymeren konzentrieren. Idealerweise sollten diese Proben mit grafting-to hergestellt und ein Protein-Polymer-Verhältnis von 1:1 angestrebt werden, um spezifische Einflüsse des Polymers und des Proteins auf das chromatographische Verhalten untersuchen zu können.

Neben SEC-MALS wurden in Zusammenarbeit mit PD Dr. Ivo Nischang, vom Jena Center for Soft Matter (JCSM) der Universität Jena, **Sedimentationsgeschwindigkeitsexperimente in einer analytischen Ultrazentrifuge** (*englisch: sedimentation velocity analytical ultracentrifugation, SV-AUC*) durchgeführt. Innerhalb eines Zentrifugalfeldes sedimentiert eine Probe entsprechend der Masse, Dichte und Form ihrer einzelnen Bestandteile, sodass diese Informationen basierend auf dem Sedimentationsverhalten der Probe gewonnen werden können. Diese Technik eignet sich besonders für Protein-Polymer-Konjugate, da die Auftrennung der Probe während der Messung erfolgt und keine langwierige Aufreinigung des Probengemischs vor der Analyse erforderlich ist. Beispielsweise bestehen Konjugat-Proben, die durch *grafting-to* hergestellt wurden, im Allgemeinen aus einem Gemisch aus unmodifiziertem Protein, Konjugat und nicht angebundenem oder umgesetztem Polymer. In den eigenen Experimenten wurde eine Fraktionierung solcher Proben erreicht und die einzelnen Komponenten identifiziert und charakterisiert. Konjugate von BSA mit PNIPAm wurden zudem unterhalb und oberhalb der Phasenübergangstemperatur der Polymerkomponente analysiert. Die Phasenübergangstemperatur, auch Trübungspunkt (*eng. cloud point*), ist definiert als die Temperatur, bei der das Polymer aufgrund veränderter Wechselwirkungen mit den umgebenden Lösungsmittelmolekülen seine Löslichkeit in dem entsprechenden Lösungsmittel ändert. Es bildet sich eine Mischungslücke, bei der die Polymerketten aggregieren bzw. sich verknäueln, um die Oberfläche und somit Interaktion mit dem sie umgebenden Lösungsmittel zu minimieren. Dieses Verhalten konnte

auf die Konjugate von BSA und dem thermoresponsiven PNIPAm übertragen und die hydrodynamischen Eigenschaften detailliert mit SV-AUC untersucht werden. Abhängig von der Temperatur der Lösung veränderte das System seine Idealität, definiert als Abweichung von einem perfekten Kugelmodell. Unterhalb der Phasenübergangstemperatur zeigte das Konjugat eine geringe Idealität, was darauf hinweist, dass in diesem Zustand das Polymer in die Lösung zeigt und kaum Interaktionen mit der Proteinoberfläche aufweist. Oberhalb der Phasenübergangstemperatur dagegen minimiert sich die Ausdehnung des Polymers aufgrund der Abstoßung vom Lösungsmittel und lagert sich an das Protein an. Dies zeigte sich in den Untersuchungen als eine Erhöhung der Idealität. Es sei erwähnt, dass das native Protein über den getesteten Temperaturbereich ein nahezu unverändertes Verhalten zeigte. Daher kann der beobachtete Effekt auf eine Anordnung der Polymerketten zurückgeführt werden, die sich je nach verwendeter Temperatur ändert. Weitere Experimente könnten genutzt werden, um einen Leitfaden für die Regulierung der hydrodynamischen Eigenschaften eines Konjugats zu erstellen. Dies ist zum Beispiel relevant für die Entwicklung neuer smarter Arzneimittel oder anderer pharmazeutischer Trägersysteme zur selektiven Anreicherung und Freisetzung des Wirkstoffes an einem bestimmten Ort.

Das letzte Teilprojekt befasste sich mit der Synthese von *ferric hydroxamate uptake protein component A* (FhuA)-Polymerkonjugaten zur Verwendung als **Bausteine für neuartige Membranmaterialien**. FhuA ist ein Membranprotein, das in der äußeren Membran von *E. Coli* vorkommt. Seine Form erinnert an eine kleine Tonne, und die Entfernung der sogenannten Korkdomäne im Inneren des Proteins führt zur Ausbildung eines passiven Kanals, der als Pore in Membransystemen genutzt werden könnte. Konjugate von FhuA wurden durch grafting-from synthetisiert. Dafür muss das Protein mit MPD als Stabilisierungsagenz anstelle klassischer Detergenzien rückgefaltet werden. Die verwendete Polymermatrix innerhalb der Biohybrid-Membran, die das Membranprotein umgibt, stabilisiert und kovalent immobilisiert, besteht aus einem Copolymer aus thermoresponsivem PNIPAm und einem Monomer, das eine UV-verlinkbare Einheit in der Seitenkette trägt. Dadurch konnte die Immobilisierung mittels eines externen Triggers ausgelöst werden. Zusätzlich kann die thermoresponsive Matrix genutzt werden, um die Membran zwischen verschiedenen Zuständen (hydrophil und hydrophob) zu schalten. Für die Membranherstellung wurde die intrinsische Amphiphilie der Membranproteine ausgenutzt. Nach Selbst-Assemblierung an der Wasser-Luft-Grenzfläche, wurden die Konjugate mit UV-Licht bestrahlt, um die kovalente Verknüpfung der verwendeten Copolymere zu initiieren. Die hergestellten Membranen wurden mit verschiedenen oberflächensensitiven Charakterisierungsmethoden analysiert und die Gesamtleistung des Systems durch Permeabilitäts- und Größenausschlussexperimente bewertet. Obwohl die Vernetzungseffizienz unter den verwendeten Bedingungen in einem vernünftigen Bereich lag (45-75 %), konnte keine ausreichend vernetzte Membran auf einem PES-Support als Trägermaterial erhalten werden. Außerdem fand der angestrebte Wechsel zwischen einem hydrophilen und einem hydrophoben Zustand der

Polymermatrix unter den getesteten Bedingungen nicht statt. Dementsprechend führten Größenausschlussexperimente nicht zu einer Retention von Analyten, die theoretisch größer sind als die durch die Dimension der verwendeten FhuA-Variante definierten Poren. Detaillierte Untersuchungen der UV-Verlinkung, der Einbau weiterer UV-verlinkbarer Einheiten in die Polymermatrix und somit die Verbesserung der Stabilität der hergestellten Membranen könnten die nächsten Schritte innerhalb dieses Projektes darstellen.

Die wichtigsten Meilensteine dieser Dissertation und eine Kurzzusammenfassung der Ergebnisse der einzelnen Kapitel sind in Abbildung 2 zusammengefasst.

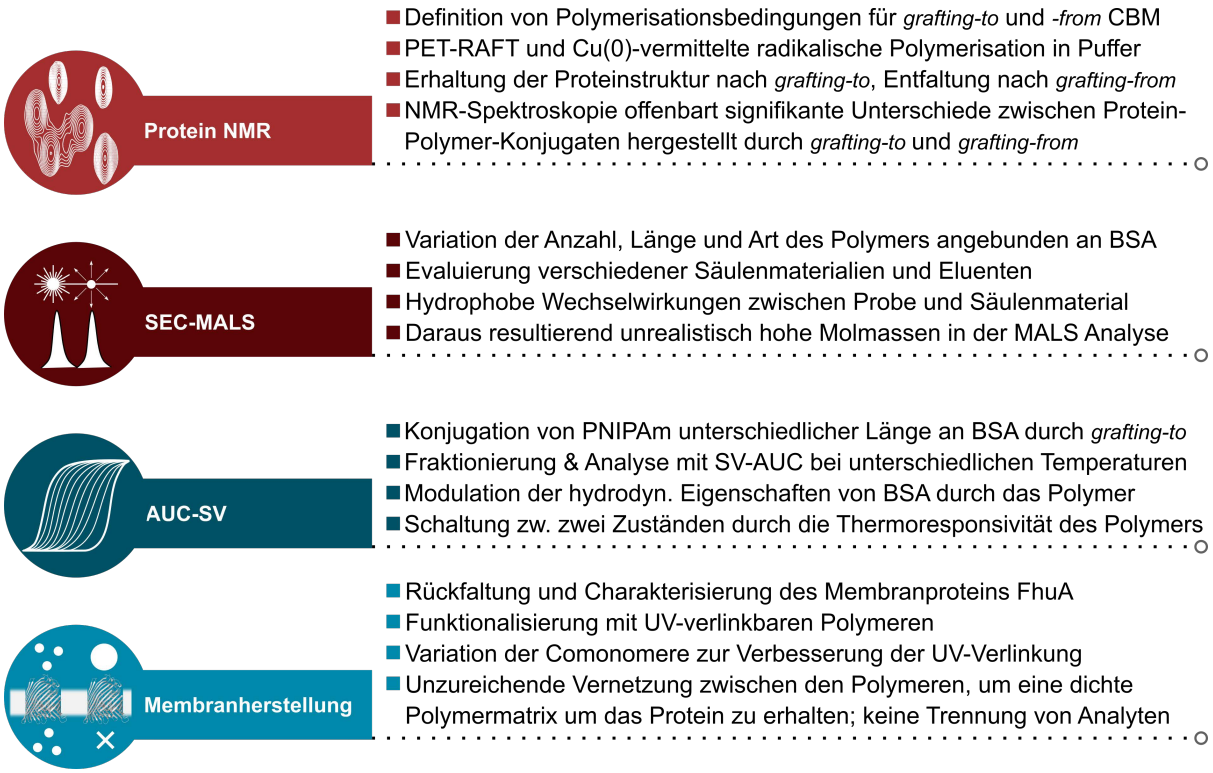


Abbildung 2: Hauptprojekte dieser Dissertation und die wichtigsten Erkenntnisse, die daraus gewonnen wurden.

Insgesamt wurden verschiedene Wege zur einfachen und effizienten Synthese von Protein-Polymer-Konjugaten durch *grafting-from* und *grafting-to* vorgestellt. Die entwickelten Methoden und gewonnenen Erkenntnisse sind ein wichtiger Schritt auf dem Weg zu neuen Hybridmaterialien. Verschiedene analytische Methoden wurden eingesetzt, um die Faltung und die hydrodynamischen Eigenschaften der Konjugate zu untersuchen, was einen tieferen Einblick in die allgemeinen Eigenschaften dieser zukunftsträchtigen Bausteine ermöglicht. Zukünftige Konjugatsynthesen können auf den erhaltenen Struktur-Eigenschafts-Beziehungen aufbauen und Biohybridmaterialien für verschiedene Anwendungen optimiert werden.

## Summary

The incorporation of proteins in artificial materials such as membranes offers great opportunities to increase on the one hand the sustainability of the product and on the other hand to avail oneself the miscellaneous qualities of proteins and enzymes perfected by nature over millions of years. One possibility to leverage proteins is the modification with artificial polymers. The obtained biohybrid materials combine the properties of both, the functionality and specificity of the biomolecules and increased stability and additional functionalities of the artificial polymers. To obtain protein-polymer conjugates, either a polymer can be grown from the protein surface (grafting-from) or a pre-synthesized polymer attached to the protein (grafting-to). Both techniques were used to synthesize conjugates of different proteins with thermo-responsive polymers in the timescale of this thesis. An overview of the different proteins and monomers and illustration of the two grafting techniques is provided in Figure 1. The obtained conjugates were characterized by advanced techniques and utilized in novel membrane systems.


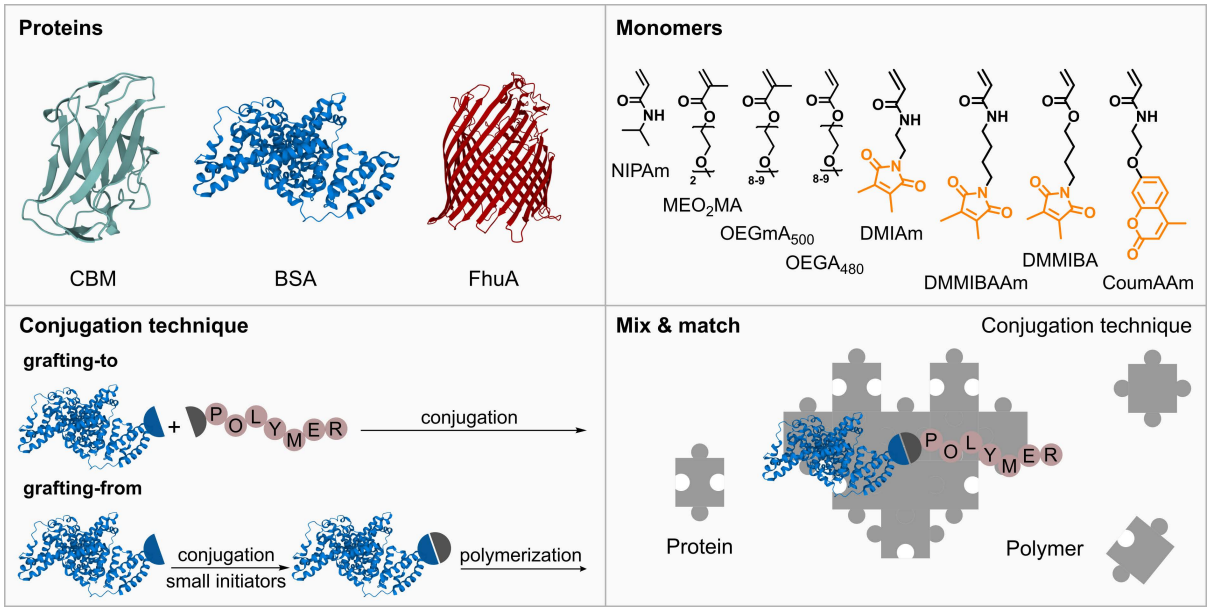


Figure 1: Overview of used proteins, monomers and conjugation techniques to synthesize protein-polymer conjugates. These conjugates were either analyzed by protein NMR spectroscopy (CBM-PNIPAm), SEC-MALS (BSA- and FhuA-PNIPAm) or SV-AUC (BSA-PNIPAm). Finally, conjugates of FhuA with PNIPAm and UV-crosslinkable monomers (highlighted with orange) were synthesized and immobilized in a membrane system.

Overall, this thesis can be subdivided into four main parts. In the first project, conjugates were analyzed by **protein NMR spectroscopy** in cooperation with Prof. Dr. Heiko Möller and Marcus Michaelis located at the University of Potsdam. Typical characterization techniques for conjugates like SDS-PAGE and CD spectroscopy can verify the successful conjugation and give hints on the secondary structure of the protein. However, the 3-dimensional protein structure, being highly important for the protein function, cannot be probed by such standard techniques. Protein NMR spectroscopy is a unique

method allowing to follow even small alterations denoted to certain amino acid positions in the protein. While this was only applied to PEGylated proteins prepared by grafting-to yet, protein NMR spectroscopy was utilized for other polymers and synthesis techniques for conjugates during my thesis. Therefore, a mutant of the carbohydrate binding module 3b (CBM3b$^{N126W}$) of the cellulosomal multimodular hydrolytic enzyme cellobiohydrolase 9A (Cbh9A) from *Clostridium thermocellum* was used as model protein and functionalized with the thermo-responsive polymer poly(*N*-isopropylacrylamide). Analysis of conjugates prepared by grafting-to or grafting-from revealed a strong impact of conjugation type on protein folding. Whereas conjugates prepared by grafting a pre-formed polymer to the protein resulted in complete preservation of protein folding, grafting the polymer from the protein surface led to (partial) disruption of the protein structure. To confirm these findings, conjugates were prepared by grafting-from using two distinct polymerization techniques, namely Cu(0)-mediated radical polymerization and photoinduced electron/energy transfer-reversible addition-fragmentation chain transfer (PET-RAFT) polymerization. Starting with the synthesis of protein-macroinitiator and macroRAFT agent by modification of Cbh9A CBM3b$^{N126W}$ with small initiator or mediator groups revealed an impact of the degree of functionalization on the protein stability. Protein structural integrity decreased with increasing extent of modification and targeted degree of polymerization. In summary, NMR spectroscopy revealed significant differences between protein-polymer conjugation via grafting-to and grafting-from and their impact on protein folding.

Next, conjugates of bovine serum albumin (BSA) as cheap and easily accessible protein were synthesized with PNIPAm and different oligoethylene glycol (meth)acrylates. The obtained protein-polymer conjugates were analyzed by an in-line combination of **size exclusion chromatography and multi-angle laser light scattering** (SEC-MALS). This technique is particular advantageous to determine molar masses, as no external calibration of the system is needed. Together with my cooperation partners Dr. Jasmin Preis und Prof. Dr. Thorsten Hofe from the company Polymer Standards Service (PSS) in Mainz, different SEC column materials and operation conditions were tested to evaluate the applicability of this system to determine absolute molar masses and hydrodynamic properties of heterogeneous conjugates prepared by grafting-from and grafting-to. Unfortunately, hydrophobic and non-covalent interactions of conjugates lead to error-prone values not in accordance to expected molar masses based on conversions and extents of modifications. A more expected chromatographic behavior was obtained for conjugates with branched PEG analogs and further experiments should focus on examination of block copolymers of BSA with these polymers prepared by grafting-to targeting a protein-to-polymer-ratio of 1:1.

Another possibility next to SEC-MALS is the characterization of conjugates by **sedimentation velocity analytical ultracentrifugation** (SV-AUC) to gain insights in the hydrodynamic properties and how they change after conjugation. Those experiments were performed in cooperation with PD Dr. Ivo Nischang, Jena Center for Soft Matter (JCSM). Within a centrifugal field, a sample moves and fractionates according to the mass, density, and shape of its individual components. This technique is especially suited for protein-polymer conjugates, as separation of the sample happens during the measurement and no tedious purification of sample mixtures prior to analysis is needed. For example, conjugate samples prepared by grafting-to are generally composed of a mixture of unmodified protein, conjugate and unreacted polymer. In the performed experiments, a fractionation of those samples was achieved and the individual components identified and characterized. Furthermore, conjugates of BSA with PNIPAm were analyzed below and above the cloud point temperature of the polymer component. The cloud point is defined as the temperature where the polymer undergoes a coil-to-globule transition as a result of changed interactions with surrounding solvent molecules. Consequently, control of conjugate hydrodynamics was achieved by utilizing the unique properties of a thermo-responsive polymer chain attached to BSA by grafting-to. It could be identified that the polymer characteristics were transferred to the conjugate molecule which than showed a decreased ideality – defined as increased deviation from a perfect sphere model – below and increased ideality above the cloud point temperature. It is mentioned that the unmodified protein showed a nearly unchanged behavior over the tested temperature range. Therefore, the observed effect can be attributed to an arrangement of the polymer chain pointing towards the solvent (expanded state) or snuggling around the protein surface depending on the applied temperature. Further experiments could provide a guideline for modulation of conjugate hydrodynamics, a property useful for example in novel drug or carrier system designs.

The last project dealt with the synthesis of ferric hydroxamate uptake protein component A (FhuA)-polymer conjugates as **building blocks for novel membrane materials**. FhuA is a membrane protein which can be found in the outer membrane of *E. Coli*. Its shape can be described as barrel and removal of a cork domain inside the protein results in a passive channel aimed to be utilized as pores in the membrane system. Conjugates were synthesized by grafting-from the protein surface when using MPD as stabilizing agent for refolding, instead of classical detergents. The polymer matrix surrounding the membrane protein is composed of thermo-responsive PNIPAm copolymerized with a monomer bearing a UV-crosslinkable moiety. Therefore, an external trigger for covalent immobilization of these building blocks in the membrane and switchability of the membrane between different states was incorporated. The conjugates and membranes prepared by a drying-mediated self-assembly approach were characterized by various surface-sensitive techniques and the overall performance of the system evaluated by permeability and size exclusion experiments. Even though crosslinking efficiency at used conditions was observed to be in a reasonable range (45–75 %), the obtained membranes displayed an insufficiency in interchain crosslinking and therefore a lack in performance. Furthermore, the aimed

switch between a hydrophilic and hydrophobic state of the polymer matrix did not occur. Correspondingly, size exclusion experiments did not result in a retention of analytes larger than the pores defined by the dimension of the used FhuA variant. Detailed investigations on crosslinking behavior to distinguish between intra- and interchain photodimerization and incorporation of more crosslinker units in the polymer matrix to increase the probability of crosslinking units to meet each other could be the next steps in this project.

The most important milestones and a short summary of the results obtained in each Chapter in this thesis are summarized in Figure 2.

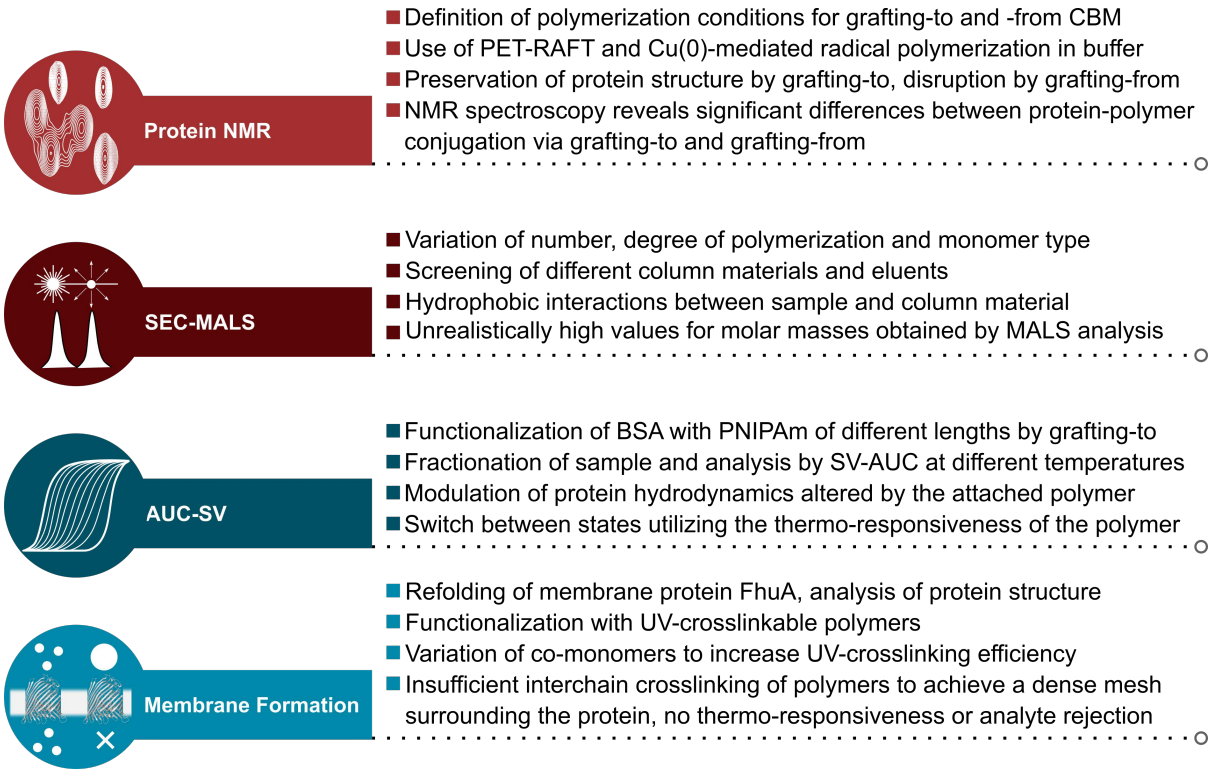


Figure 2: Take-home notes from the four main projects covered by this thesis.

Overall, different paths to generate protein-polymer conjugates in an easy and efficient way by either grafting-from or grafting-to the protein surface were presented paving the way to the generation of new hybrid materials. Different analytical methods were utilized to describe the folding and hydrodynamic properties of conjugates providing a deeper insight in the overall characteristics of these seminal building blocks. Future conjugate synthesis may build upon the obtained structure-property relationships and optimize biohybrid materials for different applications.

## Publications, Posters and Additional Projects

In cooperation with PD Dr. Ivo Nischang, the results presented in Chapter 4 will be submitted within the next months. Additionally, a manuscript will be prepared to publish results obtained throughout Chapter 2, in cooperation with Marcus Michaelis and Prof. Dr. Heiko Möller. Experience gained throughout SEC-MALS analysis of conjugates as presented in Chapter 3 are used for workshops and professional discussion on-site our cooperation partners Dr. Jasmin Preis and Prof. Dr. Thorsten Hofe.

Results obtained in an additional project not covered in this thesis are currently transferred to a manuscript. This project covered the functionalization of BSA with poly-*N*-vinylcaprolactam (PNVCL) by grafting-from and grafting-to either as homopolymer or as copolymer with 2-(dimethylamino)ethyl methacrylate (DMAEMA). Subsequent loading of conjugate nanoparticles with cis-platin resulted in a carrier system for smart drug delivery in potential anti-tumor treatments. In the course of this project, synthesis routes were established in cooperation with Prof. Dr. Marli Luiza Tebaldi and Daniel Bragança Viana (Universidade Federal de Itajubá, Brazil), supervised by me during the time of his master thesis partially performed in Potsdam.

Samples of poly(*N*,*N*-diethylacrylamide) (PDEA) and PNVCL were synthesized and provided to Huaisong Yong, research scientist at Leibniz-Institute for Polymer Research, Dresden.

**Conference Posters:**

**Berliner Chemie Symposium, Humboldt University Berlin,** 05.04–06.04.2018
M. Mathieu, H. Charan, U. Glebe, A. Böker
Transmembrane Protein-Polymer Conjugates for the Generation of Nano-Thin Membranes

**Tag der Chemie, Technische Universität Berlin,** 11.07.2019
M. Mathieu, M. Schwieters, U. Glebe, A. Böker
Transmembrane Protein-Polymer Conjugates for the Generation of Nano-Thin Membranes

**Symposium on Innovative Polymers for the Nanomedicine of the 21st Century, Friedrich-Schiller Universität Jena,** 15.07.–17.07.2019
U. Glebe, M. Mathieu, M. Schwieters, J. Martin, H. Charan, X. Dai, Z. Sun, C. Wu, A. Böker
Protein-Polymer Conjugates: Synthesis Strategies and Applications as Natural Membrane Mimics and Therapeutic Agents

**Macromolecular Colloquium, Albert-Ludwigs-Universität Freiburg,** 26.02.–28.02.2020
M. Mathieu, M. Schwieters, U. Glebe, A. Böker
Transmembrane Protein-Polymer Conjugates for the Generation of Nano-Thin Membranes

# Table of Contents

# 1 Introduction

## 1.1 From Cells to Industrial Applications and Beyond

**Proteins** are ubiquitous macromolecules, fulfilling key tasks in nature and are therefore in focus for their use in laboratory and industrial applications. They are one of the three main biopolymers in nature, namely DNA, proteins and carbohydrates.[1] Even though all proteins are built from the same building blocks called amino acids, their sequence dictates functionality of unfathomable kinds.[2] Proteins can be classified based on their structure in globular, fibrous and intermediate proteins. An alternative classification is set up according to their functionality consisting of enzymes, messengers, transporters, regulators, receptors, cell adhesion molecules, structural proteins, storage proteins and toxins.[3,4]

It is not surprising that these powerhouses of nature are widely used in industrial and biomedical applications, while new applications are constantly explored.[5,6] Especially in recent years, the need of new bio-based economically and environmentally friendly products and production processes increased significantly and circular economy became highly important for lots of industrial sectors nowadays.[7–9] Proteins as extraordinary materials with their intrinsic biodegradability could be used as alternatives for classical oil-based and synthetic resources. Enzymes could act as surrogates in chemical synthesis procedures.[10,11] As additives or raw material, proteins and enzymes are currently used in coatings, construction materials, adhesives, lubricants, and as natural detergents in the cosmetics, beverage, food, textile and paper industry.[12–14] Thereby, it is taken advantage of their various properties as foaming agents, emulsifiers, thickeners, gelling agents, wetting agents and as natural catalysts. Figure 1.1 provides some examples for industrially relevant proteins and enzymes.[5,13,14]

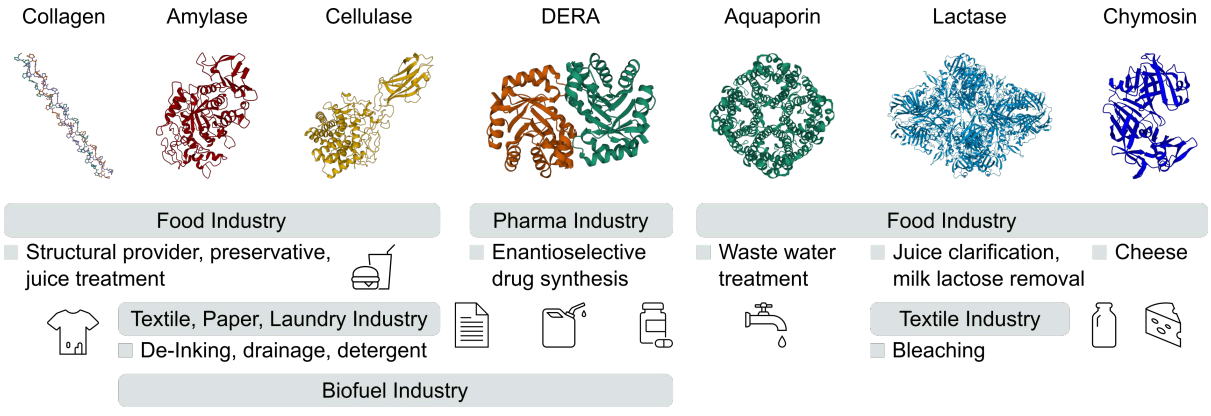


Figure 1.1: Industrially relevant enzymes and proteins categorized together with their corresponding applications.[13,14] Inset are the crystal structures of the proteins (PDB[15] IDs in order of their appearance: 1K6F,[16] 1SMD,[17] 1JS4,[18] 1VCV,[19] 1RC2,[20] 6TSK,[21] and 1CMS[22]). Structures illustrated using the Mol* web app implemented in the protein data bank (PDB) website.[23]

It is safe to say that this list will expand significantly within the next years. Current ideas for the future use of biohybrid materials are numerous. For example self-healing properties could be included into fabrics by treatment with squid ring teeth proteins.[24] When the material is torn, it can be reassembled by putting the edges together and simply adding warm water. The protein then does the magic and experiments with different fabrics already showed full recovery of material properties.[24]

Another very interesting approach is tackling the plastic pollution in the world using polymer-consuming enzymes. Bioengineers can improve those enzymes to be more efficient in their task to degrade for example polyethylene terephthalate (PET), a polymer widely used in packaging.[25] Moreover, such packaging materials could be substituted by active and smart packaging based on proteinic materials enhancing the protective and sensory functions of food packaging as well as increasing the safety, quality and convenience of food products.[13,26,27]

Some ideas already took the next step – from research into market. The founders of the company MODERN MEADOW were driven by the lack of sustainable materials when initially focusing on 3D-printing applications. Nowadays, the company provides proteins as functional components, developing and applying new technologies for bio-fabrication. As self-stated "pioneers in bio-fabrication", they provide materials that support sustainability without a lack in performance, accessibility, and aesthetics, and taking these materials to produce for example "animal products" without animals. Taking ZI™ as an example, this leather substitute developed by MODERN MEADOW provides improved properties and higher sustainability than its natural and synthetic counterparts.[13,28,29]

Another outstanding example worth mentioning is the company AQUAPORIN. As natural water purifier in all cells, proteins called aquaporins evoked interest to also work in artificial membrane systems outside the cell. This concept, already applied in academic research,[30] was successfully elevated to an industrial level by Morten Østergaard JENSEN, Peter Holme JENSEN, Claus HÉLIX-NIELSEN and Danielle KELLER. The combined know-how of biochemists, biophysicists and entrepreneurs lead to the development of membranes comprising lipid-bilayers incorporating aquaporins as functional pores. With this Aquaporin Inside® technology, one gram of protein material can filter 700 L water within 1 second. It is therefore an extraordinary example in the membrane sciences for the use of membrane proteins for ultrafiltration and desalination processes.[31–34]

## 1.2 Biomimetic Membranes

Membranes, in which a protein is incorporated in an artificial support layer composed of lipid bilayers or self-assembled block copolymers, are called **biomimicking/biomimetic or biohybrid membranes**. On the one hand, they are in focus of research as they can act as model systems to explore specific functionalities of cell membranes and membrane proteins in biology and biochemistry. On the other hand, membrane scientists can meet arising demands of costumers using new biomimetic membranes. Those may perform superior to conventional membrane systems made by high-resolution methods such as x-ray, electron beam and interference lithography. Therefore, biomimetic membranes are promising alternatives especially in the field of ultra- and nano-filtration.[35–39]

In general, a membrane is a selective layer separating a system in two or more compartments. Through this membrane, a separation of liquid or gaseous mixtures occurs due to permeation processes and different driving forces.[40] Permeation refers to the transport mechanism of the analyte through the membrane including hydromechanical (e.g., sieving) or diffusion-based processes. There are different types of separation processes classified according to their driving force, pore size of the membrane material and kind of analyte. Pressure-driven operations include micro-, ultra- and nanofiltration with pore sizes ranging from 10 µm down to < 2 nm. Reverse osmosis used for desalination and gas separation is also a pressure-driven process. In contrast, dialysis, forward osmosis and pervaporation (separation of liquid solutions through diffusion) are examples for concentration-driven processes. Additionally, an electric potential gradient and a temperature gradient can also be used for separation of analytes using membrane systems.[40]

The most prominent representative of a membrane, nowhere near beaten by its artificial imitators, is the cell membrane (Figure 1.2 a).[37] Due to the low thickness and incorporation of highly specific membrane proteins acting as “active pores”, cell membranes are outstanding regarding separation efficiency and specificity. Functionality of the incorporated proteins range from passive and active transport to signal transduction between cells. To mimic the cell membrane, proteins can be incorporated in phospholipid bilayers as natural membrane building blocks, but also block copolymer membranes can be used. Both systems tend to self-assemble under suitable conditions to 2D films making membrane formation an easy, cost- and energy-efficient straightforward process (Figure 1.2 c). Additionally, the synthetic counterparts of lipid membranes provide higher chemical and mechanical stability and the possibility to incorporate tunable properties dictated by the chosen polymeric matrix. Consequently, the functionality of the membrane proteins can be combined with the stability and robustness of synthetic membranes.[36,41–43] However, lipid and polymer membranes allow the incorporation of membrane proteins only in a comparably low density due to a ‘hydrophobic mismatch’ of protein to polymer thickness.[44,45] Furthermore, lack of covalent connection between individual components of the membrane material could lead to a decreased stability during operation.[46] Contrary,

protein-polymer conjugates can be used for simultaneous self-assembly and each building block consists of a protein pore and its polymer matrix.

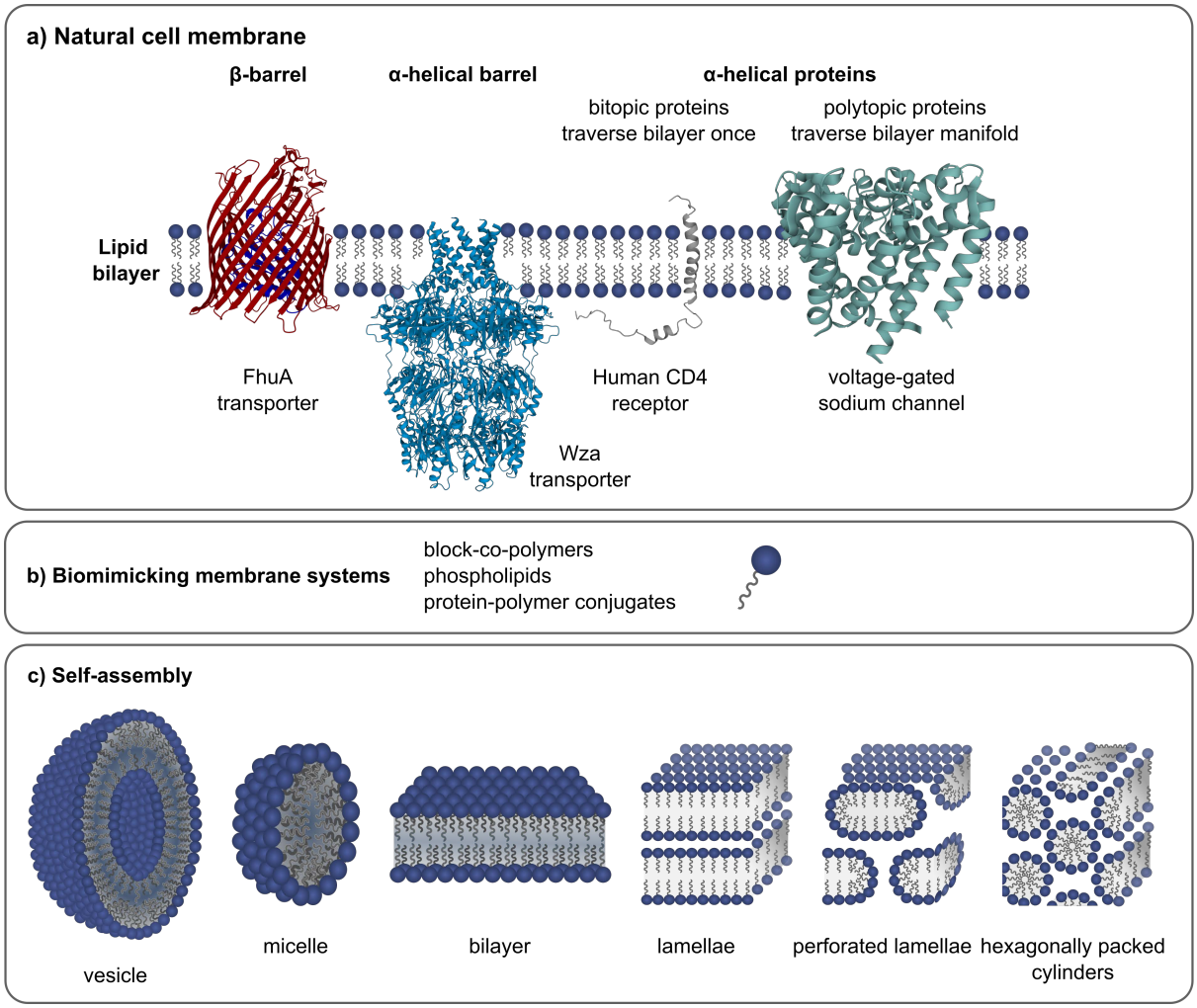


Figure 1.2: Schematics of a natural cell membrane with different membrane proteins (a). Functionalities of these membrane proteins range from active and passive transport to acting as receptors. Representative membrane proteins are shown, namely FhuA, Wza and a sodium channel (PDB[15] IDs 1BY3,[47] 2J58,[48] and 4F4L,[49] respectively). Structures illustrated using the Mol* web app implemented in the PDB website.[23] Artificial biomimicking membranes are taking advantage of the self-assembly behavior of protein-polymer conjugates, phospholipids or block copolymers (b). Higher-order structures that can be obtained by self-assembly are shown with lipids and include for example vesicles, micelles, bilayers, different kinds of lamellae or packed cylinders (excerpt). In particular, vesicle and bilayer membranes are exploited for membrane protein insertion (c). Adapted by references [35,50,51].

Besides desalination and water purification, such artificial biomimetic membranes are used as protein-based biosensors,[52,53] for size exclusion,[54] enzyme immobilization,[55–58] drug and membrane/membrane protein interaction studies,[53] and energy harvesting.[53] All these applications make use of the high specificity, selectivity and uniformity of specialized proteins performing superior to human-made pores.

## 1.3 In the Limelight as New Platform Technology - FhuA

An **idea** developed in the year 2011 by BÖKER and SCHWANEBERG aims for the incorporation of a versatile barrel-shaped protein in polymeric membrane materials.[59] As platform technology, it would provide different advantages compared to conventional methods. The membrane protein ferric hydroxamate uptake protein component A, or short FhuA, could serve as scaffold for biotechnological modification to adapt different functionalities, either on its outside or inside its channel. Protein-based materials offer a myriad of opportunities to tailor the macroscopic properties of a material by changing either the amino acid sequences of the proteins from which they are made, or by the means they are processed (protein engineering such as directed evolution).[60] Depending on the demands of the costumer, the FhuA channel could be modified to act as size separator,[61,62] chiral separator[63] or as artificial enzyme.[64] Furthermore, the polymer matrix helps to preserve the structural integrity of the protein in the membrane material, aids the formation of the active layer on top of a porous support, increases the stability of the protein against different analyte solutions and working conditions and adds additional functionalities and triggers to the overall system. Designed as **FhuA-polymer conjugate**, these hybrids serve as universal building blocks for the generation of ultra-thin membranes. Inspiration for this is the pore-forming platform technique presented by VAN RIJN et al.[41] Taking advantage of the self-assembly behavior of ferritin-polymer conjugates and subsequent denaturation of the protein, a membrane with uniformly distributed pores with small size deviation was obtained.

**FhuA** belongs to the family of porins – pore-like β-barrels which can be found in the outer membrane of Gram-negative bacteria like *Escherichia Coli* (*E. Coli*). Incorporated in the cell membrane, it plays a vital role in the transport of siderophore-mediated iron inwards the cell.[65] Its wild type is composed of 714 amino acids which assemble into two distinctive domains: a barrel composed of 22 β-strands and a plug which fills the lumen of the barrel and plugs the pore tightly.[65–68] Deletion of this cork-domain leads to a passive mass transfer channel which can be used for **size exclusion experiments** (Figure 1.3).[69]

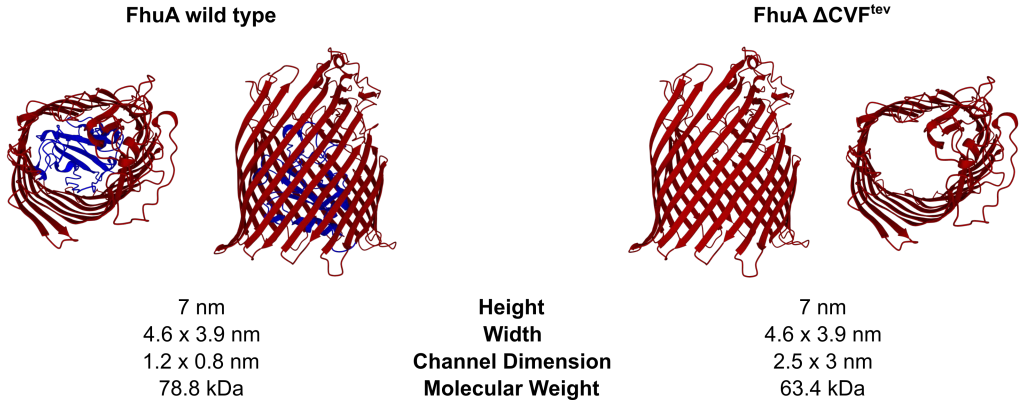


Figure 1.3: Illustration of FhuA wild type and the deletion variant with removed cork domain. Crystal structure of FhuA wild type (PDB ID 1BY3) was used and illustrated using the Mol* web app.[15,23,47]

Recently, an approach for the incorporation of FhuA molecules in **biohybrid membranes** was presented by the group of KUMAR especially designed for size exclusion based on the deletion variant.[62] In a first step, membrane proteins including FhuA were incorporated in 2D crystals and nanosheets with block copolymers using an organic solvent method. In the second step, these nanosheets were integrated in a layer-by-layer membrane with polyethylene-imine as filling material. The obtained membranes showed high water permeability outperforming commercial membranes with comparable molecular weight cut-offs while maintaining the molecular selectivity of the incorporated membrane proteins.[62] Variation of the channel diameter, as presented by SCHWANEBERG et al.,[61,70] could lead to highly precise size exclusion membranes suitable for ultra- and nano-filtration applications with high permeability while maintaining high solute selectivity.

Modification of the channel interior leads to applications beyond the scope of size exclusion. Again, the group of SCHWANEBERG provided techniques to achieve. They developed a new computer-aided whole cell screening approach to identify specific filter regions in the protein channel which can be re-engineered using multi-site saturation mutagenesis (OmniChange) libraries.[63,71] **Chiral channel protein** variants which translocate enantiomers through membranes with a preferred enantioselectivity were spotted and tested in a second step, the whole-cell screening, to test the efficiency of the variants. In initial experiments, this approach led to the identification of a FhuA variant able to resolve racemic mixtures of D- and L-arginine. The found hit showed an improved enantiomeric excess of L-arginine of ~ 24 % at 52 % conversion in the supernatant of the screening assay. In contrast, the parent variant and the blank showed and *ee* of 11 % and 8.35 % at conversions of 45 % and 43 %, respectively. However, there are still some major limitations. To identify this fit, 6000 clones were needed based on the computationally obtained possibilities. The other major drawback is the filter region approach itself, which does not provide enantioselectivity by blocking the transfer for one enantiomer, but by faster transfer of one enantiomer through the channel. This results in a delay of 300 ps for D-arginine compared to L-arginine. In equilibrium experiments as shown in the presented study, this can lead to the accumulation of one enantiomer in the supernatant compared to the other one. For membrane approaches, especially for membranes with nanometer thicknesses, this delay might not be enough to achieve a separation.[63]

Another promising application of FhuA is the generation of **biohybrid catalyst** systems. Those catalyst systems are also called artificial metalloenzymes and catalyze reactions not covered by natural enzymes. Here, the protein serves as scaffold to stabilize catalysts composed of transition metal complexes, chiefly in aqueous environments while retaining its catalytic activity. Especially for hydrophobic catalyst systems, this displays a promising approach as the sensitive catalytic center is embedded in the hydrophobic entity of the protein channel. FhuA-catalyst systems have been presented utilizing ring-opening olefin metathesis,[72] phenyl acetylene polymerization,[73] one-pot olefin cross metathesis with

sequential hydrogenation,[74] Diels-Alder reactions[75] or intermolecular alkene–alkyne coupling.[76] In a recent approach, the incorporation of such a catalyst system into a synthetic polymer film was accomplished. Therefore, FhuA was copolymerized with N-methylpyrrole. At the same time, an artificial cofactor was incorporated in the membrane which results in a catalytic biocomposite enabling ring-closing olefin metathesis in neat substrates.[64] However, all catalyst systems found in the literature belong to the Grubbs-Hoveyda type catalysts and the biohybrid catalyst systems have by far not reached their opportunities.[77]

Lastly, the possibility of utilizing FhuA to act as biosensor, either as targeted molecule or as active sensor, is exemplified here. For instance, single-molecule protein detection in a biofluid was accomplished using a protein bait-containing nanopore.[78] Here, FhuA acts as active biosensor measuring the ion current modulation in the vicinity of the pore via a polypeptide tail adaptor when a molecule penetrates the pore. The setup is comparable to a black lipid membrane. Additionally, it can be differentiated between uniform current opening and irregular current blockades. The first arises from specific protein captures and the second from nonspecific pore penetrations by nontarget components. Therefore, a quantitative sample detection and specific protein-target discrimination in a heterogeneous mixture is possible.[78] In the second example, FhuA depicts the targeted protein to detect *E. Coli* in drinking water.[79] A chimeric protein composed of a green fluorescent protein (GFP) subunit and a receptor binding protein called pb5 is used as active sensor. Here, the idea is that after binding of pb5 to its receptor FhuA in *E. Coli* bacteria, fluorescence provided by the GFP subunit of the chimeric protein after excitation with LED light is measured as direct proof of the presence of *E. Coli*. Even though this approach was not viable with FhuA, another chimeric protein targeting OmpW as relative in the family of transmembrane proteins showed exceptionally good results.[79] Nevertheless, it is imaginable that this concept can be transferred to FhuA using other chimeric proteins.

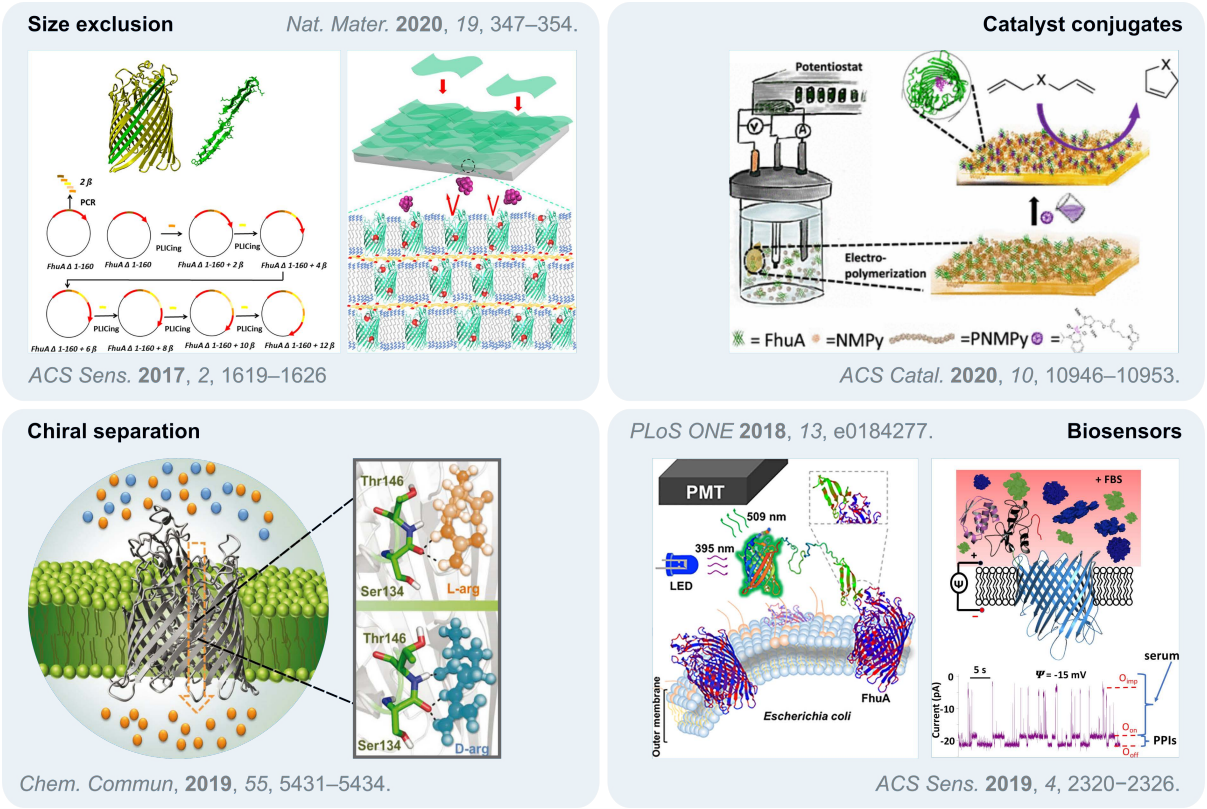


Figure 1.4: Overview of the use of FhuA in different applications. Figures reprinted with the permissions from Springer Nature,[62] the American Chemical Society (Copyright © 2017, 2019 and 2020),[61,64,78] and the Royal Society of Chemistry.[63]

The idea for FhuA-polymer membranes and the examples from literature presented above provide the basis for the current thesis. Protein-polymer conjugates based on FhuA and a thermo-responsive polymeric matrix will be assessed for constructing ultrathin membranes with a high density of FhuA pores incorporated in a polymer matrix. Hence, protein-polymer conjugates will be introduced next.

## 1.4 Protein-Polymer Conjugates

The combination of proteins with artificial polymers has shown to be a powerful tool to further improve the properties of these marvelous natural polymers with respect to solubility, stability, reusability, tunability and storability. Additionally, tailored pharmaceutical efficacy, incorporation or alteration of functionalities like stimuli-responsiveness and variation of self-assembly behavior is possible by the combination of proteins with suited polymeric materials.[11,80,81] Therefore, **protein-polymer conjugates** gained high interest within the last years based on their multipurpose usability in biomedical and industrial applications.[80–82] Most often, those conjugates are obtained by grafting a pre-synthesized polymer to the protein (**grafting-to**), in situ growth of the polymer chain from the protein surface (**grafting-from**) or by direct polymerization of biomolecule-containing monomers (**grafting-through**) (Figure 1.5).

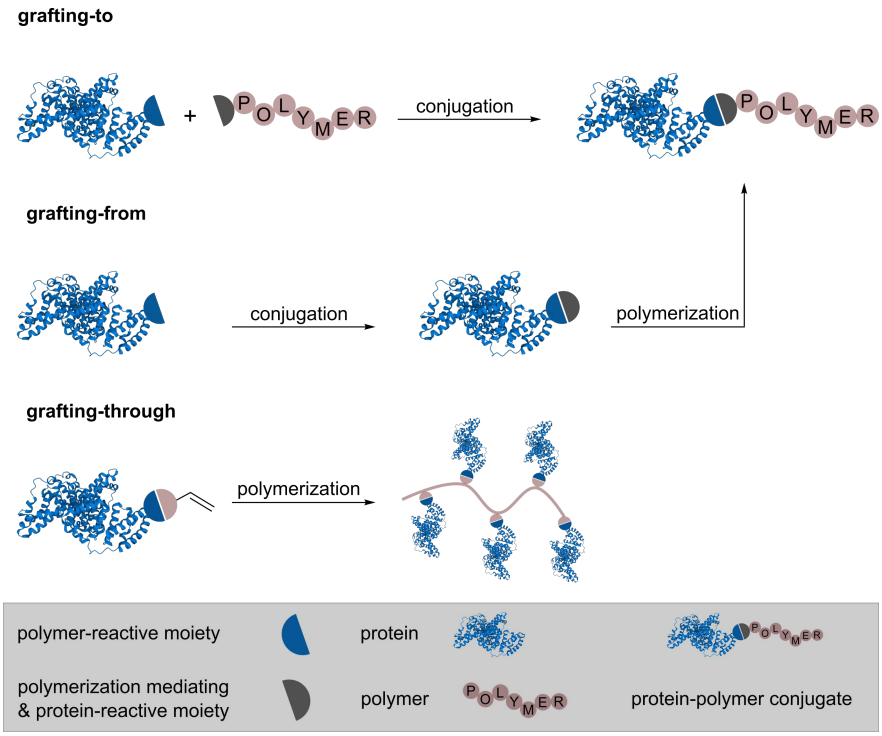


Figure 1.5: Illustration of grafting techniques for generation of protein-polymer conjugates. Bovine serum albumin (BSA, PDB ID 3F5S)[83] was used as protein for illustration.

After the discovery of reversible-deactivation radical polymerization (RDRP) with the most prominent representatives atom transfer radical polymerization (ATRP) and reversible addition-fragmentation chain transfer (RAFT) polymerization (Figure 1.6), those polymerization conditions became popular for the generation of protein-reactive polymers and in°situ generation of protein-polymer conjugates. First, the design of the polymer plays a crucial role in the performance of the conjugates and second, these techniques are applicable for a wide monomer scope and under diverse, biologically relevant conditions. Especially for in°situ bioconjugation, the polymerization must be favorably performed under aqueous conditions, at moderate monomer concentrations, the latter dictated by the applicable protein concentration, and at temperatures at or below room temperature to ensure least stress affecting the protein structure and activity.[84] In RDRP, polymer length - and as a consequence polymer structure and property - is easily varied by changing the reagent stoichiometry prior to or during polymerization.

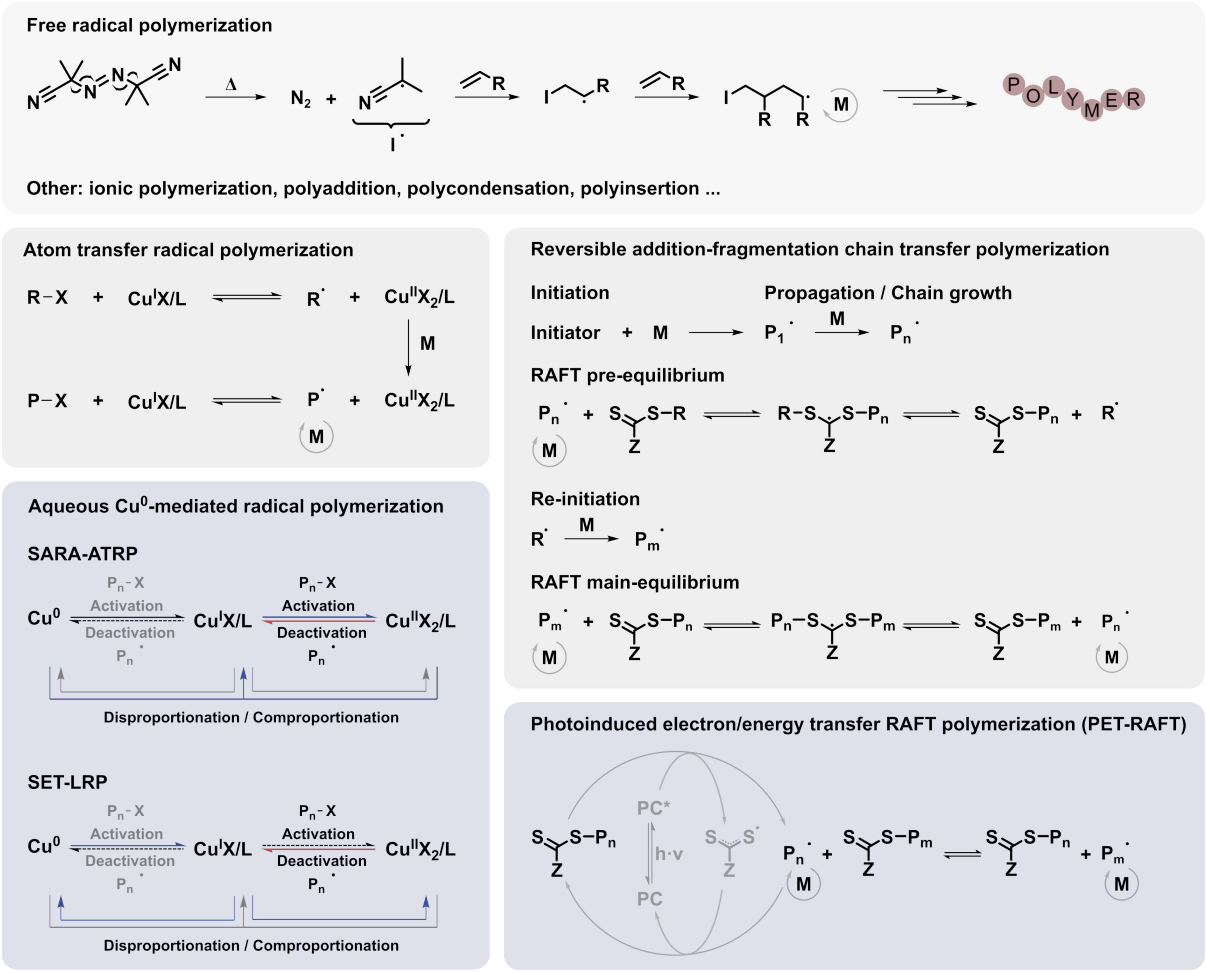


Figure 1.6: Overview of reaction mechanisms in radical polymerization as well as atom transfer radical polymerization (ATRP) and reversible addition-fragmentation chain transfer (RAFT) polymerization as commonly used techniques for the generation of protein-polymer conjugates. Aqueous copper(0)-mediated radical polymerization and photoinduced electron/energy transfer RAFT polymerization (PET-RAFT) are highlighted because of their specific relevance for grafting-from a protein.[85,86]

Recent improvements in polymerization procedures include polymerization under oxygen-tolerant conditions. Besides the possibility, that absence of oxygen and the degassing process might harm the protein, deoxygenation procedures in the presence of proteins are quite tedious. For example, degassing by bubbling with nitrogen through the solution results in foam formation as the interfacially active protein forms soap-like bubbles. THEODOROU and co-workers presented a versatile oxygen-tolerant polymerization approach using UV light initiated ATRP for the synthesis of protein-polymer conjugates using a variety of liquid monomers.[87,88] The high monomer content during polymerization acts as a co-solvent and lowers the solubility of oxygen in the reaction medium to an extent, where no further deoxygenation is needed. Furthermore, self-deoxygenating polymerization conditions as presented by HADDLETON et al. and MATYJASZEWSKI et al. following the Cu(0)-mediated radical polymerization mechanism are promising procedures, yet not transferred to protein-polymer conjugate synthesis.[89,90]

For gRAFTing-from, photoinduced electron/energy transfer (PET) RAFT as highly controllable procedure is used frequently for the synthesis of bioconjugates. The mild reaction conditions using visible light at room temperature result in precise polymerization with spatial and temporal control.[84,85,91,92] Even though PET-RAFT is not described under oxygen-tolerant conditions for gRAFTing-from a protein yet, a general oxygen-tolerant procedure using sodium ascorbate as co-reagent has already been published.[85,93–95] Throughout the years, the preparation of biomolecule-polymer conjugates by grafting-from has been described by various techniques including activators (re)generated by electron transfer (A(R)GET) ATRP,[96–98] initiators for continuous activator regeneration (ICAR) ATRP,[99] single-electron transfer living radical polymerization (SET-LRP),[100] photo-mediated ATRP[87,88] and RAFT using water-soluble thermal initiators[101,102] or metal-free PET-RAFT under visible light irradiation.[92,103,104] For grafting-to, different end-groups and their performance have been tested including active esters for amine or thiol modification of protein amino acid side chains.[105] In general, the synthesis and possible applications of protein-polymer conjugates have been frequently reviewed throughout the last years, highlighting the importance of this new field of biohybrids.[80,81,84,106–112]

Nevertheless, both grafting techniques display advantages and disadvantages. In grafting-from, a high grafting density can be achieved as small initiating groups are attached to the protein surface in a first step compared to sterically hindered polymers. In addition, the work-up after polymerization is easy as unreacted monomer and other small molecules can be separated by dialysis. However, the protein is directly involved in the polymerization process and might be harmed. In grafting-to, the protein itself is not incorporated in the polymerization process and the polymer can be precisely designed, produced and characterized prior to conjugation. Here, the disadvantage lies in the low grafting density and tedious workup procedure as a high excess of the sterically demanding polymer is needed for high conjugation yields. For both techniques, unspecific conjugation of the polymer to an arbitrary reactive group on the protein surface could lead to loss in protein functionality or enzyme activity.[81] Some approaches have been presented throughout the last years discussing site-specific conjugation methods to avoid for example modification of the enzyme active site.[82,113,114] Examples include incorporation of initiators by genetic modification, and stochiometric addition or selective blockage of highly reactive sites by dummy molecules.[50,115–117]

## 1.5 What´s the Structure?

As a result of unspecific conjugation in grafting-to and imperfections in grafting-from, **characterization of protein-polymer conjugates** to verify structural integrity of the protein after modification is an overarching challenge. Especially in grafting-from, number, distribution and initiation efficiency of initiators attached to the protein surface can vary and result in different molar masses and number of polymer chains attached per protein. Similarly, in grafting-to, a random number of polymer chains at arbitrary sites on the protein surface determined by the accessibility and reactivity of polymer-reactive groups leads to heterogeneous product mixtures, eventually also containing unreacted protein and unconjugated polymer.[81,82]

Proper folding and functionality of proteins work hand in hand. Modification can lead to changes in the protein structure and may result in reduction or complete loss of functionality, activity, structural integrity or stability. For enzymes, the remaining activity after modification can easily be probed representing the degree of structural integrity. Measuring the enzyme activity at different substrate concentrations provides a lot of information how conjugation affects the chemistry in the active site (in terms of $k_{cat}$) or the enzymes ability to bind a specific substrate (in terms of $K_M$).[118]

For proteins which do not display such kind of enzymatic activity, the analysis of structural integrity and functionality can be quite tedious. Whereas the proof of conjugation is straightforward and can be accomplished by standard biochemical characterization techniques like sodium dodecyl sulfate polyacrylamide gel electrophoresis (SDS-PAGE), size exclusion chromatography (SEC), matrix-assisted laser desorption ionization (MALDI) mass spectrometry, liquid chromatography-mass spectrometry (LC/MS) and high performance liquid chromatography (HPLC),[4] the analysis of the structural integrity of the biomacromolecule and interactions with the attached synthetic polymer is more challenging.

Characterization techniques that have been traditionally used in structural biology are nowadays emerging tools for the characterization of conjugates as well. In general, the structure of a protein is dictated by its primary amino acid sequence. The **primary structure** can be probed by sequential protein digestion and peptide sequencing by ESI-MS/MS or Edmans degradation with subsequent analysis of the products by SEC.[4] The next higher order of a protein, the **secondary structure**, arises from interactions in the backbone of the polypeptide chain. Main structural motifs are α-helices, β-sheets and random coils. Infrared (IR) and circular dichroism (CD) spectroscopy are the most frequently used techniques to analyze these structural motifs. In CD spectroscopy, the different absorption of left- and right-handed circularly polarized light is measured.[119,120] Molecules with no axis of proper rotation are referred to as chiral molecules. When a chiral molecule interacts with circularly polarized light, the absorption and refraction of left- and right-handed polarized light might happen to different extents. In

proteins, this effect arises from asymmetric or chiral α-helical or β-sheet motifs present along the polypeptide backbone. Different structural elements like α-helices, β-sheets and random coils result in characteristic CD spectra (plotted as a function of the wavelength) and can be used to differentiate between proteins of different kinds.[119,120] In IR spectroscopy, the secondary structure or more precisely the conformation of the polypeptide backbone is investigated as absorption of energy by vibrating chemical bonds. Similar to CD spectroscopy, the different structural motifs exhibit characteristic band positions and shapes revealing an overview of the overall state of the protein.[121–123]

The overall structural form of a protein is called its tertiary or quaternary structure for single polypeptide or multi-domain proteins, respectively. In addition to the backbone interactions, amino acid side chain functionalities interact with each other to fold and assemble the mature protein. Probing the tertiary or quaternary structure is most difficult as already slight deviations in folding could have a huge impact on protein functionality.

More hydrophobic amino acids such as tryptophan, phenylalanine, proline, leucine and so on, tend to hide themselves in the hydrophobic core of the protein to minimize interactions with surrounding water molecules in solution.[122] Therefore, **intrinsic or extrinsic fluorescence** of aromatic amino acids is used as probe for the tertiary structure. A shift of the emission maximum towards longer (denatured state) or shorter wavelength (folded state) provides information about the preservation of the tertiary structure.[122]

More detailed information about the state in solution such as size, shape and hydrodynamic properties can be gained by SEC coupled with different detectors like a **multi-angle laser light scattering** (MALS) detector.[124] Another possibility is the use of **analytical ultracentrifugation** (AUC), where structural information is gained by analyzing the sedimentation behavior of biomacromolecules (for more details, see Chapters 3 and 4).[125]

**Protein crystallization** and subsequent x-ray diffraction measurements represent a final confirmation of the three-dimensional arrangement of proteins in their folded state, as in all other molecule-related disciplines. Nevertheless, to find proper crystallization conditions, measurement and data analysis are quite tedious and sometimes even impossible for proteins, but even more for conjugates.[126] Cryogenic electron microscopy (Cryo-EM) might be an attractive alternative to conventional x-ray crystallography, as no crystallization is needed, making it attractive for hard to crystallize systems such as protein-polymer conjugates.[80,126] In solution and immobilized in e.g., membrane materials, other **diffraction techniques** might be handy. For example, small-angle neutron scattering (SANS) or x-ray scattering (SAXS) along with their surface sensitive techniques grazing-incidence SAXS (GISAXS) and SANS (GISANS) can provide information about size, shape, morphology, distribution and self-assembly behavior in solution or at interfaces (for more details, see Chapter 5).[126]

**Protein nuclear magnetic resonance** (NMR) spectroscopy can provide similar information as SAXS but is currently limited to relatively small proteins.[127] Especially 2D NMR techniques, where the signal shift is sensitive to the chemical environment of the studies bond, can provide versatile information about the protein folding state. Depending on the chosen technique, $^{1}H$-$^{15}N$ or $^{1}H$-$^{13}C$ heteronuclear single quantum coherence (HSQC), one obtains a fingerprint of the protein in form of chemical shifts of numerous signals in the NMR spectrum. Each signal can be assigned to a specific location in the protein. For example, each amide bond and amine containing amino acid side chain provides one or more signals in the $^{1}H$-$^{15}N$ HSQC spectrum, depending on the measurement conditions. When comparing two spectra, e.g., before and after conjugation, one gains an insight into the site of conjugation and the influence on the protein folding (see Chapter 2 for more information).[127,128]

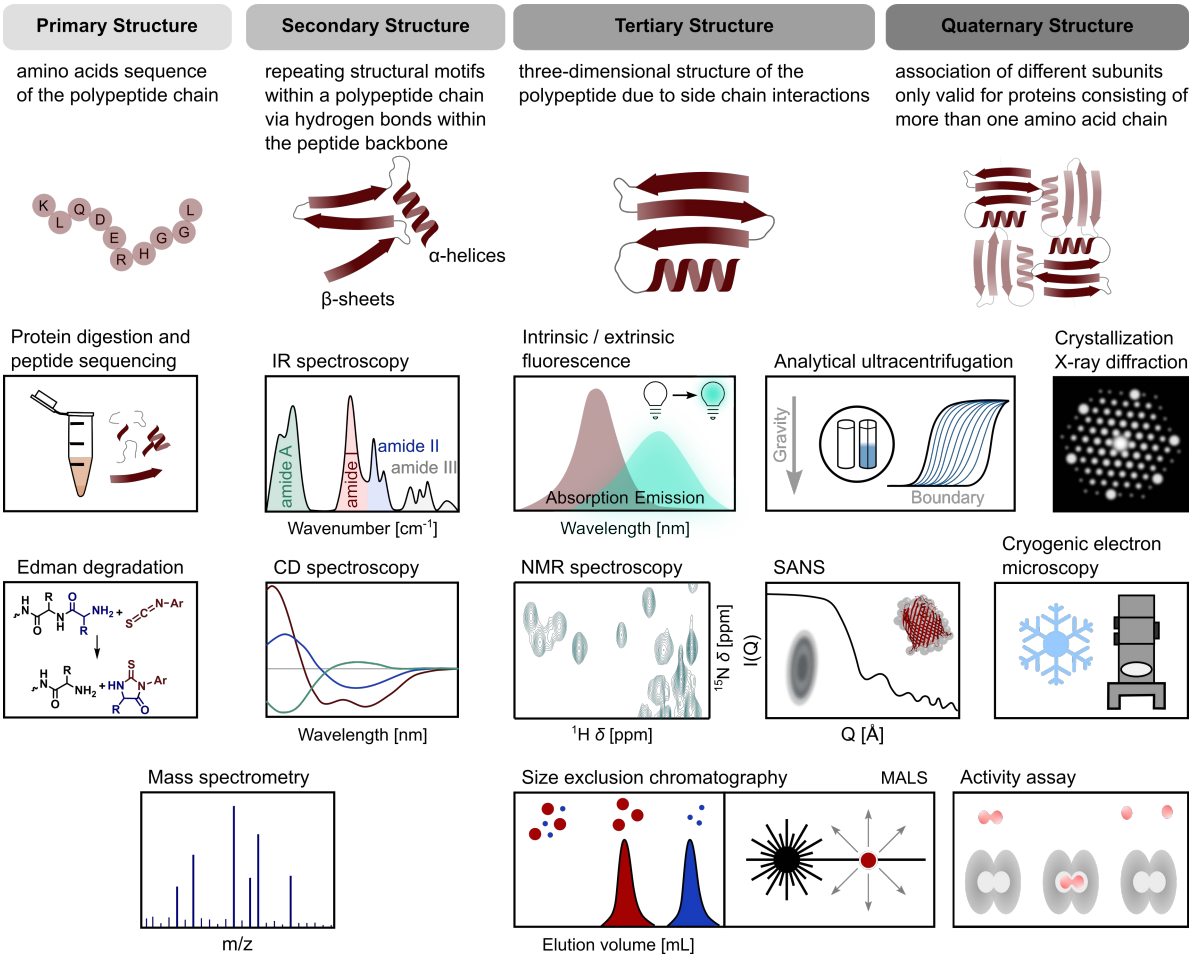


Figure 1.7: Levels of protein structure and corresponding analytical methods.[4,118–128]

## 1.6 Motivation and Scientific Goal

Polymer membranes based on proteins incorporated in polymeric materials have shown to perform superior to their classical counterparts.[33,129] Different functionalities such as size exclusion, chiral separation, sensory- or stimuli-responsiveness could be incorporated by either the chosen protein or variation of the polymer material paving the way to customized membrane designs. Combining the expertise of polymer scientists for membrane manufacturing and biotechnologists for protein modification, novel membrane concepts based on proteins can be realized and tested for future applications. The use of proteins is promising in terms of bioeconomy and sustainability. But most of all, their monodispersity as well as tailorability are yet unmet by artificial pore structures in nanometer dimensions.[130] However, protein-based membranes with a lack of covalent crosslinking demonstrate low durability, display a low density of incorporated proteins or require demanding and complicated scale-up processes.[36,46]

In the framework of this thesis, a concept for the use of protein-polymer conjugates as covalently crosslinked building blocks for membrane generation will be established to tackle the prevalent drawbacks of biohybrid membranes. The concept is based on the pore-forming platform technology developed by VAN RIJN et al. There, conjugation of the protein ferritin with a polymer and membrane formation through denaturation of the protein was established to introduce pores in a polymeric membrane material.[131] Replacement of ferritin with the transmembrane protein FhuA enables precisely defined uniform pores which can be further engineered to modulate their size and properties. Additionally, natural or artificial functionalities can be incorporated in a straight-forward way.

Preliminary work in this field was demonstrated by the group of Prof. BÖKER. Investigation of the synthesis of FhuA-polymer conjugates,[132] assembly of obtained conjugates at interfaces[133] and finally transfer of the platform technique implemented by VAN RIJN using ferritin-polymer conjugates to FhuA[134] provided the first steps towards the use of FhuA-polymer conjugates as universal building blocks for the generation of nano-thin membranes.

As the preservation of protein structure is a prerequisite for the transfer of the protein pore characteristics to the membrane material, special emphasis on the investigation of the protein structure before and after conjugation to the polymeric material is needed. Additionally, comparison between different conjugation approaches and characterization of preserved solution properties of conjugates is a special demand prior incorporation in a membrane material. Consequently, the formation of FhuA-polymer conjugates has to meet all requirements to sufficiently modify this membrane protein and incorporate the intact channel in artificial polymer membranes. Besides grafting-from, conjugation by grafting-to constitutes a promising supplemental approach worth investigating for the usability in membrane design.

Starting with the implementation of reliable polymerization conditions suitable for grafting-from under high dilution and grafting-to using end-group functionalized polymers, protein-polymer conjugates should be synthesized. The obtained conjugates of suited model proteins carbohydrate binding module 3b (CBM3b) and BSA are then planned to be analyzed using protein NMR (Chapter 2), SEC-MALS (Chapter 3) and analytical ultracentrifugation (Chapter 4) to gain further information about protein structural integrity and conjugate solution characteristics. The next step is fully devoted to FhuA (Chapter 5) taking a closer look in refolding conditions from a partially denatured state and analysis by SANS, GISAXS and x-ray reflectivity (XRR). Based on the obtained findings, FhuA-polymer conjugates are then synthesized, immobilized in membrane-like systems and intended to be characterized regarding their flux and functionality. To top it all off, an overall evaluation of the concept regarding the use of such membranes in an industrial manner will be part of this thesis.

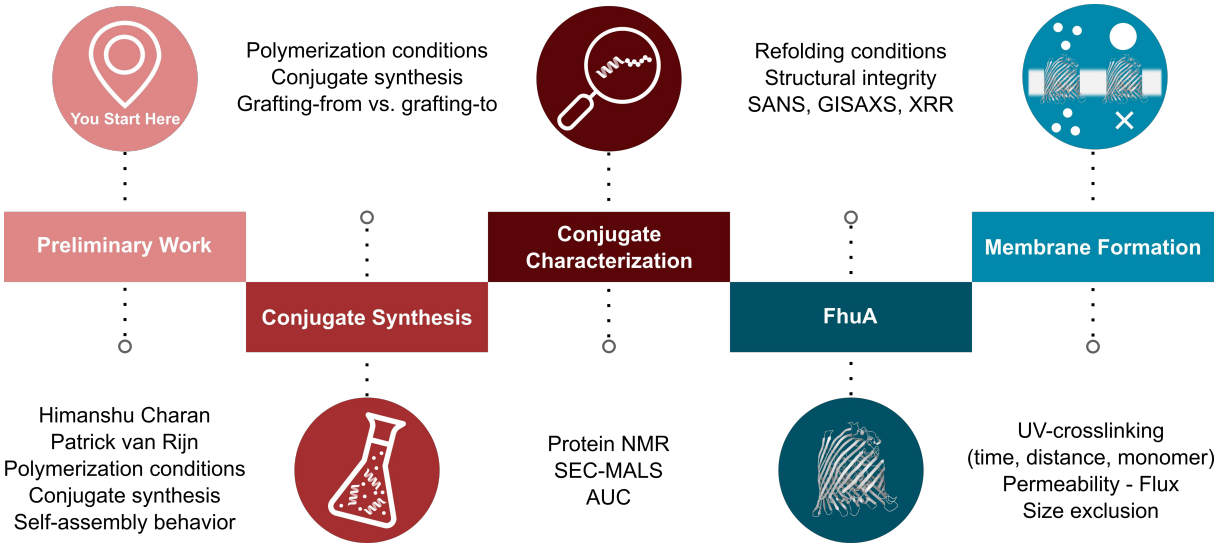


Figure 1.8: Road map for this thesis.

# 2 Probing Protein Folding by 2D NMR Techniques - Influence of Protein Modification by Polymerization Techniques

**Cooperation:** Maria Mathieu-Gaedke (conjugate synthesis, analysis, interpretation), Marcus Michaelis (NMR measurements, analysis, interpretation), Prof. Dr. Heiko Möller (conceptualization), Dr. Ulrich Glebe (conceptualization)

## 2.1 Abstract

Probing the structural integrity of proteins after modification is a challenge requiring advanced characterization techniques. Especially for proteins not displaying an enzymatic activity, to probe the preserved functionality is a major question for their ongoing use in biohybrid materials such as membranes and pharmaceuticals. Within this study, a variant of the model protein carbohydrate binding module 3b (CBM3b$^{N126W}$) of the cellulosomal multimodular hydrolytic enzyme cellobiohydrolase 9A (Cbh9A) from *Clostridium thermocellum* was used to monitor the influence of different polymerization conditions and different degrees of modification on the structural integrity of Cbh9A CBM3b$^{N126W}$ by protein nuclear magnetic resonance spectroscopy.

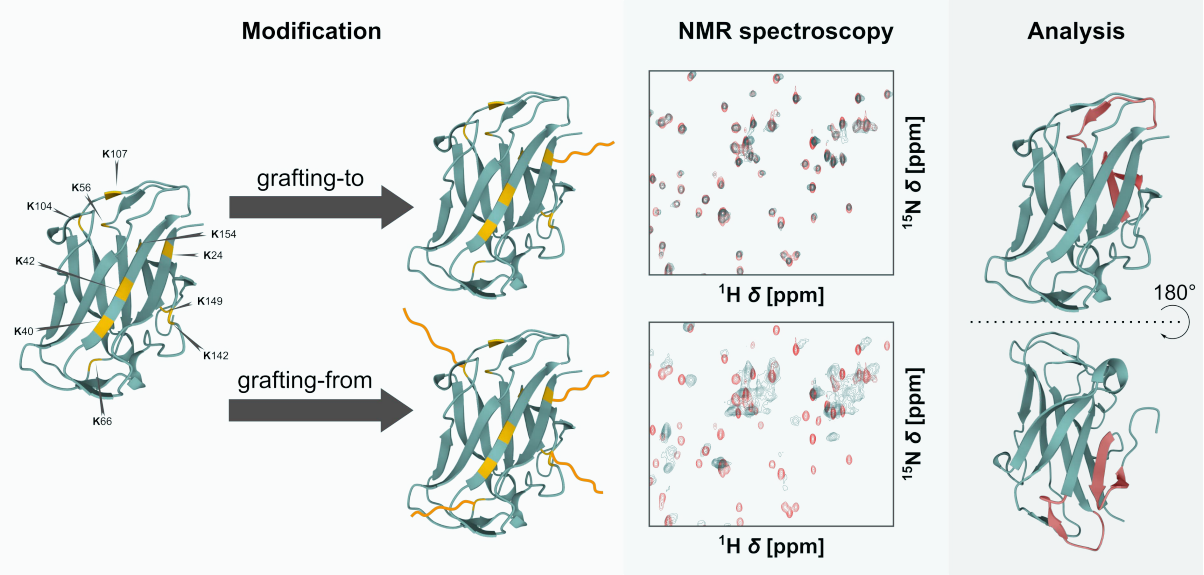


Figure 2.1: Graphical abstract for protein modification by grafting-from and grafting-to for subsequent analysis of protein folding and determination of the site of modification by protein NMR spectroscopy. Lysine residues are highlighted in yellow in the protein structure. The proposed site of modification is emphasized in red.

## 2.2 Introduction and Theoretical Background

Evaluation of protein structural integrity after modification by grafting a polymer to or from the protein surface is still a challenge in the field of biohybrid materials. Most often, characterization of conjugates is covered by CD spectroscopy to probe the secondary structure and measurement of remaining enzymatic activity as indirect proof of tertiary and quaternary arrangement. Those techniques may give hints on overall structural changes but lack to evaluate small changes at atomic level. Protein NMR spectroscopy is an advanced technique to follow these small changes by mapping chemical shifts of protein conformation in the peptide backbone or amino acid side chains. It´s therefore an alternative to classical x-ray crystallography experiments, which might be cumbersome for protein-polymer conjugates due to the low crystallinity of polymeric materials. Additionally, it can be performed in solution under non-destructive conditions and the same sample can be used for further analysis, for example measurement of the binding affinity to a substrate or remaining enzymatic activity after conjugation.[135]

Nuclear magnetic resonance (NMR) spectroscopy is a common technique in the toolbox of chemists for the characterization of small molecules. The principle behind NMR spectroscopy is the measurement of relaxation events of nuclei after excitation with an electromagnetic pulse while exposed to a strong magnetic field. Nuclei with a net spin behave like magnets. Accordingly, they orientate in a strong magnetic field along the magnetic field vector. Additionally, they spin around the main magnetic field just like a spinning top. This kind of motion is called precession. The frequency of precession $f$ is proportional to the magnetic field strength $B_0$ according to Equation (2.1).[128]

$$f = \frac{\gamma \cdot B_0}{2\pi} \tag{2.1}$$

The third variable in the equation is the gyromagnetic ratio $\gamma$, which is a characteristic constant for each nucleus. Within a molecule, additional local field differences are introduced by the variation of electron densities over the whole volume of the molecule. The higher the electron density around the nucleus, the higher the shielding from the surrounding magnetic field. A lower local field and a lower spinning frequency is observed. Therefore, the signal depends on the type of nucleus and its chemical environment within the molecule. Radio frequency pulses are used to excite the nuclei and flip the orientation of precession. As the nuclei realign to the magnetic field, the frequency of relaxation from the excited state can be measured by the current induced in a coil surrounding the sample. This process is called free induction decay, or short FID. Subsequent Fourier transformation of obtained time domain signals results in the frequency spectrum with a signal for each different nucleus. Different frequencies are called chemical shifts and they depend on the chemical structure of the nuclei and the electron density around it. In NMR spectroscopy, all nuclei are measured at once which results in a spectrum with different signals at different chemical shifts.[128] These were the fundamentals of a classical 1D

NMR experiment. Modified techniques can be used to address different nuclei and different sequences of the excitation pulse at different angles to the sample can be used to gain even more detailed information on the compound.

As the chemical shift highly depends on the chemical environment, it is a sensitive measure to observe changes in the chemical environment and, therefore, can be used to trace small changes in the structure of a protein. For large molecules, proton 1D spectra become really crowded as signals from all protons are measured at the same time frame. As an alternative, 2D spectra such as correlated spectroscopy (COSY) or $^{1}H$-$^{15}N$ heteronuclear single quantum coherence (HSQC) have been used to reduce spectral overlap in large molecules. The difference between "classical" NMR experiments and COSY and HSQC experiments is the pulse sequence used for excitation of nuclei spins. $^{1}H$-$^{15}N$ HSQC measurements have gained high interest in the protein community, as each amino acid residue (except proline) gives rise to one resonance at the position of the $^{15}N$ and $^{1}H$ frequencies of its backbone amide group and, depending on the amino acid, its side chain amide or amine group and is therefore a map of the protein amino acid composition in terms of 2D NMR signals. Because of that, it is also referred to as the amide fingerprint of a protein. Alternatively, $^{13}C$-$^{1}H$ correlation spectra are also quite frequently used to probe methyl signals in labelled proteins, called the methyl fingerprint.[136–138] Isotopic labelling of proteins to enrich the nuclei of interest, most often $^{15}N$ or $^{13}C$, is important to gain proper signal intensity in NMR analysis. This can be achieved by expression of the protein of interest in an isotope enriched medium. The isotopes are incorporated in the protein structure as they are produced by the host system.[127,138]

One major limitation in protein NMR is the assignment and spectral resolution of proteins larger than 30 kDa. As described in the section above, each backbone amide and amines in amino acid side chains give rise to a signal in the amide fingerprint. Consequently, the larger the protein, the more signals arise and spectral overlap becomes more likely.[138] In general, to fully assign the NMR spectrum of a not yet characterized protein is quite complicated. This process is lengthy and needs a lot of expertise, as different correlation spectra including 3D and 4D spectra must be measured, assigned and gained information used to depict the protein in terms of chemical shift spectra. It is comparable to an expert jigsaw puzzle. Therefore, most studies are performed using a reference protein fully assigned in previous experiments.[127,128] The range of chemical shift compared to a reference molecule, typically trimethyl silane (TMS) or sodium 3-(trimethylsilyl)propane-1-sulfonate (DSS), can be few ppm up to several 100 ppm. Figure 2.2 provides a guide for typical chemical shifts for different nuclei. In protein NMR spectroscopy, values lie typically between 100 to 135 ppm for $^{15}N$ and 4 to 11 ppm for $^{1}H$ nuclei.[127,128,139,140]

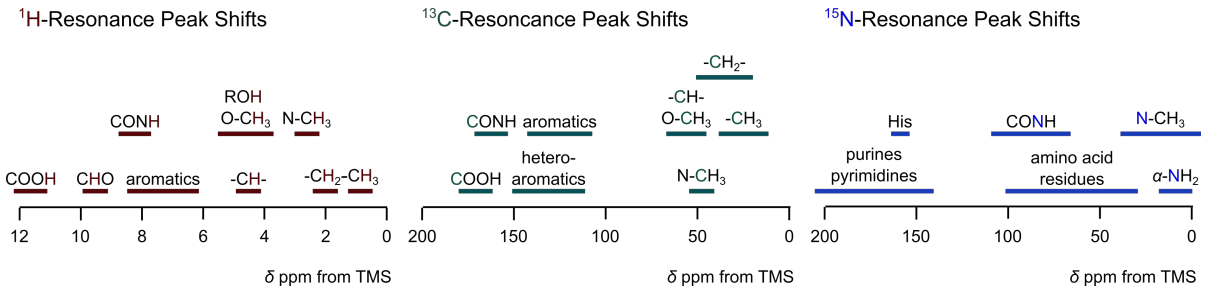


Figure 2.2: Typical chemical shifts for proton, carbon and nitrogen resonances in δ ppm from TMS. Based on reference [127].

When the reference spectrum is fully assigned, one is able to map the changes in chemical shifts. The chemical shift perturbation, also called chemical shift mapping or event-induced changes in chemical shift, can be used to determine the location of binding sites, affinities of ligands and structural changes in the protein after an event. Therefore, the geometrical distance a signal is moved is mapped against the protein sequence. The site of action can be easily identified as those shift changes are larger than the standard deviation of the shifts for all residues.[140] To compensate the relative chemical shifts of the different nuclei in heteronuclear 2D NMR experiments, a scaling or weighing factor $\alpha$ is used to obtain the Euclidean distance moved according to Equation (2.2). This scaling factor is typically ~ 0.14.[140]

$$d = \sqrt{\frac{1}{2}[\delta_H^2 + (\alpha \cdot \delta_N^2)]} \tag{2.2}$$

Research in the field of protein-polymer conjugates has focused predominantly on the investigation of therapeutic relevant proteins conjugated via grafting-to with polyethylene glycol (PEG), a FDA (abbreviation for the U.S. Food and Drug Administration) approved polymer.[141–148] In these systems, it was evaluated that the PEG chain behaves as an independent domain without any impact on protein conformation.[141,143,144,147] Decreased receptor binding and efficacy of PEGylated proteins, when noticed, where attributed to blockage of the protein binding sites by the PEG chain surrounding the protein.[142] Furthermore, the degree of PEGylation was already assessed using protein NMR spectroscopy and used to reveal structure-activity correlations, especially needed to evaluate the impact of PEGylation on therapeutics activity.[145,148]

A more detailed characterization was performed by BALBACH et al. Instead of using PEG, the studies presented branched PEG-polymers exploiting a lower critical solution temperature, abbreviated as LCST-type behavior, and studied the influence of polymer coil-globule transition at a specific temperature on protein conformation.[149] By using protein NMR spectroscopy, conjugation site, structural integrity and subsequently fibril formation of parathyroid hormone proteins (PTH) was studied. Chemical shift perturbation and plot of chemical shifts along the peptide sequence clearly revealed the influence of the polymer on protein conformation at different temperatures. Below the cloud point, only a few residues near the conjugation site were affected, whereas at temperatures above

the cloud point, the whole protein structure was affected, resulting in disappearance of signals or shift of signal positions. The authors claim that these changes can be attributed to the transition of the conjugate from an extended dumbbell conformation to a more shroud-like conformation. Interestingly, fibril formation as intrinsic feature of the investigated peptides, was not affected by conjugation.

A recent study presented by PAGE et al. utilized a block copolymer with incorporated spin labels at different positions conjugated to the protein ubiquitin.[150] The authors were able to map protein-polymer conformations in these bioconjugates with atomic precision by paramagnetic relaxation enhancement (PRE) experiments. Conjugates were prepared by an in situ activation of polymer chains with EDC-NHS and grafting-to the protein surface. The resultant data strongly suggest that the polymer snuggles to a specific area of the protein surface caused by non-covalent interactions. As a result, the protein was protected against denaturing agents and was able to withstand extreme conditions.[150]

## 2.3 Results and Discussion

Although grafting-from is widely used for the generation of protein-polymer conjugates, structural characterization of those conjugates is still not covered by protein NMR spectroscopy. This Chapter aims for a systematic synthesis of proteins modified with polymeric *N*-isopropylacrylamide (PNIPAm) by grafting-from and grafting-to followed by analysis of protein-macroinitiators (protein-MI), macro chain transfer agents (macroCTAs) and conjugates by protein NMR spectroscopy. The site-specific N126W mutant of the carbohydrate binding module 3b (CBM3b$^{N126W}$) was chosen as reference protein and the project performed in cooperation with Marcus MICHAELIS (University of Potsdam, group of Prof. Heiko MÖLLER). CBM is a protein domain of the cellobiohydrolase 9a (Cbh9A) found in *Clostridium thermocellum*.[151] The cellulosomal multimodular hydrolytic enzyme Cbh9A is involved in cellulose binding events. Although it is implied by the name, the carbohydrate binding module 3b itself does not display the ability to bind crystalline cellulose.[152] In contrast to the wild type, the point mutation in Cbh9A CBM3b$^{N126W}$ introduces this feature. The change of asparagine to tryptophane enhances the cellulose-binding ability of CBM3b by increasing the length and hydrophobicity of the putative cellulose-binding strip and reorientates one tyrosine residue (Y77) to be in plane with the two other aromatic residues Y78 and W126 to form a planar strip in the mutant protein. The structure of the protein domain can be described as nine-stranded antiparallel β-sandwich with a size of ~ 16.7 kDa and 16.9 kDa for the $^{15}$N-enriched variant, respectively.[151] For simplification, the protein variant Cbh9A CBM3b$^{N126W}$ is abbreviated as CBM without additional denotations in the rest of this Chapter. PNIPAm has been chosen as frequently used thermo-responsive polymer already used for the modification of many proteins.[92,115,132,153–155]

**Conjugates prepared by grafting-to:** First, CBM-PNIPAm conjugates synthesized by grafting-to were analyzed as they can be easily compared to literature results for PEGylated proteins as presented in the Introduction and Theoretical Background of this Chapter. Therefore, end-group functionalized PNIPAm was synthesized according to a procedure published by DE GEEST et al.[105] A RAFT agent bearing a pentafluorophenyl moiety (PFP) was synthesized and used for subsequent RAFT polymerization of NIPAm. PFP as protein-reactive end-group was chosen, as it is reported to have a higher conjugation efficiency compared to *N*-hydroxy succinimide (NHS).[105] PNIPAm was obtained by RAFT polymerization in dioxane with 4,4′-azobis(4-cyanovaleric acid) (ABCVA) as thermal initiator and reaction performed at 70 °C for 3 h. Polymers with different degrees of polymerization were used for modification, namely an oligomeric NIPAm (DP ~ 20) and a polymeric NIPAm (DP ~ 200). Prior to conjugation, the CTA end-group, more precisely the Z-group containing the trithiocarbonate moiety, was removed using a radical induced end-group removal procedure described by THEATO and co-workers.[156] An excess of a radical initiator, in the current case AIBN, was used to replace the sulfur group of the RAFT CTA and to saturate the emerging radicals with a cyanopropyl radical. Detection and quantification of the conjugate in gel filtration chromatography (GFC), or in other words aqueous SEC, by a UV–Vis detector is affected by the trithiocarbonate group of the CTA. The reason is the absorption maximum of the trithiocarbonate group around 310-320 nm, which interferes with the absorption maximum of aromatic amino acids in proteins typically used for quantification at ~280 nm.[157] Therefore, removal of the trithiocarbonate group is not mandatory, but simplifies protein detection and quantification subsequent to modification. The procedure used for conjugation of the protein-reactive polymer to CBM is as described by DE GEEST,[105] and the reaction scheme for polymerization and conjugation is shown in Scheme 2.1. CBM in phosphate buffer was first diluted with a bicarbonate stock solution (0.2 M) to a protein concentration of ~ 0.5 mg·mL$^{-1}$ and the pH adjusted to ~ 8.2. Then, the polymer pre-dissolved in dimethylsulfoxide (DMSO) was added to the protein solution and the reaction mixture stirred overnight. A 15-times molar excess of polymer with respect to protein was used for this approach.

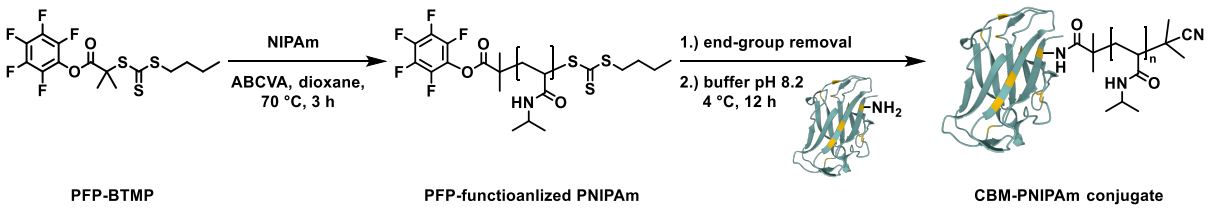


Scheme 2.1: Overview of the synthesis of CBM-polymer conjugates by grafting-to starting from a PFP-functionalized RAFT CTA. Position of lysine residues are highlighted in yellow. Crystal structure of Cbh9A CBM3b$^{N126W}$ (PDB ID 3ZQX)[151] was used for illustration.

After conjugation, the reaction mixture of both samples, namely conjugates of CBM with oNIPAm and PNIPAm, were analyzed by $^{1}$H-$^{15}$N HSQC NMR spectroscopy. In this technique, the proton and

nitrogen chemical shifts for each N-H bonded group in the protein are obtained. The result is an average spectrum over all species and conformations of the protein in the sample. Overall, CBM possesses 10 lysine residues and a solvent-exposed N-terminus which are all expected to be accessible for modification by PFP-activated o/PNIPAm. Grafting-to typically results in a mixture of unconjugated protein and conjugates with one and to a lesser extent a few attached polymer chains. Additionally, such unspecific conjugation usually leads to several positional isomers depending on the accessibility of lysine residues and N-terminus of the protein.[81,82,144] Initially, conjugates were not purified prior to the analysis. Interestingly, even though the polymer was not $^{15}N$ enriched and hence should not be visualized by this technique, the natural abundance of the $^{15}N$ isotope was sufficient to cause significant signals in 2D spectra of prepared conjugates with oligomeric and polymeric NIPAm (Figure 2.3 a). This resulted in an overlap of polymer with protein signals and a significant reduction of the native state HSQC resonances of CBM. To exclude the possibility of unfavorable interactions of the protein with unbound polymer with the protein, a reference measurement based on the protein in the presence of PNIPAm without covalent conjugation was performed. The spectrum and hence the protein structure is completely preserved (Figure 2.3 b) indicating that the unattached polymer in solution does not have any specific affinity for the protein.

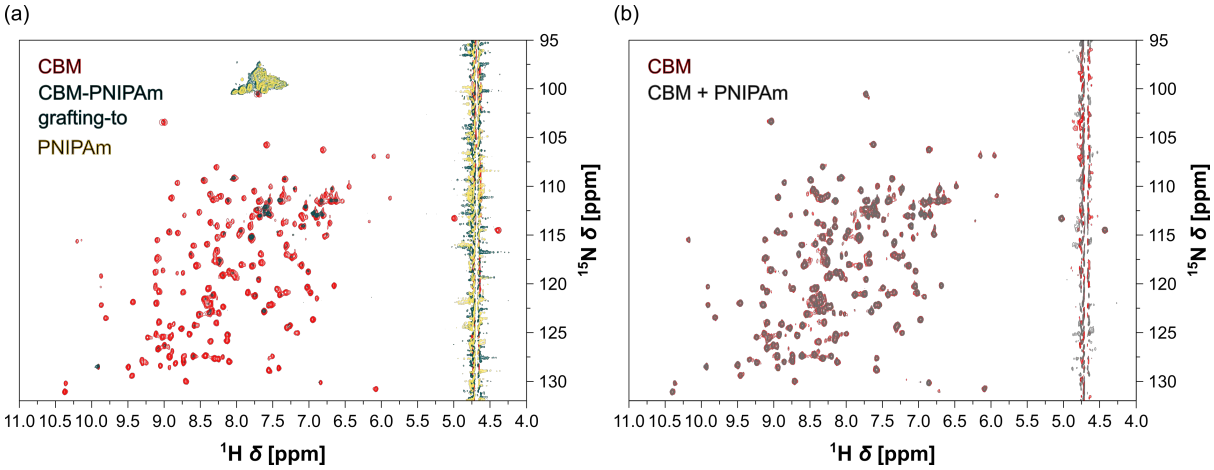


Figure 2.3: Overlay of the two-dimensional HSQC spectra of unmodified $^{15}N$-CBM (red), the crude reaction mixture of $^{15}N$-CBM-PNIPAM prepared by grafting-to (cyan) and PNIPAm in the same concentration (yellow) (a). Overlay of the two-dimensional HSQC spectra of $^{15}N$-CBM in the absence (red) and presence (grey) of PNIPAm (b). It is mentioned that the polymer concentration was reduced to a protein-to-polymer ratio of 1:1 for the reference.

As an excess of polymer is used for protein modification and a reaction mixture containing unmodified protein, conjugates and unbound polymer is usually observed for grafting-to, a purification protocol was established to separate the individual species prior to NMR characterization. Furthermore, it was decided to use only relatively short, oligomer-like polymers for both approaches, grafting-from and grafting-to to decrease unwanted polymer signals. For purification, the reaction mixture was separated by GFC and analyzed by MALDI-ToF mass spectrometry prior to further characterization with $^{1}H$-$^{15}N$ HSQC spectroscopy. In GFC, a significant shift of elution volume from ~ 100 mL for unmodified CBM

to 85 mL for the conjugate was observed, despite the fact of the relatively small increase in molar mass by conjugation (Figure 2.4 b). According to MALDI-ToF mass spectrometry (Figure 2.4 c), the molar mass increased from 17.2 kDa for CBM to 19.8 kDa for the conjugate. The mass difference of ~ 2.6 kDa fits nicely with the molar mass of one polymer chain ($M_{n,theor.}$ = 2523 g·mol$^{-1}$, $M_{n,SEC}$ = 2586 g·mol$^{-1}$) attached to the protein surface by grafting-to. Conjugation efficiency can be determined by the ratio of integrals of the two peaks obtained in GFC and was calculated to be 65 %. Due to the pronounced shift in elution volume, sufficient separation of reaction components prior to NMR analysis was achieved. The overlayed $^{1}$H-$^{15}$N HSQC spectra of unmodified CBM and conjugate are shown in Figure 2.4 a. Only minor changes in chemical shifts and slight decreases of peak intensities in some regions of the spectra were observed. Analysis of this sample in terms of chemical shift perturbation, as explained in Section 2.2 to identify the site of modification, was performed and the results shown at the end of this chapter. In summary, the CBM conformation is retained after modification via grafting-to. These findings are in agreement with literature reports for PEGylated proteins.[141,143,144,147] Similar to PEG, a PNIPAm chain seems to have a negligible effect on the protein structure.

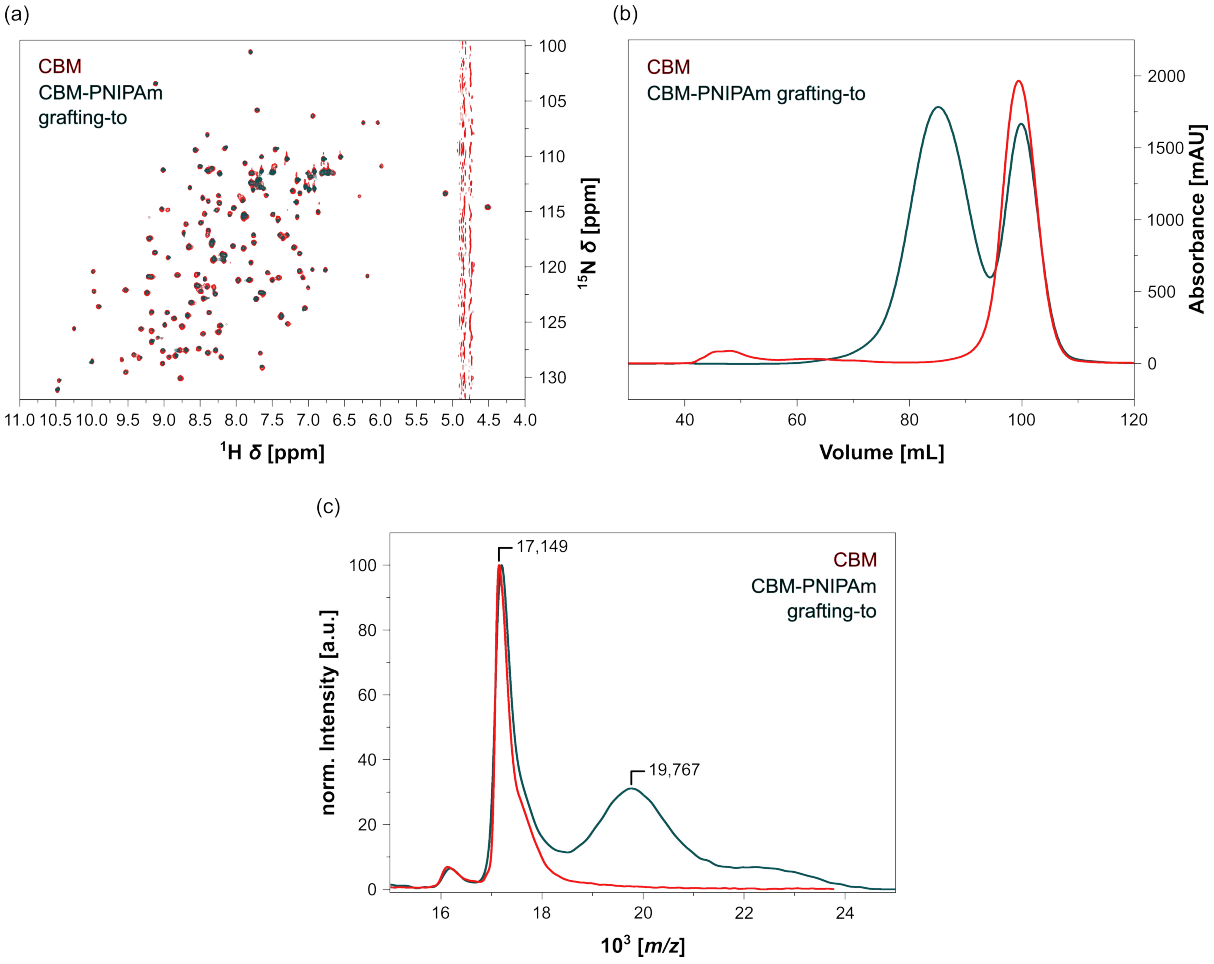


Figure 2.4: Overlay of the two-dimensional HSQC spectra of $^{15}$N-CBM (red) and synthesized conjugate by grafting-to (cyan) after purification by GFC (a). GFC chromatogram of CBM (red) and the crude reaction mixture after grafting oNIPAm to the protein (cyan) (b). MALDI-ToF mass spectra of unmodified (red) and modified CBM (cyan) (c).

**Polymerization procedures for grafting-from CBM:** Two different procedures to obtain protein-polymer conjugates by grafting-from were chosen to modify CBM as model protein with PNIPAm, namely Cu(0)-mediated radical polymerization and PET-RAFT. Even though both techniques have already been used in literature reports to modify different kinds of proteins, reaction conditions are not in agreement with general requirements for mild protein modification. As stated by KONKOLEWICZ et al. in their review from 2018, polymerization at low protein and monomer concentration and ambient temperature are favorable features for protein modification.[84] Additionally, irradiation with moderate light intensities preferable in the visible light regime for photochemical polymerization procedures is advantageous to reduce light damage of the protein. A selection of procedures employed for conjugate synthesis by the stated polymerization types is provided in Table 2.1.

**Table 2.1: Selection of reported reaction conditions utilized previously to obtain protein-polymer conjugates by grafting-from under ATRP-like and RAFT conditions.**

| # | Procedure | Protein | β [mg·mL$^{-1}$] | Conditions Ratio / [mM] | | | | Ref. |
|---|---|---|---|---|---|---|---|---|
| | | | | **Initiator** | **Monomer** | **CuBr** | **Me$_6$TREN** | |
| **1** | | - | - | 1 [17.7] | 50 [884] | 0.4 [7.1] | 0.4 [7.1] | [90] |
| **2** | **Cu(0)-** | CalB | 11.4 | 1 [0.17] | 589 [100] | 23.2 [4] | 23.2 [4] | [158] |
| **3** | **RDRP** | BSA | 6.7 | 1 [2.5] | 67 [166] | 1.25 [3.1] | 1.25 [3.1] | [100] |
| **4** | | | | **Initiator** | **Monomer** | **CuBr** | **HMTETA** | [159] |
| | | Myoglobin | 0.63 | 1 [0.037] | 3000 [111] | 100 [3.7] | 300 [11] | |
| **5** | **ATRP** | | | **Initiator** | **Monomer** | **CuBr /CuBr$_2$** | **Me$_6$TREN** | [131] |
| | | Ferritin | 1 | 1 [0.16] | 1750 [280] | 100/50 [16/8] | 187.5 [30] | |
| **6** | **Photo-** | | | **Initiator** | **Monomer** | **Cu$_2$Br** | **Me$_6$TREN** | [88] |
| | **ATRP** | BSA | 23 | 1 [0.23] | 5000 [1150] | 1.5 [0.345] | 12 [2.76] | |
| **7** | **Thermal** | | | **CTA** | **Monomer** | **Initiator** | | [153] |
| | **RAFT** | Lysozyme | 13.4 | 1 [1.22] | 219 [267.5] | 1.3 [1.6] | | |
| **8** | **PET-** | | | **CTA** | **Monomer** | **Eosin Y** | **PMDETA** | [92] |
| | **RAFT** | Lysozyme | 4.6 | 1 [1] | 99 [99] | 0.01 [0.01] | 1 [1] | |

Common polymerization conditions for the generation of protein-polymer conjugates by grafting-from presented in the literature either regard high protein concentrations (Table 2.1, entries 6 & 7), high extent of modification with small initiating groups (Table 2.1, entry 3) or a high degree of polymerization to increase monomer concentration during polymerization (Table 2.1, entries 2–6). These conditions limit the scope of the synthetic accessibility of various conjugates. Protein concentration is a limiting factor since lots of proteins, especially membrane proteins or in general more hydrophobic proteins have an upper boundary for solubility with regard to the protein concentration.

High monomer concentrations have the impact that they act as a kind of co-solvent and may have an influence on the protein structure or the general characteristics of the resulting protein-polymer conjugates.

In absence of sacrificial initiator/CTA, which is additional initiator/CTA added to the protein-macroinitiator or -macroCTA to increase the abundance of initiating sites during ATRP and RAFT polymerization and thus to gain more control over the polydispersity, a high protein or monomer concentration is usually required to induce polymerization.[107] The protein concentration is variable, as the protein concentration in $mg \cdot mL^{-1}$ needed for polymerization depends on the number of initiators/CTAs attached to the protein surface. CBM possesses 10 lysine residues which can be modified by bromine containing initiators or CTA moieties to initiate a polymerization under Cu(0)-mediated radical polymerization or RAFT conditions, respectively. For the shown reaction conditions, this would correlate to a CBM concentration of approximately 2–20 mg/mL, depending on the extent of modification and needed concentration of initiator/CTA to initiate the polymerization as stated in Table 2.1. Therefore, prior to applying the polymerization conditions to the synthesis of conjugates, they were altered to fulfil the stated requirements by KONKOLEWICZ and co-workers for polymerizations at a CBM concentration of 1–2 $mg \cdot mL^{-1}$.[84] Consequently, polymerization conditions for the synthesis of PNIPAm under high dilution of monomer and initiator were defined based on modified procedures presented in the literature.[90,92,132] Conversion was monitored by NMR spectroscopy and resulted polymers analyzed by size exclusion chromatography (SEC). Used reaction conditions and obtained results are summarized in Tables 2.2 and 2.3 for PET-RAFT and Cu(0)-mediated radical polymerization, respectively.

For PET-RAFT, a water-soluble chain transfer agent (CTA) bearing a short PEG-group on the Z-site, abbreviated PEG-CTA, was used. Details regarding the choice of this CTA are discussed in a later section of this chapter. Eosin Y was used as photocatalyst under mild visible light irradiation by blue LEDs ($\lambda_{max}$= 460-465 nm, ~ 375 $lm \cdot m^{-1}$, 60 $LEDs \cdot m^{-1}$) and in the presence of PMDETA as tertiary amine. High conversion at low CTA concentration was achieved at increased eosin Y concentration with respect to initiator. Dispersities of synthesized polymers were around Đ = 1.3, which is slightly higher than the ones reported in literature with ~ 1.01.[92] Entries 1 and 2 in Table 2.2 represent conditions as stated in the literature article (irradiation at 0.9 $W \cdot ft^{-1}$, 16459 $mcd \cdot ft^{-1}$, 50 cm, 30 LEDs, ~ 170 lm, SMD 5050, beam angle 180°).[92] It has to be noted, that initial experiments were performed at much higher light intensities (2.95 m, 177 LEDs, 4.8 $W \cdot m^{-1}$, 82 $lm \cdot W^{-1}$, 1160 lm, SMD 3528, beam angle 120°). As a consequence, polymerization was fast and resulted in broader dispersities of resulting polymers and were not comparable to literature results. Thereupon, light intensity was adjusted by a dimmer to 15 % of initial light intensity (~174 lm) and reaction kinetics slowed down to moderate rates with full conversion after 6 hours (Table 2.2, entry 5). SEC profiles of the polymers showed a

monomodal peak skewed towards higher molar masses (fronting) indicating interactions of the polymer with the column material and/or the presence of polymer chains with lower molar masses. Moreover, the polymers have a significantly higher molar mass than theoretically expected. This could be due to fast propagation relative to initiation or slower chain transfer in the RAFT mechanism. Taking a closer look at the literature, this phenomenon is described as side effect of high photocatalyst concentrations and high light intensities in PET-RAFT procedures.[92] Conditions from Table 2.2 entry 14 were chosen to be optimal for the subsequent polymerization from protein-macroCTA. These conditions represent a protein concentration of 1–10 mg·mL$^{-1}$, depending on the extent of modification of CBM with CTA units. To avoid high protein concentration, sacrificial CTA was added to account for the lower number of attached chain transfer agents.

**Table 2.2: Conditions screened for the PET-RAFT polymerization under high dilution in aqueous buffer.**

| # | Conditions Ratio / [mM] | | | | Conv.[a] | $M_{n,theor.}$[a] [g·mol$^{-1}$] | $M_{n,SEC}$ [g·mol$^{-1}$] | $M_{w,SEC}$ [g·mol$^{-1}$] | Đ |
|---|---|---|---|---|---|---|---|---|---|
| | CTA | NIPAm | EY | PMDETA | | | | | |
| **1** | 1 [5] | 20 [100] | 0.01 [0.05] | 1.1 [5.5] | > 99 % | 2 606 | 4 791 | 7 295 | 1.52 |
| **2** | 1 [1] | 100 [100] | 0.01 [0.01] | 1.1 [1.1] | 78 % | 9 161 | 14 166 | 17 038 | 1.20 |
| **3** | 1 [0.5] | 20 [10] | 0.01 [0.005] | 1.1 [0.55] | - | - | - | - | - |
| **4** | 1 [0.1] | 100 [10] | 0.01 [0.001] | 1.1 [0.11] | - | - | - | - | - |
| **5** | 1 [0.5] | 20 [10] | 0.1 [0.05] | 1 [0.5] | > 99 % | 2 606 | - | - | - |
| **6** | 1 [0.1] | 100 [10] | 0.1 [0.01] | 1 [0.1] | 50 % | 6 000 | - | - | - |
| **7** | 1 [0.5] | 20 [10] | 0.05 [0.025] | 1 [0.5] | 50 % | - | - | - | - |
| **8** | 1 [0.2] | 50 [10] | 0.05 [0.01] | 1 [0.2] | 20 % | - | - | - | - |
| **9** | 1 [0.1] | 100 [10] | 0.05 [0.005] | 1 [0.1] | - | - | - | - | - |
| **10** | 1 [0.05] | 200 [10] | 0.05 [0.0025] | 1 [0.05] | - | - | - | - | - |
| **11** | 1 [0.2] | 50 [10] | 0.25 [0.05] | 1 [0.2] | 75 % | 4 586 | - | - | - |
| **12** | 1 [0.1] | 100 [10] | 0.5 [0.05] | 1 [0.1] | 60 % | 7 132 | - | - | - |
| **13** | 1 [0.05] | 200 [10] | 0.1 [0.05] | 1 [0.05] | 45 % | 10 527 | - | - | - |
| **14** | 1 [0.5] | 20 [10] | 0.1 [0.05] | 1 [0.5] | 75 % | 2 040 | 4 063 | 5 375 | 1.32 |
| **15** | 1 [0.5] | 50 [20] | 0.1 [0.05] | 1 [0.5] | 87 % | 5 265 | 11 621 | 15 526 | 1.32 |
| **16** | 1 [0.5] | 100 [50] | 0.1 [0.05] | 1 [0.5] | 76 % | 8 943 | 18 073 | 23 673 | 1.31 |
| **17** | 1 [0.5] | 200 [100] | 0.1 [0.05] | 1 [0.5] | 88 % | 20 259 | 39 300 | 49 672 | 1.26 |

[a] According to NMR spectra of the crude reaction mixtures. Polymerizations were conducted using a commercially available blue LED light strip wound insight a cardboard parcel box (2.95 m, 177 LEDs, 4.8 W·m$^{-1}$, 82 lm·W$^{-1}$, 1160 lm, SMD 3528, beam angle 120°, longlife-led.de, order number 1596). Light intensity was reduced to 17 % for entries 5–17. *N,N,N′,N″,N″*-pentamethyldiethylenetriamine (PMDETA) was used as tertiary amine to improve control over molar masses according to reference [92]. All polymerizations were performed in buffer containing 10 mM phosphate and 30 mM NaCl, pH 7.4.

To explore conditions for Cu(0)-mediated radical polymerization, α-bromoisobutyric acid (BiBa) was chosen as controlled radical polymerization (CRP) initiator due to its high solubility in water. Additionally, BiBa carries a carboxylic acid group which can be modified to allow protein functionalization by active ester chemistry.[160] Polymerizations at low monomer and initiator concentrations were accomplished by the choice of a suitable catalyst concentration. Different reaction conditions used and analysis of obtained polymers are summarized in Table 2.3. It was found that low concentration of monomer and initiator and correspondingly low radical concentration during polymerization can be balanced out by a higher catalyst concentration resulting in fast synthesis of polymers within minute time frames and dispersities as low as Đ = 1.12. Again, experimentally determined molar masses do not correlate to the theoretically expected ones. A reasonable explanation is a low efficiency of the chosen initiator in the current system. This problem was already described in the case of BiBa among other initiators and seems to be a common issue in Cu(0)-RDRP.[96,161,162]

Nevertheless, overall three different cases of catalyst/ligand ratios were studied within this approach. An equimolar ratio, excess copper and excess ligand was used to study the impact on polymer characteristics despite the fact of the chosen initiator. High conversions were observed for all tested conditions when handling of the different solutions was appropriate. In all experiments, no degassing prior to polymerization was needed according to the recent findings by HADDLETON et al.[90] Polymerization was performed in a syringe and removal of head space was sufficient to eradicate the need for degassing. First, CuBr was placed in the syringe along with a stirring bar and a solution containing ligand in water or buffer was added, head space eliminated and the solution stirred until complete disproportionation was observed. Then, a solution containing initiator and monomer was added, headspace eliminated and polymerization proceeded under rapid stirring and decreased temperature, typically 4 °C. The lower temperature helps to disperse the colloidal copper particles in the reaction medium and to assure a homogeneous reaction mixture. Additionally, the rate of polymerization is slowed down at lower temperature leading to a better control over the polymerization. It should be mentioned that the order of adding the reaction components is crucial to obtain controlled polymerization and that the monomer/initiator solution is suggested to be added to the initiator/ligand solution rather than the other way around, to prevent loss of copper particles during the transfer step.

There are currently two proposed models to describe the mechanism of aqueous Cu(0)-mediated radical polymerization. In supplemental activator and reducing agent atom transfer radical polymerization (SARA ATRP), $Cu^{I}$ serves as the major activator of alkyl halides (initiator) and $Cu^{0}$ as supplemental activator and reducing agent of $Cu^{II}$ through comproportionation. Conversely, in single electron transfer living radical polymerization (SET-LRP), $Cu^{0}$ is the major activator and disproportionation is the major fate of $Cu^{I}$ in the system. In both theories, deactivation of alkyl radicals is regulated by $Cu^{II}$.[86,163,164] In water, a rapid and complete disproportionation of CuBr to $CuBr_2$ and dispersed $Cu^{0}$ particles is obtained,

despite the suggested mechanism of polymerization.[90,96,163,165,166] The SET-LRP is strongly supposed by HADDLETON.[163] Contrary, the SARA ATRP mechanism is defended by MATYJASZEWSKI. Even though the system starts in a fully disproportionated state, he justifies this assumption with the hypothesis, that the only pathway for the systems is comproportionation after addition of monomer and initiator to the priorly disproportionated catalyst/ligand solution.[86]

It is described, that an excess CuBr to ligand provides a higher amount of $Cu^{II}$ in the reaction medium, thus more efficient deactivation and better control.[165] Correspondingly, at copper/ligand ratios of 2:1, a lower polymer dispersity compared to a ratio of 1:1 was observed (Table 2.3, entries 3–10). Surprisingly, even though the control over polymerization increased, initiator efficiency decreased resulting in a bigger gap between expected and determined molar masses. In contradiction to the stated deactivation by $Cu^{II}$, an excess of ligand and therefore higher amount of $Cu^{I}$ in the reaction medium did not result in loss of control (Table 2.3, entries 12 and 13). In the presence of an additional halide salt, in the own studies sodium chloride, monodisperse polymers were obtained even at a copper/ligand ratio of [1]:[1.2]. Halide salts are reported to increase the control over polymerization as they provide a higher amount of deactivating species.[96] Furthermore, use of sodium chloride in the reaction mixture was found to help to disperse the colloidal copper particles even further. Nevertheless, high amount or excess of ligand should be avoided as the pH of the reaction solution is changed significantly. Furthermore, high ligand ratios are reported to decrease end-group fidelity of polymers at high conversion.[167,168]

With the presented methods in mind, further investigations in the field of polymerization under high dilution should focus on the control of the initial state of polymerization in both, Cu(0)-mediated radical polymerization and PET-RAFT. Further modification of reaction components, variation of irradiation source and intensity for PET-RAFT and CuBr concentrations and impact of additional salts on control of polymerization should be investigated. Additionally, variation of ATRP initiator to match the rate of initiation and polymerization to obtain a high initiation efficiency is recommended. When different monomers are aimed for, variation of ligand could be important to match reaction rates of monomer and catalyst system to increase control over polymerization.[167,169] Conditions from Table 2.3 entry 5 were chosen to be optimal for the subsequent modification of CBM by grafting-from via Cu(0)-mediated radical polymerization. Comparable to the PET-RAFT procedure, these conditions represent a protein concentration of 1–10 $mg \cdot mL^{-1}$, depending on the extent of modification of CBM with small CRP initiators. To avoid high protein concentration, sacrificial initiator could be added to account for the lower number of attached initiating groups at the protein surface.

**Table 2.3: Conditions screened for the Cu(0)-mediated radical polymerization of NIPAm under high dilution in aqueous buffer.**

| # | Conditions Ratio / [mM] | | | | CuBr dispr. [mM] | Conv.[a] | $M_{n,theor.}$[a] [g·mol$^{-1}$] | $M_{n,SEC}$ [g·mol$^{-1}$] | $M_{w,SEC}$ [g·mol$^{-1}$] | Đ |
|---|---|---|---|---|---|---|---|---|---|---|
| | Initiator | NIPAm | CuBr | $Me_6TREN$ | | | | | | |
| **1** | 1 [8.9] | 100 [884] | 0.8 [7.1] | 0.4 [3.6] | 49.5 | 45 % | 5 259 | 9 983 | 12 320 | 1.23 |
| **2** | 1 [2.4] | 67 [164] | 1.25 [3.0] | 1.25 [3.0] | 18.8 | > 99 % | 7 749 | 13 127 | 23 936 | 1.82 |
| **3** | 1 [0.5] | 100 [47] | 7.5 [3.5] | 7.5 [3.5] | 24.8 | > 99 % | 11 483 | 21 226 | 29 838 | 1.41 |
| **4** | 1 [0.5] | 100 [47] | 15 [7] | 7.5 [3.5] | 49.5 | 92 % | 10 578 | 24 426 | 28 187 | 1.15 |
| **5** | 1 [0.5] | 50 [23] | 7.5 [3.5] | 7.5 [3.5] | 24.8 | > 99 % | 5 825 | 9 877 | 13 427 | 1.36 |
| **6** | 1 [0.5] | 50 [23] | 15 [7] | 7.5 [3.5] | 49.5 | 89 % | 5 203 | 18 884 | 21 914 | 1.16 |
| **7** | 1 [0.5] | 100 [47] | 7.5 [3.5] | 7.5 [3.5] | 24.8 | > 99 % | 11 483 | 17 041 | 23 663 | 1.39 |
| **8** | 1 [0.5] | 100 [47] | 15 [7] | 7.5 [3.5] | 49.5 | 92 % | 10 578 | 27 306 | 32 203 | 1.18 |
| **9** | 1 [0.5] | 200 [94] | 7.5 [3.5] | 7.5 [3.5] | 24.8 | > 99 % | 22 799 | 35 417 | 48 022 | 1.36 |
| **10** | 1 [0.5] | 200 [94] | 15 [7] | 7.5 [3.5] | 49.5 | 75 % | 17 141 | 42 127 | 47 013 | 1.12 |
| **11**[b] | | | | | | - | - | - | - | - |
| **12** | 1 [0.5] | 100 [47] | 7.5 [3.5] | 11 [5.4] | 24.8 | 72 | 8 315 | 19 231 | 22 287 | 1.16 |
| **13**[c] | | | | | | 87 | 10 012 | 21 743 | 24 563 | 1.13 |

[a] According to NMR spectra of the crude reaction mixtures. All polymerizations were performed in buffer containing 10 mM phosphate and 30 mM NaCl, pH 7.4, except otherwise noted. [b] Phosphate concentration set to 100 mM. [c] NaCl concentration set to 150 mM.

**Grafting-from using Cu(0)-mediated radical polymerization and PET-RAFT conditions:** In general, grafting-from is composed of two individual steps. First, small initiating groups (functional CRP initiators or CTAs) are attached to amino acid side chains of the protein or its termini. The ε-amino group of lysine was chosen as functional group, because of its natural abundance on the proteins' outer surface and the possibility to map occurring changes by $^{1}H$-$^{15}N$ HSQC NMR spectroscopy. In the second step, the polymerization is performed and the polymer grows directly from the protein surface. An overview is provided in Scheme 2.2 for the chosen reaction conditions to grow PNIPAm from CBM in buffer by Cu(0)-mediated radical polymerization (top) and PET-RAFT polymerization (bottom).

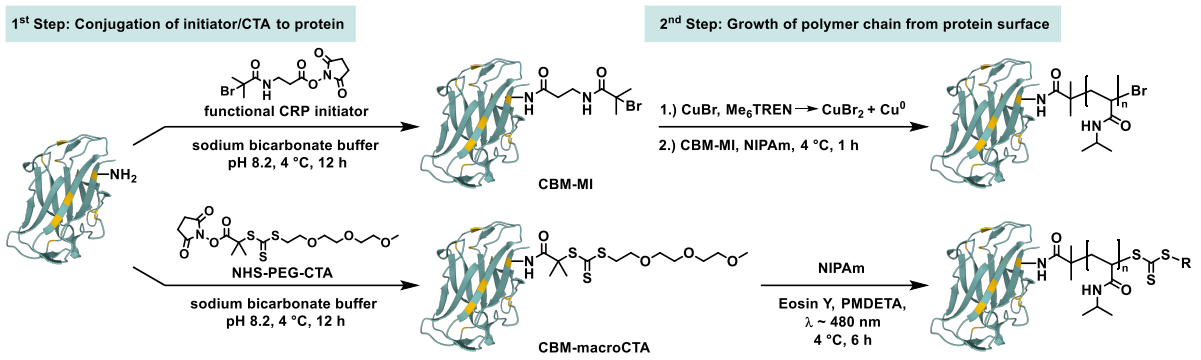


Scheme 2.2: Grafting-from CBM by Cu(0)-mediated radical polymerization (top) and PET-RAFT (bottom) to obtain CBM-PNIPAm conjugates. Crystal structure of Cbh9A CBM3b$^{N126W}$ (PDB ID 3ZQX)[151] used for illustration. A part of the functional CRP initiator is not displayed in the final conjugate for simplification.

Modification of CBM with *N*-2-bromo-2-methylpropanoyl-*β*-alanine *N*'-oxysuccinimide ester as the functional CRP-initiator and an NHS-functionalized CTA (Scheme 2.2, 1st step) was performed at various pH values of the reaction medium, in order to modulate the modification degree. For macroCTA synthesis, a suitable water-soluble CTA was designed for modification of CBM in order not to have a detrimental effect on the solubility of the macroCTA. CTAs reported in the literature for protein modification had the disadvantage, that protein solubility was decreased after modification as a result of the high hydrophobicity of the CTA moiety.[170] To circumvent this solubility problem, KONKOLEWICZ presented a combined grafting-to and grafting-from strategy. There, a small water-soluble oligomer was synthesized, attached to the protein with moderate conjugation efficiency and the polymer grown from the protein-macroCTA. As this strategy is close to the grafting-to strategy already investigated in the section above, a typical grafting-from strategy should be conducted in the framework of this thesis as this was not investigated by NMR spectroscopy before. Consequently, a new RAFT CTA inspired by systems presented in literature bearing a triethylene glycol moiety as Z-group was designed.[92,171] Details on CTA chemical structure and synthesis is provided in the Experimental Part of this Chapter. The synthesized PEG-CTA showed exceptional water-solubility and high modification efficiency in test studies using BSA as cheap and universal reference protein (data not shown).

Previous studies have shown that conjugation efficiency of proteins with NHS-active esters can be modulated by the applied excess of functional initiator/CTA to accessible primary amine groups present at the protein surface and the chosen pH value of the reaction medium.[134] The impact of the extent of modification on protein structure was therefore studied prior to polymerization. Conjugation of NHS-activated functional CRP initiator and PFP-activated PEG-CTA to CBM to obtain the respective macroinitiator (MI) and macroCTA was performed at pH 7.4 and 8.2, representing a lower and a higher extent of modification. The extent of modification was estimated by dividing the measured differences in molar masses of unmodified CBM and CBM-MI/CBM-macroCTA as determined by MALDI-ToF mass spectrometry by either 220 or 325, the mass of one attached initiator or CTA unit, respectively.

At pH 7.4, a mass increase of ~ 1 kDa after initiator attachment was observed corresponding to approximately 4–5 initiators attached per CBM molecule. For CBM-macroCTA the mass increase was found to be ~ 0.56 kDa corresponding to approximately 1–2 CTA units attached per CBM molecule. The respective MALDI-ToF mass spectra are depicted in Figure 2.5 a. At pH 8.2, extent of modification increased and was determined to be nearly quantitative (~ 9–10 lysine residues) for CRP initiators and approximately 50 % (~ 5 lysine residues) for CTA units.

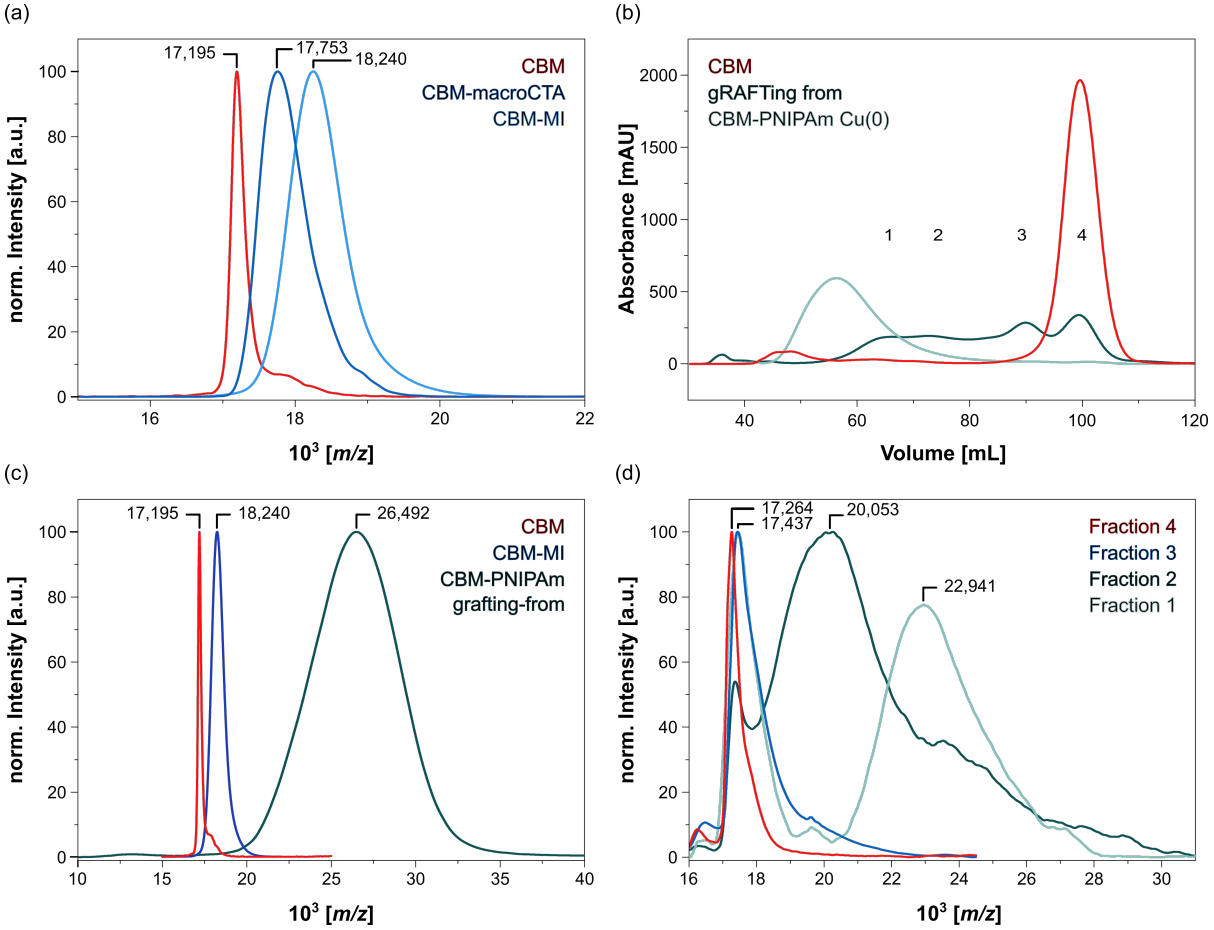


Figure 2.5: Analysis of CBM-MI, CBM-macroCTA (a) and corresponding protein-polymer conjugates by MALDI-ToF mass spectrometry (c and d) and GFC (b). Conjugates were obtained by grafting PNIPAm from the protein surface using either the Cu(0)-mediated radical polymerization approach (b light green curve, c) or PET-RAFT (b and d). By PET-RAFT, a mixture composed of unmodified CBM (red curves in b and d), CBM-macroCTA (blue curve in d) and two different conjugates (green curves in d) was observed and separated by GFC (dark green curve in b) prior to analysis with NMR spectroscopy.

The influence on the protein structure can be evaluated by inspection of the corresponding overlayed $^{1}H$-$^{15}N$ HSQC spectra shown in Figure 2.6 for CBM-MI (a and b) and CBM-macroCTA (c and d). The modification at lower pH only caused minimal perturbations in the protein's NMR spectra. Signal position, intensity and spectral resolution indicate a minor influence on the protein folding properties. The spectrum and hence the protein structure is overall preserved and was therefore analyzed in more detailed by chemical shift perturbation plots shown and discussed at the end of this chapter.

Interestingly, even though the degree of functionalization with CTA units is lower compared to CRP initiators, the general inspection of the NMR spectra implicates a higher impact of CTA on the protein structure compared to initiator units. A possible explanation could be the higher hydrophobicity of the CTA moieties influencing the general amphiphilicity of the protein.

At pH 8.2, and hence higher degrees of modification, the discrepancy between reference and sample spectrum increased significantly, indicating a negative effect on the protein structural integrity. $^{1}$H-$^{15}$N HSQC spectra revealed a significant reduction in peak intensity of the native state HSQC resonances, decreased spectral resolution and more pronounced chemical shift changes. From a theoretical point of view, long correlation times in NMR measurement after excitation result in broad signals, less signal intensity and ultimately in a higher signal overlap (for more details, see the theoretical part in the beginning of this Chapter). This can originate from sample precipitation, changes in sample solubility or mobility and structural changes. Additionally, a cluster of peaks at 110–115 ppm for $^{15}$N signals and 6.5–7.75 ppm for $^{1}$H signals was observed, characteristic for unfolding events of the protein.[172–174] As a consequence of the presented results, for grafting the polymer from the protein surface, CBM-MI and CBM-macroCTA derived at pH 7.4 were used exclusively.

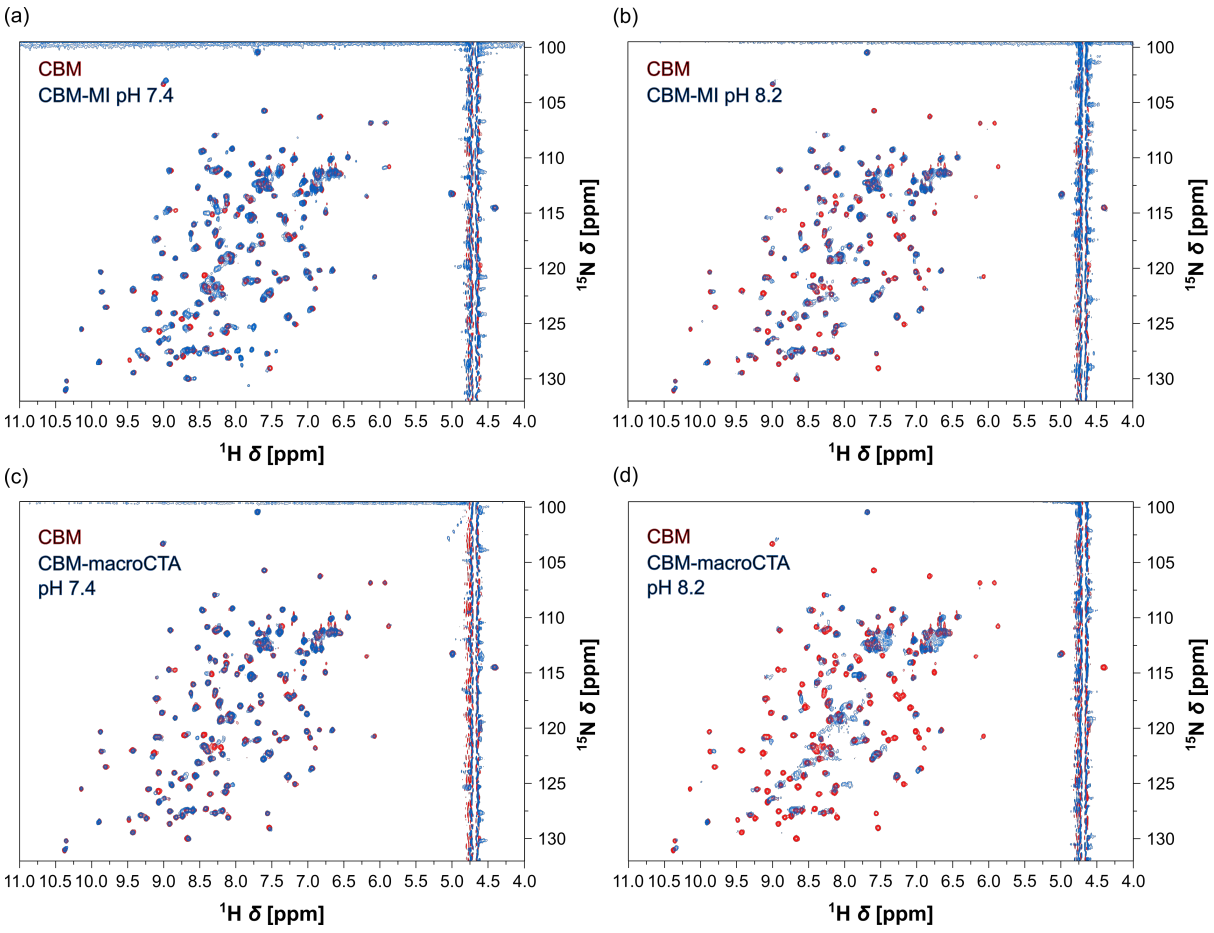


Figure 2.6: Overlap of NMR spectra prior and subsequent to modification with small ATRP initiators and CTA moieties at pH 7.4 and 8.2.

For the subsequent polymerization, conditions from Table 2.2 entry 14 for PET-RAFT and Table 2.3 entry 5 for Cu(0)-mediated radical polymerization were used. The targeted degree of polymerization for both conditions was set to 20, corresponding to a theoretical molar mass of the polymer of ~ 2.2 kDa per chain. Conjugates were analyzed by size exclusion chromatography (Figure 2.5 b) and MALDI-ToF mass spectrometry (Figure 2.5 c and d) to separate different reaction components and determine the molar mass of the conjugates, respectively.

First, conjugates obtained by the Cu(0)-approach were synthesized and analyzed by protein NMR spectroscopy. Starting from CBM-MI, an additional mass increase of 8.25 kDa was determined after polymerization (Figure 2.5 c). This correlates to a degree of polymerization of 14.6–18.2 or a molar mass of 1.65–2.1 kDa per polymer chain assuming approximately 4–5 initiating groups to be present at the protein surface and that the polymerization started evenly from every initiator attached to the protein surface. Based on the GFC chromatogram (Figure 2.5 b), the protein was transformed completely into a conjugate as no peak for unmodified CBM is visible. As already described for conjugates derived by grafting-to, the elution volume is shifted towards significantly lower values as expected.

In the overlayed spectra (Figure 2.7) it is clearly visible, that most signals decreased in intensity after polymer was grown from the protein surface. Signal clusters have formed in the region around 110–115 ppm for $^{15}$N signals and 6.5–7.75 ppm for $^{1}$H signals, which was already observed at high modification rates with small initiator molecules. Additionally, a new cluster was found between 125–128 ppm for $^{15}$N signals and 7.5–8.0 ppm for $^{1}$H signals. Overall, this result strongly suggests a negative impact of grafted polymer chains on the protein structural integrity. Compared to one attached polymer chain by grafting-to, approximately four to five chains were grown by grafting-from via Cu(0)-mediated radical polymerization. The high density of polymers around a rather small protein could be one reason for the high impact on the protein structure. A possible explanation could be that the growing polymer acts as leverage forcing the protein structure to open. This result is in contrast to common literature, where protein modification by grafting-from is stated to increase to protein structural integrity as tested by enzyme activity assays.[77,118,175] It could be assumed, that the enzyme´s active site still maintains its general structure and might be a little bit more exposed and therefore accessible to its substrate explaining the increase in enzyme activity of the conjugate. It should be noted that these experiments were repeated several times under different conditions and that the impact of the catalyst/ligand system at high concentration was tested as reference, showing no impact on the protein structure as determined by NMR spectroscopy.

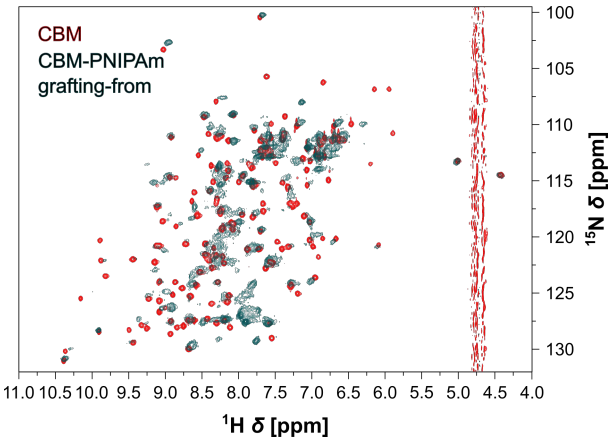


Figure 2.7: CBM prior to (red) and after (green) modification with PNIPAm by grafting-from using the Cu(0)-mediated radical polymerization approach. Cluster formation and decrease in peak intensity and spectral resolution is observed.

Second, conjugates synthesized by PET-RAFT were analyzed. As described above, at pH 7.4, the modification with PEG-CTA units led to the attachment of approximately 1–2 CTA moieties per protein molecule. To increase the amount of CTA units during polymerization, sacrificial CTA was added to the reaction mixture. Correspondingly, a mixture of different species was obtained after polymerization. The sample was fractionated by GFC (Figure 2.5 b), assigned by MALDI-ToF mass spectrometry (Figure 2.5 d) as unmodified protein, CBM-macroCTA and protein-polymer conjugates and the individual fractions analyzed by NMR spectroscopy. Numeration of peaks is in accordance with the elution volume with the lowest elution volume denoted as Fraction 1 and the fraction with the highest elution volume as Fraction 4. According to GFC and MALDI-ToF analysis, Fraction 4 can be assigned to unmodified CBM. Correspondingly, overlayed spectrum of Fraction 4 matches the spectrum of native CBM (Figure 2.8 a). All protein signals are visible and no significant chemical shift changes were observed. Peak intensity and resolution dropped slightly but can be assigned to insufficient separation of the fractions by GFC and the presence of residual CBM-macroCTA (Fraction 3) in the sample. For Fraction 3, assigned to be the CBM-macroCTA which did not take an active part in polymerization, resolution and chemical shift changes are more pronounced. They correlate strongly to the spectrum obtained for CBM-macroCTA prior to polymerization as presented in Figure 2.6 c in the section above. Fractions 2 and 1 were assigned as conjugates with either one or two attached polymer chains, based on the mass increase measured by MALDI-ToF mass spectrometry. The measured mass differences correspond to polymers with a mass of ~ 2.4–2.7 kDa which matches to a degree of polymerization of ~ 21–24. This is higher than the anticipated one, but reinforces the assumption, that not all CBM-macroCTA contributed to the polymerization. Although different lengths of one grown polymer chain could be also possible, the separation and isolation of two fragments with a doubled mass increase makes it more likely that fraction 1 consists of a conjugate with two polymer chains. For obtained conjugates, spectral shift changes increased and peak intensity decreased drastically with increasing

degree of functionalization (Figure 2.8 c and d). The deviations likely arise from structural changes and/or decreased sample solubility and mobility.

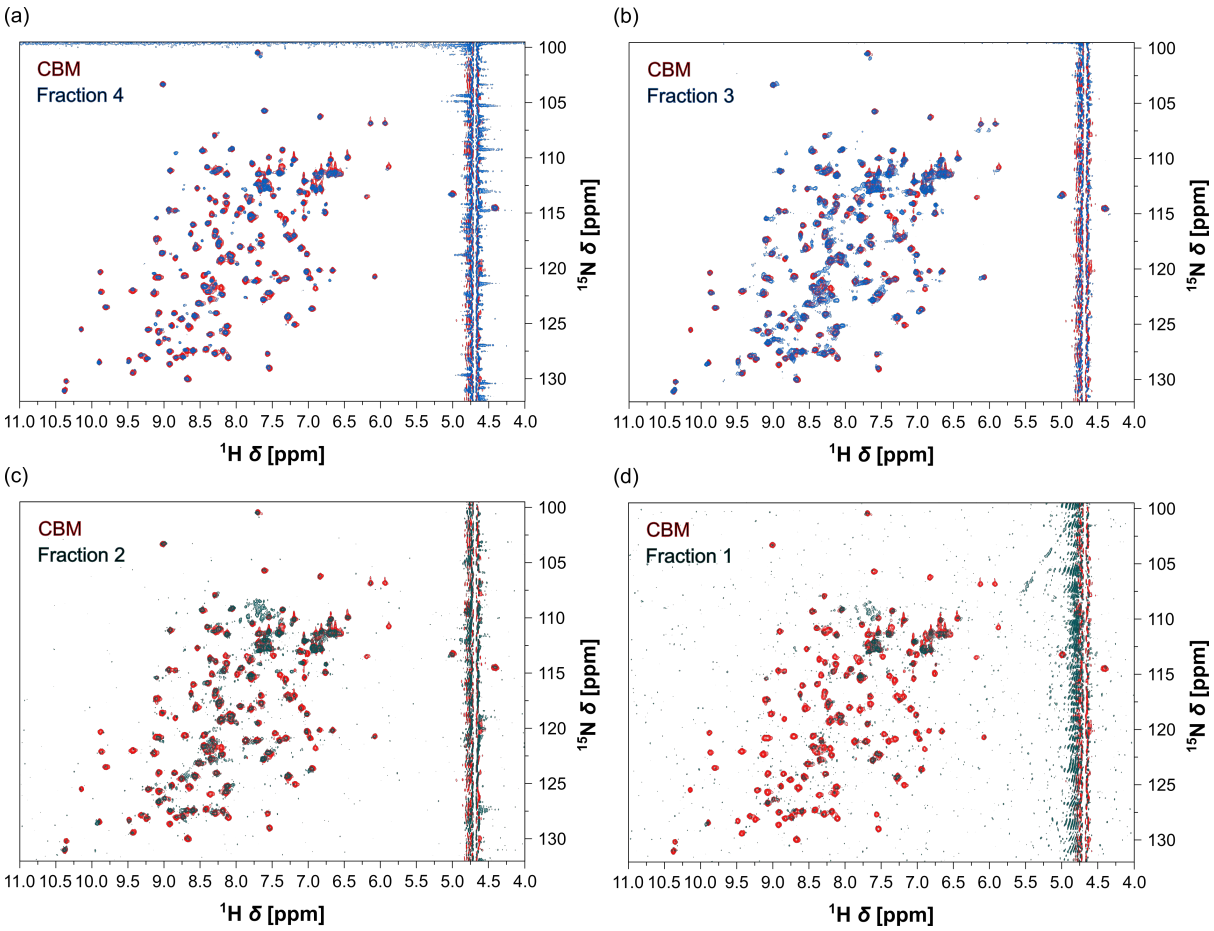


Figure 2.8: Corresponding $^{1}$H-$^{15}$N HSQC spectra of unmodified CBM (red) and fractions obtained by GFC of the crude reaction mixture after grafting-from by PET-RAFT polymerization. Fraction 4 can be correlated to unmodified CBM (a) and Fraction 3 to a mixture of unmodified CBM and CBM-macroCTA (b). Fraction 2 and fraction 1 correlate to protein-polymer conjugates with either one (c) or two polymer chains (d) grown from the protein surface.

In summary, modification of CBM with small initiating groups for RAFT and Cu(0)-mediated radical polymerization and subsequent in situ polymerization from the protein surface has a distinct impact on the protein structure, solubility and/or sample mobility. With increasing extent of modification, this effect seems to be more pronounced. It is imaginable that different factors play a part in contributing to the observed impact: the site and extent of modification as well as the chemical nature of immobilized groups at the protein surface.

**Chemical shift perturbation plots**: Spectra obtained from conjugates prepared by grafting-to as well as CBM-MI and CBM-macroCTA synthesized in buffer at pH 7.4 were analyzed in more detail to evaluate sites of modification and determine reactive lysine residues in the protein. Figure 2.9 shows the individual NMR signals corresponding to the 10 lysine residues in CBM of the reference spectrum

(red) and after modification (green for conjugate, blue for MI and macroCTA). It can be roughly evaluated, that for conjugation of the relatively large polymer chain to the protein surface, lysine residues K66 and K154 were preferred for modification. For better clarity it should be mentioned that modification can be assigned based on pronounced chemical shift perturbation either obtained for the signals corresponding directly to the functionalized lysine residues or other amino acid residues near the site of modification. Furthermore, new signals may arise from the newly formed amide bonds after conversion of the ε-amino groups. For conjugates, those new signals were ambiguously observed. More precisely, signal splitting for residues K142, K66 and Q145 was found rather than the rise of new signals. Overall, it can be assumed that polymer chains were attached to the protein or entangled around the protein directly at or near these mentioned residues. It should be mentioned that signals in the NMR spectra may overlap and do not reveal the exact site of modification as performed functionalization was not site-specific and a mixture of different structural isomers was probably obtained.

For CBM-MI, the highest number of chemical shift changes for lysine residues was observed, as expected from the degree of functionalization determined by MALDI-ToF mass spectrometry, namely ~ 5 functional CRP initiators attached per CBM. The most significant changes were found for K104 and K154, but also K56, K24, K107 and K149 showed significant changes in signal position. For CBM-macroCTA, the most significant change was again observed for K154. Here, extent of modification was found to be up to 2 CTA units per protein molecule.

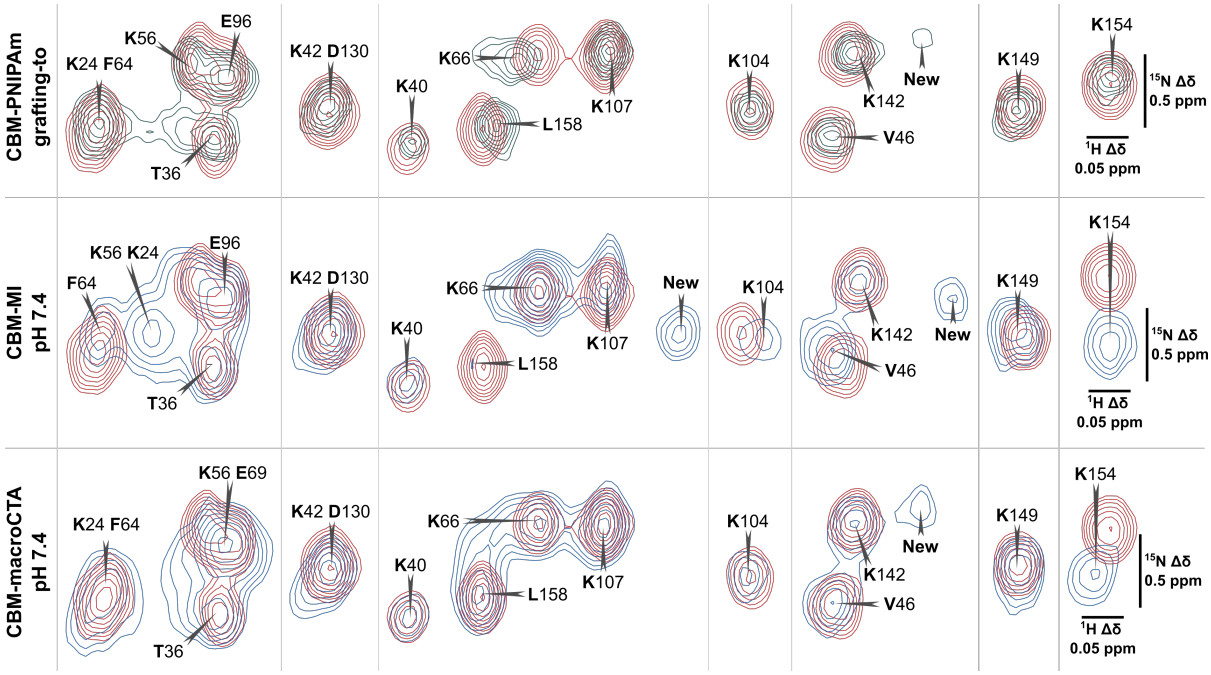


Figure 2.9. Excerpts of overlayed spectra derived for CBM-PNIPAm synthesized via grafting-to, CBM-MI and CBM-macroCTA showing all lysine related signals denoted alongside their numerical position in the protein structure. Unmodified CBM is represented in red.

For both samples, new signals have arisen (Figure 2.10). It can be seen that the intensity and number of new signals is higher for CBM-MI, which exhibits more attached groups, compared to CBM-macroCTA. These were not assigned to a specific amino acid. To do that, additional 2D and 3D NMR experiments would be needed. The corresponding image for CBM-oNIPAm prepared by grafting-to is not added but correlated strongly to the signals observed for CBM-macroCTA.

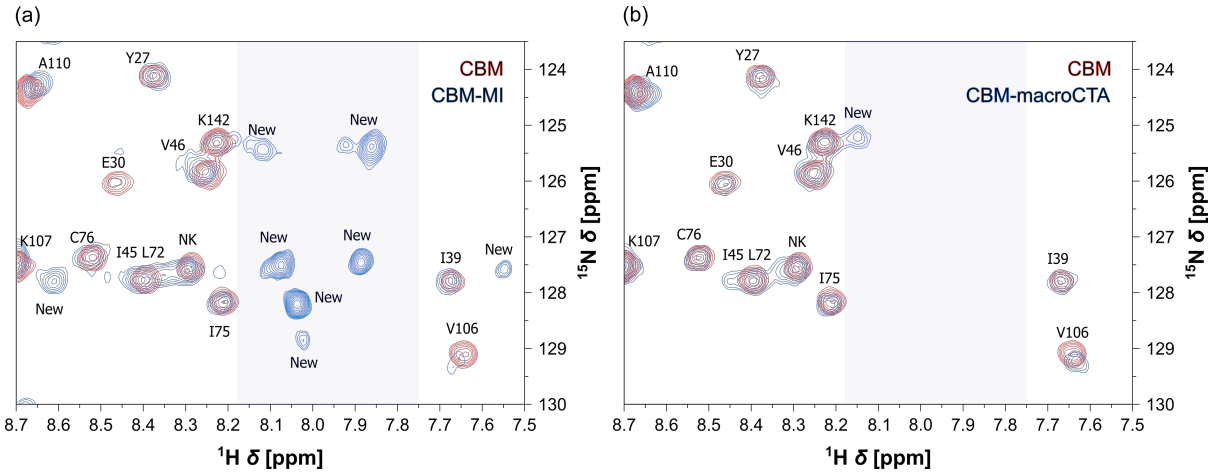


Figure 2.10: Position of new signals observed after modification with small CRP-initiators (a) or PEG-CTA units (b).

In summary, K154 showed the highest probability for modification with small initiator and CTA molecules whereas this residue seems not to be modified by the comparably large oligomeric NIPAm. While for large molecules, the site of conjugation depends highly on the accessibility of the lysine residue, the nucleophilic character and reactivity is a key parameter for modification with small molecules.[170] It is mentioned, that for the N-terminus, which is generally also accessible for conjugation and modification, no significant chemical shift changes were observed and that it was therefore concluded, that it remained unmodified in the presented studies. Indeed, solely observation of protein structure and orientation of lysine residues did not show a significant difference in steric demand. For better visualization, Figure 2.11 shows the CBM protein structure with the positions of the lysine residues highlighted in yellow (Figure 2.11 a) and excerpts showing the ball-and-stick representation of K154, K56 and K66 (Figure 2.11 b). It has to be mentioned, that the steric demand of adjacent amino acids has a considerable effect on the accessibility of amino acid side chains. For better clarity and to avoid an overcrowded picture, adjacent amino acid side chains are not included in Figure 2.11 b.

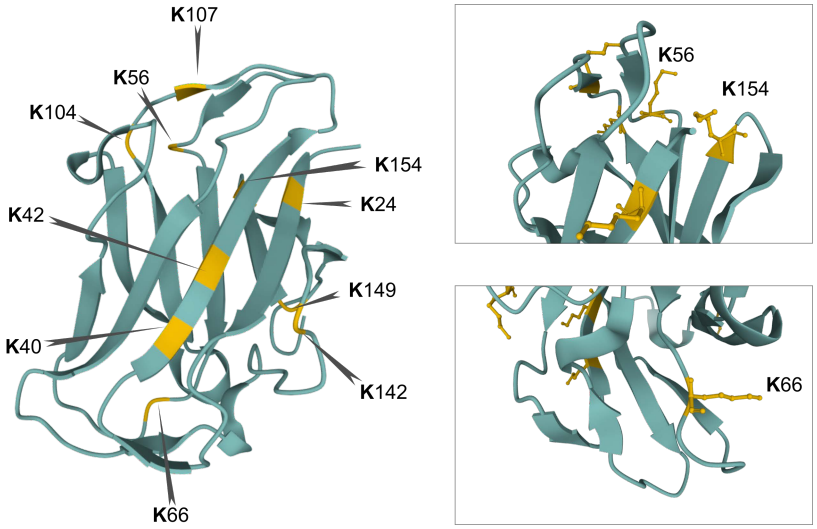


Figure 2.11: Cbh9A CBM3b$^{N126W}$ crystal structure (PDB entry 3ZQX)[151] with lysine residues highlighted in yellow (left). Excerpts to illustrate the accessibility of K56, K154 and K66 (right). Illustrations were generated using the Mol* web app.[23]

Last of all, plots of the chemical shift changes along the peptide sequence for CBM-MI (Figure 2.12 a), CBM-macroCTA (Figure 2.12 c) and CBM-PNIPAm obtained by grafting-to (Figure 2.12 b) were generated. In general, a higher impact of macroCTA and MI synthesis on protein structure is observed compared to grafting a polymer chain to the protein. Even though all are subject to the same reaction mechanism, namely modification of lysine ε-amine functionality with an active ester, the higher rate of modification by the small CRP initiators seems to already lead to a significant impact on chemical shifts. As a result of the chemical modification of lysine residues, chemical shifts of adjacent amino acids are altered as well and shift changes are induced. Taking a look at the chemical shift perturbation plot along the peptide sequence in Figure 2.12, most events after modification happen between β-strand 2 and 3 in addition to β-strands 8 and 9 for all samples. The corresponding region in the protein structure is highlighted in Figure 2.12 d.

Modification seems to exclusively happen at this site of the protein based on the performed measurements. Further investigations are needed, to specifically describe the mode of modification and resulting preference of the highlighted areas in the protein structure. For example, a CBM mutant with different blocked lysine residues could be designed to probe the reactivity for modification with small initiators, CTA units or polymer chains.

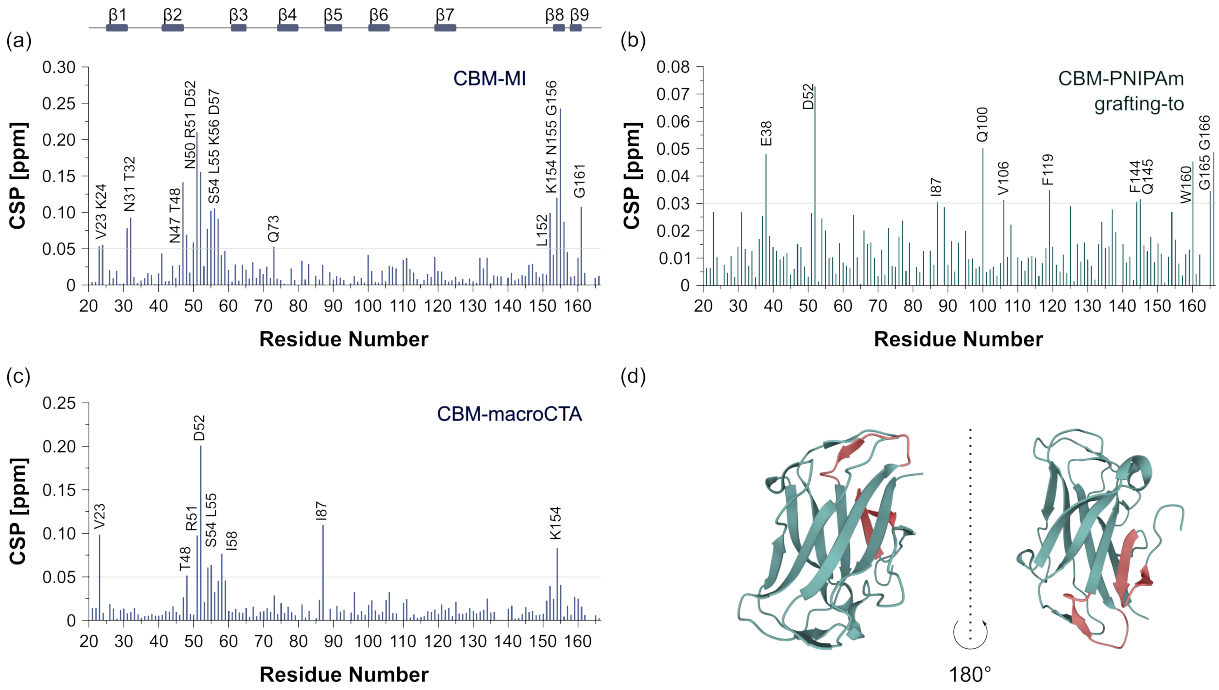


Figure 2.12: Chemical shift perturbation of CBM-MI (a), CBM-macroCTA (c) and CBM-PNIPAm conjugate prepared by grafting-to using a PFP-functionalized oligomeric polymer chain (b). Site of action as determined by the plots is marked in the Cbh9A CBM3b$^{N126W}$ protein structure (d) (PDB entry 3ZQX).[151] Illustrations were generated using the Mol* web app.[23]

## 2.4 Conclusion and Outlook

The aim of this work was to broaden the current knowledge in the field of protein modification by either grafting a polymer from or to the protein surface. So far, few researchers have focused on the structural characterization of conjugates by advanced technique to probe the three-dimensional structure. Protein NMR spectroscopy can be used as alternative to protein crystallization to probe structural integrity at atomic level. Until now, this methodology has only been applied to conjugates obtained by grafting-to and it was assumed that grafting-from similarly does not have a detrimental effect on the protein. However, the results shown in this chapter demonstrate that grafting-from and grafting-to the model protein CBM lead to significant differences in the protein structure. Likewise PEGylation, PNIPAm that was grafted to CBM has nearly no influence on the protein structure. However, already the attachment of functional initiators or CTAs, commonly used for grafting-from, alter the CBM structure significantly. Unlike other research carried out in this area, the found results strongly suggest a negative effect on protein structural integrity after modification with grafting-from. This effect is aggravated with increasing degree of modification and proceeding polymerization.

Ongoing work should cover the determination of the cellulose binding efficiency as intrinsic functionality of Cbh9A CBM3b$^{N126W}$ in comparison for different conjugates and unmodified protein. Proposed cellulose-binding residues are Y77, Y78 and W126 located in the β4-strand of the protein.

This binding site is opposite to the region highlighted in Figure 2.12. If possible, similar experiments should be carried out with a second reference protein as protein stability depends on various factors and results obtained for CBM may not display a general behavior of all proteins.

In an ongoing project, the influence of protein modification by a new site-specific grafting-to strategy is investigated. There, sortase A, an enzyme able to covalently ligate specific peptide sequences, is used to attach end-group functionalized polymers to either the C- or N-terminus of engineered CBM. As the ligation site is predefined, the impact of different polymer types on the protein structure can be more easily compared. This project is currently performed in cooperation between Johannes MARTIN, Marcus MICHAELIS, Prof. Dr. Heiko MÖLLER and Dr. Ulrich GLEBE.

## 2.5 Experimental Part

**Materials:** All materials were received as stated and used as received unless otherwise noted. Deuterated solvents $CDCl_3$ and $D_2O$ were obtained from Deutero. Tris-[2-(dimethylamino)ethyl]amine ($Me_6$TREN, 99+ %) was purchased from Fisher Scientific. *N*-Isopropylacrylamide (NIPAm, > 98 %) was purchased from Tokyo Chemical Industry (TCI) and purified by recrystallization from ethanol. Tetrabromofluorescein (eosin Y, > 95 %) and triethylene glycolmonomethyl ether (> 98 %) were purchased from TCI and used without further purification. CuBr (> 99 %) was purchased from Sigma-Aldrich and purified by stirring in glacial acetic acid overnight, filtered, washed with ethanol and diethyl ether and dried in vacuo. Azobisisobutyronitrile (AIBN, 98 %) was purchased from Sigma-Aldrich and purified by recrystallization in methanol and stored at 4 °C. 4,4'-Azobis(4-cyanovaleric acid) (ABCVA, ≥ 75 %), *N*,*N*,*N*′,*N*″,*N*″-pentamethyldiethylenetriamine (PMDETA, 99 %), α-bromoisobutyric acid (BiBa, 98 %), *N*-hydroxysuccinimide (NHS, 98 %) and 1-butanethiol (99 %) were used from Sigma-Aldrich as received. *N,N*′-Diisopropylcarbodiimide (DIC, 98 %) and pentafluorophenol (PFP, 98 %) were purchased from Carbolution Chemicals. Super-DHB as matrix substance for MALDI-MS (≥ 99 %) was used from Fluka. 4-Dimethylaminopyridine (DMAP, ≥ 99 %) and thiourea (≥ 99 %) were purchased from Roth. Carbon disulfide (99+ %) was purchased from Alfa Aesar. Bovine serum albumin fraction V (BSA) was purchased from Roth (≥ 98 %). CBM was provided by Marcus Michaelis (University of Potsdam) according to an established procedure.[176] Phosphate buffer refers to a buffer containing 10 mM sodium phosphate and 30 mM NaCl, pH 7.4. Stock solutions of buffers were designed to adjust the buffer to the corresponding pH when diluted with protein solution for modification with functional CRP initiator or NHS-PEG-CTA (buffer composition for 0.1 M multiplied by 2). Buffers were made using ultrapure water (Milli-Q®) with a resistivity of 18.2 MΩ·cm at 25 °C. Dialysis tubing cellulose membrane with a molecular weight cut-off (MWCO) 3.5 kDa was purchased from Sigma-Aldrich. *N*-2-Bromo-2-methylpropanoyl-β-alanine *N*'-oxysuccinimide ester (functional

CRP initiator) was synthesized according to reference [175]. 2-(Butylthiocarbonothioylthio)-2-methylpropionic acid (BTMP) and PFP-BTMP as RAFT CTA were synthesized according to literature procedures.[105,177] Thiol containing starting material for PEG-CTA synthesis was obtained starting from triethylene glycolmonomethyl ether following a procedure presented by FOOS et al.[178]

**Instrumentation:**

**$^{1}$H NMR and $^{19}$F NMR** spectra of the intermediates and final polymers were recorded at 25 °C at 400 MHz on a Bruker AVANCE NEO 400 spectrometer. Chemical shifts δ are given in ppm referring to the respective solvent peak at δ ($^{1}$H) 7.26 ppm for $CDCl_3$ or δ ($^{1}$H) 4.79 ppm for $D_2O$. **Protein NMR** data were collected on a Bruker AVANCE III 600 spectrometer. Since all samples were measured in aqueous buffers, $D_2O$ was added to each sample to a final concentration of 5 % (vol.) for the field lock. Chemical shifts were referenced to internal 4,4-dimethyl-4-silapentane-1-sulfonic acid (DSS) at 0.0 ppm. **UV–Vis** absorption spectra were recorded on a SPECORD 210 (Analytik Jena) spectrometer using 1 cm pathlength disposable cuvettes. Temperature-dependent **turbidimetry measurements** were performed with a Cary 5000 (Varian) spectrometer with heating rate of 0.5 $K \cdot min^{-1}$ and data acquisition every 0.2 K (temperatures are precise within 0.5 K). Sample concentration was adjusted to 1 $mg \cdot mL^{-1}$ for each measurement. **Size exclusion chromatography** (SEC) measurements were obtained using either THF or NMP + 0.5% LiBr as mobile phase with simultaneous UV and RI detection at 25 °C and a flow rate of 0.5 $mL \cdot min^{-1}$. The stationary phase used was a 300 × 8 $mm^2$ PSS SDV-Linear-M (3 µm particle size) column for THF and a 300 × 8 $mm^2$ PSS GRAM-Linear (3 µm particle size) column for NMP. Samples were filtered through 0.45 µm filters and the injected volume was 100 µL. Narrowly distributed polystyrene standards (PSS, Mainz, Germany) were used for calibration. **Sodium dodecyl sulfate-polyacrylamide gel electrophoresis** (SDS-PAGE) was performed with a 4-20% polyacrylamide gradient gel, using the Mini-PROTEAN Tetra Cell from Bio-Rad and Roti®-Mark TRICOLOR XTRA was applied as standard protein ladder. Protein samples were treated with a denaturing buffer and heated to 85 °C for 10 mins prior to use. Bands were visualized using a standard silver-staining or Coomassie blue staining protocol. **Matrix-assisted laser desorption/ionization time-of-light mass spectra** (MALDI-ToF) were acquired using a 337 nm Bruker microflex MALDI-ToF spectrometer with pulsed ion extraction. Masses were determined in positive ion reversed mode. Sample solutions were applied on a ground steel target using the dried droplet technique. Either Millipore ZipTipC4 pipette tips were used (unmodified protein samples) or the sample applied on the target first and the matrix solution on top after evaporation of the solvent. In all cases, a volume of 0.5 µl was applied on the target. Super-DHB, a 9:1 mixture of 2,5 dihydroxybenzoic acid (DHB) and 2-hydroxy-5-methoxybenzoic acid, was used as matrix substance in a 50 mg/ml solution in Milli-Q water:acetonitrile 1:1 with 0.1 % trifluoroacetic acid. Mass calibration was performed with external calibration.

**Procedures:**

**2-(Butylthiocarbonothioylthio)-2-methylpropionic acid (BTMP)** was synthesized according to a procedure adapted from MONTEIRO et al.[177] To a stirred suspension of $K_3PO_4$ (33.2 g, 156 mmol, 1.0 equiv.) in acetone (260 mL), 1-butanethiol (13.44 g, 16 mL, 149 mmol, 2.1 equiv.) was added and stirred for 30 min. Carbon disulfide (22.9 g, 18.2 mL, 300 mmol, 4.3 equiv.) was added dropwise and the reaction mixture turned yellow immediately. After 45 min, α-bromoisobutyric acid (11.7 g, 70 mmol, 1.0 equiv.) was added in one portion and the reaction mixture stirred for further 2 hours. Afterwards, the solution was filtered (Whatman grade 2), the solvent removed under reduced pressure and the resulting oil stirred in 5% HCl overnight. The formed precipitate was filtered and the obtained solid purified by column chromatography (silica gel, *n*-hexane/ethyl acetate, 4:1) to yield the product as bright yellow solid after removal of solvents in vacuo (7.5 g, 29.7 mmol, 42%).

**$^1$H NMR** (400 MHz, $D_1$-chloroform) δ: 3.32 – 3.24 (m, 2H, -SC$H_2$), 1.72 (s, 6H, -SC(C$H_3$)), 1.70 – 1.61 (m, 2H, -SC$H_2$C$H_2$), 1.42 (dq, *J* = 14.6, 7.3 Hz, 2H, -C$H_2$C$H_3$), 0.93 (t, *J* = 7.3 Hz, 3H, -C$H_2$C$H_3$) ppm.

**Pentafluorophenyl (PFP) BTMP** was synthesized according to a procedure described by DE GEEST et al.[105] BTMP (2.52 g, 10 mmol, 1 equiv.), PFP-OH (2.054 g, 11 mmol, 1.1 equiv.) and DMAP (122 mg, 1 mmol, 0.1 equiv.) were introduced in a round bottom flask and dissolved in 100 mL $CH_2Cl_2$. The reaction mixture was cooled in an ice bath and DIC (1.288 g, 1.7 mL, 11 mmol, 1.1 equiv.) added dropwise while vigorously stirring. The reaction mixture was stirred overnight in the thawing. The solvent was removed under reduced pressure and the crude product purified by column chromatography (silica gel, $CH_2Cl_2$). The first fraction was collected, the solvent removed, and the product obtained as an orange oil (2.83 g, 6.7 mmol, 67%).

**$^1$H NMR** (400 MHz, $D_1$-chloroform): δ = 3.36 – 3.29 (m, 2H, -SC$H_2$), 1.86 (s, 6H, -SC(C$H_3$)$_2$), 1.74 – 1.62 (m, 2H, -SC$H_2$-C$H_2$), 1.43 (dq, *J* = 14.6 Hz, 7.3 Hz, 2H, -C$H_2$C$H_3$), 0.97 – 0.88 (m, 3H, -C$H_2$C$H_3$) ppm.

**$^{19}$F NMR** (376 MHz, $D_1$-chloroform): δ = -151.48 – 151.64 (m, 2F, Ar-$F_{ortho}$), -155.75 (t, *J* = 21.9 Hz, 1F, Ar-$F_{para}$), -162.27 – 162.45 (m, 2F, Ar-$F_{meta}$) ppm.

The spectra are in accordance with literature data.[105]

**RAFT Polymerization of NIPAm:** The functionalized PFP-BTMP was used for the RAFT polymerization of NIPAm in unstabilized dioxane (monomer concentration 2 M) at 70 °C using ABCVA as initiator. Ratios of [NIPAm]:[CTA]:[ABCVA] of [200]:[1]:[0.1] or [20]:[1]:[0.1] were chosen for the polymeric and oligomeric product, respectively. All components were introduced to a

Schlenk tube, deoxygenated by three freeze-pump-thaw cycles, and transferred to a preheated oil bath at 70 °C. The polymerization was stopped after 2.5 h by immersing the flask in an ice bath. The polymer was precipitated in cold diethyl ether whereas the oligomeric NIPAm was purified by column chromatography (silica gel, $CH_2Cl_2$/MeOH, 8:2). The final protein-reactive polymer and oligomer were dried in vacuo and characterized by NMR spectroscopy, SEC and turbidimetry.

**Table 2.4: Characterization of oNIPAm and PNIPAm by NMR spectroscopy, SEC and turbidimetry.**

| Sample | DP | Conv.[a] | $M_{n,theor}$[a] [g·mol$^{-1}$] | $M_{n,SEC}$ [g·mol$^{-1}$] | $M_{w,SEC}$ [g·mol$^{-1}$] | Đ | $T_{CP}$ [°C] |
|---|---|---|---|---|---|---|---|
| oNIPAm | 20 | 93 % | 2 523 | 2 586 | 2 880 | 1.11 | 22.6 |
| PNIPAm | 200 | 90 % | 20 787 | 17 600 | 20 256 | 1.15 | 35.5 |

[a] According to NMR spectra of the crude reaction mixtures.

**Conjugation of protein-reactive polymer to CBM:** A solution of native CBM (10 mg, 0.59 µmol, 5.93 µmol accessible lysine residues, 1 equiv.) in 10 mL phosphate buffer was diluted with 10 mL 0.2 M sodium bicarbonate stock solution to adjust the pH to 8.2. A 25-times excess referred to CBM of oligomeric NIPAm (DP = 20) or polymeric NIPAm (DP = 200) dissolved in 200 µL DMSO (DMSO concentration in CBM solution < 1 vol%) was added and stirred at 4 °C overnight. Afterwards, the solution was centrifuged (7500xg for 10 min) and the supernatant passed through a 0.2 µm PVDF sterile syringe filter to get rid of undissolved side products. To get rid of pentafluorophenol as side product of conjugation, the reaction mixture was dialyzed (MWCO 3.5 kDa) against phosphate buffer for 5 days with water exchange every 24 h.

**PEG-CTA** was synthesized by combining two literature procedures.[177,178]

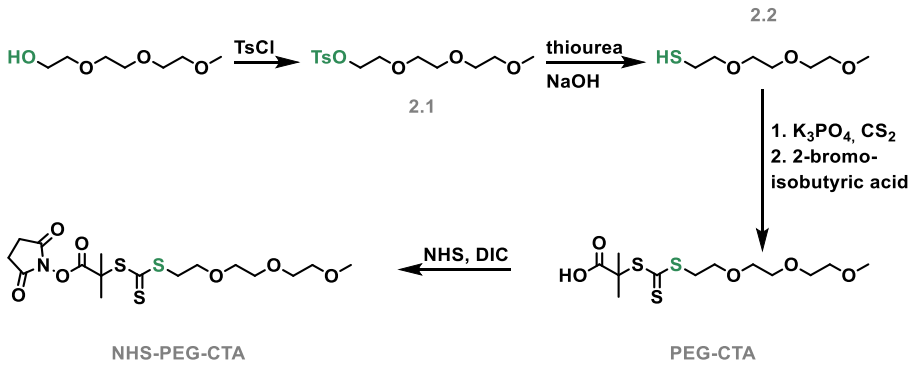


Scheme 2.3: Synthesis of NHS-PEG-CTA starting from triethylene glycol monomethyl ether.

Sodium hydroxide (7.15 g, 180 mmol, 1.8 equiv.) dissolved in 25 mL distilled water and triethylene glycol monomethyl ether (16.6 g, 100 mmol, 1 equiv.) dissolved in 25 mL THF were placed in a round bottom flask and cooled with an ice bath. A solution of 4-toluenesulfonyl chloride (19.1 g, 12.9 mL, 100 mmol, 1 equiv.) in 30 mL THF was added dropwise under nitrogen atmosphere. The mixture was stirred overnight at room temperature and then extracted 2-times with diethyl ether. The organic phase

was washed with water, dried with sodium sulphate, filtered and the solvent evaporated under reduced pressure without heating. The product **2.1** was obtained as colorless liquid (27.2 g, 86 mmol, 86 %).

A solution of **2.1** (13.5 g, 42.5 mmol, 1 equiv.) in 25 mL ethanol abs. was placed in a two-neck round bottom flask equipped with a reflux condenser. Thiourea (3.25 g, 42.5 mmol, 1 equiv.) in 17 mL water was added and the mixture heated to reflux for 2.5 h. Then, a solution of sodium hydroxide (2.05 g, 51 mmol, 1.2 equiv.) in 12.5 mL water was added and reflux continued for further 1.75 h. After concentration in vacuo, fresh water was added and pH adjusted with aq. hydrochloric acid to neutral pH and the solution extracted with $CH_2Cl_2$. The organic phase was dried with sodium sulphate, filtered and the solvent removed in vacuo to yield the product **2.2** as colorless liquid (7.0 g, 38.8 mmol, 91 %).

Thiol compound **2.2** (3.5 g, 19.4 mmol, 1.5 equiv.) and potassium phosphate (4.7 g, 22 mmol, 1.7 equiv.) were placed in a round-bottom flask along with 70 mL acetone and stirred for 30 min. Carbon disulfide (2.96 g, 2.35 mL, 38.8 mmol, 3 equiv.) was added in one portion and stirring continued for 45 min. Then, α-bromoisobutyric acid (2.16 g, 12.9 mmol, 1 equiv.) was added in one portion and the reaction mixture stirred overnight. Formed potassium bromide was filtered off, solvent removed under reduced pressure and crude mixture purified by column chromatography (silica gel, gradient $CH_2Cl_2$/EtOH, 97:3 to 8:2). The second fraction was collected and solvent removed to obtain the product **PEG-CTA** as orange liquid (2.74 g, 8 mmol, 62 %).

**$^1$H NMR** (400 MHz, chloroform-$d_1$) δ = 3.73 (t, *J* = 6.3 Hz, 2H, -S-C*H*$_2$-CH$_2$-), 3.67 – 3.60 (m, 6H, -C*H*$_2$-O-C*H*$_2$-C*H*$_2$-O-), 3.58 – 3.51 (m, 4H, -C*H*$_2$-C*H*$_2$-O-CH$_3$), 3.38 (s, 3H, -CH$_2$-O-C*H*$_3$), 1.86 (s, 6H, 2 -C*H*$_3$) ppm.

**PEG-CTA was functionalized with NHS** according to a protocol reported by DE GEEST et al.[105] PEG-CTA (820 mg, 2.4 mmol, 1 equiv.) and *N*-hydroxysuccinimide (276 mg, 2.4 mmol, 1 equiv.) were placed in a round-bottom flask and dissolved in 20 mL $CH_2Cl_2$ and cooled with an ice bath. *N*,*N*'-Diisopropylcarbodiimide (302 mg, 377 µL, 2.4 mmol, 1 equiv.) in 4 mL $CH_2Cl_2$ was added dropwise while vigorously stirring. After stirring overnight, the mixture was filtered and purified by column chromatography (silica gel, $CH_2Cl_2$/acetonitrile, 9:1). Solvent was removed under reduced pressure and the product **NHS-PEG-CTA** obtained as orange oil (865 mg, 2.0 mmol, 82 %).

**$^1$H NMR** (400 MHz, chloroform-$d_1$) δ = 3.73 (t, *J* = 6.3 Hz, 2H, -S-C*H*$_2$-CH$_2$-), 3.66 – 3.60 (m, 6H, C*H*$_2$-O-C*H*$_2$-C*H*$_2$-O-), 3.57 – 3.52 (m, 4H, -C*H*$_2$-C*H*$_2$-O-CH$_3$), 3.38 (s, 3H, -CH$_2$-O-C*H*$_3$), 2.80 (s, *J* = 31.1 Hz, 4H, NHS unit), 1.86 (s, 6H, 2 -C*H*$_3$ ) ppm.

**Polymerization from PEG-CTA** was accomplished using a modified procedure described by SUMERLIN et al.[92] Polymerizations were conducted using a commercially available blue LED light strip (www.longlife-led.de, serial number 1596, 2.95 m, 4.8 $W \cdot m^{-1}$, 82 $lm \cdot W^{-1}$, 1160 lm, SMD 3528, beam angle 120°) wound inside a parcel box. In a typical experiment, PEG-CTA (3 mg, 8.8 µmol, 1 equiv.), NIPAm (19.8 mg, 175.2 µmol, 20 equiv.), eosin Y (0.57 mg, 0.88 µmol, 0.1 equiv.), and PMDETA (1.8 µL, 8.8 µmol, 1 equiv.) were dissolved in 17.5 mL 10 mM phosphate buffer in $D_2O$, pH 7.4, transferred to a syringe equipped with a magnetic stirring bar, the tip sealed with a small septum and purged with $N_2$ for 20 min. Polymerization was initiated by irradiation with blue light (LED strip) and conversion monitored by NMR spectroscopy. Reaction was quenched after 6 h (92 % conversion) by turning off the light and exposure to air. After lyophilization, the crude reaction mixture was washed with *n*-hexane to get rid of unreacted starting material. The final polymer was characterized by SEC.

**Polymerization from BiBa** was performed using two modified methods from HADDLETON et al.[90,100] Procedure I: In a typical experiment, CuBr (4.0 mg, 28.1 µmol, 1.25 equiv.) was placed in a syringe along with a magnetic stirring bar. A solution of $Me_6$TREN (4.7 µL, 28.1 µmol, 1.25 equiv.) in 1.48 mL 10 mM phosphate buffer were added and headspace eliminated. The solution was left for disproportionation at 4 °C under rapid stirring for 15 min. Then, a solution containing initiator (3.75 mg, 22.5 µmol, 1 equiv.) and NIPAm (51 mg, 450 µmol, 20 equiv.) in 7.5 mL phosphate buffer were added to the syringe and polymerized for 1 h at 4 °C under rapid stirring. An upright position of the syringe to ensure proper mixing of copper particles in the time course of the polymerization was found to be important. Afterwards, the solution was passed through a 0.2 µm PVDF syringe filter to remove solid copper particles, conversion determined by NMR spectroscopy and residual reaction solution dialyzed using an appropriate dialysis tubing against Milli-Q water for 3 days. The final polymers were analyzed by SEC. Here, ratios between CuBr, $Me_6$TREN, initiator and monomer were kept at [1.25]:[1.25]:[1]:[monomer] and initiator concentration fixed to 2.5 mM. CuBr concentration during disproportionation was set to 18.8 mM. Procedure II: Here, initiator concentration was fixed at 0.45 mM, CuBr concentration at 3.5 mM during polymerization and 24.8 mM during disproportionation and catalyst/ligand ratio was set to [1]:[1]. Monomer concentration was varied depending on the targeted degree of polymerization. Method is analogous to procedure I.

**Synthesis of CBM-MI and CBM-macroCTA** was performed using the standard procedure established in the BÖKER group. A solution of native CBM (10 mg, 0.59 µmol, 5.93 µmol accessible lysine residues, 1 equiv.) in 5 mL phosphate buffer was diluted with 5 mL 0.2 M sodium bicarbonate stock solution or 0.2 M phosphate buffer to adjust the pH to 8.2 or 7.4, respectively. Functional CRP initiator (5.0 mg, 14.9 µmol, 2.5 equiv., as solid) or NHS-PEG-CTA (6.5 mg, 14.9 µmol, 2.5 equiv., dissolved in 500 µL DMSO) was added to the protein solution and the reaction mixture stirred at 4 °C for 12 h. Afterwards, the solution was filtered through a 0.2 µm sterile PVDF syringe filter, transferred to a

3.5 kDa MWCO dialysis membrane and purified by 3-times dialysis against 10 mM phosphate buffer, 10 mM NaCl, pH 7.4.

**Preparation of CBM-PNIPAm conjugates by Cu(0)-mediated radical polymerization or metal-free PET-RAFT polymerization under visible light irradiation:** Procedures were similar to the previous described methods for polymerization in absence of protein. Ratios refer to the number of initiators/CTA units attached to the protein as determined by MALDI-ToF mass spectrometry.

For Cu(0)-mediated radical polymerization, procedure II as indicated above using the ratios stated in Table 2.3 entry 5 was used for polymerization from CBM-MI prepared at pH 7.4 bearing ~ 4–5 initiating groups per protein. In a typical experiment, CuBr (4.3 mg, 30.1 µmol, 7.5 equiv.) was placed in a syringe along with a magnetic stirring bar. A solution of $Me_6$TREN (8.0 µL, 30.1 µmol, 7.5 equiv.) in 1.21 mL 10 mM phosphate buffer was added and headspace eliminated. The solution was left for disproportionation at 4 °C under rapid stirring for 15 min. Then, a solution containing CBM-MI (13.5 mg, 0.8 µmol, 4.0 µmol attached initiating units, 1 equiv.) and NIPAm (9 mg, 80 µmol, 20 equiv.) in 7.5 mL phosphate buffer was added to the syringe and polymerized for 1 h at 4 °C under rapid stirring. Afterwards, the solution was filtered through a 0.2 µm sterile PVDF syringe filter, transferred to a 3.5 kDa MWCO dialysis membrane and purified by 3-times dialysis against 10 mM phosphate buffer, 10 mM NaCl, pH 7.4. For samples prepared according to procedure I, sacrificial initiator was added to the CBM-MI solution to reach a total concentration of 2.5 mM initiating units. Results obtained for this approach were similar to these shown in the Results and Discussion part and are therefore not added.

For PET-RAFT polymerization, the same procedure as stated above was used applying conditions as indicated in table Table 2.2 entry 14 starting from CBM-macroCTA prepared at pH 7.4 bearing ~ 1–2 CTA units per protein. In a typical experiment, CBM-macroCTA (8.5 mg, 0.5 µmol) in 8.5 mL phosphate buffer was mixed with sacrificial PEG-CTA (1.45 mg, 4.25 µmol) to reach a total amount of CTA units of 4.75 µmol. To this solution, NIPAm (10.7 mg, 94.9 µmol, 20 equiv.), eosin Y (0.31 mg, 0.48 µmol, 0.1 equiv.), and PMDETA (1.0 µL, 4.8 µmol, 1 equiv.) were added. The reaction mixture was transferred to a syringe equipped with a magnetic stirring bar, the tip sealed with a small septum and purged with $N_2$ for 20 min and the polymerization initiated by irradiation with blue light (LED strip). The reaction was quenched after 6 h by turning off the light and exposure to air. Afterwards, the solution was transferred to a 3.5 kDa MWCO dialysis membrane and purified by 3-times dialysis against 10 mM phosphate buffer, 10 mM NaCl, pH 7.4.

# 3 Characterization of Globular and β-Barrel Protein-Polymer Conjugates by SEC in-line with Multi-Angle Laser Light Scattering

**Cooperation:** Maria Mathieu-Gaedke (conjugate synthesis, analysis, interpretation), Dr. Jasmin Preis (SEC-MALS measurements, method development), Prof. Dr. Thorsten Hofe (conceptualization), Dr. Ulrich Glebe (conceptualization)

## 3.1 Abstract

To study the composition of biohybrid materials and to determine their molar mass is a main challenge in the field. The heterogeneity of protein-polymer conjugates, resulting from conjugation of a different number and length of the polymer chains, arises the need for advanced characterization methods to determine relevant information about the individual macromolecules. Two different methods, analytical ultracentrifugation and gel permeation chromatography in combination with a multi-angle laser light detector, were used to gain a deeper insight into bioconjugate hydrodynamics and accessibility of molar mass information of the sample.

Within this chapter, the usability of SEC-MALS for detailed characterization of hydrodynamic properties and calibration-free determination of conjugates molar masses is investigated. Conjugates were synthesized by grafting-from and grafting-to and analyzed in cooperation with Dr. Jasmin PREIS and Prof. Dr. Thorsten HOFE, scientist and co-founder, respectively, of the company PSS in Mainz. Bovine serum albumin (BSA) and ferric hydroxamate uptake protein component A (FhuA) were chosen as representatives of globular and membrane proteins and a variation of water-soluble polymers used. The aim was to establish a robust method to analyze protein-polymer conjugates and membrane proteins. The analysis by AUC is covered in the next chapter of this thesis.

## 3.2 Introduction and Theoretical Background

**Size exclusion chromatography (SEC)**, also referred to as gel permeation chromatography (GPC), is a chromatographic technique to separate and analyze sample components based on their size - or more precisely - by their Stokes radii. Therefore, the sample is dissolved in a respective solvent or buffer system called the mobile phase and passed through a column packed with porous beads, called the stationary phase. Partitioning by SEC is driven entirely by entropic processes and retention of analyte particles is defined by the intraparticle pore volume that is accessible to the analyte. Large analyte particles are excluded from the pores and elute first whereas small analyte particles are able to enter the pores in the stationary phase and are thus delayed on their way through the column. The process is visualized in Figure 3.1 for the separation of two particles of different sizes.[179–181] Favorably, separation occurs exclusively based on size differences and no other interactions between sample and the stationary phase.[179]

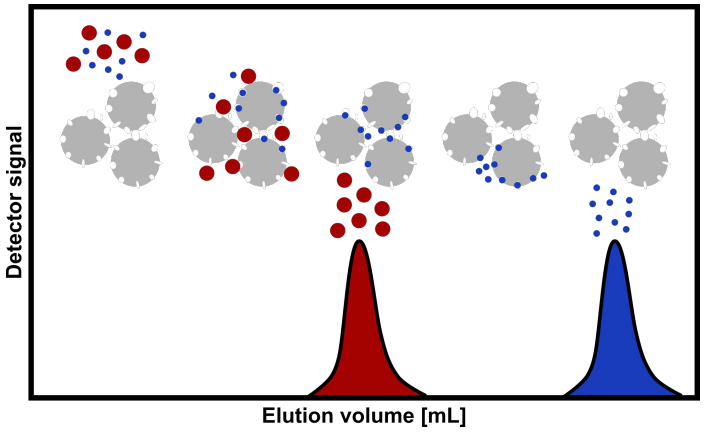


Figure 3.1: Principal concept of particle separation by size exclusion chromatography.

By SEC, composition, molar mass and mass distributions (dispersity) of analyte particles (of the individual components) in the sample can be estimated by their retention time. Therefore, the system is calibrated with standards of known molar masses. Comparison of the retention time or retention volume of the analyte to that of the standards gives access to the relevant information. However, analysis of molar masses by SEC relies on several key assumptions. First, the reference and the analyte share an overall similar conformation and specific volume and therefore the same relationship between diffusion properties and molar mass. Second, both do not interact with the column material in terms of adhesion, van-der-Waals and hydrophobic interactions. Consequently, if the analyte of interest is different in shape or compactness or interacts with the column material, retention might be influenced to a large extent and molar mass determination based on the reference becomes invalid.[180–183] SEC is widely used in the analysis of macromolecules, especially proteins and polymers. Depending on the intrachain interactions of the polymer or biomacromolecule, packing density might vary. As a result, for more loosely packed particles, molar mass estimation based on SEC is overestimated, whereas for small, tightly packed particles the molar mass is underestimated. Generally speaking, proteins vary in shape and their Stokes radii do not correlate directly with their molar mass.[180,182,183]

**Multi angle laser light scattering** (MALS) can provide information about the sample molar mass, conformation, macromolecule architecture and hydrodynamic properties based on basic physical considerations instead of external calibration. A MALS detector measures the proportion of light scattering by an analyte at multiple angles relative to the incident beam. This method relies on the Rayleigh theory which describes the elastic scattering of light and the correlation between molar mass and hydrodynamic radius based on Equation (3.1).[179,182,184]

$$M = \frac{R_0}{Kc\left(\frac{d_n}{d_c}\right)^2} \tag{3.1}$$

Here, molar mass $M$ is defined by the fraction of the reduced Rayleigh ratio – the amount of scattered light by the analyte relative to the laser intensity - extrapolated to angle zero $R_0$ and a term including the weight concentration of the particle in the sample mixture $c$, the refractive index increment $d_n/d_c$ and an optical constant $K$, which describes the characteristic parameters of the used system. In some sources, $R_0$ is also denoted as $\Delta LS$ and describes the light scattering as the excess of light scattered at a given angle $\theta$ by the solution containing the scattering particles.[182,184]

Data obtained at different known concentrations of the sample components can be used for generation of a Zimm plot. Here, intensity of scattered light as function of incident angles is used to derive hydrodynamic properties such as radius of gyration and molar mass.[179,185] Usually, $\frac{Kc}{R_\theta}$ is plotted against $\sin^2\frac{\theta}{2} + kc$. A stretch factor $k$ is needed to put the concentration in the same numerical order as the other factors. A representative Zimm plot is shown in Figure 3.2. It has to be mentioned, that this is just one method to analyze data obtained from MALS experiments.

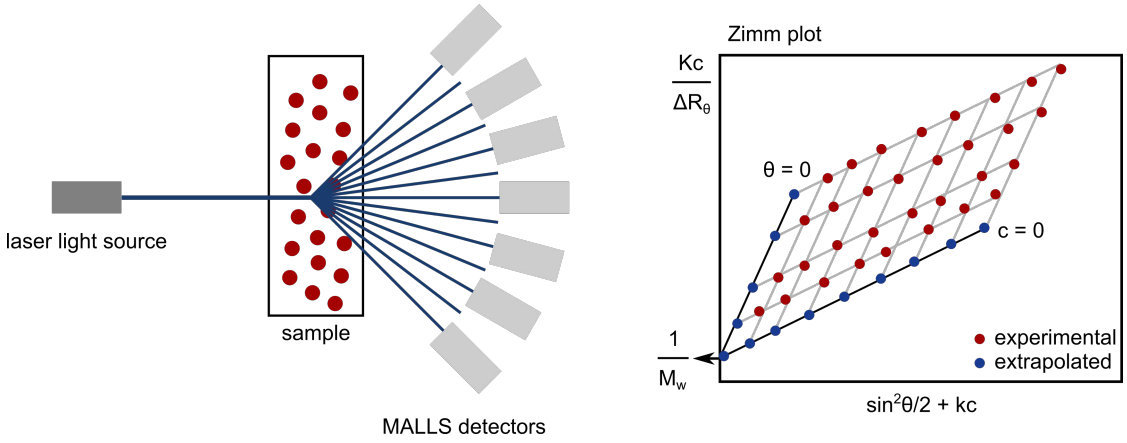


Figure 3.2: Illustration of a MALS experiment (left) and a typical Zimm plot (right). Extent of scattering of a laser beam by a sample is measured by detectors at different angles with respect to the incident beam. Plot of scattered light intensity as function of incident angle measured at different sample concentrations and extrapolation of the plot to zero angle and zero concentration yields the mean square radius of the macromolecules from the initial slope and the molar mass of the compound at the point where both concentration and angle equal zero. According to reference [186].

**Information** available by the combination of SEC and MALS are manifold ranging from purification, separation and analysis of individual components from a sample mixture, determination and quantification of oligomeric states, assessment of stoichiometry in complex systems to the evaluation of post-functionalization. By analysis of angular variation of scattering intensity, MALS can determine shape and size of macromolecules.[179,180,182] One major advantage of this technique is that mass calculation can be performed at any point of the elution chromatogram.

Furthermore, analysis of membrane proteins not accessible by other techniques might be accomplished. The intrinsic problem with membrane proteins is their arrangement in detergent micelles or association with stabilizing agents. This often results in overestimation of molar mass and misinterpretation of data as the parameters of the complex of membrane protein with its detergent or stabilizing agent is analyzed rather than the characteristics of the membrane protein alone.[182,187] Additionally, SEC-MALS is especially suited for heterogeneous sample as the sample is fractionated by the column chromatography prior to analysis with the MALS detector.[182] Therefore, it is an ideal candidate for the characterization of protein-polymer conjugates.

For **example**, association of membrane proteins in detergent complexes was studied by ALTEGOER et al. By analysis with SEC-MALS, the ratio of bound detergent per protein was determined. Additionally, information gained from SEC-MALS strongly indicated a formation of protein-detergent complexes rather than embedment of protein into detergent micelles.[188] Another study presented by BLOUNT and co-workers focused on determining the contribution of protein to the molar mass of protein-detergent complexes. In other words, the composition of complexes was determined and associated to the respective components, namely the protein and the detergent. The obtained results indicated a difference in oligomerization of SaMscL as target protein when solubilized by different detergents. These findings are relevant to understand quaternary structure stabilization in protein refolding and solubilization.[189]

Even though the use of SEC-MALS for characterization of protein-polymer conjugates is reported in literature, determination of molar mass of conjugates after grafting-from the protein sample is the mainly reported use. For example, CHILKOTI and co-workers demonstrated the analysis of myoglobin conjugates with different water soluble polymers.[159] Comparison of expected and experimentally determined molar masses provided solid proof of a controlled still facile copper(0)-mediated radical polymerization.

Until now, this methodology has only been applied on few samples and there is a lack in systematic characterization to proof or disproof the feasibility of this technique for the characterization of protein-polymer conjugates.

### 3.3 Results and Discussion

In this chapter, the question of conjugation efficiency and absolute molar mass determination of protein-polymer conjugates was tackled using SEC in combination with a MALS detector. Therefore, bovine serum albumin (BSA) as cost-effective, easily accessible and frequently used reference protein was modified with different water-soluble polymer materials by grafting-from and grafting-to. Additionally, FhuA as representative of the membrane protein family was functionalized as well and analyzed using a buffer system containing a stabilizing agent needed for membrane protein stabilization and solubilization.

**Theoretical considerations:** For analysis with MALS when coupled on-line to separation by SEC, quantitative recovery of the sample from each injection is necessary for accurate quantification of molar mass averages and distributions. As can be seen in Equation (3.1), the concentration directly affects the calculation of molar mass and loss of sample in the column would negatively affect the molar mass determination. Additionally, specific refractive index increments ($\partial n/\partial c$) of individual sample components are important variables for appropriate data analysis as defined by the Rayleigh Equation (3.1). Therefore, mass separation by SEC must occur exclusively based on size and not by interactions of sample with column material. Parameters which can be varied to achieve a successful separation in terms of SEC are the flow rate, column length, mass and volume load, the working range of the columns defined by the exclusion limit of the void volume, the column volume, column material and the mobile phase.[179–181,183]

For this purpose, different column materials, mobile phases and flow rates were screened for their applicability for size separation of protein-polymer conjugates. Furthermore, the focus was set to achieve a reliable separation method by SEC prior to further characterization with MALS. Within the next sections, only representative results are presented in terms of SEC chromatograms. Additional parameters used are summarized in tables or discussed in textual form.

**Synthesis of PNIPAm conjugates and analysis:** First, conjugates of both proteins, FhuA and BSA, with PNIPAm were prepared by grafting-from using the same methodology as described in Chapter 2.3. In a first step, proteins were modified with functional CRP initiators using a 5-times excess of NHS-activated initiator per lysine group present at the protein surface. To obtain nearly quantitative modification, reaction was performed at pH 8.2. Hence, 36 initiators are assumed for both proteins. Next, PNIPAm was grown from the protein-MI surface and different degrees of polymerization, namely 50, 100 and 200 repeating units, were targeted by varying the ratio of monomer per initiator group. Additionally, conjugates of BSA and PNIPAm prepared by grafting-to as described in Chapter 2.3 were synthesized. The same polymers, namely a PNIPAm with degree of polymerization ~ 200 and oligomeric oNIPAm with ~ 20 repeating units, were used for protein modification. Conjugates were analyzed by SDS-PAGE to verify conjugation and results presented in Figure 3.3. After modification, molar mass and surface properties of conjugates change which results in a reduced mobility within the SDS-PAGE gel. Broad and faded bands typical for protein-polymer conjugates were observed. Conjugates prepared by grafting-to contain approximately one polymer chain per protein and the band moved within the gel. In contrast, the conjugates obtained by grafting-from contain many polymer chains (up to 36 when assuming high initiation efficiency) and are mostly stuck at the top of the gel.

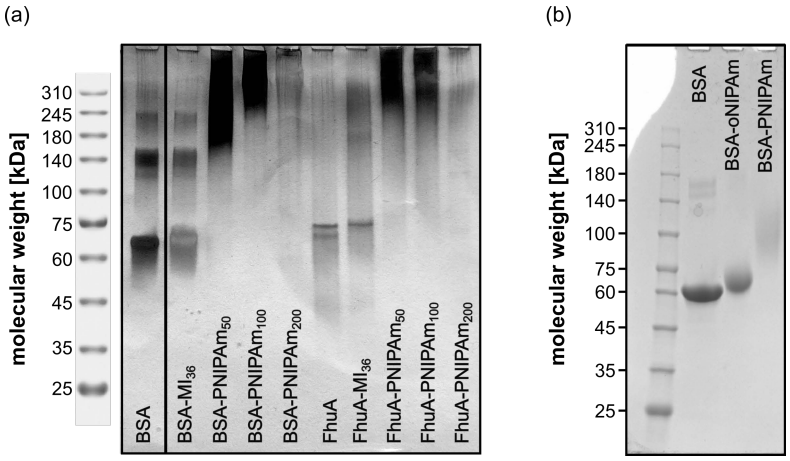


Figure 3.3: SDS-PAGE of conjugates prepared by grafting-from (a) and grafting-to (b) FhuA and BSA using PNIPAm as polymer. Degrees of polymerization are denoted in the subscript. For (a), protein ladder intensity was too low. Therefore, a reference ladder as provided from the manufacturer is shown. SDS PAGE cropped for clarity between sample BSA and BSA-$MI_{36}$. Additional bands observed for BSA correspond to protein dimers and trimers.

Afterwards, unmodified protein, protein-macroinitiator and conjugates were analyzed by SEC. Prior to analysis, samples were dialyzed to get rid of unreacted monomer (grafting-from) and other side products (grafting-to). In the first experiments, a PSS PROTEEMA column with bead size of 5 µm, porosity of 1000 Å and column dimension of 8x300 mm was used. The stationary phase in this column type consists of a specifically modified silicate material and is suited for protein samples ranging in molar mass between 1–7.5 kDa (based on protein calibration). The injection volume was set to 20 µL at a sample concentration of 1 mg·$mL^{-1}$. Even though the molar mass regime suggested for this column is not in correlation with expected molar masses of protein-polymer conjugates, hydrodynamic size defined by the porosity of stationary phase beads was estimated to be suited for these samples by my cooperation partners. The expected molar masses of macroinitiators and conjugates are summarized in Table 3.1. For conjugates prepared by grafting-from, a quantitative modification with small initiating groups and quantitative conversion during polymerization is assumed. This assumption is based on MALDI-ToF mass spectrometry performed by CHARAN[134] and NMR experiments following the conversion of polymerization over time. A mass increase per attached initiator of 220 Da and per monomer repeating unit of 113 Da was used for calculations. For both proteins, 36 addressable lysine residues are present at the protein surface.[134] Representative studies for the modification of BSA are shown in one of the following sections. For non-conjugated homopolymers of PNIPAm prepared by Cu(0)-mediated radical polymerization (Table 3.1, entries 13–15), molar mass based on conversion determined by NMR spectroscopy multiplied by 2 was used for estimation. The factor 2 accounts for the lower initiator efficiency as described and discussed in Chapter 2.3.

**Table 3.1: Expected molar masses of proteins, protein-macroinitiators and conjugates prepared by grafting-from and grafting-to.**

| # | Sample | Expected composition[a] [%] | | $M_{w,calc.}$[b] [Da] |
|---|---|---|---|---|
| | | Protein | Polymer | |
| **1** | **FhuA** | 100 | 0 | 78 853 |
| **2** | **FhuA-MI$_{36}$** | 100 | | 86 773 |
| **3** | **FhuA-PNIPAm$_{50}$** | 29.9 | 70.1 | 290 173 |
| **4** | **FhuA-PNIPAm$_{100}$** | 17.6 | 82.4 | 493 573 |
| **5** | **FhuA-PNIPAm$_{200}$** | 9.6 | 90.4 | 900 373 |
| **6** | **BSA** | 100 | | 66 463 |
| **7** | **BSA-MI$_{36}$** | 100 | | 74 383 |
| **8** | **BSA-PNIPAm$_{50}$** | 26.8 | 73.2 | 278 017 |
| **9** | **BSA-PNIPAm$_{100}$** | 15.4 | 84.6 | 481 651 |
| **10** | **BSA-PNIPAm$_{200}$** | 8.4 | 91.6 | 888 919 |
| **11** | **BSA-PNIPAm$_{200}$ grafting-to** | 76.2 | 23.8 | 87 250 |
| **12** | **BSA-PNIPAm$_{20}$ grafting-to** | 96.4 | 3.6 | 68 986 |
| **13** | **PNIPAm$_{50}$** | - | 100 | 11 650 |
| **14** | **PNIPAm$_{100}$** | - | 100 | 22 966 |
| **15** | **PNIPAm$_{200}$** | - | 100 | 45 598 |

[a] Percent of protein in conjugate by $M_{w,MI}/M_{w,conjugate}$ for conjugates prepared by grafting-from and $M_{w,Protein}/M_{w,}$conjugate for conjugates prepared by grafting-to. [b] Molar masses for conjugates prepared by grafting-from estimated based on expectable mass increase after initiator attachment as $M_{w,MI} = M_{w,protein} + (M_{w,initiator}\cdot$#modified lysine) and after polymerization as $M_{w,conjugate} = M_{w,MI} + (DP\cdot M_{w,monomer}\cdot$#modified lysine). Samples were prepared using Procedure II as stated in the Experimental Part of Chapter 2 for grafting-from protein-MIs.

Starting with the membrane protein FhuA, flow rate and buffer composition were varied between 0.5–1.0 mL·min$^{-1}$ and MPD content of 50–150 mM, respectively. 2-Methyl-2,4-pentandiol (MPD) is a stabilizing agent used for FhuA solubilization and stabilization. Despite classical detergents for membrane proteins, MPD does not block the protein surface leaving it available for protein surface modification.[132] More details about FhuA can be found in Chapter 5. MPD buffer in this Chapter is defined as a 10 mM phosphate buffer pH 7.4 with the denoted amount of MPD added. MPD is mixable with water in every ratio, can be considered as organic co-solvent and, thus, could affect the properties of the mobile phase. Exemplary chromatograms of FhuA, FhuA-MI and FhuA-PNIPAm conjugates are presented in Figure 3.4. Irrespective of flow rate and buffer composition, the elution volume was found to be ~ 9.75 mL for FhuA, ~ 9.25 mL for FhuA-MI and between 6–9 mL for conjugates, depending on the targeted degree of polymerization. Samples partially eluted near the exclusion volume of the column – defined by the void volume of the pores – indicating that the used column system is not suited for analysis of these samples and segregation corresponding to their hydrodynamic radii. Furthermore,

broad asymmetric elution bands were observed for all species, leading to the assumption of non-covalent interactions between the membrane protein and the column material. Additionally, an asymmetric peak shape was observed for all samples based on FhuA further supporting the theory of non-covalent and hydrophobic interactions of protein with the column material.

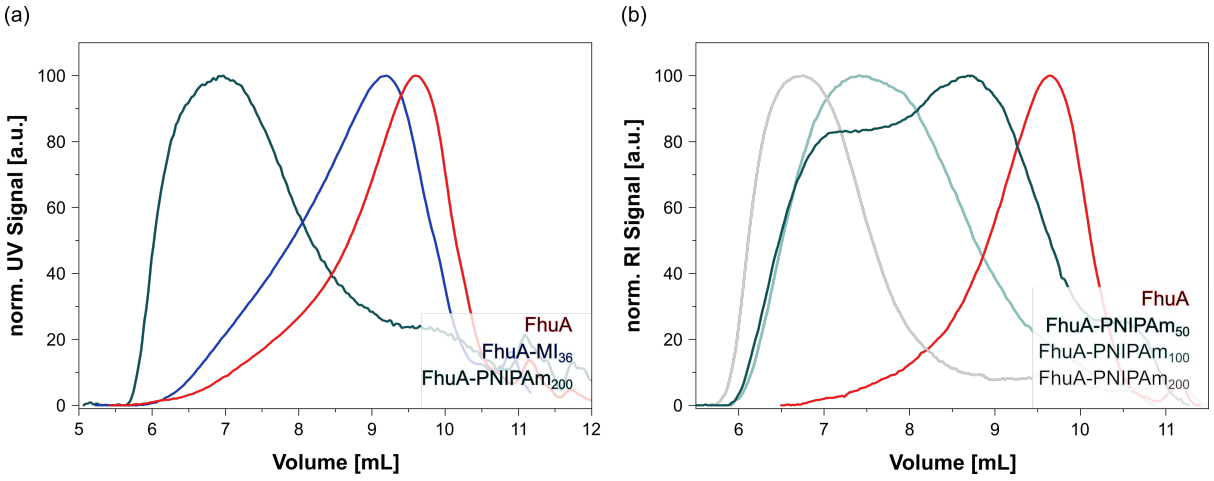


Figure 3.4: FhuA, FhuA-MI and FhuA-PNIPAm conjugates analyzed by SEC chromatography using a PSS PROTEEMA 5 µm column. Either a 50 mM MPD buffer as eluent and a flow rate of 0.5 mL·min$^{-1}$ (a) or 150 mM MPD buffer as eluent and a flow rate of 1.0 mL·min$^{-1}$ (b) was used. Temperature was fixed at 23 °C for all measurements.

The same conditions were applied to conjugates based on the globular protein BSA. Results are presented in Figure 3.5 for conjugates prepared by grafting-from (a), grafting-to (b) and PNIPAm (c) as reference analyte. In general, peak symmetries and molar mass distributions are narrower for BSA-derived materials compared to FhuA. For conjugates prepared by grafting-from, the elution volume decreased with increasing molar mass of the conjugates as required to achieve a successful separation by SEC based on molar mass and hydrodynamic radius. However, bimodal molar mass distributions – recognizable by the higher molar mass shoulder – were observed. It is conceivable that interactions between protein and conjugate with column material were not as pronounced as for FhuA samples, but still present. Furthermore, the severe increase in molar mass from 66.4 kDa for unmodified BSA to 74.4 kDa for BSA-MI and further to 278 kDa, 482 kDa and 889 kDa for the conjugates is not represented by the elution volume. Either the distance between BSA and BSA-MI is too large or the difference between MI and conjugates too small. It can be inferred that either BSA and BSA-MI or conjugates possess unspecified interactions with the column material.

For conjugates prepared by grafting-to, a mixture of different species is typically obtained. This reaction mixture is generally composed of unmodified protein, protein-polymer conjugate and unbound polymer used in excess to increase conjugation yield (detailed description can be found in Chapter 2.3). When the larger PNIPAm with a degree of polymerization of ~ 200 repeating units was used ($M_w$ ~ 20 kDa), a bimodal molar mass distribution resulting from the different species in the reaction mixture was

observed. The peak at ~ 11.3 mL can be attributed to unbound polymer whereas the peak at ~ 10.6 mL represents a mixture of unmodified protein and protein-polymer conjugates. Furthermore, conjugates based on the smaller polymer with ~ 20 repeating units ($M_w$ ~ 2.5 kDa), elute at the same volume as the conjugate based on the larger polymer with ~ 200 repeating units ($M_w$ ~ 20.8 kDa). For this sample, no additional elution band for unbound polymer is observed, probably due to the small size of the oligomeric macromolecule. It is mentioned that analysis of these samples with MALDI-ToF mass spectrometry revealed a mass increase of ~ 4.3 kDa after modification with oNIPAm and 20.4 kDa after modification with PNIPAm. This can be correlated to two oNIPAm chains attached per BSA molecule in contrast to one longer PNIPAm chain. Furthermore, unmodified BSA is visible in the MALDI-ToF spectrum after modification with the larger PNIPAm chain (spectra and detailed characterization can be found in Chapter 4.3, Figure 4.5). Overall, differences in molar masses upon conjugation did not result in the expected shift in elution volumes. Especially for conjugates based on the large polymer, a significant shift in elution volume to smaller values is expected. Instead, elution volumes of unmodified BSA, BSA-PNIPAm and BSA-oNIPAm were found to be 10.66 mL, 10.63 mL plus the additional peak for unconjugated polymer at 11.3 mL, and 10.61 mL, respectively.

Even though the homopolymer is considerably smaller in hydrodynamic size than the protein-based materials, the obtained elution volume was relatively large and differences between the samples relatively small. Even though peak symmetry for $PNIPAm_{200}$ is multimodal under the used conditions, change to DMSO/LiBr eluent led to a single, symmetrical peak (chromatograms not shown). Therefore, the unexpected elution behaviour demonstrated in Figure 3.5 can be accounted to non-covalent interactions of PNIPAm with the column material.

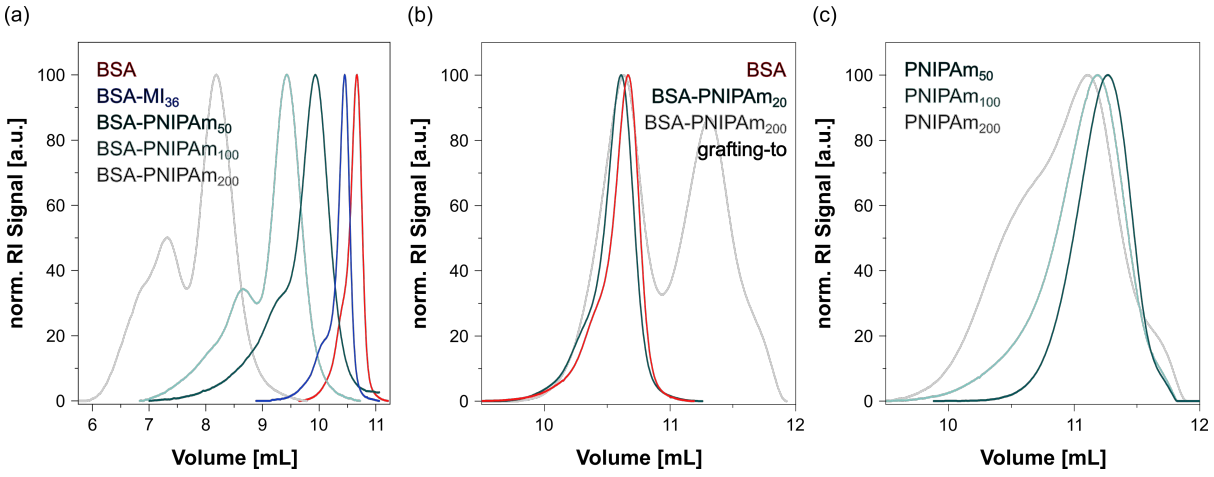


Figure 3.5: SEC chromatograms of BSA, BSA-MI and BSA-PNIPAm conjugates prepared by grafting-from (a) or grafting-to (b). Chromatograms of PNIPAm homopolymers are shown in (c). PSS PROTEEMA 5 µm column was used (eluent: 150 mM MPD buffer, flow rate: 0.5 mL·min$^{-1}$, temperature: 23 °C).

Next, a 50 vol% mixture of MPD buffer and DMSO was used with the aim to reduce interactions of samples with column material and suppress hydrophobic interactions of FhuA. It must be mentioned

that the samples used for all measurements were from the same batch. For unmodified BSA, a bimodal distribution profile was observed in contrast to the SEC experiments in pure MPD buffer. Contrary, unimodal and symmetrical peaks were obtained for BSA-MI and BSA-PNIPAm conjugates. This difference can be explained by the reduced stability of BSA in DMSO buffer mixtures leading to unfolding of the protein and increased hydrophobic interactions of the exposed hydrophobic core with the membrane material.[190] In contrast, conjugates generally experience an increased stability against co-solvents and it can be assumed that denaturation of conjugates is prevented by the polymer corona surrounding the protein.[77] Additionally, the elution volume was shifted to lower values for conjugates compared to the measurements in pure MPD buffer. Unfortunately, the higher the ratio of polymer, the lower the solubility of the conjugates in the new eluent system. As a result, BSA-PNIPAm$_{200}$ was not soluble and hence not analyzed by SEC. Nevertheless, the lower elution volume for the other two conjugates seems more realistic (see discussion above). For samples based on FhuA, no improvement was observed. Whereas conjugates seem to perform slightly better (narrower distribution profile), unmodified protein and macroinitiator showed enhanced interactions with column material. Therefore, this eluent in combination with the chosen column was not suited for further investigations.

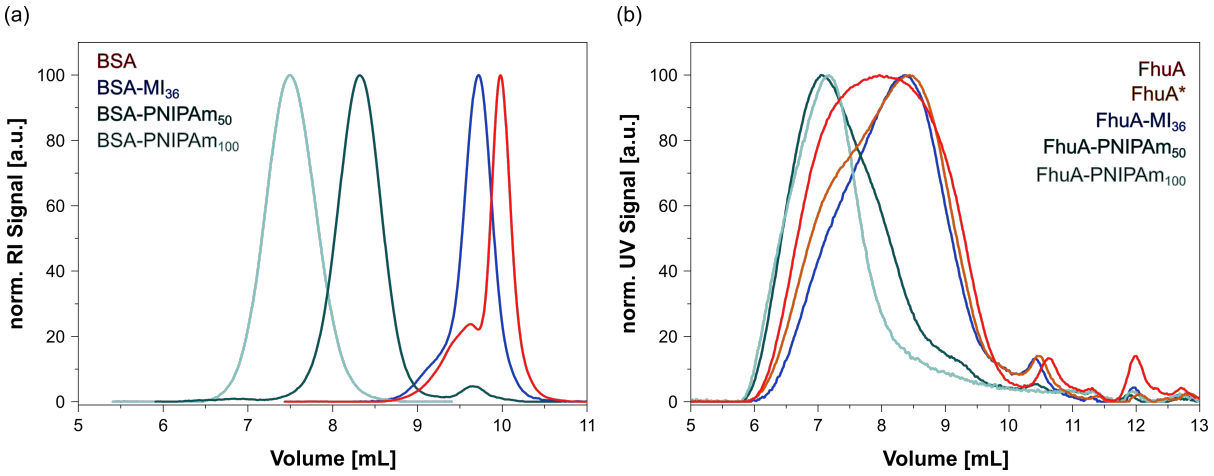


Figure 3.6: SEC chromatograms of BSA-conjugates (a) and FhuA-conjugates (b) prepared by grafting-from protein-MI measured in 50 vol% DMSO eluent. PSS PROTEEMA 5 µm column was used (eluent: 25 mM MPD buffer and 50 vol% DMSO in Milli-Q, flow rate: 0.5 mL·min$^{-1}$, temperature: 23 °C). The sample denoted with an asterisk was dissolved directly in the eluent buffer whereas all other samples were prepared in MPD buffer and mixed with DMSO.

When only DMSO was used as eluent, conjugates of both proteins were completely soluble and passed the column. Nevertheless, interactions between samples and column material occurred. Additionally, unmodified proteins tended to stick to the column material leading to partial or complete retention. Corresponding to the experiments in DMSO-MPD buffer mixtures, a partial or complete unfolding of unmodified proteins can be assumed. Consequently, molar mass analysis based on calibration with pullulan resulted in unrealistic molar masses and broad molar mass distributions (Table 3.2). Depending on the eluent, either interactions of unmodified proteins and MI or conjugates with the column material

were observed, as shown by the presented chromatograms of samples in the sections above and the deviation of expected and measured molar masses.

**Table 3.2: Analysis of SEC chromatograms of FhuA, FhuA-MI and FhuA-PNIPAm conjugates as well as BSA-MI, BSA-PNIPAm conjugates and PNIPAm homopolymer.**

| Sample | $M_{w,calc.}$ [kDa] | Eluent System | | | | | |
|---|---|---|---|---|---|---|---|
| | | MPD buffer | | DMSO/MPD 50 vol% | | DMSO, 0.05 M LiBr | |
| | | $M_w$ [kDa] | Đ | $M_w$ [kDa] | Đ | $M_w$ [kDa] | Đ |
| **FhuA** | 78.8 | 204 | 1.60 | - | - | - | - |
| **FhuA-MI$_{36}$** | 86.8 | 337 | 1.44 | - | - | - | - |
| **FhuA-PNIPAm$_{200}$** | 900 | - | - | - | - | 762 | 1.45 |
| **FhuA-PNIPAm$_{100}$** | 494 | - | - | 755 | 1.45 | 357 | 1.38 |
| **FhuA-PNIPAm$_{50}$** | 290 | - | - | 635 | 1.49 | 387 | 1.38 |
| **BSA-MI$_{36}$** | 74.4 | 92.5 | 1.06 | 140 | 1.04 | - | - |
| **BSA-PNIPAm$_{200}$** | 889 | - | - | - | - | 362 | 1.25 |
| **BSA-PNIPAm$_{100}$** | 482 | - | - | 444 | 1.04 | 182 | 1.12 |
| **BSA-PNIPAm$_{50}$** | 278 | - | - | 292 | 1.04 | 115 | 1.17 |
| **PNIPAm$_{200}$** | 45.6 | - | - | - | - | 82.5 | 1.36 |

PSS PROTEEMA, 5 µm, 1000 Å, 8x300 mm, flow rate 0.5 ml·min$^{-1}$, sample concentration 1 mg·mL$^{-1}$, injection volume 20 µL, column oven set to 23 °C, molar masses estimated based on a pullulan calibration of the column, higher molar mass shoulders were neglected.

**Additional column and eluent systems:** Different columns, column materials, column combinations and eluent systems were tested for their suitability to separate proteins, MIs and conjugates and the results are summarized in Table 3.3. For entries 7 and 8, further analysis in terms of molar mass and distribution determination based on calibration with standards is provided in the Experimental Part of this Chapter (Table 3.13). Generally, column combinations are used to enhance resolution by combination of columns that differ in porosity, pore size distribution and covered molar mass range. Besides the already harnessed PROTEEMA column, a new column type, namely PSS SUPREMA, was used. In contrast to PROTEEMA, which is especially recommended for proteins, SUPREMA is suggested for all kinds of neutral and anionic polymers. The column material is composed of a modified acrylate-copolymer network and the separation regime denoted as 0.1 kDa up to 30 kDa.

To test the thermo-responsive properties of the attached PNIPAm, measurements at temperatures above the $T_{CP}$ of the polymer were performed (Table 3.3, entry 1). As expected, the coil-globule transition enhanced the hydrophobic interactions of the samples with the column materials. Furthermore, buffer modification by addition of MeOH did not result in an improved performance of the system. Overall, either interactions of the unmodified protein or conjugates with the column material occurred and no suited conditions to analyze all samples with the same method were found.

**Table 3.3: Qualitative description of column and eluent systems probed for separation of proteins and protein-polymer conjugates prior analysis with MALS detector.**

| # | Specifications | Results & Interpretation |
|---|---|---|
| **1** | Column: PSS PROTEEMA, 5 µm, 1000 Å<br>Eluent: 50 mM MDP buffer<br>Temperature: 40 °C | • Complete retention of FhuA-PNIPAm conjugates and PNIPAm homopolymers<br>• Coil-globule transitions enhanced hydrophobic interactions with the column material |
| **2** | Column: PSS PROTEEMA, 5 µm, 1000 Å<br>Eluent: 50 mM MDP buffer + 0.1 M NaCl | • FhuA sample not completely soluble in buffer systems (salting-out effect)<br>• Complete retention of conjugates by column<br>• Perceivable interactions of homopolymer with column |
| **3** | Column: PSS PROTEEMA, 5 µm, 1000 Å<br>Eluent: 50 mM MDP buffer + 20 vol% MeOH | • Large shift in elution volume between protein and MI<br>• Partial retention of conjugates and homopolymer<br>• Perceivable interactions of all samples with column |
| **4** | Column: PSS PROTEEMA, 5 µm, 2000 Å<br>Eluent: 50 mM MDP buffer | • Better resolution for BSA samples<br>• Almost complete retention of FhuA samples |
| **5** | Column: PSS SUPREMA, 10 µm, ultrahigh<br>Eluent: 50 mM MPD buffer | • Decreased resolution<br>• Monomodal distribution for protein and MI<br>• Complete retention of conjugates and homopolymer |
| **6** | Column: PSS SUPREMA, 10 µm, ultrahigh<br>Eluent: MPD buffer + 20 vol% MeOH | • Monomodal distribution for protein and MI<br>• Complete retention of conjugates and homopolymer |
| **7** | Column: PSS PROTEEMA, 5 µm<br>Combination: 300 - 1000 - 2000 Å<br>Eluent: 150 mM MPD buffer | • Enhanced resolution of homopolymers<br>• Almost complete retention of FhuA samples<br>• Interactions of BSA samples with column |
| **8** | Column: PSS PROTEEMA, 5 µm<br>Combination: 100 - 1000 - 2000 Å<br>Eluent: 150 mM MPD buffer | • Enhanced resolution of homopolymers<br>• Partial retention of FhuA samples<br>• Interactions of BSA samples with column |

Column dimension 8x300 mm, flow rate 0.5 ml·min$^{-1}$, sample concentration 1 mg·mL$^{-1}$, injection volume 20 µL for entries 1–5 and 50 µL for entries 6–8, column oven set to 23 °C except otherwise noted.

**Conjugates based on PMEO$_2$MA:** The measurements so far were not very promising. Either the conjugates or the unmodified proteins exhibited non-covalent and hydrophobic interactions with the column material. Additionally, retention of PNIPAm homopolymers by the tested columns was observed. Even though PNIPAm is a water-soluble polymer, proper analysis by SEC was found to occur solely in DMSO, dimethylformamide (DMF) or dimethylacetamide (DMAc) eluent systems. Unfortunately, these eluent systems were not suited for complete solubilization of either the proteins or respective protein-polymer conjugates. Furthermore, such solvents do not come into consideration for proteins as pure organic solvents probably harm the protein structure even in conjugates, despite the stabilization by the polymer chains.

Consequently, the used monomer for conjugate synthesis was varied in order to test alternative conjugated polymers for their elution and separation properties during SEC. Di(ethylene glycol) methyl ether methacrylate ($MEO_2MA$) was chosen next. The respective thermo-responsive polymer undergoes a coil-globule transition at ambient temperatures of ~ 26 °C and was therefore thought to be a comprehensive substitute for PNIPAm.[191] The conjugates were synthesized analogous to the described procedures in Chapter 2.

In addition to the variation of the polymer type, the number of initiating groups deposited on the protein surface was varied. In the previous experiments, either the protein properties or the polymer properties denoted the solubility and interactions with the column material. Therefore, a variation of conjugate composition appeared to be the next logical step to understand these interactions in more detail. For the different macroinitiators, the pH value of the reaction medium was varied between pH 6.5 – 9.2 and a 5-times excess of NHS-activated functional CRP initiator per lysine residue used for modification. The resultant BSA-MIs were analyzed by MALDI-ToF mass spectrometry and the obtained spectra are shown in Figure 3.7. The extent of modification was assessed by dividing the difference in molar mass of BSA-MI and unmodified BSA by the mass of one attached initiator unit, namely 220 Da. In average, the extent of modification was determined to be 15, 19, 25 and 36 at pH 6.5, 7.0, 7.4 and 8.2, respectively. At pH 8.2, all accessible lysine residues at the protein surface were modified. Consequently, further increase in pH did not result in further modification. For conjugate synthesis, $BSA\text{-}MI_{15}$, $BSA\text{-}MI_{25}$ and $BSA\text{-}MI_{36}$ were used, and targeted degree of polymerization was set to 20 or 50 repeating units.

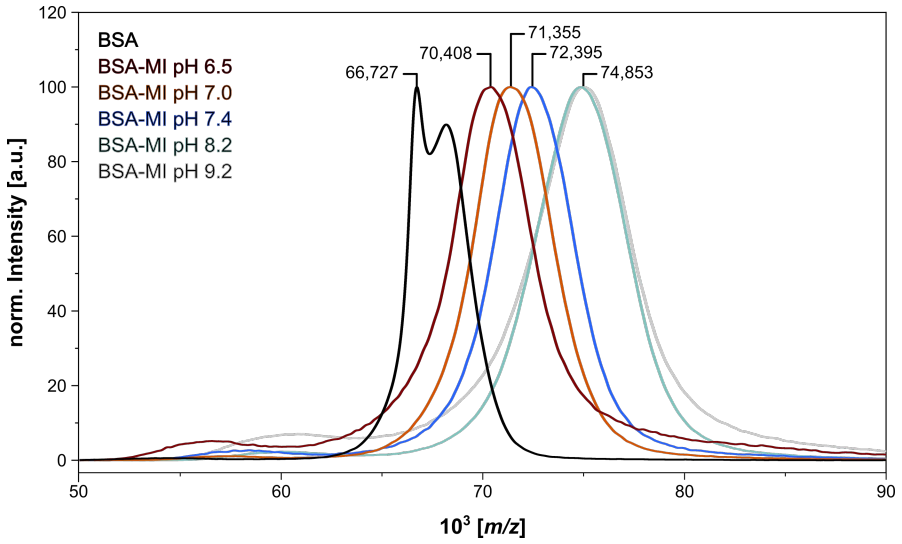


Figure 3.7: MALDI-ToF mass spectra of BSA (black) and macroinitiators synthesized at different pH values of the reaction medium. Molecular mass difference of MI and unmodified BSA was used to determine the approximate amount of initiating groups attached to the protein surface.

For the synthesis of $PMEO_2MA$ homopolymers and conjugates, the reaction time for the Cu(0)-mediated radical polymerization was adjusted to obtain sufficient conversion. Instead of 1 h as used for PNIPAm homopolymers and conjugates, time was increased to 4.5 h based on kinetic analysis with NMR spectroscopy. Two different degrees of polymerization, namely 20 and 50 repeating units, were targeted and conversions of 65 % and 70 %, respectively, reached after 4.5 h.

**Table 3.4: Expected molar masses of proteins, protein-macroinitiators and conjugates prepared by grafting-from using $MEO_2MA$.**

| Sample | Expected composition[a] [%] | | $M_{w,calc.}$[b] [Da] |
|---|---|---|---|
| | Protein | Polymer | |
| **BSA** | 100 | | 66 463 |
| **BSA-$MI_{15}$** | 100 | | 69 763 |
| **BSA-$PMEO_2MA_{20}$** | 65.5 | 34.5 | 106 466 |
| **BSA-$PMEO_2MA_{50}$** | 41.4 | 58.6 | 168 579 |
| **BSA-$MI_{25}$** | 100 | | 71 963 |
| **BSA-$PMEO_2MA_{20}$** | 54.1 | 45.9 | 133 135 |
| **BSA-$PMEO_2MA_{50}$** | 30.4 | 69.6 | 236 656 |
| **BSA-$MI_{36}$** | 100 | | 74 383 |
| **BSA-$PMEO_2MA_{20}$** | 45.7 | 54.3 | 162 925 |
| **BSA-$PMEO_2MA_{50}$** | 23.8 | 76.2 | 311 995 |
| **$PMEO_2MA_{20}$** | - | 100 | 5 228 |
| **$PMEO_2MA_{50}$** | - | 100 | 13 510 |

[a] Calculations performed analogous to Table 3.1. [b] Molar masses for conjugates prepared by grafting-from estimated based on expectable mass increase after initiator attachment as $M_{w,MI} = M_{w,protein} + (M_{w,initiator} \cdot \#\text{modified lysine})$ and after polymerization as $M_{w,conjugate} = M_{w,MI} + (DP \cdot M_{w,monomer} \cdot \#\text{modified lysine})$. DP is defined as the targeted degree of polymerization times observed conversion as determined by NMR spectroscopy. Mass increase per $MEO_2MA$ repeating unit of 188.22 $g \cdot mol^{-1}$ was used for calculations. Samples were prepared using Procedure II as stated in the Experimental Part of Chapter 2 for grafting-from protein-MIs.

Then, the macroinitiators and protein-polymer conjugates were analyzed by SEC and the respective chromatograms are shown in Figure 3.8. Here, a combination of two series-connected PSS SUPREMA 10 µm ultrahigh plus columns and an eluent composed of 0.5 $mg \cdot mL^{-1}$ sodium azide in Milli-Q water was used. For macroinitiators, this combination resulted in monomodal and narrow molar mass distributions. For unmodified BSA, a distortion to lower molar masses was observed. In general, the difference in elution volume between unmodified protein and respective macroinitiators is highly developed which indicates again the appearance of non-covalent interactions. For conjugates, the solubility decreased with increasing extent of modification. For the lower degree of polymerization of 20 repeating units, monomodal and narrow distribution profiles were observed whereas for the higher degree of polymerization of 50 repeating units, a distortion towards higher molar masses was obtained.

Changes in elution volume were quite subtle with 18.8 mL–18.5 mL and 18.6 mL–18.2 mL for DP = 20 and 50, respectively. Unfortunately, it was not possible to analyze homopolymers as they were not soluble under the chosen conditions. This might be explained by the low $T_{CP}$ of these homopolymers, which is typically around 26 °C.[191]

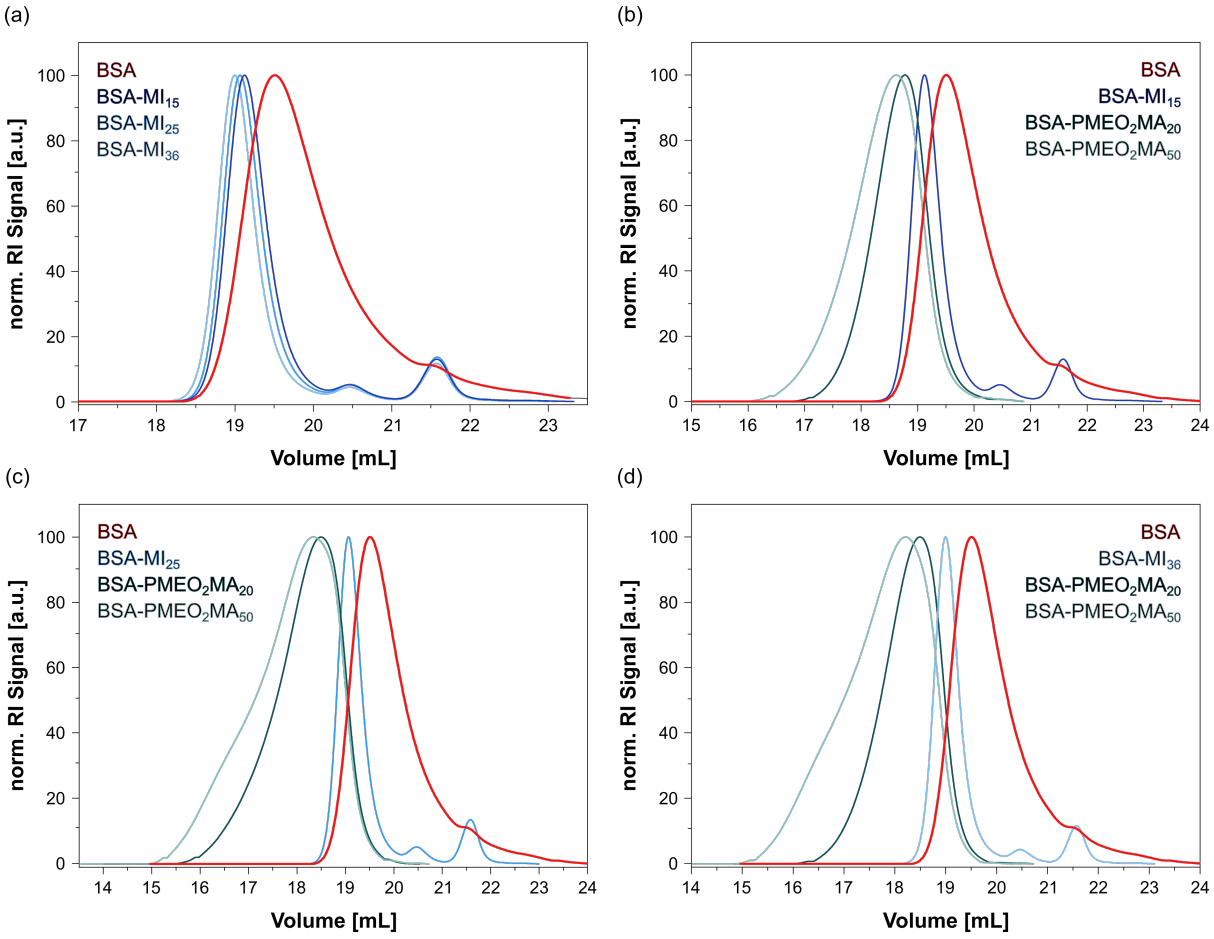


Figure 3.8: SEC chromatograms of BSA-MIs synthesized at pH 6.5, 7.4 and 8.2 (a) and BSA-PMEO$_2$MA conjugates (b–d) prepared by grafting-from the respective protein-MI. Combination of two series-connected PSS SUPREMA 10 µm ultrahigh plus columns were used (eluent: 0.5 mg·mL$^{-1}$ sodium azide in Milli-Q water, flow rate: 0.5 mL·min$^{-1}$, temperature: 23 °C).

Overall, these samples eluted in a much more favorable way than the PNIPAm conjugates. The elution volume and elution volume differences between the samples appeared much more realistic. Therefore, they were analyzed by SEC and molar masses estimated by external standard calibration of the column system and determination by an in-line connected MALS detector (Table 3.5).

**Table 3.5: Analysis of BSA, BSA-MI and BSA-PMEO$_2$MA conjugates.**

| Sample | $M_{w,calc.}$ [kDa] | $M_{w,PEO}$ [kDa] | $M_{n,PEO}$ [kDa] | Đ | $M_{w,MALS}$ [kDa] |
|---|---|---|---|---|---|
| **BSA** | 66.5 | 86.9 | 85.7 | 1.01 | 95.9 |
| **BSA-MI$_{15}$** | 69.8 | 75.8 | 59.2 | 1.28 | 78.5 |
| **BSA-PMEO$_2$MA$_{20}$** | 106.5 | 283 | 143 | 1.98 | 1 050 |
| **BSA-PMEO$_2$MA$_{50}$** | 168.6 | 507 | 192 | 2.64 | 3 020 |
| **BSA-MI$_{25}$** | 72.0 | 84.9 | 67.0 | 1.27 | 89.6 |
| **BSA-PMEO$_2$MA$_{20}$** | 133.1 | 783 | 86.3 | 9.15 | 6 170 |
| **BSA-PMEO$_2$MA$_{50}$** | 236.7 | 1 410 | 119 | 11.88 | 3 150 |
| **BSA-MI$_{36}$** | 74.4 | 90.3 | 66.8 | 1.35 | 96.6 |
| **BSA-PMEO$_2$MA$_{20}$** | 163.0 | 537 | 67.0 | 9.41 | 3 540 |
| **BSA-PMEO$_2$MA$_{50}$** | 312.0 | 1 470 | 152 | 9.66 | 73 300 |

In-line combination of 2 x PSS SUPREMA, 10 µm, ultrahigh plus, 8x300 mm, eluent 0.5 g·L$^{-1}$ $NaN_3$ in Milli-Q water, flow rate 0.5 ml·min$^{-1}$, sample concentration 1 mg·mL$^{-1}$, injection volume 100 µL, column oven set to 23 °C, molar masses estimated based on a polyethylene oxide (PEO) calibration of the column system or measured by an in-line connected MALS detector, higher molar mass shoulders were neglected.

In summary, molar masses estimated using an external calibration of the used column system and PEO as calibrant resulted in lower values than expected (underestimation of molar masses), whereas the analysis of the individual sample components by the in-line connected MALS detector resulted in higher values than expected (overestimation of molar masses). Whereas molar masses based on external calibration rely on the chosen calibrant and deviations may arise from differences in the analyte and calibrant relationship between Stokes radii, molar mass and diffusion properties, variance in MALS data mainly occur because of misestimation of the refractive index increment or sample concentration. Both are represented in the denominator in Equation (3.1). When the concentration of the analyte is reduced because of interactions with the column material or misestimation of the sample concentration, the overall term for molar mass increases. Furthermore, the square value of the refractive index increment ($d_n/d_c$) is used for molar mass determination by light scattering and deviations of this value from the real value have a huge impact. For copolymers and protein-polymer conjugates, this value is not constant and difficult to determine.

**Conjugates based on POEGA and POEGmA:** The inconvenient $T_{CP}$ of the PMEO$_2$MA polymer material near ambient temperature resulted in a difficult handling of the samples. Even though SEC results were more promising compared to PNIPAm, the system proved to be insufficient for further analysis. As the inconveniences were accounted to the low cloud point and not to the general polymer characteristics, a longer side chain of the branched PEG analog was thought to improve the chromatographic behavior of the samples. Therefore, oligo(ethylene glycol) (meth)acrylates (OEG(m)A) with side chain lengths of 8-9 ethylene oxide repeating units were chosen for further investigations. The longer oligoethylene glycol side chain increases the hydrophilicity of the system

and shifts the cloud point to values higher than 90 °C.[191–193] The more hydrophilic nature of these monomers and corresponding polymers was hoped to disrupt non-covalent interactions of the conjugates with the column material. Nevertheless, slight deviations of polymer backbone hydrophilicity determined by the additional methyl group in methacrylate made both monomers, acrylate and methacrylate, interesting for conjugate synthesis and characterization by SEC-MALS. Chemical structures and respective cloud points of $PMEO_2MA$ compared to oligo(ethylene glycol) (meth)acrylates with $M_n$ of 475 and 500 g·mol$^{-1}$ for OEGA and OEGmA, respectively, are shown in Figure 3.9.

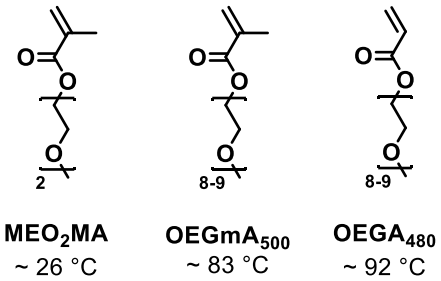


Figure 3.9: Chemical structures of monomers for branched PEG analogs chosen for conjugate synthesis and the respective $T_{CP}$ of the resulting polymers.[191–193]

Initial studies using oligo(ethylene glycol) methacrylate (OEGmA) polymers ($M_n$ of 500 g·mol$^{-1}$ per repeating unit) with various molar masses ranging from ~ 10 kDa up to 50 kDa synthesized by RAFT polymerization and measured in a sodium azide buffer exploiting a combination of two PSS SUPREMA 10 µm ultrahigh plus columns arranged in series provided promising results (Table 3.6). Independent of the chosen column system and used calibration standard, experimental results near the expected values were obtained for all polymers indicating a chromatography without non-covalent interactions between sample and column material.

**Table 3.6: Characteristics of POEGmA synthesized by RAFT and analyzed by SEC and MALS.**

| Sample | $M_{w,theor.}$[a] [Da] | $M_{w,PS}$[b] [Da] | $M_{n,PS}$[b] [Da] | Đ[a] | $M_{w,PEO}$[c] [Da] | $M_{n,PEO}$[c] [Da] | Đ[b] | $M_{w,MALS}$[c] [Da] |
|---|---|---|---|---|---|---|---|---|
| **$POEGmA_{50}$** | 25 291 | 29 165 | 20 066 | 1.45 | 32 000 | 19 800 | 1.61 | 47 400 |
| **$POEGmA_{100}$** | 50 291 | 39 674 | 28 510 | 1.39 | 43 600 | 43 600 | 1.65 | 70 500 |

[a] According to NMR spectra of the crude reaction mixtures. [b] PSS SDV linear M column was used, 3 µm, 8x300 mm, eluent THF, flow rate 0.5 ml·min$^{-1}$, sample concentration 1 mg·mL$^{-1}$, injection volume 100 µL, column oven set to 23 °C and molar masses estimated based on a polystyrene (PS) calibration. [c] In-line combination of 2 x PSS SUPREMA columns was used, 10 µm, ultrahigh plus, 8x300 mm, eluent 0.5 g·L$^{-1}$ $NaN_3$ in Milli-Q water, flow rate 0.5 ml·min$^{-1}$, sample concentration 1 mg·mL$^{-1}$, injection volume 100 µL, column oven set to 23 °C and molar masses estimated based on a PEO calibration. Higher molar mass shoulders were neglected.

In initial experiments for grafting POEG(m)A from BSA by Cu(0)-mediated radical polymerization at high dilution and using an excess of ligand per catalyst of [1]:[1.2], incomplete conversion was observed. Accordingly, conditions were optimized to adjust the system to the new monomers and reach full conversion under ambient conditions. As POEGA and POEGmA are acrylates and methacrylates, respectively, their activity differs and catalyst/ligand ratios and source of ligand have to be adjusted accordingly.[169] Different ligands are reported that facilitate the disproportionation of $Cu^{I}$ in aqueous systems needed for this type of polymerization to work under controlled conditions. In a comprehensive study presented by HADDLETON and co-workers, POEGA and POEGmA were synthesized using either $Me_6$TREN or PMDETA as ligand. The former is described to match the activity of acrylates and the latter for methacrylates. It should be mentioned that, in the published studies, an equimolar amount of catalyst and ligand was used rather than an excess of ligand. A higher amount of ligand compared to catalyst shifts the equilibrium towards [$Cu^{I}$(ligand)Br] and hence increases the overall activity of the system (for more mechanistic considerations please see Chapter 1.4 and Chapter 2). In the own studies, cessation of polymerization for POEGA was observed before quantitative conversion indicating a poor end-group fidelity which might be explained by the lack of [$Cu^{II}$(ligand)Br]Br acting as deactivating agent. In contrast, for POEGmA good conversions were achieved. The resultant polymers were analyzed by SEC and results summarized in Table 3.7. Surprisingly, when PMDETA was used, the discrepancy of expected and observed molar mass was not as pronounced as for $Me_6$TREN indicating a better match of reactivities of initiator, monomer and catalyst/ligand system. Nevertheless, the obtained dispersity increased significantly when PMDETA was utilized. Furthermore, when a lower degree of polymerization was targeted, cessation of polymerization was observed indicating a lack in deactivation by [$Cu^{II}$(ligand)Br]Br during polymerization. Decrease of ligand with respect to catalyst was therefore thought to increase amount of Cu(II) in the system and facilitate polymerization to achieve near quantitative conversion.

**Table 3.7: Ligand influence on the Cu(0)-mediated polymerization of $OEGA_{475}$ and $OEGmA_{500}$.**

| # | Ligand | monomer | Conversion | $M_{n,theor.}$[a] [Da] | $M_{n,SEC}$ [Da] | $M_{w,SEC}$ [Da] | Đ |
|---|---|---|---|---|---|---|---|
| **1** | **$Me_6$TREN** | **OEGA** | 50 | 24 167 | - | - | - |
| **2** | **PMDETA** | | - | - | - | - | - |
| **3** | **$Me_6$TREN** | **OEGmA** | 90 | 45 167 | 84 927 | 113 619 | 1.34 |
| **4** | **PMDETA** | | 70 | 35 167 | 32 361 | 50 405 | 1.56 |

Concentration of reaction components were fixed for all polymerization and were initiator [0.465 mM], monomer [46.5 mM], CuBr during polymerization [3.5 mM], during disproportionation [24.8 mM], ligand [4.2 mM]. The ratio of reaction components was set to [1]:[100]:[7.5]:[9]. SEC analysis performed with a PSS SDV linear M column, 3 µm, 8 x 300 mm, eluent THF, flow rate 0.5 ml·min$^{-1}$, sample concentration 1 mg·mL$^{-1}$, injection volume 100 µL, column oven set to 23 °C and molar masses estimated based on a PS calibration. [a] According to NMR spectra of the crude reaction mixtures.

For further investigations, POEGA was prioritized over POEGmA. Polymerization conditions for OEGA by aqueous copper(0)-mediated radical polymerization in water under ambient conditions and from BSA by grafting-from were already described in the literature.[90,108] Characteristics of synthesized polymers derived under various conditions are summarized Table 3.8. At optimized reaction conditions, full conversion was achieved within 60–240 min, depending on the catalyst/ligand ratio. In general, low dispersity was observed with good agreement between expected and measured molar masses.

**Table 3.8: Conditions screened for the Cu(0)-mediated polymerization of $OEGA_{475}$.**

| # | Conditions Ratio / [mM] | | | | CuBr dispr. [mM] | Conv. | $M_{n,theor.}$[a] [g·mol$^{-1}$] | $M_{n,SEC}$ [g·mol$^{-1}$] | $M_{w,SEC}$ [g·mol$^{-1}$] | Đ |
|---|---|---|---|---|---|---|---|---|---|---|
| | Initiator | OEGA | CuBr | $Me_6$TREN | | | | | | |
| **1** | 1 [11.4] | 20 [227] | 0.4 [4.6] | 0.4 [4.6] | 32 | 90 | 8 807 | 15 601 | 19 313 | 1.24 |
| **2** | 1 [2.5] | 67 [167] | 1.25 [3.1] | 1.25 [3.1] | 18.8 | > 99 | 32 000 | 35 933 | 48 487 | 1.35 |
| **3** | 1 [2.5] | 67 [167] | 2.5 [6.2] | 1.25 [3.1] | 36.2 | 95 | 30 719 | 30 177 | 33 167 | 1.10 |
| **4** | 1 [0.465] | 20 [9.3] | 7.5 [3.5] | 7.5 [3.5] | 24.8 | > 99 | 9 671 | 9 421 | 12 318 | 1.31 |
| **5** | 1 [0.465] | 20 [9.3] | 15 [7] | 7.5 [3.5] | 50 | - | - | - | - | - |
| **6** | 1 [0.465] | 100 [46.6] | 7.5 [3.5] | 7.5 [3.5] | 24.8 | > 99 | 47 687 | 25 579 | 33 239 | 1.30 |
| **7** | 1 [0.465] | 100 [46.6] | 15 [7] | 7.5 [3.5] | 50 | 71 | 34 247 | 27 030 | 29 977 | 1.11 |

SEC analysis performed with a PSS SDV linear M column, 3 µm, 8x300 mm, eluent THF, flow rate 0.5 ml·min$^{-1}$, sample concentration 1 mg·mL$^{-1}$, injection volume 100 µL, column oven set to 23 °C and molar masses estimated based on a PS calibration. Polymerizations for entries 1–3 were performed according to procedures presented in the literature. The corresponding citation is added in the first column. [a] According to NMR spectra of the crude reaction mixtures.

Protein-polymer conjugates of BSA with POEGA were formed using conditions as stated in Table 3.8 entry 2. These conditions were already used in the literature to produce BSA-POEGA conjugates. At the same time, BSA-PNIPAm conjugates were re-synthesized using the same conditions. The samples presented in the sections above were synthesized using an excess of ligand with respect to catalyst. In contrast to the previously performed polymerization, at high extent of modification and high targeted degree of polymerization, gel formation of the samples was observed. Increase of $Cu^{I}$ to shift the equilibrium to [$Cu^{II}$(ligand)Br]Br did not result in a further increase in control over polymerization when conjugates were targeted despite the fact, that higher amount of [$Cu^{II}$(ligand)Br]Br led to a better control in the synthesis of homopolymers (Table 3.8 entry 3). This might be explained by the close proximity of initiator groups at the protein surface and unfavorable adsorption/desorption events at the nascent $Cu^0$ particles promoted by hydrophobic interactions of functionalized macroinitiator.[194]

Additional attempts such as addition of sodium chloride to increase protein solubility by the salting-in effect,[195] addition of sodium dodecyl sulfate to suppress hydrophobic interactions,[100] and performing the polymerization at lower protein concentration with and without the use of a sacrificial initiator did not result in a better performance. Gel formation was observed, when high degrees of polymerizations

were targeted. Therefore, DPS were adjusted to lower values. For BSA-$MI_{15}$ and $MI_{25}$, degree of polymerization of 20 and 100 were achieved without gel formation. For BSA-$MI_{36}$, degree of polymerization was set to 20 and 60 for both, NIPAm and OEGA monomers. SDS-PAGEs of obtained protein-polymer conjugates are shown in Figure 3.10. The typical faded bands for conjugates were observed. With increasing extent of modification with POEGA, the faded band disappeared, indicating a blocking of the protein by the polymer corona and hence a suppressed sensitivity to SDS-PAGE silver staining. The respective expected compositions and molar masses of protein, macroinitiator and conjugates based on the conversion during polymerization are summarized in Table 3.9.

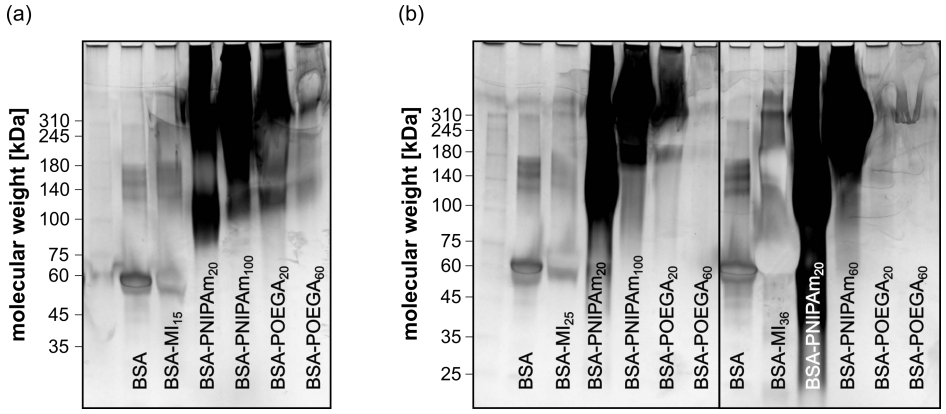


Figure 3.10: SDS-PAGE of BSA, BSA-macroinitiators and conjugates with PNIPAm and POEGA starting from BSA-$MI_{15}$ (a), BSA-$MI_{25}$ or BSA-$MI_{36}$ (b). 4-15 % gradient gels were used and bands visualized by silver staining protocol.

The respective expected compositions and molar masses of protein, macroinitiator and conjugates based on the conversion during polymerization are summarized in Table 3.9.

**Table 3.9: Expected molar masses of proteins, protein-macroinitiators and conjugates prepared by grafting-from BSA-macroinitiators with different numbers of attached initiators per BSA molecule.**

| | Sample | Expected composition[a] [%] | | $M_{w,calc.}$[b] [kDa] |
|---|---|---|---|---|
| | | Protein | Polymer | |
| **BSA-$MI_{15}$** | BSA-$PNIPAm_{20}$ | 66.2 | 33.8 | 100.4 |
| | BSA-$PNIPAm_{100}$ | 28.1 | 71.9 | 236.2 |
| | BSA-$POEGA_{20}$ | 31.6 | 68.4 | 210.5 |
| | BSA-$POEGA_{60}$ | 13.3 | 86.7 | 498.5 |
| **BSA-$MI_{25}$** | BSA-$PNIPAm_{20}$ | 54.0 | 46 | 123.0 |
| | BSA-$PNIPAm_{100}$ | 28.1 | 71.9 | 236.2 |
| | BSA-$POEGA_{20}$ | 21.7 | 78.3 | 306.5 |
| | BSA-$POEGA_{60}$ | 8.5 | 91.5 | 786.5 |

**Table 3.9: Expected molar masses of proteins, protein-macroinitiators and conjugates prepared by grafting-from BSA-macroinitiators with different numbers of attached initiators per BSA molecule.**

| | Sample | Expected composition[a] [%] | | $M_{w,calc.}$[b] [kDa] |
|---|---|---|---|---|
| | | Protein | Polymer | |
| **BSA-$MI_{36}$** | BSA-$PNIPAm_{20}$ | 44.9 | 55.4 | 147.9 |
| | BSA-$PNIPAm_{60}$ | 21.4 | 78.6 | 310.8 |
| | BSA-$POEGA_{20}$ | 16.1 | 83.9 | 412.0 |
| | BSA-$POEGA_{60}$ | 6.0 | 94.0 | 1 103.3 |

[a] Calculations performed analogous to Table 3.1. [b] Molar masses for conjugates prepared by grafting-from estimated based on expectable mass increase after initiator attachment as $M_{w,MI} = M_{w,protein} + (M_{w,initiator} \cdot \#\text{modified lysine})$ and after polymerization as $M_{w,conjugate} = M_{w,MI} + (DP \cdot M_{w,monomer} \cdot \#\text{modified lysine})$. DP is defined as the targeted degree of polymerization times observed conversion as determined by NMR spectroscopy. Mass increase per OEGA and NIPAm repeating unit of 480 $g \cdot mol^{-1}$ and 113 $g \cdot mol^{-1}$ was used for calculations, respectively. Samples were prepared using Procedure I as stated in the Experimental Part of Chapter 2 for grafting-from protein-MIs.

As control system and to maintain consistency with the previous experiments performed with PNIPAm, conjugates of BSA with POEGA and POEGmA were aimed to be prepared by grafting-to. Therefore, end-group functionalized polymers were synthesized by RAFT polymerization analogous to the procedure described in Chapter 2. Unfortunately, as the steric demand of these branched polymers is too large, no modification of BSA by grafting-to using PFP-functionalized POEGA and POEGmA was achieved. This phenomenon was already described in the literature.[196] In further experiments, a spacer between active ester and polymer chain could be used to increase the accessibility of the end-group and therefore the conjugation efficiency.[196] However, this could not be accomplished in the time frame of this thesis. Table 3.9 summarizes the characteristics of the synthesized protein-polymer conjugates in terms of composition and expected molar masses.

While PNIPAm conjugates were already analyzed in detail, focus was set to the new POEGA conjugates. The chromatograms obtained using the same column and eluent system as for the $PMEO_2MA$ conjugates are shown in Figure 3.11. The higher the degree of conjugation, the worse the resolution and obtained molar mass distributions of the samples. When lyophilized and redissolved in the eluent buffer, samples with high amount of POEGA tended to form hydrogels instead of monodispersed solutions. As a result, these samples are certainly present as aggregates and were retained by the column system.

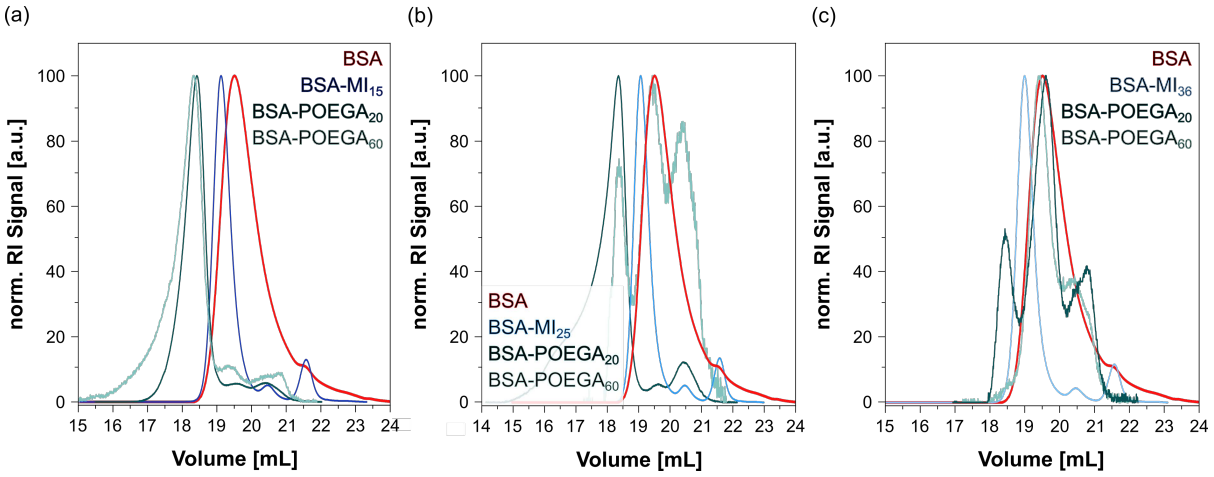


Figure 3.11: SEC chromatograms of BSA, BSA-MI and POEGA conjugates prepared by grafting-from the respective protein-MI with varying number of attached initiating groups. Combination of two series-connected PSS SUPREMA 10 µm ultrahigh plus columns were used (eluent: 0.5 mg·mL$^{-1}$ sodium azide in Milli-Q water, flow rate: 0.5 mL·min$^{-1}$, temperature: 23 °C.

Consequently, analysis by column chromatography and molar mass estimation based on external calibration and light scattering was error-prone and resulted in unrealistic values, as shown in Table 3.10.

**Table 3.10: Analysis of BSA, BSA-MI and BSA-POEGA conjugates.**

| Starting from | Sample | $M_{w,calc.}$ [kDa] | $M_{w,PEO}$ [kDa] | $M_{n,PEO}$ [kDa] | Đ | $M_{w,MALS}$ [kDa] |
|---|---|---|---|---|---|---|
| **BSA-MI$_{15}$** | **BSA-POEGA$_{20}$** | 210.5 | 282 | 43 | 6.56 | 624 |
| | **BSA-POEGA$_{60}$** | 498.5 | 709 | 37 | 19.18 | 55 100 |
| **BSA-MI$_{25}$** | **BSA-POEGA$_{20}$** | 306.5 | 1 020 | 39,9 | 25.63 | 11 700 |
| | **BSA-POEGA$_{60}$** | 786.5 | 67,1 | 7,8 | 8.59 | - |
| **BSA-MI$_{36}$** | **BSA-POEGA$_{20}$** | 412.0 | 60,7 | 7,6 | 8.05 | - |
| | **BSA-POEGA$_{60}$** | 1 103.3 | 31,3 | 8,1 | 3.87 | - |

In-line combination of 2 x PSS SUPREMA, 10 µm, ultrahigh plus, 8x300 mm, eluent 0.5 g·L$^{-1}$ $NaN_3$ in Milli-Q water, flow rate 0.5 ml·min$^{-1}$, sample concentration 1 mg·mL$^{-1}$, injection volume 100 µL, column oven set to 23 °C, molar masses estimated based on a polyethylene oxide (PEO) calibration of the column, higher molar mass shoulders were neglected.

Lastly, samples were measured with a buffer system containing 50 % methanol and 0.1 M sodium nitrate to increase on the one hand the solubility of the samples in elution buffer and on the other hand to further decrease hydrophobic interactions of samples with the column material. The results are summarized in Table 3.11. A huge discrepancy between the chromatographic behavior of conjugates derived from PNIPAm and POEGA was observed. PNIPAM-conjugates were partially retained by the system and molar mass values based on external calibration are massively underestimated. Contrary, MALS measurements gave higher values than theoretically expected, again based on the partial

retention of the sample. POEGA-conjugates performed slightly better, but still showed huge discrepancies between expected and observed molar masses.

**Table 3.11: Analysis of BSA and conjugates with PNIPAm and POEGA using 50 vol% MeOH as eluent.**

| | Sample | $M_{w,calc.}$ [kDa] | $M_{w,PEG\text{-}PEO}$ [kDa] | $M_{n,PEG\text{-}PEO}$ [kDa] | Đ | $M_{w,MALS}$ [kDa] |
|---|---|---|---|---|---|---|
| | **$POEGA_{20}$** | | 7.45 | 4.57 | 1.63 | 12.3 |
| | **$POEGA_{100}$** | | 25.6 | 10.8 | 2.37 | 50.4 |
| | **$POEGmA_{20}$** | | 9.54 | 5.85 | 1.63 | 16.2 |
| | **$POEGmA_{100}$** | | 41.1 | 18.0 | 2.29 | 83.6 |
| **$BSA\text{-}MI_{15}$** | **$BSA\text{-}PNIPAm_{20}$** | 100.4 | 14.2 | 4.96 | 2.87 | 1 640 |
| | **$BSA\text{-}PNIPAm_{100}$** | 236.2 | 14.6 | 7.27 | 2.01 | 1 590 |
| | **$BSA\text{-}POEGA_{20}$** | 210.5 | 153.0 | 26.2 | 5.85 | 1 860 |
| **$BSA\text{-}MI_{25}$** | **$BSA\text{-}PNIPAm_{20}$** | 123.0 | 56.6 | 16.8 | 3.37 | 1 060 |
| | **$BSA\text{-}PNIPAm_{100}$** | 236.2 | 12.3 | 7.52 | 1.64 | 684 |
| | **$BSA\text{-}POEGA_{20}$** | 210.5 | 1 310 | 50 200 | 26.20 | 22 100 |

In-line combination of 2 x PSS SUPREMA, 10 µm, ultrahigh plus, 8x300 mm, eluent 50 vol% MeOH and 0.1 M $NaNO_3$ in Milli-Q water, flow rate 0.5 ml·$min^{-1}$, sample concentration 1 mg·$mL^{-1}$, injection volume 100 µL, column oven set to 23 °C, molar masses estimated based on a PEG-PEO calibration, higher molar mass shoulders were neglected

To sum up, the tested protocols were not suited for the successful fractionation and analysis of protein-polymer conjugates by MALS in-line connected to SEC. Even though highlighted in a review by RUSSEL as highly promising technique for detailed analysis of protein-polymer conjugates,[81] the studies performed in cooperation with the company Polymer Standards Service uncovered major disadvantaged and challenges still to be solved.

In the literature, two applications of SEC-MALS to characterize protein-polymer conjugates were found. CHILKOTI et al. successfully used SEC-MALS to characterize myoglobin (Mb) functionalized site-specifically with water-soluble polymers.[159] The resulting protein-to-polymer ratio of 1:1 was achieved by exclusive modification of the N-terminus with a small CRP initiator. Subsequent polymerization of 2-(dimethylamino)ethyl methacrylate (DMAEMA) and POEGmA (average $M_n$ ~ 500 g·$mol^{-1}$) was performed by in situ ATRP from the N-terminus of Mb. Targeted degrees of polymerization were 3000 and 1500 for DMAEMA and POEGmA, respectively. Analytical SEC was performed using an Agilent Bio SEC-5 Column (300 Å, 4.6 x 300 mm, 5 µm) series-connected to an Agilent Bio SEC-5 guard column (150 Å, 4.6, 50 mm, 5 µm). Flow rate was set to 0.4 mL·$min^{-1}$ and 0.1 M sodium phosphate buffer, pH 7.0 with 5 % MeOH used as the eluent at 25 °C. The molar mass of the conjugates was determined as 425 kDa and 612 kDa for Mb-DMAEMA and Mb-POEGmA, respectively. Mb has a molar mass of approximately 17 kDa. Considering the molar mass of the

monomers to be 157 g·mol$^{-1}$ and 500 g·mol$^{-1}$, the obtained degree of polymerization amounts to 2595 and 1190. It can be assumed that the obtained molar masses by SEC-MALS correlate to the expected values. Unfortunately, the authors did not provide any information, neither about the achieved conversion during polymerization, nor their expected molar mass of the conjugate. Furthermore, analysis with SEC revealed the presence of unreacted protein in the reaction mixture. Nevertheless, the presented study provides realistic values.

FINN and co-workers modified virus-like particles (VLPs) via an azide-alkyne cycloaddition procedure of azide-functionalized VLPs derived from the bacteriophage Qβ and alkyne-terminated polymers.[197] SEC-MALS was used to determine the number of attached polymer chains per VLP rather than comparison of expected and obtained molar masses. Therefore, a Superose 6 10/300 GL size exclusion column (GE Healthcare), 0.1 M $KPO_4$ buffer pH 7.4 as eluent and a flow rate of 0.4 mL·min$^{-1}$ was used. Samples were detected using a UV–Vis detector (Agilent), a Viscotek SEC-MALS 20 multi-angle light scattering detector (Malvern), and a Viscotek VE3580 refractometer (Malvern). Measured differences in molar mass between the conjugate and starting material was used to determine extent of modification. Sample molar masses varied between 2770–4000 kDa. Curiously, SDS-PAGE of conjugates showed unreacted starting material not visible in the corresponding SEC chromatograms. Furthermore, no purification protocol is provided by the authors and protein quantification performed using a bicinchoninic acid (BCA) assay calibrated with BSA. This assay is reported to be inappropriate for accurate protein quantification and to yield different responses for different proteins.[198,199] Unfortunately, both studies do not discuss procedures used to calculate refractive index increments. Therefore, their shown results might be treated with caution.

## 3.4 Conclusion and Outlook

Within the time frame of this thesis, we were not able to establish a successful and universal method for the separation and characterization of protein-polymer conjugates with SEC-MALS. The interaction of either the protein or the polymer shell with the column material led to chromatographic properties not suited for the detailed analysis of the hydrodynamic state, the molar mass and dispersity of the conjugates synthesized. It is assumed that conjugates prepared by grafting-to or site-specific grafting-from with preferably one polymer chain attached per protein molecule might be easier to analyze, comparable to the studies presented by CHILKOTI and co-workers.[159] These systems behave more like classical block copolymers and the influence of the polymer chain on elution behavior might be more easily accessible.

Therefore, further experiments should deal with the synthesis of BSA-polymer conjugates with POEGA or POEGmA, as these systems were found to be the most promising. The branched PEG analogs are highly hydrophilic suppressing hydrophobic interactions with the column material. To achieve this, grafting-to of end-group functionalized POEG(m)A polymers with a spacer between the branched polymer and the protein-reactive group could be used. Alternatively, a 1:1 modification of BSA with a functional CRP initiator could be established. Therefore, the BSA cysteine thiol group present at the protein surface could be targeted. In native BSA, only one free thiol group is present at the protein surface and was used frequently in the literature to achieve a 1:1 modification of BSA.[88,114]

## 3.5 Experimental Part

**Materials:** All materials were received as stated and used as received unless otherwise noted. Di(ethylene glycol) methyl ether methacrylate ($MEO_2MA$), poly(ethylene glycol) methyl ether acrylate (OEGA, average $M_n$ ~ 480 g·mol$^{-1}$) and poly(ethylene glycol) methyl ether methacrylate (OEGmA, average $M_n$ ~ 500 g·mol$^{-1}$) were purchased from Sigma-Aldrich and passed through basic alumina twice, before use, to remove inhibitors. 2-Methyl-2,4-pentanediol (MPD, ≥ 99 %) was purchased from Roth. 2-(Butylthiocarbonothioylthio)-2-methylpropionic acid (CTAM) was received from Johannes MARTIN and functionalized with PFP according to the procedure presented in Chapter 2. Phosphate buffer refers to a buffer containing 10 mM sodium phosphate and 10 mM NaCl, pH 7.4. MPD buffer refers to a buffer containing 10 mM sodium phosphate, 10 mM NaCl and 50 mM MPD, pH 7.4. FhuA was received from the group of SCHWANEBERG and the detailed preparation is discussed in Chapter 5. Dialysis tubing cellulose membrane with MWCO 12–14 kDa was purchased from Sigma-Aldrich.

**Instrumentation:** All used instruments are listed in the Experimental Part of Chapter 2.

**Procedures:**

**Conjugation of protein-reactive polymer to BSA** was performed analogous to the procedure described for CBM in Chapter 2. 100 mg native BSA (Mw~66.5 kDa, 1.5 µmol) was dissolved in 10 mM phosphate buffer pH 7.4 at a concentration of 1 mg·mL$^{-1}$. After complete dissolution, the protein solution was diluted with 0.2 M carbonate-bicarbonate buffer pH 9.2 to a protein concentration of 0.5 mg·mL$^{-1}$ and a final pH of 8.2. A 15-times excess referred to BSA of oligomeric NIPAm (DP = 20) or polymeric NIPAm (DP = 200) dissolved in 1 mL DMSO (DMSO concentration in BSA solution <0.5 vol%) was added and stirred at 4 °C overnight. Afterwards, the solution was centrifuged (7500xg for 10 min) and the supernatant passed through a 0.2 µm PVDF sterile syringe filter to get rid of undissolved side products. To get rid of pentafluorophenol as side product of conjugation, the reaction mixture was dialyzed against Milli-Q water for 5 days with water exchange every 24 h. A small amount of sample was used for characterization and the remaining part lyophilized to obtain BSA-oNIPAm and BSA-PNIPAm, respectively, as a fluffy powder.

**FhuA-MI and BSA-MI** were synthesized according to the presented procedure described in Chapter 2. The number of attached initiators was varied by adjusting the pH during the macroinitiator synthesis using either a sodium bicarbonate or carbonate-bicarbonate buffer stock solution (0.2 M for pH 8.2 and 9.2 respectively, resulting in complete modification of the protein) or a phosphate buffer stock solution (0.2 M for pH 7.4, 7.0 and 6.5 for a reduced number of attached initiators). The relation of pH and degree of modification can be found in Figure 3.7.

**FhuA-polymer and BSA-polymer conjugates by grafting-from** were synthesized according to the procedures described in Chapter 2 as detailed below. After polymerization, a small amount of sample was used for characterization and the remaining part dialyzed against Milli-Q water for 5 days with water exchange every 24 h. After lyophilization, the respective protein-polymer conjugates were obtained as fluffy powders.

**Polymerization from FhuA-MI according to Procedure II:** In a typical experiment, CuBr (8.0 mg, 55.8 µmol, 7.0 equiv.) was placed in a syringe along with a magnetic stirring bar. A solution of $Me_6$TREN (22.0 µL, 80.0 µmol, 10.0 equiv.) in 2.5 mL 10 mM phosphate buffer containing 50 mM MPD was added and headspace eliminated. The solution was left for disproportionation at 4 °C under rapid stirring for 15 min. Then, a solution containing FhuA-MI (17.0 mg, 0.22 µmol, 8.0 µmol attached initiating units, 1 equiv.) and NIPAm (180 mg, 1600 µmol, 200 equiv.) in 15 mL MPD buffer was added to the syringe and polymerized for 1 h at 4 °C under rapid stirring. Afterwards, the solution was filtered through a 0.2 µm sterile PVDF syringe filter, transferred to a 14 kDa MWCO dialysis membrane and purified by dialysis. The degree of polymerization was adjusted by varying the ratio of monomer to initiator to obtain FhuA-PNIPAm$_{50}$ and FhuA-PNIPAm$_{100}$.

**Polymerization from BSA-MI according to Procedure I:** In a typical experiment, CuBr (1.8 mg, 12.4 µmol, 1.25 equiv.) was placed in a syringe along with a magnetic stirring bar. A solution of $Me_6$TREN (3.3 µL, 12.4 µmol, 1.25 equiv.) in 650 µL 10 mM phosphate buffer containing 50 mM MPD was added and headspace eliminated. The solution was left for disproportionation at 4 °C under rapid stirring for 15 min. Then, a solution containing BSA-MI (18.2 mg, 0.275 µmol, 9.9 µmol attached initiating units, 1 equiv.) and NIPAm (112 mg, 990 µmol, 100 equiv.) in 3.32 mL phosphate buffer was added to the syringe and polymerized for 1 h at 4 °C under rapid stirring. Afterwards, the solution was filtered through a 0.2 µm sterile PVDF syringe filter, transferred to a 14 kDa MWCO dialysis membrane and purified by dialysis. For BSA-$MI_{15}$ and BSA-$MI_{25}$ the protein concentration was adjusted to keep the initiator concentration constant. The procedure was the same when synthesizing conjugates with $MEO_2MA$ as monomer.

**Polymerization from BSA-MI according to Procedure II:** In a typical experiment, CuBr (12.0 mg, 83.4 µmol, 7.0 equiv.) was placed in a syringe along with a magnetic stirring bar. A solution of $Me_6$TREN (32.0 µL, 120.0 µmol, 10.0 equiv.) in 3.6 mL 10 mM phosphate buffer containing 50 mM MPD was added and headspace eliminated. The solution was left for disproportionation at 4 °C under rapid stirring for 15 min. Then, a solution containing BSA-MI (22.0 mg, 0.33 µmol, 11.9 µmol attached initiating units, 1 equiv.) and NIPAm (270 mg, 2380 µmol, 200 equiv.) in 22 mL phosphate buffer containing 50 mM MPD was added to the syringe and polymerized for 1 h at 4 °C under rapid stirring. Afterwards, the solution was filtered through a 0.2 µm sterile PVDF syringe filter, transferred to a 14 kDa MWCO dialysis membrane and purified by dialysis. For BSA-$MI_{15}$ and BSA-$MI_{25}$ the protein concentration was adjusted to keep initiator concentration constant. The procedure was the same when synthesizing conjugates with $OEGA_{475}$ as monomer.

**RAFT polymerization of POEGA and POEGmA** were synthesized using standard RAFT procedures. PFP-functionalized BTMP and CTAM were used as RAFT agents for the polymerization of OEGA and OEGmA, respectively. All reaction components were dissolved in unstabilized dioxane at a monomer concentration of 50 wt% and polymerization performed at 80 °C using ABCVA as initiator. Ratios of [monomer]:[CTA]:[ABCVA] of [100]:[1]:[0.1] or [20]:[1]:[0.1] were chosen to obtain lower and higher molar mass products, respectively. All components were introduced to a Schlenk tube, deoxygenated by three freeze-pump-thaw cycles, and transferred to a preheated oil bath at 80 °C. The polymerization was stopped after 6 h by immersing the flasks in an ice bath. The polymers were precipitated in cold *n*-hexane. The final protein-reactive polymers were dried in vacuo and characterized by NMR spectroscopy and SEC.

**Table 3.12: Characterization of POEGA and POEGmA and the respective protein-reactive polymers by NMR spectroscopy and SEC.**

| Sample | DP | Conv.[1] | $M_{n,theor.}$[a] [g·mol$^{-1}$] | $M_{n,SEC}$ [g·mol$^{-1}$] | $M_{w,SEC}$ [g·mol$^{-1}$] | Đ |
|---|---|---|---|---|---|---|
| PFP-POEGA | 20 | > 99 % | 9 922 | 6 504 | 7 401 | 1.14 |
| | 100 | > 99 % | 47 938 | 12 269 | 16 212 | 1,32 |
| PFP-POEGmA | 20 | 94 % | 9 857 | 8 916 | 10 049 | 1.13 |
| | 100 | 79 % | 39 957 | 18 626 | 24 702 | 1.33 |

[a] According to NMR spectra of the crude reaction mixtures.

## Appendix:

**Table 3.13: Analysis of FhuA, FhuA-MI and FhuA-PNIPAm conjugates.**

| Sample | $M_{w,calc.}$ [kDa] | Column Combination 1 | | | | Column Combination 2 | |
|---|---|---|---|---|---|---|---|
| | | 100 mM MPD | | 150 mM MPD | | 150 mM MPD | |
| | | $M_w$ [kDa] | Đ | $M_w$ [kDa] | Đ | $M_w$ [kDa] | Đ |
| **FhuA** | 78.8 | | | 416.9 | 1.20 | 255.4 | 1.30 |
| **FhuA-MI$_{36}$** | 86.8 | | | 34.7 | 2.34 | 27.0 | 1.96 |
| **FhuA-PNIPAm$_{200}$** | 900 | | | | | | |
| **FhuA-PNIPAm$_{100}$** | 494 | | | 227.7 | 5.15 | | |
| **FhuA-PNIPAm$_{50}$** | 290 | | | | | 34.6 | 1.56 |
| **BSA** | 66.5 | 50.0 | 1.05 | 52.0 | 1.05 | 45.6 | 1.05 |
| **BSA-MI$_{36}$** | 74.4 | 61.4 | 1.04 | 63.8 | 1.04 | 51.4 | 1.05 |
| **BSA-PNIPAm$_{200}$** | 889 | 371.8 | 1.17 | 202.6 | 1.15 | 117.3 | 1.76 |
| **BSA-PNIPAm$_{100}$** | 482 | 154.8 | 1.13 | 133.7 | 1.05 | 44.9 | 1.69 |
| **BSA-PNIPAm$_{50}$** | 278 | 136.9 | 1.12 | 56.5 | 1.05 | 44.9 | 1.07 |
| **PNIPAm$_{200}$** | 45.6 | 36.0 | 1.89 | 35.2 | 1.82 | 32.3 | 1.47 |
| **PNIPAm$_{100}$** | 22.9 | 26.4 | 1.97 | 24.5 | 1.7 | 26.8 | 1.83 |
| **PNIPAm$_{50}$** | 11.7 | 15.1 | 1.6 | 14.1 | 1.47 | 14.2 | 3.18 |

Combination 1: PSS PROTEEMA, 5 µm, 8x300 mm, 300 Å - 1000 Å - 2000 Å; Combination 2: PSS PROTEEMA, 5 µm, 8x300 mm, 100 Å - 1000 Å - 2000 Å; flow rate 0.5 ml·min$^{-1}$, sample concentration 1 mg·mL$^{-1}$, injection volume 50 µL, column oven set to 23 °C, molar masses estimated based on a pullulan calibration.

# 4 Protein-Polymer Conjugates Analyzed by Analytical Ultracentrifugation - Control of Protein Hydrodynamics by Conjugation and Temperature

**Cooperation:** Maria Mathieu-Gaedke (conjugate synthesis, characterization), PD Dr. Ivo Nischang (AUC concept, measurements, and analysis), Dr. Ulrich Glebe (conceptualization)

## 4.1 Abstract

Analytical ultracentrifugation (AUC) is an absolute, dispersive and destruction-free characterization technique allowing to assess particle properties in solution. PEGylated proteins have been characterized by AUC before and a parachute effect through the attachment of the synthetic polymer observed. Here, the influence of a thermo-responsive polymer on the protein hydrodynamics is studied for the first time by AUC. Therefore, two conjugates of the model protein bovine serum albumin (BSA) with either a long poly-*N*-isopropylacrylamide (PNIPAm) chain or a short oligomer were synthesized by grafting-to, a fast and easy method to obtain conjugates under biologically relevant conditions. Sedimentation velocity analytical ultracentrifugation (SV-AUC) experiments showed that the hydrodynamic properties of BSA can be modified at molecular level using the well-studied thermo-responsive polymer PNIPAm. Moreover, measurements at temperatures below and above the cloud point temperature ($T_{CP}$) of the polymer showed a significant temperature-dependent tailoring of the hydrodynamic properties dominated by the polymer chain.

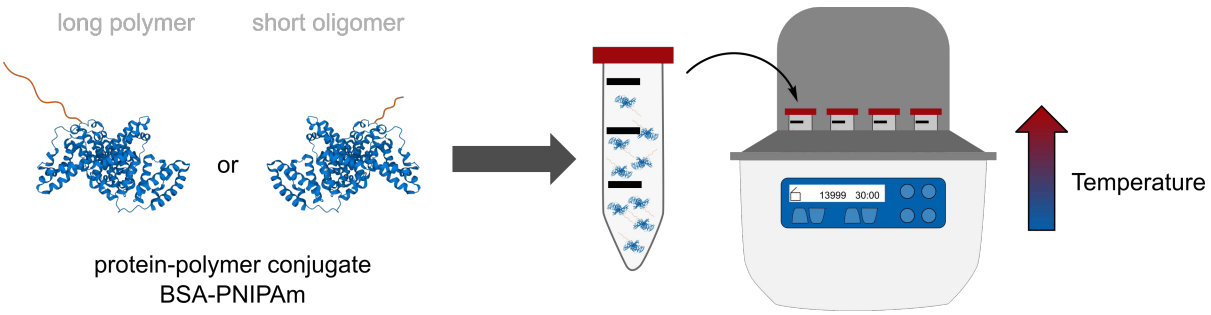


Figure 4.1: Schematic representation of the different conjugate types synthesized to study their temperature-dependent properties by AUC.

## 4.2 Introduction and Theoretical Background

The application of analytical ultracentrifugation (AUC) in structural biology and for the analysis of naturally and synthetically derived macromolecules regained interest within the last years along with the rise of data processing software.[136,200] Information available from this technique is manifold, ranging from destruction-free analysis of molar mass, dispersity or structural homogeneity, stoichiometry of oligomeric associations and thermodynamic binding constants. With approximately

50 µg of sample, a broad overview about the state of the target molecule and its interaction with ligands or other molecules in the solution can be gained, including all relevant hydrodynamic properties of the system.[125,201] Therefore, AUC is a powerful method in the toolbox of (structural) biologists, biochemists, and chemists. It can be utilized for molecules ranging in the size from several hundred Dalton (e.g., lignin-like isoeugenols, $M_w$ ~ 0.4–0.9 kDa) up to thousands of kilodalton (e.g., glycoconjugates with protein tristetraprolin, $M_w$ ~ 7300 kDa).[202]

Examples in **structural biology** include the characterization of surfactant-protein interactions and the solubilization and isolation efficiency of surfactant-free systems for membrane protein handling,[203–206] as well as the study of protein-protein interactions especially in the context for the use as therapeutic proteins or antibodies.[200,207] One outstanding work is provided by RIVAS et al.[208] who studied the assembly of the bacterial division machinery by a combination of AUC, light scattering and fluorescence spectroscopy. The use of complementary techniques resulted in a robust description of the bacterial cell division process including a quantitative description of the involved species, functional energetics of macromolecular complexes, their modes of association and the relative abundance of assemblies (Figure 4.2).[209] AUC contributed to confirm the importance of the division protein FtsZ within the initial state of bacterial cell division and for the formation of the dynamic division ring (Z-ring) that drives bacterial cytokinesis.

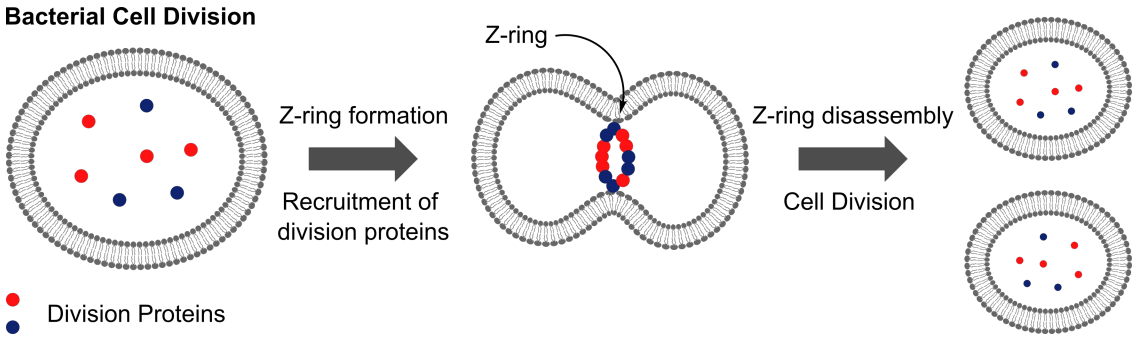


Figure 4.2: Illustration of the bacterial cell division. Within a first initiation period, division proteins including FtsZ are recruited, forming assemblies and result in the development of the Z-ring. Exchange of proteins between cell and Z-ring promotes the final cell division process.[209]

In **polymer chemistry**, AUC is utilized to study colloids,[210] nanoparticles[211,212] and polymeric materials.[213] Similar to the characterization of proteins, one can obtain information about the heterogeneity, molar mass, conjugation efficiency and uptake or accumulation of macromolecules by/in specific cells.[214] Size, shape and morphology of nanoparticles prepared under various conditions can be mapped by AUC which provides guidelines for other researchers based on derived structure-property

relationships.[215] Similarly, for pharmaceutical applications, AUC can provide guidelines for polymeric materials to function as PEG alternatives or protein-mimetics and define relationships between molar mass and hydrodynamic parameters.[216–218] AUC has also proven to be highly accurate in the prediction of particle size and molar mass also for complex compound mixtures as demonstrated for ionic polymers and ionomers.[219,220]

At the intersection of both disciplines, **protein-polymer conjugates** are highly interesting candidates for the analysis with AUC. Those conjugates, obtained commonly by grafting-to (prefabricated polymer conjugated to the protein) or grafting-from (in situ polymerization directly from proteins modified with initiator), display highly interesting properties defined by both components, the protein and polymer. They are in focus of research due to their potential biomedical applications. Conjugation of polymers like polyethylene glycol (PEG) and its alternatives, e.g. polyoxazolines (POx), to proteins increases their pharmacokinetic properties as elongated circulation time in the body and increased stability due to the shielding effect of the polymer shell.[221,222] Even though the scope of synthesis and application for protein-polymer conjugates increases, characterization of conjugates in solution is quite rare. After conjugation, the samples are mostly of a heterogeneous kind making the analysis with analytical ultracentrifugation especially interesting as no tedious workup is needed prior to measurement. Examples found are almost exclusively protein-PEG conjugates and AUC was used to measure conjugation efficiency, purity of the sample, molar mass of species and their tendency for aggregation before and after conjugation.[144,223–226]

Detailed investigation of the behavior of protein-polymer conjugates in solution and how the conjugates hydrodynamic properties are affected by the attached polymer by AUC is rarely reported. Even though examples found in the literature highlight the possibilities of AUC, conjugate characterization by AUC have been addressed by only a few researchers, despite the high potential of this technique. It was found, for example, that the properties of the polymer were effectively transferred to the protein upon PEGylation and the polymer chain functions as a "parachute", affecting substantially the sedimentation behavior of the protein upon conjugation.[144,227] This effect was perceived for other PEGylated proteins and is supposed to be a result of an increased asymmetry of the conjugate compared to the unmodified protein. In other words, the shape of the conjugate with the attached polymer chain differs markedly from the approximately spherical protein. It is assumed, that this change is caused by the attached PEG chain hanging freely in the surrounding solution rather than wrapping itself around the protein molecule.[228]

Motivated by these investigations, the aim of this chapter is to follow the presented examples and go one step further. We aim to change two parameters, the chosen polymer and the temperature range investigated. The shown examples utilized AUC at room temperature, even though for biomedical applications an investigation at higher temperatures would be interesting.[212] PNIPAm as temperature-

responsive polymer conjugated to BSA was investigated in a temperature range between 10 to 40 °C. At around 32 °C, PNIPAm undergoes a coil-globule transition from a former elongated state.[229] Therefore, a strong temperature-dependent influence of the polymer on the conjugate hydrodynamics is assumed. These findings could provide a deeper understanding for the tailoring of conjugate hydrodynamics, especially in the context for biomedical applications and drug targeting at physiological temperature.[230] Furthermore, these measurements could contribute to the detailed description how polymers arrange in conjugates and if they wrap around the protein and/or hang freely into the solution. These questions are still a matter of debate.

The **concept of AUC** is based on the sedimentation behavior of macromolecules at a given gravitational force. In general, the rate of sedimentation in the normal gravitational field of a molecule is defined but also limited by its mass. To fasten up this process, in his pioneering work from the 1920´s, SVEDBERG and co-workers employed centrifugal forces and used the relationship between velocity of sedimentation and hydrodynamic properties of the investigated macromolecules to determine the molar mass of proteins.[231,232]

Within a centrifugal field, the sample experiences three forces namely sedimentation ($F_s$), buoyancy or back diffusion ($F_b$) and friction ($F_c$). Due to these forces, the sample moves and fractionates in the centrifugal field according to the mass, density, and shape of the individual components. The resulting concentration boundary of the fractions can be tracked by different optics implemented in the centrifuge, for example UV–Vis, turbidimetry, refractive index differences, interference optics or fluorescence. Since the separation of the sample happens during the measurement, no tedious purification of sample mixtures prior to analysis with AUC is needed. Also, the measurement takes place in solution and buffer systems suitable to ensure intactness of the measured species can be easily used without disturbing the measurement.[233]

Figure 4.3 illustrates a typical measurement chamber and the three experiments most often applied in analytical ultracentrifugation. In a typical experiment, sample and blank solution are measured simultaneously and exposed to a centrifugal field defined by the rotor velocity and the radial position of the sample. Within this centrifugal field, the former uniformly distributed sample starts to form a concentration boundary of the sedimenting particles according to the molar mass, size and shape of the (macro-)molecules. At high rotor speed and consequently a strong centrifugal field, this boundary is forced to completely move towards the bottom of the measurement cell leading to complete sedimentation of the particles. The motion of this boundary is measured over time and defined as sedimentation velocity of the individual molecules or components within the sample. Therefore, these experiments are commonly named **sedimentation velocity** experiments (SV-**AUC**).[234]

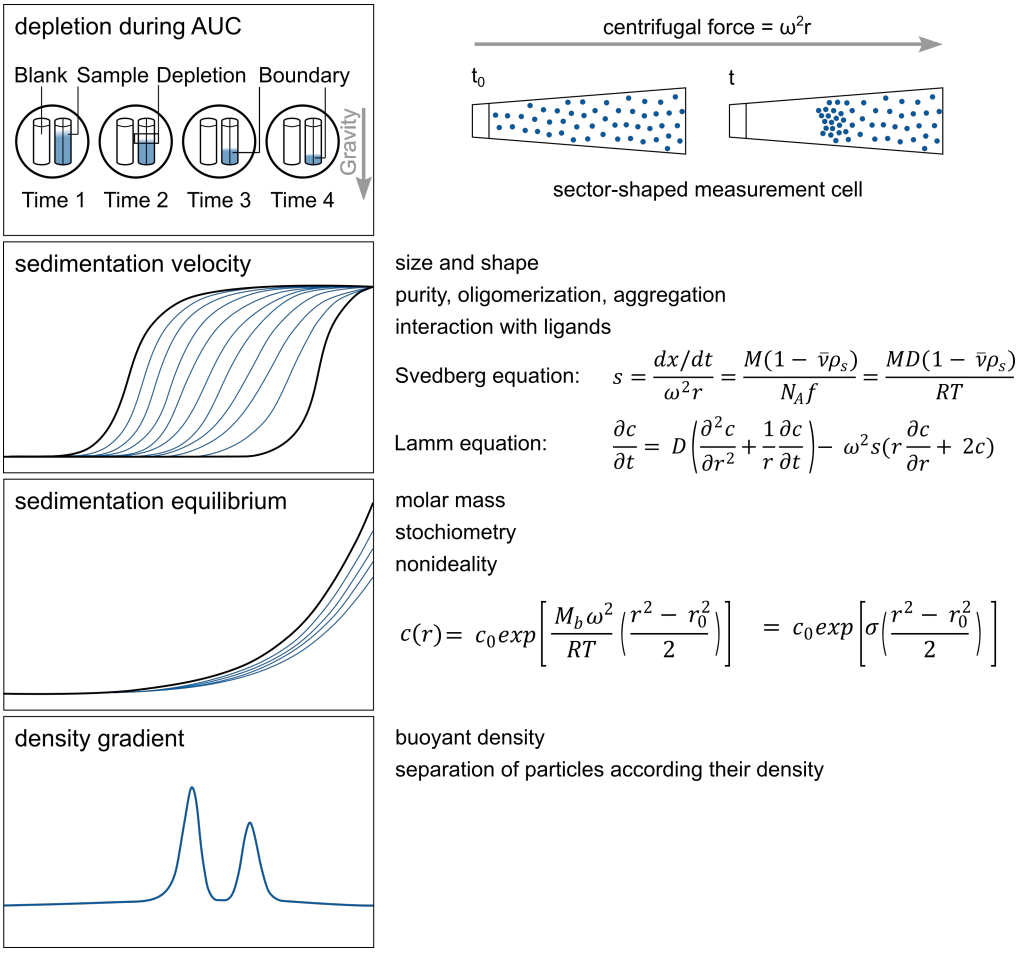


Figure 4.3: Overview of the most common AUC experiments and their corresponding mathematical considerations. Figure adapted based on reference [234]. The x-axis represents the time and the y-axis the intensity of the detector signal.

The relationship between sedimentation coefficient *s*, diffusion coefficient *D* and molar mass *M* of the sedimenting species is given by the Svedberg Equation (4.1).[235] The migration of the time-dependent boundary of the migrating species *dx/dt* within the measurement cell is monitored and at constant angular velocity $\omega$ and radial position *r* the sedimentation coefficient is defined as

$$s = \frac{dx/dt}{\omega^2 r} = \frac{M(1-\bar{\nu}\rho_s)}{N_A f} = \frac{MD(1-\bar{\nu}\rho_s)}{RT} \tag{4.1}$$

where $N_A$ is the Avogadro number, *R* the universal gas constant, *T* the temperature in units *K*, $\rho_s$ the density of the solvent, *f* the translational friction coefficient or frictional force and the partial specific volume of the sample $\bar{\nu}$. The sedimentation coefficient can be understood as the ratio of the sedimentation velocity to the centrifugal field $\omega^2 r$. The right part of the equation arises from the Stokes-Einstein relationship $D = \frac{RT}{N_A f}$ defining the diffusion coefficient *D* to be proportional to the frictional force *f*. This equation can be rearranged and solved for the molar mass based on the sedimentation behavior.[136,218,233–235]

Measuring the concentration-dependent sedimentation coefficient *s* at different concentrations of the macromolecule in solution and extrapolation to infinite dilution leads to the determination of $s_0$

$$s^{-1} = s_0^{-1}(1 + k_s c) \tag{4.2}$$

with $k_s$ being the concentration-sedimentation coefficient (Gralen coefficient). Besides the definition of the migrating species as ideal molecule, one can take the polymer chain end-to-end distance $<h^2>$ into account yielding Equation (4.3) and (4.4) for $s_0$ and $k_s$, respectively.

$$s_0 = \frac{M(1 - \upsilon\varrho_0)}{N_A P \eta_0 < h^2 >^{1/2}} \tag{4.3}$$

$$k_s = B\frac{\langle h^2\rangle^{3/2}}{M} \tag{4.4}$$

*P* is the Flory hydrodynamic parameter that is a function of the contour length *L* and the Kuhn segment length *A* and the diameter of the macromolecular chain *d* being widely used in the description of linear polymer chains. The factor *B* is a parameter for the given macromolecule system and depends on the relative contour length and relative diameter of the macromolecular chain.[136,218,233–235]

Based on Equation (4.1) in combination with the Stokes equation $f_0 = 6\pi\eta R_0$, where $f_0$ is the translational friction coefficient of a spherical particle, $\eta$ is the viscosity of the solution, and $R_0$ is the radius of the sphere, one can describe the sedimentation coefficient for smooth, compact spherical particles or globular proteins $s_{sphere}$ as:

$$s_{sphere} = \frac{M(1 - \bar{\nu}\rho_s)}{N_A f} = \frac{M(1 - \bar{\nu}\rho_s)}{N_A 6\pi\eta R_0} = \frac{M(1 - \bar{\nu}\rho_s)}{N_A 6\pi\eta\left(\frac{3M\bar{\nu}}{4\pi N_A}\right)^{1/3}} = 0.012\frac{M^{\frac{2}{3}}(1 - \bar{\nu}\rho_s)}{\bar{\nu}^{1/3}} \tag{4.5}$$

This $s_{sphere}$-value is the maximum sedimentation coefficient that can be derived for a particle of a given mass. As compact sphere, the particle holds its minimum surface area and therefore the minimal contact with the surrounding solvent molecules. Consequently, the protein or particle experiences its minimum translational friction coefficient $f_0$.[136,218,233–235]

$$D_0 = \frac{k_B T}{P\eta_0\langle h^2\rangle^{1/2}} = \frac{k_B T(1 - \nu\rho)^{1/2}}{\eta_0^{3/2} 9\pi\sqrt{2}((f/f_{sphere})_0)^{3/2}(s_0\nu)^{1/2}} \tag{4.6}$$

The left part of Equation (4.6) is based on the relationship provided by SVEDBERG and the right part additionally takes the hydrodynamic equivalent sphere concept into account. It allows the estimation of the translational diffusion coefficient at infinite dilution based on the numerical solution of the Lamm

equation through the hydrodynamic equivalent sphere concept and determination of $f/f_{sphere}$. An overview of factors determining the properties of particles with the same mass and their influence on particle diameter, diffusion and sedimentation is given in Figure 4.4.[136,218,233–235]

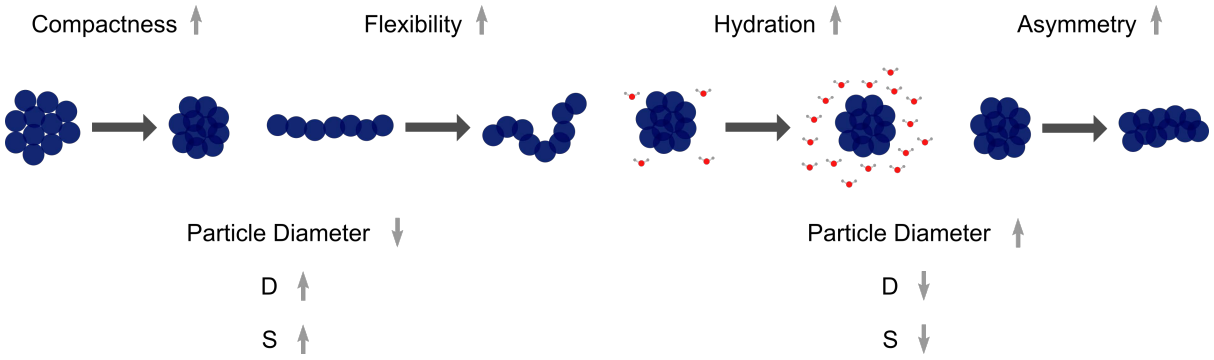


Figure 4.4: Overview of factors determining properties of particles with same molar mass. The light grey arrows indicate an increase (↑) or decrease (↓) in compactness, flexibility, hydration, asymmetry, particle diameter or of the sedimentation coefficient (*S*) and the translational diffusion coefficient (*D*).[208]

Based on these considerations, different information can be obtained by SV-AUC experiments. First, the sedimentation coefficient distribution profile *c(s)* provides information about the oligomerization and aggregation behavior of the particles in solution. Based on theoretical considerations alongside experimental evaluation of sedimentation behavior, further assertions about the system can be made. For example, the ratio of $s_{sphere}$ to the experimentally obtained *s*-value, which is correlated to the ratio of experimentally derived frictional coefficient *f* to the minimum frictional coefficient $f_0$, is a measure for the maximum shape asymmetry from a sphere. Besides asymmetry, this ratio is influenced by the roughness, degree of hydration and expansion (asymmetry) of the targeted molecule. One can simulate different oligomeric states, shapes and molar masses and compare them with the experimentally derived state to get an idea of the appearance of the molecule of interest in solution.[136,218,233–235]

Even though the Svedberg equation and their counterparts provide a solid theoretical understanding of the AUC technique, practically, the Lamm equation is used for the analysis of sedimentation velocity. In simple words, it describes the time evolution of the radial concentration distribution *c(r,t)* during sedimentation within a sector-shaped cell. Based on the numerical solution of this equation, a concentration profile in dependence of the sedimentation coefficient *c(s)* is obtained.

$$\frac{\partial c}{\partial t} = D\left(\frac{\partial^2 c}{\partial r^2} + \frac{1}{r}\frac{\partial c}{\partial t}\right) - \omega^2 s\left(r\frac{\partial c}{\partial r} + 2c\right) \tag{4.7}$$

Based on the determined sedimentation coefficients, relevant characteristics of the investigated system can be evaluated using the equations described above.

While sedimentation velocity experiments are performed at high rotor speed and therefore induce a complete sedimentation of the sample, **sedimentation equilibrium** (AUC-SE) experiments are conducted under moderate to low centrifugal forces. Therefore, competing events take place, namely sedimentation and back diffusion resulting in a thermodynamical equilibrium state. This measurement, in contrast to the sedimentation velocity, is time-independent and yields absolute, calibration free information about the molar mass, nonideality, stoichiometry and binding coefficients in e.g., host-guest systems. Based on Equation (4.7) and considering that $c(t)$=0 and instead, a concentration gradient $c(r)$ along the radius $r$ is established, the equilibrium radial concentration is given by Equation (4.8) with $c_0$ being the concentration at a reference distance $r_0$, $M_b$ the buoyancy molar mass and $r$ the radial distance of the boundary.[234]

$$c(r) = c_0 exp\left[\frac{M_b \omega^2}{RT}\left(\frac{r^2 - r_0^2}{2}\right)\right] = c_0 exp\left[\sigma\left(\frac{r^2 - r_0^2}{2}\right)\right] \quad (4.8)$$

The last experiment presented in Figure 4.3 is the **density gradient** experiment in AUC. For this kind of experiment, a self-forming gradient material is used to obtain a density gradient within the measurement cell during the centrifugation process. Along this density gradient, the sample components accumulate at the radial position where their density matches the density of the surrounding solution. Therefore, it is an alternative towards classical methods like hydrometer or pycnometer. This technique might be familiar to the reader regarding its historical relevance for the support of the hypothesis about the semiconservative replication of DNA by Meselson and Stahl and is still used for the characterization of DNA and genome sequences.[234]

## 4.3 Results and Discussion

**Conjugate Synthesis:** Experiments using unmodified BSA, BSA-oNIPAm and BSA-PNIPAm conjugates were performed at different temperatures to measure the impact of the thermo-responsive behavior of the polymer chain on the hydrodynamic properties of the conjugate in sedimentation velocity experiments. In a first step, conjugates of BSA with oligomeric NIPAm (~ 20 repeating units) and PNIPAm (~ 200 repeating units) were synthesized according to a procedure described by DE GEEST et al. (Scheme 4.1).[105] To evaluate whether an oligomeric short molecule displays same effects in changing the hydrodynamic properties of the targeted protein as its polymeric counterpart, these two length were chosen for initial studies. As described in Chapter 2, PFP-functionalized BTMP was used as RAFT CTA for synthesis of oligomers and polymers and subsequent conjugation to BSA because of the high conjugation efficiencies described for PFP-ester in the literature.[105]

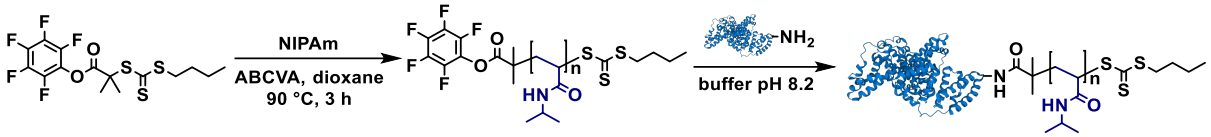


Scheme 4.1: Synthesis of protein-polymer conjugates by the grafting-to approach starting from PFP-functionalized CTA. The polymer was synthesized by a standard RAFT procedure.

The obtained conjugates were analyzed to evaluate the degree of functionalization by SDS-PAGE and MALDI-ToF mass spectrometry (Figure 4.5a & b). Higher molar mass bands in SDS-PAGE indicated a successful modification of BSA. According to the obtained mass differences in MALDI-ToF mass spectrometry, it can be assumed that approximately one to two oNIPAm chains or one PNIPAm chain were attached per BSA molecule, respectively. By using the sterically less hindered oNIPAm, the degree of functionalization by grafting-to BSA was higher compared to the larger PNIPAm, as already described in the literature.[170] As a result, BSA-oNIPAm seems to be composed mainly of the conjugate species whereas the conjugation with the longer PNIPAm leads to a mixture of unmodified protein and conjugate. In addition, both samples contain unconjugated polymer which is not sufficiently removed by dialysis. For complete separation of the mixtures, size exclusion chromatography could be used analogous to the procedure used in Chapter 2.

The thermo-responsive behavior of the polymers and the protein-polymer conjugates was analyzed by turbidimetry and dynamic light scattering (DLS) and the spectra shown in Figure 4.5c and d, respectively. Cloud point temperatures for oNIPAm and PNIPAm were found to be ~ 24 °C and ~ 35 °C, respectively, by turbidimetry measurements. The difference in cloud point can be explained on the one hand by the different molar masses and on the other hand by the more pronounced end-group effect of the hydrophobic RAFT CTA on the oligomer.[236] After conjugation, the cloud point for BSA-oNIPAm shifted to higher temperature as the end-group effect of the hydrophilic protein is more pronounced as the hydrophobic RAFT CTA.[237] Whereas DLS measures the increase in particle diameter as function of the scattered light (derived count rate), turbidimetry measures the decrease in transmittance of the sample. Therefore, cloud point temperatures derived by DLS are slightly lower than the respective ones measured by turbidimetry. As particle diameter increases, turbidity of the solution does not simultaneously increase.

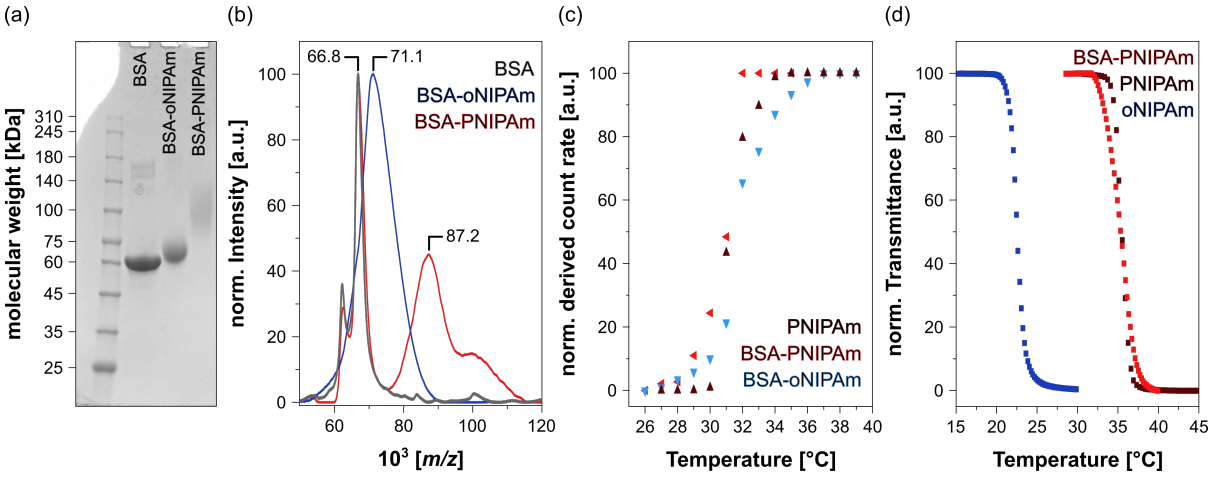


Figure 4.5: SDS-PAGE (a) and MALDI-ToF mass spectra (b) of BSA and the synthesized protein-polymer conjugates. The thermo-responsive behavior of oNIPAm, PNIPAm and the respective protein-polymer conjugates was determined by dynamic light scattering (c) and turbidimetry (d).

**Analysis of Conjugates by SV-AUC:** The conjugates were used for analysis by SV-AUC without further purification as mixtures are typically separated and identified during analysis. The obtained SV data were analyzed using SedFit software and the *c(s)* model based on the numerical solution of the Lamm Equation (4.7) to gain sedimentation and diffusion coefficients which both unveil all details of the sample. For simplification, the same translational frictional ratio $\frac{f}{f_{sphere}}$ for each sedimenting macromolecule with a given concentration is assumed. Measurements at different analyte concentrations and extrapolation of the obtained data to infinite dilution was used for the determination of $s_0$ and $k_s$ according to Equation (4.2) and (4.4), respectively. The corresponding graphs are given in Figure 4.6 showing the concentration profile in dependence of the sedimentation coefficient (a) and the translational friction ratio (b), values for the sedimentation coefficient at infinite dilution (c) and the concentration-sedimentation coefficient (d) in dependence to the analyte temperature. The concentration profiles of native BSA and BSA-oNIPAm conjugates showed two species corresponding to protein or conjugate monomer and dimer based on UV–Vis detection. For BSA-PNIPAm only a single peak was observed. Additionally to UV–Vis, refractive index differences were detected revealing the presence of dimers and trimers in all samples (data not shown). Furthermore, two concentrations were investigated revealing nearly the same distribution profiles and ratios between monomeric, dimeric and trimeric protein (data not shown). As concentration does not seem to have a significant influence on the measurements, further experiments were performed at a sample concentration of 1 mg·mL$^{-1}$ to reduce amount of sample needed per measurement. The sedimentation coefficient $s_0$ for both, BSA-PNIPAm and BSA-oNIPAm is lower than the one determined for the unmodified protein, despite their increased molar mass after conjugation. With increasing temperature, $s_0$ increases monotonically for all samples which is a result of the lower viscosity of the surrounding solution and therefore a lower friction. The concentration-sedimentation coefficient $k_s$ increases after conjugation.

With increasing temperature, $k_s$ decreases for both conjugates and stays almost stable for the unmodified protein. For all measurements, a more pronounced influence on the conjugate hydrodynamic parameters bearing the longer polymer chain were observed.

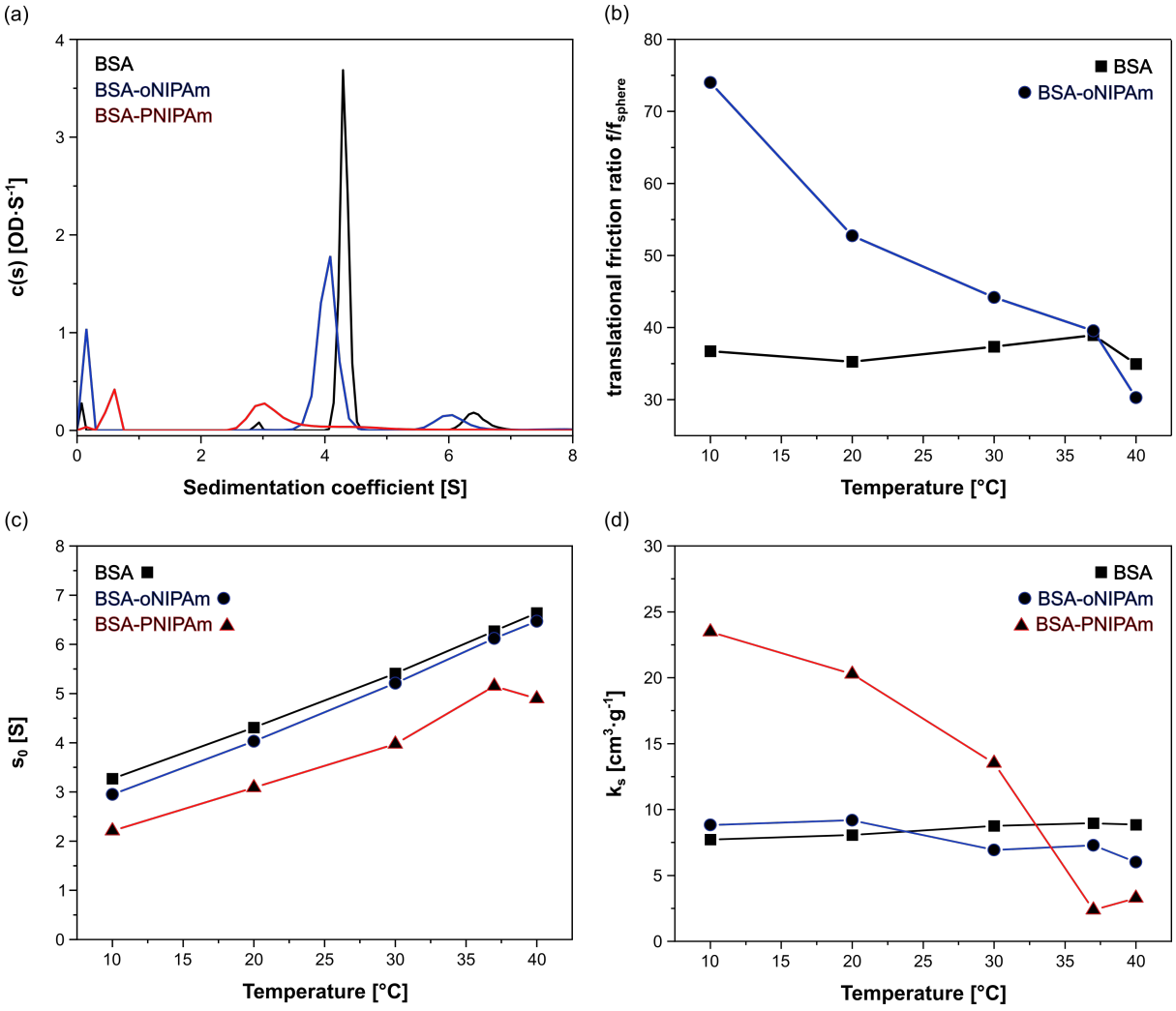


Figure 4.6: Date obtained by SV-AUC of unmodified protein and prepared protein-polymer conjugates. Concentration profiles in dependence on sedimentation coefficient for BSA based on the refractive index traces (a) were measured at 22 °C. The translational friction ratios of BSA and modified BSA-oNIPAm (b), sedimentation coefficients at infinite dilution (c) and Gralen coefficients (d) were determined at various temperatures below and above the $T_{CP}$ of PNIPAm. A sample concentration of 1 mg·mL$^{-1}$ was used for the measurements except otherwise noted.

As already seen in the literature using protein-polymer conjugates derived by PEG and PEG analogs a "parachute" effect is observed in the elongated state of polymer ($T < T_{CP}$) when attached to the globular protein.[144,227,228] The polymer acts as a parachute and decelerates the proteins despite increased molar masses of the conjugate. This effect can be described as deviation from the theoretically assumed sedimentation behavior considering the increase in mass after conjugation. The molecule sediments slower as expected and therefore, the polymer acts as a parachute for the protein. In other words, the polymer modulates BSA´s hydrodynamics, $f/f_{sphere}$ increases wherefore $s_{0,exp} < s_{0,theor}$.

Thus, BSA-oNIPAm and BSA-PNIPAm behave similar as PEGylated proteins at 20 °C. The other observation undescribed in literature so far is the temperature-dependent behavior of a LCST-type polymer when attached to a protein. At temperatures below the cloud point of the polymer, the non-ideality of the system increases after conjugation identified by higher $k_s$- and $k_f$-values of conjugates compared to the native protein. The polymer can therefore be assumed to extend the compact structure of BSA, an observation in accordance to literature reports for PEG-derived conjugates of several proteins.[144,227,228] In contrast, at temperatures above the transition temperature, a coil-globule transition of the polymer chain occurs, and the non-ideality of the system decreases to a value comparable to the unmodified protein. This effect is more pronounced for the longer polymer chain but also barely noticeable for the small, oligomeric NIPAm. An illustration of the assumed effect is given in Figure 4.7. The values derived for $k_s$ at different temperatures provide strong evidence that, after the coil-globule transition, the polymer snuggles in its collapsed state into the protein surface.

We want to point out that this is not a sharp transition as compared to the obtained turbidimetry and DLS results, but still happens within the same region for the predetermined cloud point as measured with the mentioned techniques.

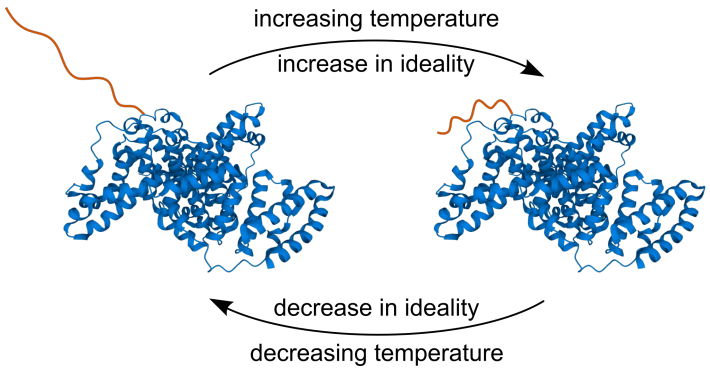


Figure 4.7: Illustration on the temperature dependent behavior of a thermo-responsive polymeric chain attached to a protein as hypothesized based on the findings of the presented research.

In summary, the behavior of the protein-polymer conjugate is mainly dominated by the specific properties of the polymer chain, as already described for conjugates with PEG.[144,228] This effect is amplified with increasing molar mass of the polymer. It becomes significant at a protein-to-polymer molar mass ratio of 3:1, as demonstrated in the shown experiments. Presumably, these properties could be tailored to the characteristics of the chosen polymer component and its specific physicochemical properties.

It must be mentioned that this effect probably depends on the kind and nature of the polymer. We assume, for example, that charged or zwitterionic polymers show a completely different behavior in such an experiment due to interactions of charged polymer and amino acid side chains present at the protein surface. Nevertheless, these experiments were a first step towards the detailed screening of the hydrodynamic behavior of protein-polymer conjugates providing deeper insights in the dynamics effected by the conjugation of polymers to proteins.

### 4.4 Conclusion and Outlook

The influence of smaller and larger thermo-responsive polymers on the hydrodynamic properties of protein bioconjugates were investigated with the model protein BSA using analytical ultracentrifugation sedimentation velocity experiments at different temperatures. The conjugates exhibited different sedimentation behavior below and above the cloud point temperature of the attached thermo-responsive polymer opening the possibility to tailor the temperature-dependent solution properties of conjugates by parameters like polymer type and molar mass.

Next, investigations of more heterogeneous conjugate samples derived by grafting-from are planned. Here, the impact of the number of attached polymer chains per protein and respective mass increase could be evaluated. Therefore, conjugates bearing different numbers of polymer chains but with comparable molar mass increase were synthesized. BSA was modified with either 3 or 30 initiating sites for Cu(0)-mediated radical polymerization and the ratio of initiator to monomer modified to be 200 or 20, respectively. Assuming a complete conversion in both cases, a molar mass increase of 67.8 kDa corresponds to 3 long or 30 short polymer chains. However, measurement of these samples by AUC could not be realized in the time frame of this thesis.

Additionally to these experiments, variation of the polymer itself represents an interesting next step. To elucidate the solution behavior in such kind of experiment, where electrostatic interactions also with the proteins' surface charges and the polymer could take place, could be envisaged.

## 4.5 Experimental Part

**Materials:** All materials used as received and further specified in Chapter 2.5 of this Thesis.

**Instrumentation: Sedimentation velocity experiments** were performed using a Optima Analytical Ultracentrifuge (Beckman Coulter Instruments, Brea, CA) with an An-50Ti eight-hole rotor using double-sector Epon centerpieces with a 12 mm optical solution path length. The radial sedimentation velocity profiles in respect to time were observed using interference optics. All experiments were performed at a rotor speed of 42.000 rpm for 24 h and at specified temperatures.

The cells were filled with 410 µL of the sample in phosphate buffered saline (PBS) and with 440 µL of the solvent PBS as the reference. Sedimentation velocity data were analyzed with SEDFIT (version 15.01b) and the *c(s)* model with a maximum entropy regularization procedure. This model accounts for a numerical solution of the Lamm equation, yielding weight-average translational frictional ratios, $f/f_{sphere}$, and differential distributions of sedimentation coefficients according to Equation (4.6) and (4.7). Density and viscosity of the solvent were estimated as follows. The density of PBS was determined to 1.0056 g $cm^{-3}$ at a temperature of 20 °C with a density meter DMA 4100 (Anton Paar, Graz, Austria). The dynamic viscosity of PBS was measured to be 1.03 mPa·s with an AMVn Automated Micro Viscometer from Anton Paar. The partial specific volumes of the protein-polymer conjugates was approximated from the values of BSA and PNIPAm by linear interpolation, taking their mass fractions into account. The value for BSA was set to 0.733 $cm^3 \cdot g^{-1}$ as predicted by SCHUCK et al.[238] and for the polymers of different degrees of polymerization to 0.842 $cm^3 \cdot g^{-1}$ according to reported values by WINNIK.[239] For PNIPAm, no significant increase in partial specific volume with increasing polymer chain length is assumed according to studies reported by NISCHANG et al.[213,240] Radial profile scans were taken in 3 min time intervals. A suitable selection of scans was used for data evaluation.

**Methods:** Synthesis of PFP-BTMP, subsequent polymerization of NIPAm with degree of polymerization of ~ 200 (PNIPAm) or ~ 20 (oNIPAm) repeating units and conjugation of obtained protein-reactive polymers to BSA was accomplished as described in detail in Chapter 2.5.

# 5 FhuA as Building Block for the Generation of Nano-Thin Membrane Systems - Refolding, Modification, Characterization and Performance as Biohybrid Membrane

**Cooperation:** Maria Mathieu-Gaedke (conjugate synthesis, characterization, membrane design, performance tests), Magnus Schwieters (direct crosslinking of FhuA, characterization, TEM), Dr. Marco Grull (protein expression, extraction & purification), Dr. Deepak Anand (design, expression, extraction and purification of chiral variant), Dr. Tayebeh Mirzaei Garakani (project coordination), Prof. Dr. Ulrich Schwaneberg (conceptualization), Prof. Dr. Alexander Böker (conceptualization), Dr. Ulrich Glebe (conceptualization)

## 5.1 Abstract

This chapter addresses the formation of ultra-thin self-assembled membranes with channel proteins acting as the functional pores as part of the BMBF tandem project “Chiral Membranes II”. Protein-polymer conjugates as building blocks for these membranes were synthesized with copolymer chains incorporating crosslinkable monomers. Due to the high interfacial activity of these protein-polymer conjugates, they can be assembled at the air/water interface. Crosslinking of the polymer chains leads to a stable thin membrane which lies planar on top of a support after evaporation of water. Consequently, the membranes consist of a polymer matrix surrounding the transmembrane proteins. The targeted protein was the well-studied iron transporter FhuA. Using FhuA as nanochannel has the advantage that the channel interior can be functionalized for specific separations. Therefore, membranes could be developed in future not only for separation processes based on size exclusion, but also for interactions based on e.g., charge and chirality. Here, engineered variants of FhuA with modified channels (e.g., open channel variant) and/or varied number of anchoring points for polymer attachment were produced in the group of Prof. SCHWANEBERG (RWTH Aachen) and used for membrane formation. Thermo-responsive polymer chains were conjugated to FhuA, which can be switched from hydrophilic to hydrophobic by increasing the temperature of the analyte solution. Due to this responsivity, the analyte should be forced to pass the membrane barrier preferentially through the protein channels rather than through the polymer matrix.

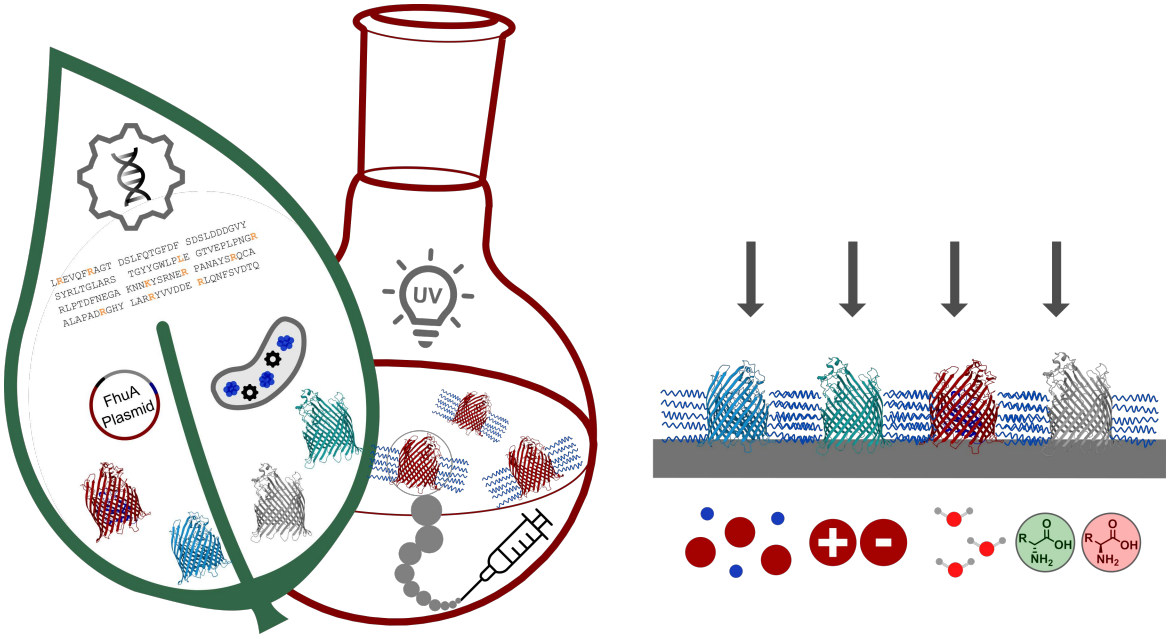


Figure 5.1: The project presented in this chapter combines the know-how of biotechnologists and polymer scientists to create novel protein-based membrane materials. Rational design and directed evolution lead to protein variants expressed in *E. Coli*. Modification of these protein variants and immobilization in a membrane system leads to novel membranes able to adapt the functionality of the protein to fulfill different separation demands such as size exclusion, separation of molecules based on their charge, switchable water permeability or chiral resolution.

## 5.2 Introduction and Theoretical Background

The incorporation of **protein-polymer conjugates in membrane materials** has been shown to be a promising route for the generation of highly precise and energy-efficient alternatives for solely polymeric membranes.[36,38,41] Combining the uniformity, specificity and tailorability of proteins with variable functionalities of polymeric materials, novel materials can be obtained. Taking advantage of the self-assembly behavior of proteins and protein-polymer conjugates in solution and at interfaces, easy and cost-efficient membrane formation can be established.[43] Such membranes have already been prepared by VAN RIJN and co-workers using ferritin-PNIPAm conjugates.[131,241] By a drying-mediated self-assembly procedure, asymmetric membranes lying on top of a porous support were generated. Within his approach, proteins act solely as templates for size, distribution and uniformity of pores desired to be implemented in the membrane material. After a denaturing step, an ultrafiltration membrane with nano-sized pores of uniform size and distribution was obtained.[131]

To test the **performance of a membrane**, water permeability and size exclusion experiments are usually performed. Transport of analyte molecules through pores happens convectively, i.e. due to a concentration and/or pressure gradient at the membrane between upstream and downstream side.[40,242,243] Consequently, for size exclusion, the size of the pore must be smaller than the size of the particle desired to be rejected. Accordingly, Au nanoparticles were rejected by the mentioned conjugate membranes when they were larger in diameter than the protein-templated pores.[131] Another

observation was made during operation of these membranes. When using PEG polymers of different sizes, no rejection was obtained. A possible explanation is the solution-diffusion model for membrane systems. Here, the analyte is dissolved in the membrane material itself, which is mostly composed of polymers. The analyte diffuses through the membrane and desorbs at the downstream side of the membrane. This process commonly occurs in gas permeation membranes in non-porous membrane systems but could also happen as side-effect in other membrane systems.[242]

The introduced protein-polymer conjugate membranes make use of stimuli-responsive polymers. **Stimuli-responsiveness** is a concept widely used to modify the gating-behavior and to switch the permeability of membrane systems.[57,244–247]. Such "smart" polymer materials undergo a phase transition upon applying a specific stimulus such as temperature, pH, presence of specific ions or molecules, UV light, ion strength, or an oxidation process.[247] Membranes shown in literature were either composed of stimuli-responsive building blocks or the pores of a premanufactured membrane subsequently modified by grafting respective polymers from or to the surface. In the first approach, membranes are commonly composed of smart hydrogel systems based on thermo-responsive polymers with LCST behavior. LCST-type polymers undergo a coil-globule transition above a specific temperature resulting in collapse of the former elongated polymer chains and increase in hydrophobicity.[248] Therefore, smart hydrogel membranes exhibit a loose, hydrophilic state before and a dense, hydrophobic state after an increase of analyte temperature above the cloud point (Figure 5.2 left). In this example, the permeability is reduced above the cloud point.[247] For the second approach, also called smart gating pores, the permeability can be increased or decreased, depending on the grafting yield and branching of the polymer grafted to or from the membrane pore surface (Figure 5.2 right). For low grafting yield, an opening of the pore and an increase in permeability is obtained. In this case, a contraction of the polymer corona is more likely than aggregation events to happen. In contrast, at high grafting yield, polymer chains are in closer proximity to each other and aggregation is more favored and leads to a tighter blockage of the pore and a decrease of permeability.[247,249,250] The shown examples demonstrate the effect on permeability for polymers undergoing a coil-globule phase transition at higher temperatures. On the other end of the spectrum, an upper critical solution temperature (UCST)-type polymer is in a globule state at lower temperatures and elongates as temperature increases. For these polymers, the described effects are the other way around.[247,251–254]

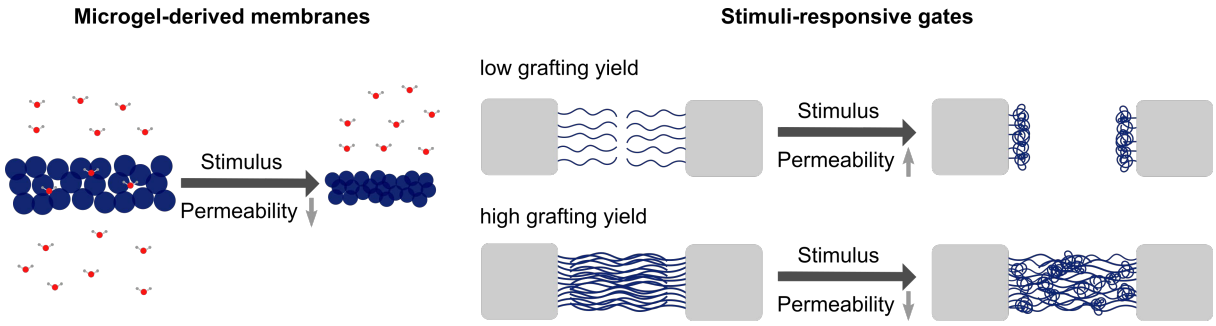


Figure 5.2: Stimuli-responsive membrane systems can be polymer- or microgel-derived. Depending on grafting- and packing density, permeability of the membrane is increased (↑) or decreased (↓). Inspired by reference [247].

Different techniques can be used to characterize protein-derived building blocks in solution on the one hand and at the interface within the generated membrane materials on the other hand.[126] Frequently used in material sciences is **scanning force microscopy** (SFM), a surface sensitive technique able to derive membrane thickness, surface topography including roughness and sample stiffness.[255–257] In simple words, the interaction of a tip mounted on a spring-like cantilever with the sample is measured. In contact mode, the feedback signal required to keep the cantilever at a constant position as measure for deflection of the cantilever is used. In tapping mode, also called dynamic contact mode, the cantilever oscillates up and down at or near its resonance frequency. When the tip comes close to or reaches the sample surface, frequency and amplitude of the cantilever oscillation are altered and used as feedback signal for the device to adjust the height of the cantilever to maintain a pre-set oscillation amplitude. In non-contact mode, additionally to the pre-set oscillation amplitude an average tip-to-sample distance is defined. Change in oscillation as a result of long-range forces acting between tip and sample are the basic principles for this scanning force microscopy mode.[255–257]

Above and beyond SFM, more detailed information from soft-matter materials can be gained using **scattering techniques**. Depending on whether x-ray or neutron irradiation is used, sample to detector distance and angle of incidence, one distinguishes between techniques under small angle (SAXS and SANS), wide angle (WAXS and WANS) or grazing-incidence small angle (GISAXS and GISANS) scattering conditions.[258–260] In SAXS and SANS, a collimated beam of monochromatic x-rays or neutrons is used to illuminate a sample in transmission mode. At any interface with a change in electron density or nuclear/spin density, elastic scattering leads to deflection of the beam from its incident trajectory. The scattered waves interfere with each other leading to an increase or decrease of the reflected wave amplitude. A 2D-detector measures the position (angle) and intensity of the interference pattern from these reflected waves. The resulting image represents the spatial mapping of changes in material density. Integration along azimuthal angle results in a scattering signal curve, also referred to as scattering profile. Finally, fitting of these curves is used to gain information about the state of the sample such as size, shape and spatial organization (Figure 5.3).[258,259,261,262] In small-angle experiments, the measurement is performed close to the primary beam or in other words, small 2θ-values. Therefore,

the sample-detector distance is in long range to obtain a sufficient resolution. Contrary, in wide-angle experiments such as WAXS and WANS, the measurement is performed at large 2θ-values and the detector is positioned close to the sample. Based on this, either an atomic resolution by WAXS/WANS or nanoscale resolution by SAXS/SANS can be achieved.[258,259,261,262]

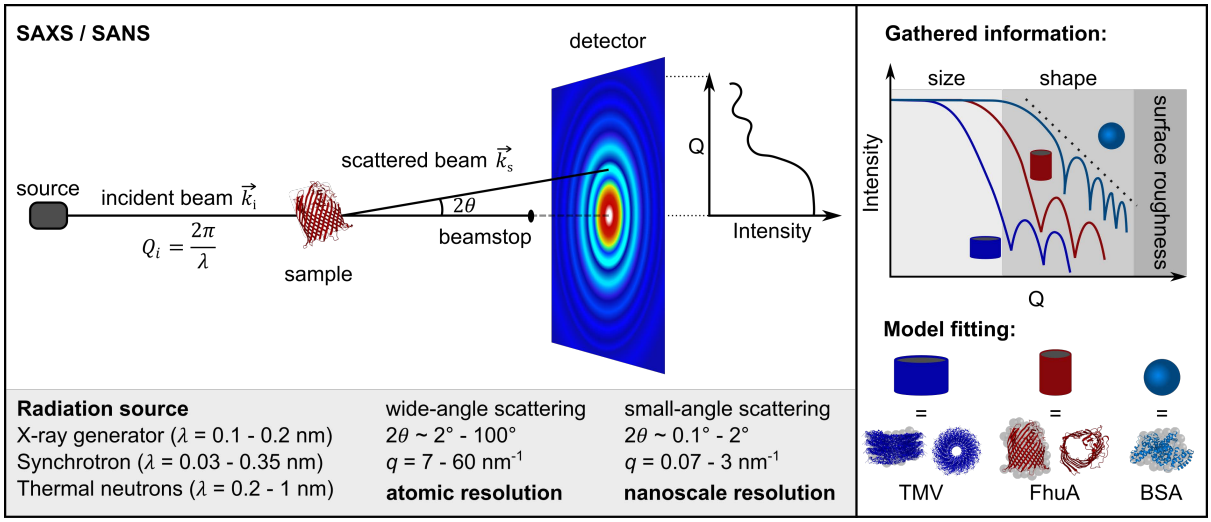


Figure 5.3: Visualization of wide/small angle x-ray and neutron scattering experiments. The sample is illuminated by a collimated beam of monochromatic x-rays or neutrons in transmission mode. The detector is placed directly behind the sample and measures the intensity in correlation to the scattering angle θ. The intense reflected beam and scattering in the incident plane is attenuated by a rod-shaped beam stop. Integration along the azimuthal angle results in a scattering signal curve providing information about size, shape and surface roughness of the investigated particles. Inset are the crystal structures (PDB IDs 2XEA,[263] 1BY3,[47] and 4F5S)[83] of proteins TMV, FhuA and BSA, respectively. Figures inspired by references [261,262].

Changing the sample from bulk to thin films, small-angle scattering techniques suffer from a low sensitivity and low signal intensity because of the small scattering cross-section in transmission mode. GISAXS, where a very shallow incident angle of the beam below the critical angle for total external reflection is used, is a surface sensitive method more sophisticated for thin film analysis.[260,264–267] At such narrow angles, a foot-print effect is observed, where the beam travels a significantly long path alongside the sample. In other words, at narrow incident angles, the scattering cross-section is increased horizontally. In contrast to SAXS experiments, those experiments are operated in reflection geometry (detector placed vertically behind the sample). Structural information in the horizontal plane of the sample is obtained by this technique, such as long-range ordering. As in SAXS, the diffuse scattering arising from the sample is measured by a 2D detector and a mapping of scattering as function of the scattering angle 2θ is observed, providing information normal to the surface plane (z-axis), along the surface plane (x-axis) and perpendicular to the surface plane (y-axis). As the interference occurs at every layer with a difference in electron density, multilayer thin film analysis of each individual layer in the film can be accomplished (Figure 5.4 top).[260,264–267]

In x-ray reflectivity (XRR), the same principles as for SAXS and GISAXS apply. First, the sample is illuminated by a collimated beam around the critical angle for total external reflection. At every interface, where electron density or refractive index changes, a portion of the beam is reflected whereas the rest is refracted and penetrates deeper into the sample until it reaches the next interface. Again, the intensity of the interference pattern of the reflected waves is measured. Whereas in SAXS and GISAXS the angle of incidence is fixed and interference pattern as function of 2θ is measured using a 2D detector, the incident angle is varied in XRR and the intensity of reflection for a range of angles around the critical angle is measured by a point detector providing a reflectivity curve (reflectometry pattern). In specular XRR, as by the definition of specular reflection, the angle of incidence equals the angle in which the reflection intensity is detected. As the incident angle defines the penetration depth, specific layer parameters in vertical direction such as density (critical angle), thickness (oscillation) and roughness (dampening of signal, curve shape, amplitude) can be evaluated from these reflectivity curves based on well-known mathematical and physical considerations (Figure 5.4 bottom).[267–269]

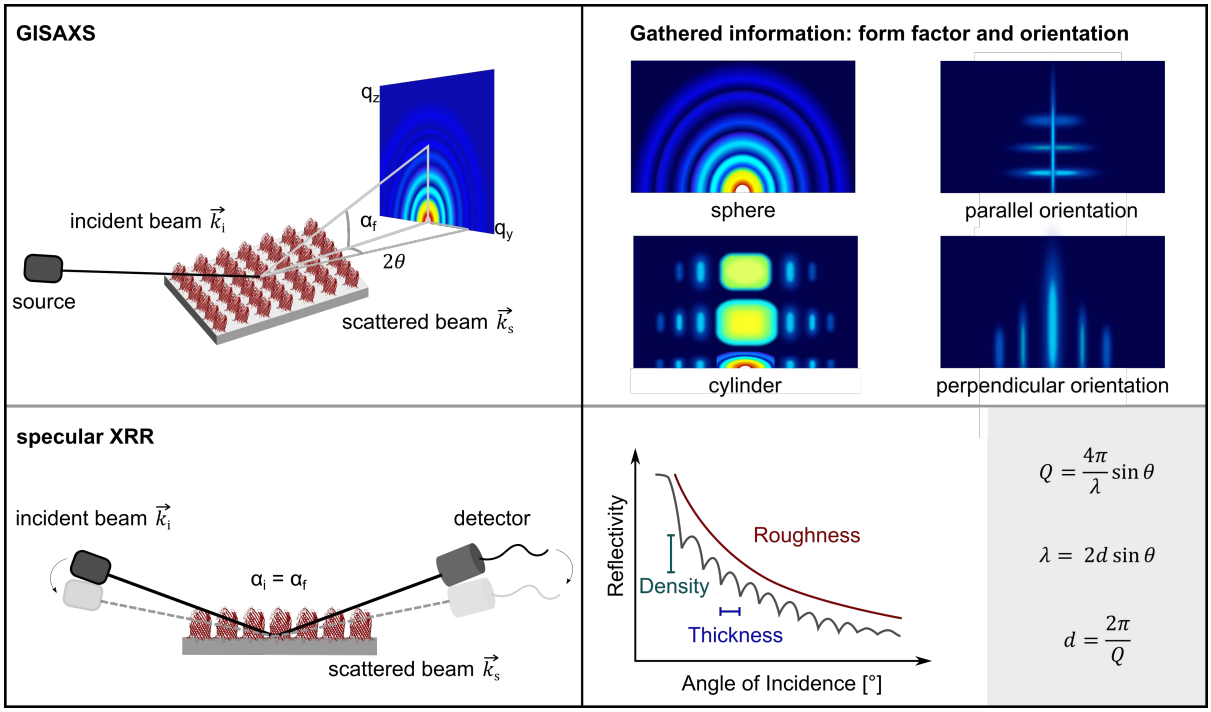


Figure 5.4: Illustration of GISAXS and specular XRR experiments. A flat surface is illuminated by a collimated and monochromatic beam under very small incident angles. The incident angle defines the penetration depth in the surface by the beam. Scattering intensity is either measured at fixed incident angle in relation to scattering angle θ (GISAXS) or at varied incident angles (XRR) by a 2D-detector or point-detector, respectively. 2D scattering patterns and reflectivity curves provide information about shape, orientation, surface density, thickness and roughness of the investigated material. Figure inspired by references [260,265,269].

**Examples** found in the literature impressively show the usability of such advanced techniques for protein-polymer derived materials.[126] Especially improved modelling systems make structure determination of protein-polymer conjugates highly precise and more achievable nowadays. Pioneering

work has been done in the group of OLSEN using the model protein mCherry. They demonstrated the use of advanced scattering techniques to study protein-polymer interactions in semidilute blends,[270] to determine the shape of protein-polymer conjugates by SANS and SAXS,[271,272] study ordering and self-assembly behavior for a variety of copolymers in concentrated solutions,[51,155,273] and in thin films.[274] In a recent study, libraries of different proteins have been investigated to propose guidelines for predetermination of self-assembly behavior of protein-polymer block copolymers. Correlation between protein size and quality of ordering was determined by SAXS showing an initial increase in quality up to a protein size of 30 kDa. Above this point, the quality began to decrease again with increasing protein size.[275] Those findings are essential for the development of protein-polymer hybrid membranes where performance correlates with protein orientation and ordering within the membrane material.

Channel-forming proteins, such as mCherry from the example above, are especially favorable for the incorporation in novel membrane materials. To obtain those proteins in high quantities, **recombinant protein production** is often utilized in biotechnology.[276] Recombinant genes, blueprints of the desired protein of interest in form of a cloning vector, are used to manipulate an organism to express large amounts of the recombinant gene. Additional modifications in the gene sequence as part of protein engineering lead to generation of mutant variants.[60,277] Bacterial and eucaryotic systems with *Escherichia Coli* and yeast as most prominent examples are frequently used for large-scale protein production. In addition, novel cell-free systems to produce the protein of interest are a promising alternative route to cell-based systems.[278,279] In such, components of crude cellular lysates of microorganisms, plants, or animals are used as reaction mixture to produce the protein of interest exocellular.[278] After overexpression, protein material is extracted and isolated from the (cell) components and other protein products either from the cell lysate, membrane or generated inclusion bodies.[280]

**Inclusion bodies** are aggregates of proteins in different folding states. They are a result of enforced overexpression up to a point, where the cell cannot handle the huge amount of protein anymore. Highly hydrophobic proteins, such as membrane proteins, are more predestinated to form inclusion bodies than their hydrophilic counterparts.[281–283] Those aggregates must be extracted from the cell under relatively harsh conditions as cell membrane and interactions of proteins entrapped in inclusion bodies must be interrupted. Typically, denaturing conditions are used for protein extraction and solubilization. SDS is widely used for this step due to its near-universal denaturing and solubilization properties. Unfortunately, already a low concentration of SDS leads to denaturation of proteins in solution. As a result, a refolding step is needed after extraction and solubilization. Refolding of a protein from denatured state can be visualized in a refolding funnel, with the final folded state at the bottom of the funnel (Figure 5.5).

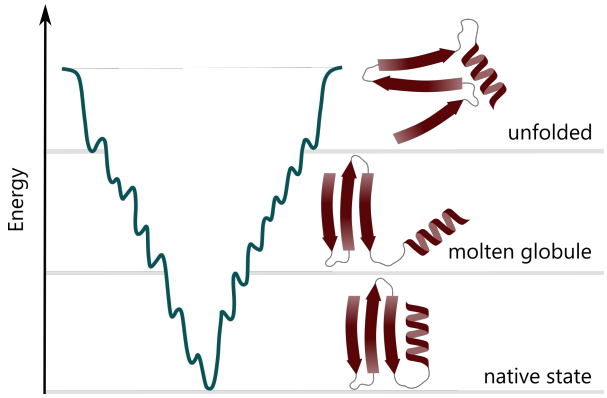


Figure 5.5: Energy landscape for the refolding of proteins starting from a tertiary structure denatured state. The protein undergoes different transitions from unfolded stated to a molten globule state until it reaches its final native state.

As a rule of thumb, refolding after denaturation happens to an extent of ~ 60 – 70%, depending on the refolding procedure.[284,285] Those procedures can be one-step dialysis, step-wise dialysis, descending denaturant concentration, buffer exchange by gel filtration, either rapid, slow, pulsed (protein/denaturant solution is added into refolding buffer) or reverse dilution (refolding buffer is added in protein/denaturant solution), or mixing and solid phase refolding.[280,285–287]

For **membrane proteins** having both hydrophobic and hydrophilic regions, detergents like phospholipids or block copolymers mimicking the natural cell membrane are favorably used for solubilization and refolding. An alternative strategy has been presented by PRIVÉ. He utilized specific properties of the small amphipathic molecule 2-methyl-2,4-pentanediol (MPD). It has been found that the addition of MPD to a protein solution prior to addition of SDS leads to a significantly higher concentration of SDS required to inactivate proteins. The concept was transferred to reactivate SDS-denatured proteins by the addition of high quantities of MPD.[288,289] Refolding efficiencies up to 67% have been achieved after screening of various conditions to define the optimum for refolding. It has to be noted that no refolding was achieved in the absence of SDS, indicating that the performance depends on the balance between SDS and MPD.[289]

## 5.3 Results and Discussion

Within this chapter, an approach for the use of FhuA-polymer conjugates as universal building blocks for nano-thin membrane generation is presented. Integrated in a BMBF tandem project, part of this thesis is the proof of concept for the immobilization of FhuA pores in a membrane matrix composed of thermo-responsive PNIPAm and UV-crosslinkable moieties for covalent tethering using an external trigger. Taking advantage of the thermo-responsive behavior of PNIPAm, generated membranes were put into service at different temperatures below (hydrophilic, water permeable matrix) and above (hydrophobic, water impermeable matrix) the cloud point temperature of the polymer. Parallel to this work, the direct crosslinking of FhuA after assembly at the air/water interface in a Langmuir trough

using a homo-bifunctional crosslinker was studied by Magnus SCHWIETERS and the results presented in his thesis with the title "Protein nanopore membranes prepared by a simple Langmuir approach".[290] After Langmuir-Schaefer transfer of the crosslinked films to a solid support, membranes comprised of mono-, double or multilayers were characterized by surface sensitive techniques such as SFM, XRR, GISAXS, transmission electron microscopy (TEM) and helium ion microscopy (HIM). Their performance in terms of permeability for water and ions was tested as well. Results were successfully published in *small* and the reader is encouraged to take a look in the publication to gain a deeper insight in this topic.[291] In this approach, the protein is not functionalized prior to membrane formation and mono- as well as multilayers are accessible comprising highly packed proteins in the film. Hence, this system perfectly serves as reference for the present thesis. Some of the data shown within this section will therefore cover denoted membranes/protein films using the approach established by Magnus SCHWIETERS.

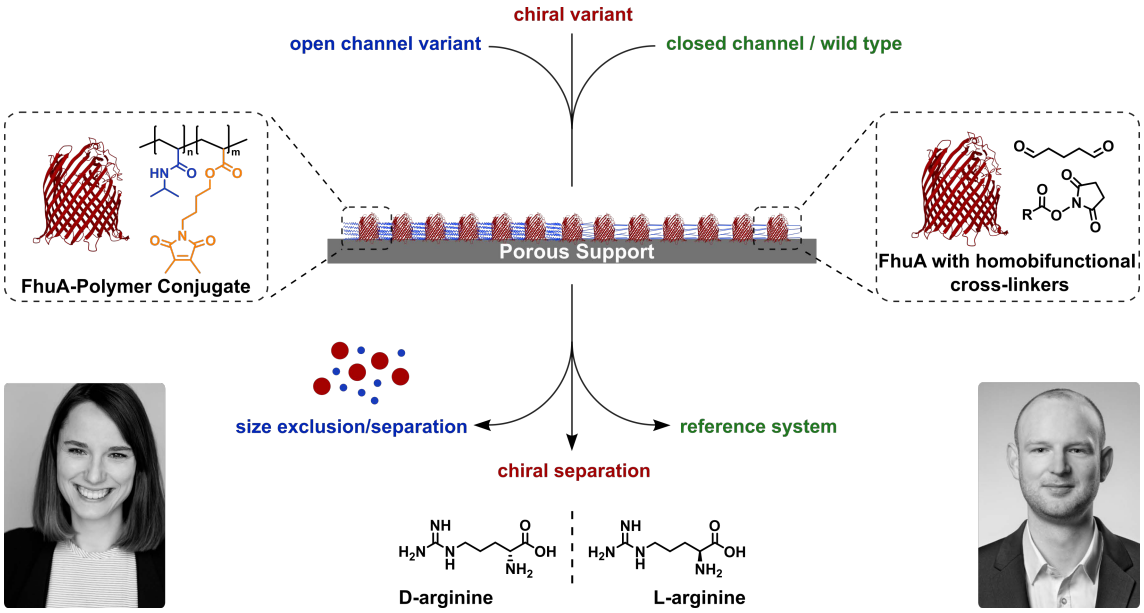


Figure 5.6: Protein-derived membranes as objective in "Chiral Membranes II" were investigated in two doctoral theses. In the first approach, presented in this thesis, protein-polymer conjugates are used as building blocks covalently crosslinked on top of a porous support. In the second approach, investigated by Magnus SCHWIETERS, FhuA is directly used as building material. Therefore, the protein is self-assembled at the air/water interface, immobilized by crosslinking using glutaraldehyde and transferred to support materials by Langmuir-Schaefer approach. Variants explained in detail in the following section.

**Variants of FhuA:** Within the scope of this thesis, FhuA wild type (FhuA WT), an open channel variant FhuA $\Delta CVF^{tev}$ and a modified open channel variant with reduced number, but optimized position of lysine residues FhuA $\Delta CVF^{tev}K_{11}^{up}$ (FhuA A2a) were investigated.[132] The number of anchoring points for initiator or polymer conjugation to the protein outer surface is equal to the amount of accessible lysine residues. This number varies between the different protein variants used in the present thesis and an overview of those variants is provided in Figure 5.7. FhuA A2a was found to be very sensitive towards modification leading to precipitation of the protein after MI synthesis and polymerization.

Thus, analysis with this variant is quite rare and most investigations had to be performed with FhuA WT and FhuA ΔCVF$^{tev}$. Additionally, the significantly reduced number of anchoring points in FhuA A2a will lead to a more porous polymer mesh around the protein by the grafting-from approach. As a result, membrane performance was shifted towards higher permeability as less material is deposited on top of the porous support material compared to the reference system with wild type and a closed pore.[134] Misinterpretation of the data assuming the higher permeability to be due to the open channel constitutes a great risk and contributions of permeability through the protein pore and through the polymer matrix can probably not be distinguished. Therefore, a new variant should be designed with an open channel but same number of anchoring points as in the wild type. First simulations to design such a variant were performed in the group of SCHWANEBERG, but final development was not accomplished in the anticipated time scope.

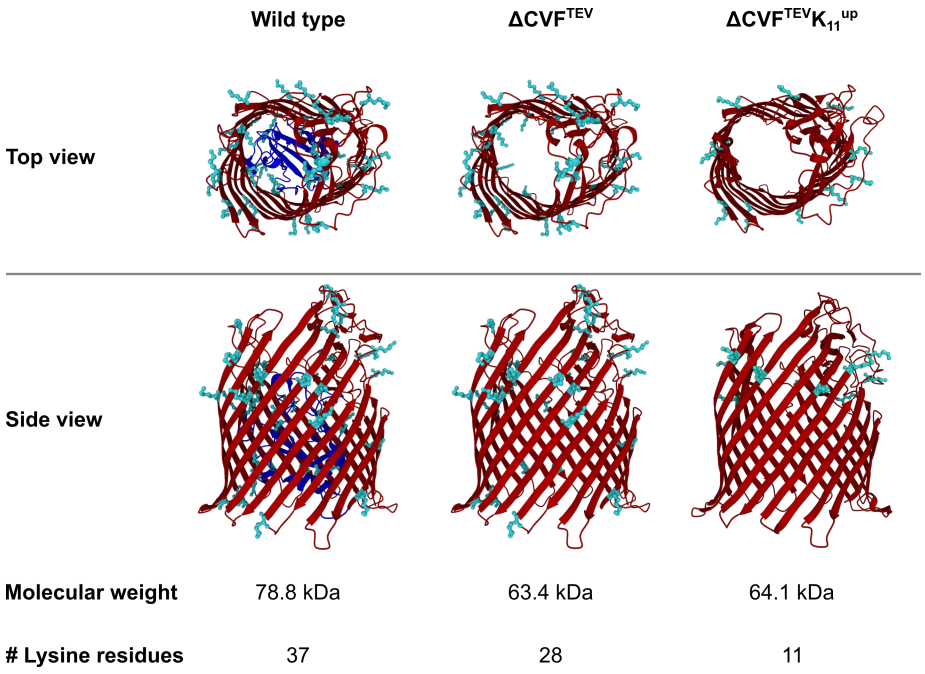


Figure 5.7: Overview of different FhuA variants used within this thesis. Lysine residues are highlighted in cyan. Point mutations were simulated using the respective tool provided with the PyMOL[292] software based on provided sequences by KINZEL.[293] Protein structures illustrated using MOL 3D web app implemented in the protein data bank website and PDB ID of FhuA WT 1BY3.[23,47]

Initial studies for polymer conjugation, membrane generation and performance were focused on FhuA WT and the newly developed chiral variant P6F4 and its parent variant 3G.[63] The main scope of the project “Chiral Membranes II” was to obtain a membrane system for chiral resolution. Unfortunately, the obtained variants have shown to be not suited for downstream processes limited by the separation process within the protein channel. Separation occurs due to a time delay, where one enantiomer passes the functionalized channel protein 300 ps faster compared to the other enantiomer. In the published experimental setup, enantiomeric excess was obtained using an equilibrium setup.[63]

For downstream processes like membrane or column systems, an amount of protein unrealizable in a thin membrane or a very long column filled with protein would be needed, to have a sufficient time delay to separate the enantiomeric mixture. Therefore, experiments using these variants were discontinued.

**Protein refolding:** FhuA as natural membrane protein can be found in the outer membrane of *E. Coli*. Nevertheless, recombinant protein production and isolation of the protein from the outer cell membrane under non-denaturing conditions yields only a few milligrams of material. To obtain FhuA in gram scale, biotechnologists at the RWTH Aachen established the production of FhuA by overexpression in *E. Coli*. Refolding after extraction of protein from inclusion bodies using SDS was accomplished using the small amphiphilic molecule MPD. The method presented by PRIVÉ et al.[288,289] was adapted and modified by SCHWANEBERG and co-workers to induce refolding of FhuA while simultaneously removing SDS by a refolding protocol. Former protocols using detergents and block copolymers resulted in a shielding effect making modification of the protein unachievable.[73] MPD as small amphipathic molecule stabilizes the hydrophobic transmembrane area of FhuA without provoking this shielding effect.[73,132] To estimate the refolding efficiency, I performed dialysis of SDS-denatured FhuA under various conditions (Table 5.1) and analyzed the samples by CD spectroscopy.

**Table 5.1: Summary and description of refolding protocols for FhuA WT after SDS extraction from inclusion bodies using either MPD, MPD/SDS protocol or dialysis without refolding agent.**

| # | Sample | Conc. FhuA [mg·mL$^{-1}$] | T [°C] | Buffer Composition | Description |
|---|---|---|---|---|---|
| 1 | SDS denatured | | | | Prior to refolding |
| **2** | FhuA protocol 1 | 1 | 4 | 10 mM phosphate buffer, 50 mM MPD | Buffer change every 24 h, 3 days in total |
| **3** | FhuA protocol 2 | 2 | 4 | | |
| **4** | FhuA protocol 3 | 4 | 20 | 10 mM phosphate buffer, 250 mM MPD | |
| **5** | FhuA protocol 4 | 1 | 4 | 10 mM phosphate buffer, 250 mM MPD, 0.1 mM SDS | Buffer change every 48 h, 6 days in total |
| **6** | FhuA protocol 5 | 0.1 | 4 | | |
| **7** | Refolding w/o MPD | 1 | 4 | 10 mM phosphate buffer | Buffer change every 24 h, 3 days in total |
| **8** | SDS/MPD protocol | 0.5 | 20 | 50 mM phosphate buffer, 60 mM SDS, 1.5 M MPD | 1 mg/mL FhuA WT in 50 mM phosphate buffer and 120 mM SDS mixed 1:1 with 3 M MPD in 50 mM phosphate buffer and stirred for 24 h |
| **9** | Autoclaved | 1 | 120 | 10 mM phosphate buffer, 50 mM MPD | After refolding (protocol 1) autoclaved for 30 min |

Figure 5.8 compares the respective CD spectra of protein samples prepared by the different refolding procedures. A reference spectrum of a FhuA WT sample extracted from the outer membrane under non-denaturing conditions is shown for comparison. The respective data were obtained from the Protein Circular Dichroism Data Bank (PCDDB),[294] entry CD0000108000.[295] For clarity, excerpts for protocols 1–5 are added (Figure 5.8 c & d). Respective spectra for SDS-denatured sample prior to refolding, after refolding and denaturation with an autoclave, after refolding using the SDS/MPD protocol as presented by PRIVÉ et al. and after dialysis against phosphate buffer in the absence of stabilizing agents including MPD are shown in Figure 5.8 b. The CD spectrum of intact, folded FhuA WT resembles the typical shape for β-sheets and has a minimum around 215 nm. In general, no major difference between the tested protocols was observed. For protocol 4 and 5, a slightly higher content of α-helices in the sample was present, deduced by the double minimum around 213 nm.[198] Compared to the reference spectrum, all samples showed a significant deviation indicating an incomplete refolding. This result was not unexpected, considering the limitations of refolding efficiency by classical dialysis protocols.[285] Surprisingly, similar results were observed for refolding in the absence of the refolding agent MPD, most likely due to residual SDS present in the sample, which could also act as stabilizing agent.[296]

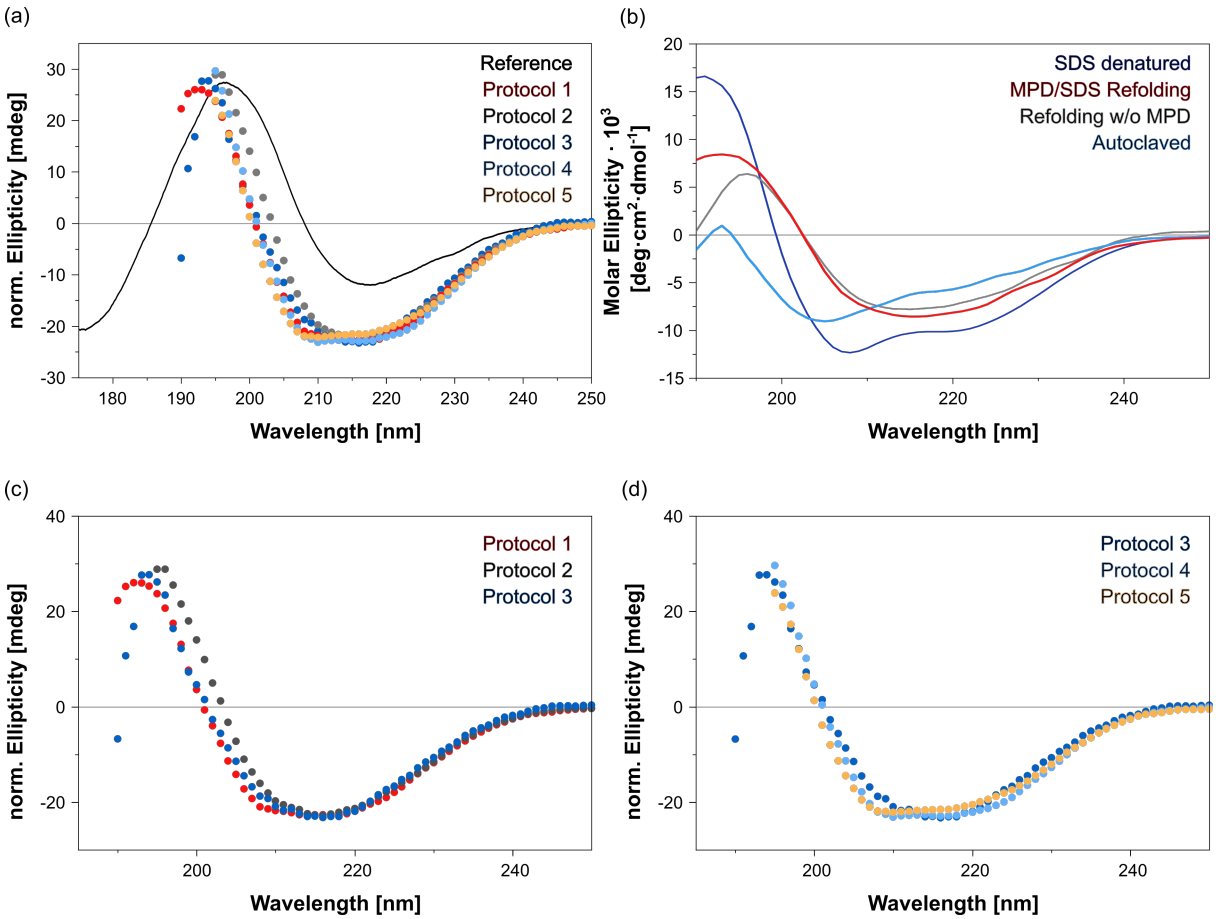


Figure 5.8: CD spectra of SDS-denatured, autoclaved and refolded FhuA WT samples using the stated conditions summarized in Table 1.

Even though CD spectroscopy is considered to test the secondary structure of proteins rather than their tertiary structure, deviations between CD spectra of different membrane proteins can be seen (Figure 5.9). Based on the structural variations, huge differences in shape, position of maxima and minima and intercept with the x-axis occur. On the other side, only slight changes are expected for small structural deviations, like in the case of FhuA WT and BTuB. Interestingly, refolded FhuA WT is more comparable to pectate lyase, a β-helical protein as can be seen in Figure 5.9 b. Other refolding protocols to increase the percentage of functional protein after recombinant protein production under the chosen conditions or at least a proper test of functionality after refolding need to be established. However, this was beyond the scope of this thesis. For preparation of protein samples, protocols 1 and 2 were preferably used throughout the whole thesis and expected to result in FhuA samples consisting of a large amount of refolded protein.

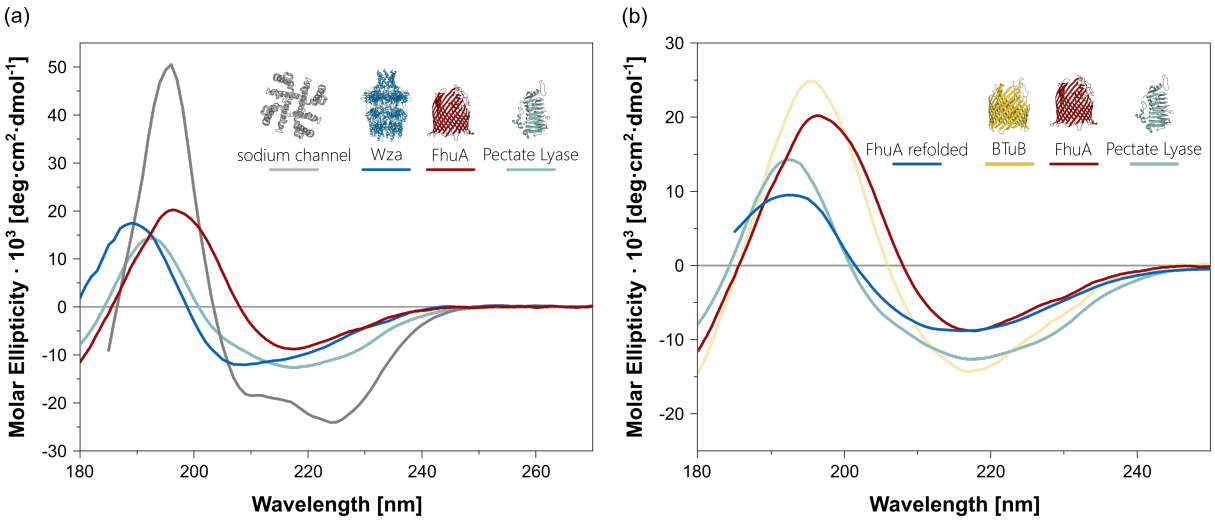


Figure 5.9: CD spectra of different membrane proteins (a) and overlay with measured spectrum of FhuA refolded by dialysis with MPD using protocol 1 (b). Typical membrane proteins composed of different secondary structure types were used and depicted as inserts: sodium channel pore (grey, predominantly antiparallel alpha-helical bundle); Wza (blue, mixed helical, beta sheet and unordered structure); FhuA (red, predominantly beta barrel); pectate lyase (green, beta helical structure); BTuB (yellow, predominantly beta barrel). The CD spectra correspond to PCDDB[294] IDs CD0004012000,[49] CD0000128000,[295] CD0000108000,[295] CD0000054000,[297] and CD0000102000,[295] respectively. Inset are the crystal structures (PDB[15] IDs 4F4L,[49] 2J58,[48] 1BY3,[47] 1AIR,[298] and 1NQE,[299] respectively) of these proteins depicted in the same color scheme.[198]

The refolded protein samples were then investigated by small angle neutron scattering (SANS) for further insights in refolding efficiency and protein three-dimensional structure. As SDS-PAGE (Figure 5.14) and transmission electron microscopy (TEM, sample prepared by Magnus SCHWIETERS and measured by Thomas BICK in the group of Prof. Dr. Petra WENDLER, University of Potsdam) showed the presence of protein impurities and aggregation, size exclusion chromatography was performed prior to SANS measurement using the in-line SEC-SANS measurement set-up at Institute Laue-Langevin (ILL, Grenoble, France), beamline D22. The SEC chromatogram supported the findings obtained by SDS-PAGE and TEM revealing a rather heterogeneous sample. Data acquisition and evaluation was

therefore not straightforward, as the amount of monomeric protein in the sample was too low. Analysis and interpretation of the data, performed by Dr. Anne MARTEL, Dr. Andrea LASSENBERGER and Dr. Andrea TUMMINO, on-site cooperation partners at ILL, supported the findings obtained so far. After refolding, a significant amount of misfolded protein and/or protein aggregates was present. Accordingly, SANS data were of poor quality and no reasonable model representing tested FhuA WT and open channel variants FhuA ΔCVF$^{tev}$ and FhuA A2a was found which would be in accordance with the measured data. Nevertheless, those proteins were used for protein-polymer synthesis and subsequent incorporation in polymeric materials.

**Synthesis of protein-polymer conjugates:** FhuA-polymer conjugates were synthesized by Cu(0)-mediated radical polymerization in buffer using the grafting-from approach as already presented in Chapter 2. In a first step, small initiating groups were attached to the amine functionality of the lysine side chain present at the protein surface to yield the protein-macroinitiator. A high degree of modification was targeted, and the reaction performed at pH 8.2 according to own experiments with BSA (see Chapter 3.3, Figure 3.7) and previous reports with an excess of initiator per lysine residue of 5.[132] In a second step, polymer chains were grown in situ from the protein surface. As results in Chapter 2 suggested a significant influence of grafting-from conditions on protein structure, grafting-to was performed as alternative in the generation of FhuA-polymer conjugates as well (Scheme 5.1). For this procedure, the same conditions as described for CBM and BSA in the Chapters 2 and 3 were used.

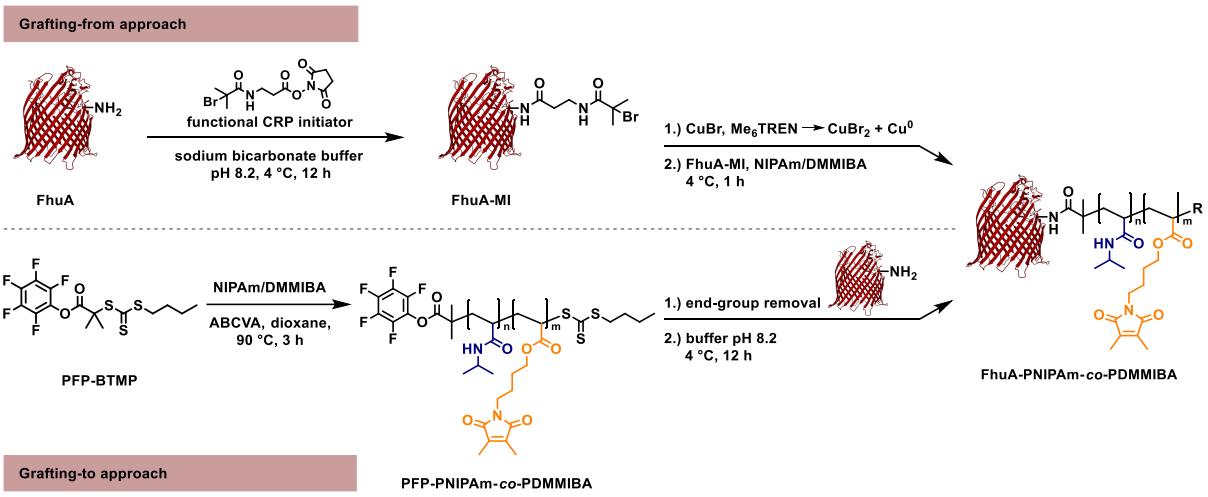


Scheme 5.1: Synthesis of FhuA-polymer conjugates by grafting-from (left) and grafting-to (right) using NIPAm (blue) and DMMIBA (orange) as monomers for in situ generation of protein-polymer conjugates or synthesis of protein-reactive polymers.

**Variation of crosslinkable monomers:** For covalent immobilization of protein-polymer conjugates as building blocks in the membrane, UV-crosslinkable monomers were incorporated in the polymer. A variety of compounds bearing either a dimethyl maleimide or coumarin moiety were synthesized, polymerized and compared regarding their crosslinking efficiency under various conditions. The chemical structures of monomers are presented in Figure 5.10. These UV-crosslinkers were either inspired (DMMIBAAm) or adapted from compounds described in the literature (DMIAm, DMMIBA, CoumAAm).[300–302] Synthesis was performed according to described literature procedures and detailed description is provided in the Experimental Part of this Chapter. For DMMIBAAm, the same procedure as described for DMIAm was used. NMR spectra of obtained monomers are in accordance to published data.[300–302]

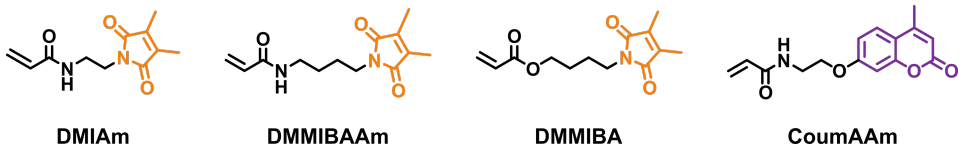


Figure 5.10: Chemical structure of the different monomers bearing either a maleimide (orange) or a coumarin moiety (violet) for UV-crosslinking.

**Copolymerization of UV-crosslinkable monomers with NIPAm:** Initial studies for the copolymerization of NIPAm with DMIAm and DMMIBA in aqueous system using copper(0)-mediated radical polymerization conditions as applied for grafting-from the protein, were already performed by CHARAN and the results presented in his thesis.[134] It was found, that the higher the concentration of crosslinkable monomer was set in the feed solution prior to polymerization, the lower the polymerization yield. Additionally, higher amount of crosslinkable monomer did not result in a higher amount of crosslinker incorporated in the polymeric material. Therefore, amount of crosslinkable monomer in relation to NIPAm was set to 5 %. The same results were obtained in the current thesis in test studies using DMIAm, DMMIBAAm, DMMIBA and CoumAAm in aqueous Cu(0)-mediated radical polymerization. Two different factors were accounted for the poor incorporation and polymerization efficiency at higher co-monomer concentrations in the feed. First, the co-monomers, especially DMMIBA and CoumAAm, displayed a low water solubility. Second, the double bonds in maleimide and coumarin moieties tend to interrupt the polymerization leading to radical chain termination events.[303]

It should be mentioned that an increase in crosslinking points between the copolymers and thus a more stable polymer mesh in the membranes later could be obtained by incorporating a higher amount of co-monomer in the polymer material. Therefore, polymerizations were tested in organic solvent by RAFT polymerization with screening of different reaction conditions including varied monomer concentration, initiator concentration and polymerization temperature. However, none of the tested reaction conditions led to a higher incorporation of crosslinkable monomer at moderate polymerization efficiency. Therefore, for membrane generation the amount of crosslinkable monomer in PNIPAm was kept unchanged to 5 %. The generated polymers were characterized by NMR spectroscopy, SEC and cloud points arising from the thermo-responsive PNIPAm chains determined by turbidimetry. Ratios of NMR signals arising from the dimethyl maleimide groups (2 -$CH_3$ at $\delta$ = 3.95 ppm) or the coumarin group (-CH group at $\delta$ = 7.45 ppm, the most low-field shifted group) in the copolymers to the dimethyl groups in the PNIPAm side chain (2 -$CH_3$ groups at $\delta$ = 1.10 ppm) were used to calculate the amount of incorporated co-monomer in the final polymer and was found to be roughly 5 % for all copolymers synthesized by RAFT polymerization. For polymers incorporating the more hydrophobic co-monomers DMMIBA and CoumAAm, the cloud point shifted to lower values. In general, a range of cloud points between 25–30 °C was observed ($T_{cp,PNIPAm}$ = 32 °C).[229] For detailed information see the Experimental Section of this Chapter.

Literature procedures for the polymerization of the chosen monomers consist either of free radical polymerization or synthesis of block copolymers. The latter were used for the formation of polymersomes taking advantage of the self-assembly behavior of prepared amphiphilic materials or hydrogel formation using extremely large polymers with degrees of polymerization up to ~ 1000.[301,302,304,305] These conditions were not suited for the generation of protein-polymer conjugates by grafting-from or grafting-to. Incorporation of block copolymers could have a negative impact on the self-assembly behavior of bioconjugates at planar interfaces and free radical polymerization lacks the possibility of directed attachment of polymer chains to the protein surface.

**Crosslinking efficiency in aqueous solution:** In the case of dimethyl-maleimide, the precursor dimethyl maleimide ethylene amine hydrochloride salt (DMMI-HCl) is water soluble and was used in initial experiments to determine the crosslinking efficiency at different distances to the UV source and irradiation times. Crosslinking efficiency can be estimated by UV–Vis spectroscopy following the change of the absorption maximum of the maleimide C=C double bond (Figure 5.11 a).[302,306] Depending on the reaction medium, the formation of an asymmetric dimer (in aqueous medium) or a [2+2] cycloadduct (in organic media) was reported and classified by the new absorption maximum visible in the UV–Vis spectrum (Figure 5.11 b).[302,306]

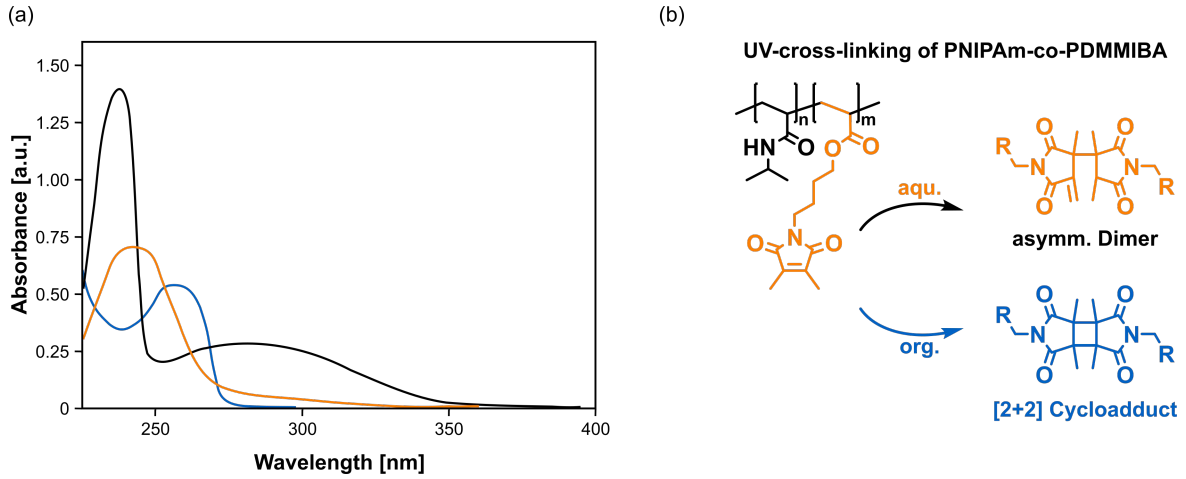


Figure 5.11: Characteristic UV spectra of dimethylmaleimide before (black) and after UV-crosslinking (orange and blue, a).[306] Depending on the reaction medium, an asymmetric dimer (orange) or a [2+2] cycloadduct (blue) is obtained (b).[302]

First, experiments at varying distances between the dimethyl-maleimide solution to the UV source were performed. A 5 mM solution was used in order to achieve an absorbance of approximately 1 for the maximum around 300 nm. As the crosslinking of FhuA-copolymer conjugates has to be performed in aqueous solution, the compound was solubilized in Milli-Q water where the formation of the asymmetric dimer was demonstrated in literature.[302,306] Samples were taken at different time points and the respective UV–Vis spectra can be found in Figure 5.12. First, a decrease of absorbance at 305 nm from maximum 1.2 to minimum 1.0 arbitrary units for a distance of 5 cm and an irradiation time of 120 min was observed. Second, a shift of the absorbance boundary from ~ 250 nm towards higher wavelengths up to 280 m for the highest crosslinking degree can be seen. This value indicates the formation of a cycloadduct after irradiation of the maleimide derivative in aqueous conditions. This is contradictory to common literature, as an asymmetric dimer is more favored in aqueous solution.[302] The cycloadduct was shown to cause a stronger redshift of the absorption than the asymmetric dimer (Figure 5.11)[302,306] as observed during my measurements. These differences can be attributed to the fact, that a mixture of products and starting compound was used for the measurements. A clear indication for the formed crosslinking product could only be obtained when the reaction mixture would be separated and each compound analyzed separately. Determination of the absorption maximum would then allow for further interpretation. Nevertheless, only a successful crosslinking reaction irrespective of the formed product is important in the framework of this thesis. To get an idea of the needed set-up for membrane generation, the obtained results were sufficient to continue. Further irradiation beyond 120 min has been shown to result in a higher crosslinking efficiency (graphs not shown) at longer irradiation period. Nonetheless, prolonged irradiation and therefore higher irradiance and flux of photons may lead to polymer and/or protein degradation.[307–310] As a result, an irradiation time of 120 min and a sample-to-UV source distance of 15 cm was chosen for further experiments.

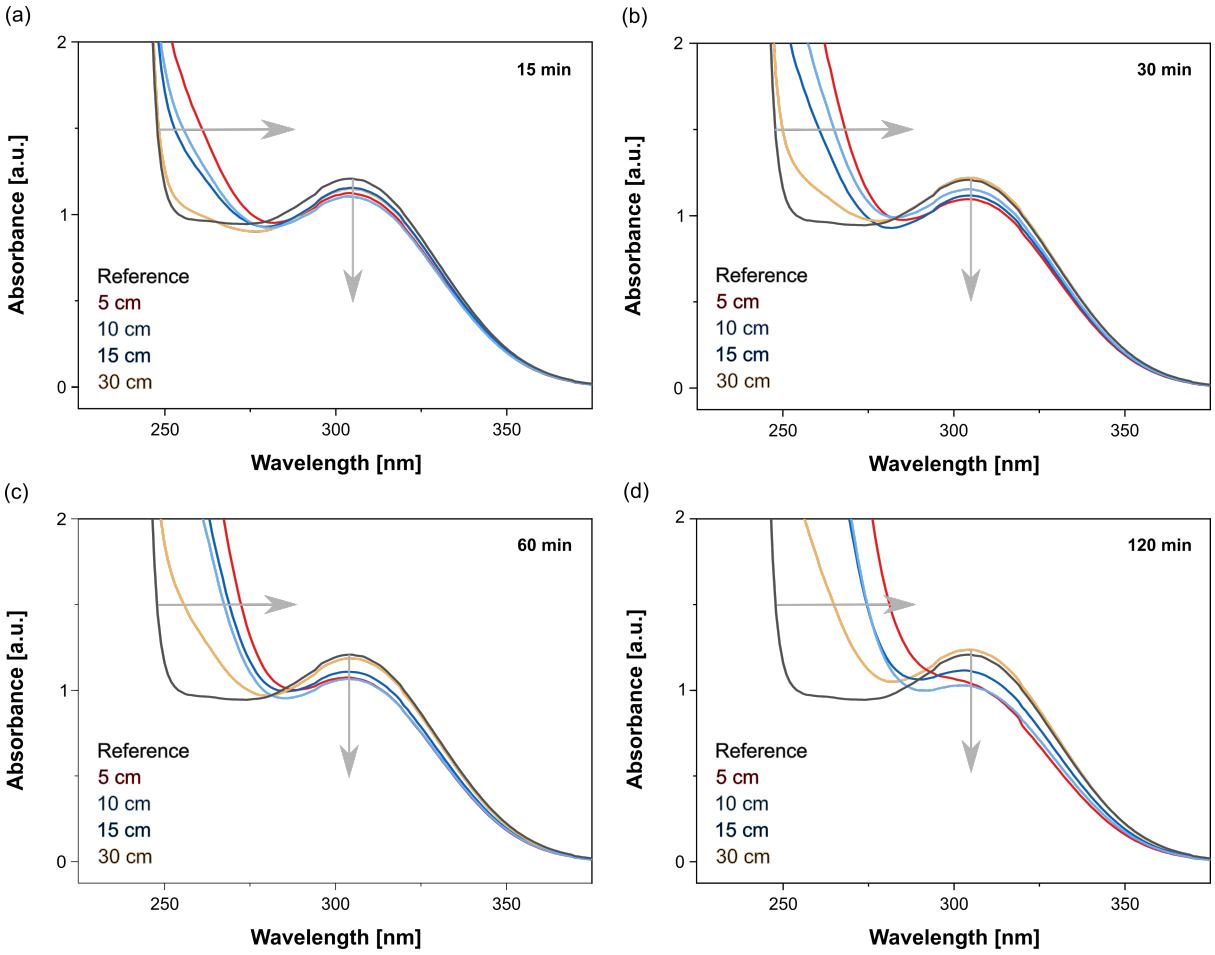


Figure 5.12: Efficiency of UV-crosslinking reaction in dependence on irradiation time and distance to UV source. DMMI-HCl as reference compound was dissolved in Milli-Q water at a concentration of 5 mM and characterized by UV–Vis spectroscopy before and after UV irradiation.

Next, those experiments were transferred to the copolymers of NIPAm and UV-crosslinkable monomers. The amount of crosslinkable monomer was set to 5% and the overall degree of polymerization to 100 repeating units. This degree of polymerization was selected to keep consistent with previous studies in the field of protein-polymer conjugates for membrane generation performed in the BÖKER group.[134] The distance between sample and UV source was fixed to 15 cm based on the experiments presented above. The photodimerization degree or crosslinking efficiency can be calculated from $1 - A_t/A_0$, were $A_0$ and $A_t$ are the initial absorbance and the absorbance after irradiation time *t*, respectively.[311] For evaluation of crosslinking efficiency, only the decrease of the absorption band at ~ 305–310 nm for maleimide-derived monomers and at 320 nm for the coumarin-based monomer was used. As PNIPAm itself has a strong absorbance at ~ 200 nm, the shift of the absorption boundary at ~ 260 nm was not measurable. For all samples, a decrease of the absorption band was observed after irradiation indicating successful crosslinking. The best efficiency was found for coumarin-derived copolymers with approximately 75 % after 120 min and 84 % after 300 min. For maleimide-based polymers, the performance of DMMIBA and DMMIBAAm are the same with an

efficiency of 47 % and 67 % after 120 min and 300 min irradiation, respectively. The poorest efficiency was found for the DMIAm monomer with only 24 % and 36 % after the same time periods. The difference between the maleimide-based monomers can be ascribed to an increase in crosslinking efficiency with increasing spacer-length between polymer backbone and functional group as described by VOIT et al.[300] As the increase of crosslinking degree slows down significantly throughout the investigated time frame, irradiation time for generation of membrane systems was set to 120 min.

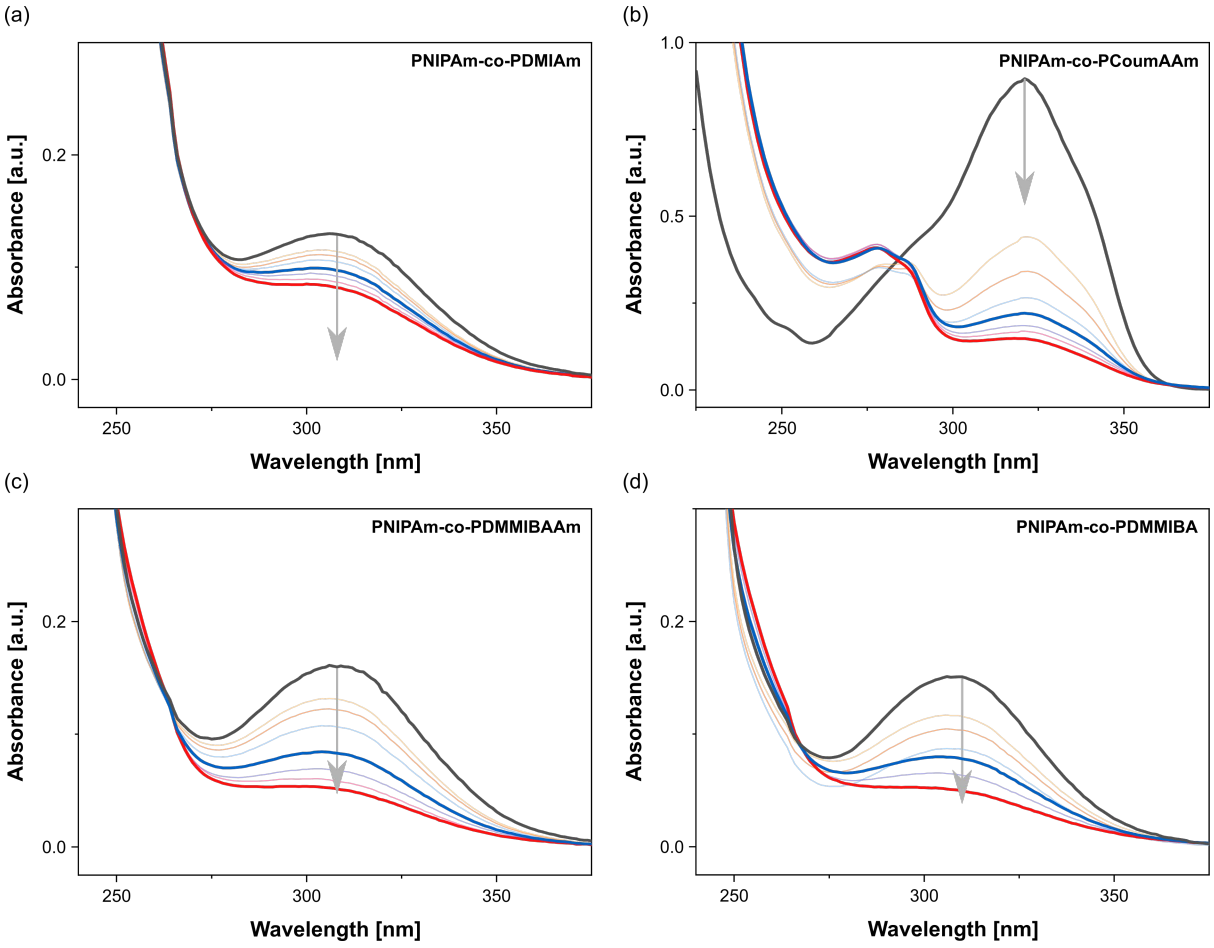


Figure 5.13:Crosslinking efficiency of copolymers based on PNIPAm and crosslinkable monomers bearing a maleimide moiety (PDMIAm, PDMMIBAAm, PDMMIBA) or coumarin moiety (PCoumAAm). Copolymers were dissolved in Milli-Q water at a concentration of 2 mM and further diluted to 0.13$\overline{3}$ mM. 200 µL of this solution were used for the measurements which represents the amount of polymer deposited in a 25 layer equivalents FhuA WT membrane. The term layer equivalent is described in the section "calculation of the amount of FhuA needed for membrane generation" below. Absorbance was measured in dependence on irradiation time at a distance to the source of 15 cm (black = 0 min; purple = 120 min; grey = 300 min).

It should be mentioned that these studies were only performed to measure crosslinking efficiency in solution and not in membrane materials, bulk or at interfaces. Information on photodimerization degree in bulk could in general be gained by following the decrease in peak intensity using FT-IR spectroscopy of solid membrane material. As the generated membranes in the course of this thesis were only several

100 nm thick, amount of deposited material on top of a silicon wafer was not sufficient for those measurements.

**Grafting-from and -to FhuA:** Detailed information about reaction conditions for grafting-from and grafting-to are already discussed in Chapter 2.3 and an overview for generation of protein-polymer conjugates based on FhuA is provided in Scheme 5.1. For grafting-from, proof of conjugation was accomplished by SDS-PAGE showing an increase in molar mass of the respective band after initiator attachment and polymerization (Figure 5.14 a).

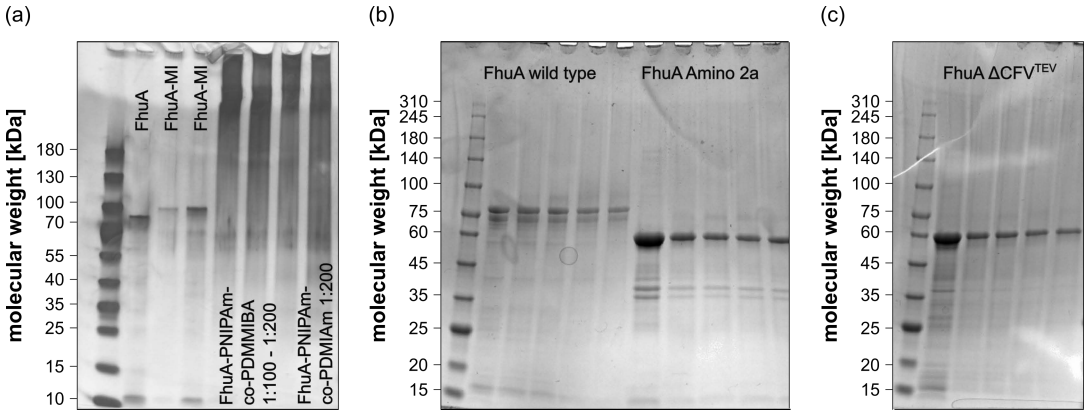


Figure 5.14: SDS-PAGE of FhuA, FhuA-MI and FhuA-polymer conjugates synthesized using different ratios of monomer to initiator during polymerization (a). SDS-PAGE of FhuA WT, FhuA A2a (b) and FhuA ΔCVF$^{tev}$ (c) prior (first lane of each set) and after conjugation with the four different PFP-functionalized copolymers.

Even though protein conjugation by grafting-to was already accomplished using CBM (Chapter 2) and BSA (Chapter 3), findings using FhuA were contradictory as no conjugation was observed. One reasonable explanation could be the used buffer composition. While CBM and BSA were modified in phosphate buffer, MPD is additionally present in buffers for FhuA. MPD as diol could interact with the activated ester polymers used for conjugation and prevent polymer attachment. Nevertheless, this result was not expected as conjugation with the active ester functionalized ATRP initiator was highly efficient and further investigations are recommended to elucidate limiting factors within this system. Those could be the excess of reactant to protein or lysine residues and the steric demand of large polymers making the reaction much less favored and susceptible to be affected by the presence of MPD. Overall, future experiments for grafting-to with BSA or CBM in MPD buffer are recommended to test this hypothesis.

All in all, protein-polymer blends, i.e. a mixture of unmodified protein and unconjugated polymer, were obtained instead of conjugates. Nevertheless, the obtained blends were used for membrane generation in addition to the conjugates synthesized by grafting-from. It was assumed that proteins might be entrapped in the polymer mesh obtained after UV-crosslinking. Therefore, the functionality of the protein might be transferred to the membrane system without the need of covalent modification of the protein prior to membrane generation. Those synergistic properties obtained by blending two polymeric

materials with each other are already established in polymer blends for pervaporation and gas separation.[312] Within the FhuA/copolymer blend, a domain-formation is assumed based on findings by OLSEN et al. In SANS experiments of protein/PNIPAm blends, polymer-induced depletion interactions were obtained.[270] Protein/polymer blends based on PNIPAm can therefore be treated analogous to partially miscible blends. To clarify the difference in the next sections, annotation of protein-polymer conjugates with covalently attached polymer chains obtained by grafting-from will be FhuA-polymer (with polymer being the respective copolymer) whereas the blends are denoted as FhuA/polymer.

**Calculation of the amount of FhuA needed for membrane generation:** In our approach, membrane generation is achieved by a drying-mediated self-assembly procedure (Figure 5.15). Here, a drop of conjugate solution is placed on top of a porous support and after a short self-assembly period, irradiated by UV light to achieve covalent crosslinking of the membrane. During this process, water evaporates and the local concentration of conjugate in bulk and at the air/water interface increases gradually.

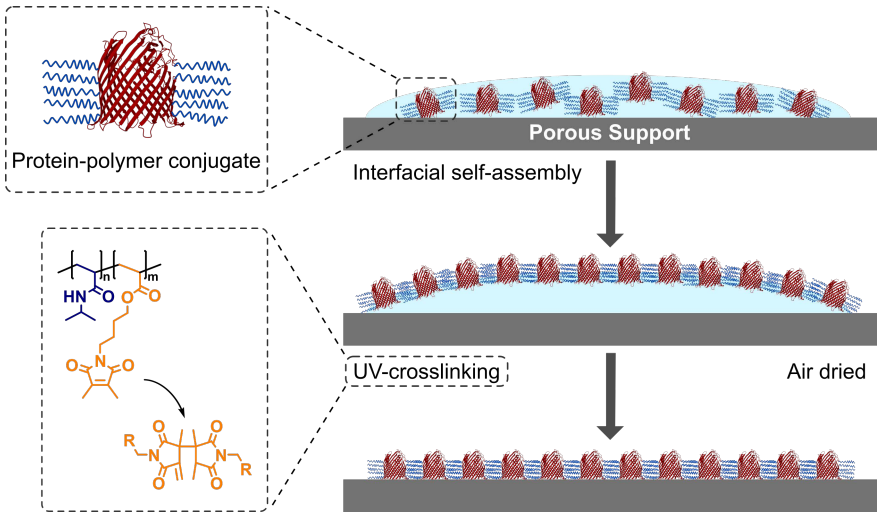


Figure 5.15: Illustration of the drying-mediated self-assembly process used for the generation of nano-thin protein-polymer derived membranes deposited on top of a porous support. First, conjugate solution is placed on top of a porous support. After self-assembling, building blocks are covalently crosslinked by applying UV light. Simultaneously, water evaporates leaving an asymmetric membrane with an active layer made from protein-polymer conjugates.

Based on the dimension of FhuA (6.9 nm x 3.9 nm x 4.6 nm) and assuming an upright orientation of the protein during the self-assembly process as a result of the intrinsic amphiphilicity of membrane proteins, an average area of 14.1 $nm^2$ per protein can be expected assuming the top of the barrel to be equal an asymmetric top base of a cylinder with the area calculated by $A = \pi \cdot r_1 \cdot r_2$, with $r_1$ and $r_2$ being 1.95 and 2.3 nm of the unmodified FhuA protein, respectively. The following estimations assume that all conjugates assemble at the interface irrespective of forming a mono- or multilayer. Considering the average end-to-end distance of a PNIPAm chain with ~ 100 repeating units as used for membrane formation) to be ~ 3 nm,[313] the area of the respective protein-polymer conjugate is calculated to be 41.2 $nm^2$ using the equation described above with adjusted $r_1$ and $r_2$ values of 4.95 and 5.3 nm,

respectively, for the protein-polymer conjugate. The area per FhuA molecule based on its crystal structure is estimated to be 40.5 $nm^2$ (protein data bank entry 1BY3).[47] It is further assumed that the polymer chains fill up the interstitial space between the protein molecules which is present in the crystal structure as well as the arrangement at the interface due to the elliptical shape of the proteins instead of increasing the space required for a conjugate. Moreover, polymer chains of neighboring conjugates are expected to overlap to a large extent. Based on the presented considerations, 4.1 pmol protein-polymer conjugate was used per $cm^2$ membrane to imitate a monolayer. This amount of protein-polymer conjugate is referred to as one "layer equivalent" in the course of this thesis. This term is solely a theoretical consideration to simplify the reader's imagination of the generated membranes. To aim at the formation of multilayers, the value of 4.1 pmol was multiplied with the number of requested layers. In case of reference systems composed solely of polymer to imitate the polymer mesh or matrix surrounding the proteins in obtained protein-polymer membranes, the number of polymer chains per protein was considered. FhuA wild type bears 37 lysine residues on the outside and therefore 37 anchoring points for polymer/initiator molecules. Previous studies have shown, that all lysine residues are modified in a grafting-from approach.[132] Consequently, the amount of polymer to imitate one layer of conjugate membrane is multiplied by the factor 37, hence 151.7 pmol per layer equivalent.

**Membrane generation and characterization at room temperature:** Asymmetric membranes with the active layer composed of protein-polymer conjugates were produced by the drying-mediated self-assembly procedure and covalent crosslinking under UV light irradiation as presented in Figure 5.15. Protein-polymer conjugates of FhuA WT and FhuA A2a prepared by grafting-from using PDMMIBA as co-monomer or blend materials of FhuA WT, FhuA A2a or FhuA $\Delta CVF^{tev}$ with copolymers of DMIAm, DMMIBAm, DMMIBA and CoumAAm with NIPAm prepared by RAFT polymerization were used. Irradiation time was set to 120 min and the distance to the UV source was fixed at 15 cm based on the crosslinking experiments described above. To increase the mechanical stability of the ultra-thin membranes, a porous polyether sulfone (PES) support was used for stabilization (Supor® PES Membrane Disc Filters, product ID 60301). A pore size of 0.2 µm of the PES was chosen to keep the set-up consistent with experiments performed by CHARAN.[134] For analysis by GISAXS, XRR and SFM, membranes were prepared analogously on top of a silicon wafer.

Performance in terms of permeability at different hydrostatic pressures at room temperature was measured to evaluate the stability of the membranes *in operando*. In general, flux $J$ is defined as the permeate stream flowrate $Q$ divided by the membrane surface area $A$. Permeate flow is the amount of water that passes the membrane in a certain amount of time. Therefore, flux can be expressed in terms of permeate volume $V$ per area $A$ per time $t$ as summarized in Equation (5.1) or defining a membrane permeability coefficient $K$ (also called mass-transfer coefficient) times the difference between transmembrane pressure $P_T$ and the osmotic pressure of the feed solution $P_O$. The transmembrane

pressure is the difference between feed pressure and permeate pressure after passing the membrane. To provide a positive driving force for the feed solution to flow through the membrane, the transmembrane pressure must be higher than the osmotic pressure.[243,314]

$$J = \frac{Q_{water}}{A_{membrane}} = \frac{V_{water}}{A_{membrane} \cdot t} = K \cdot (P_T - P_O) \tag{5.1}$$

Those measurements were performed using a custom-made in-house device as shown in Figure 5.16.

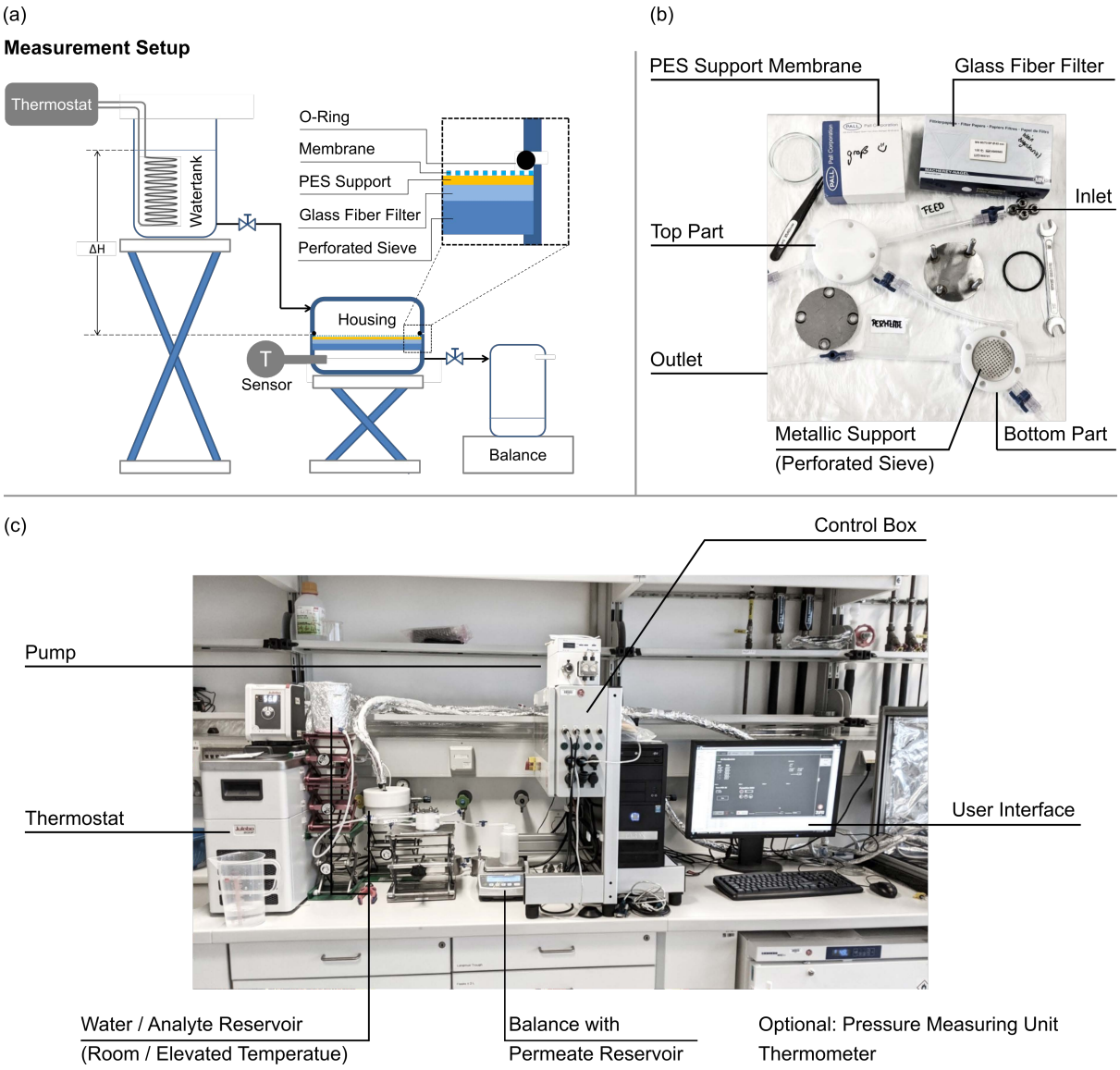


Figure 5.16: Schematic representation of the water flux measurement setup (a) and photographs of the realized setups in the lab (b and c).

Membrane thicknesses and protein arrangement in protein-polymer based and directly crosslinked protein films at the air/water interface using a Langmuir trough or prepared on top of silicon substrates were analyzed by SFM, GISAXS and specular XRR. SFM measurements of directly crosslinked protein

films obtained by Langmuir-Schaefer transfer after assembly, compression and crosslinking using glutaraldehyde at the air/water interface revealed a film thickness of monolayer and bilayer films of ~ 5.5 and 10 nm, respectively. Specular XRR measurements (performed at SIRIUS beamline of Synchrotron SOLEIL, France, with kind help of Dr. Stephanie TAßLER) and analysis of obtained reflectivity curves to deduce the electron density confirmed the results obtained by SFM. Fitting of electron density profiles provided film thicknesses of 5 nm and 9 nm, respectively, for mono- and bilayer films. XRR data are shown in Figure 5.17.

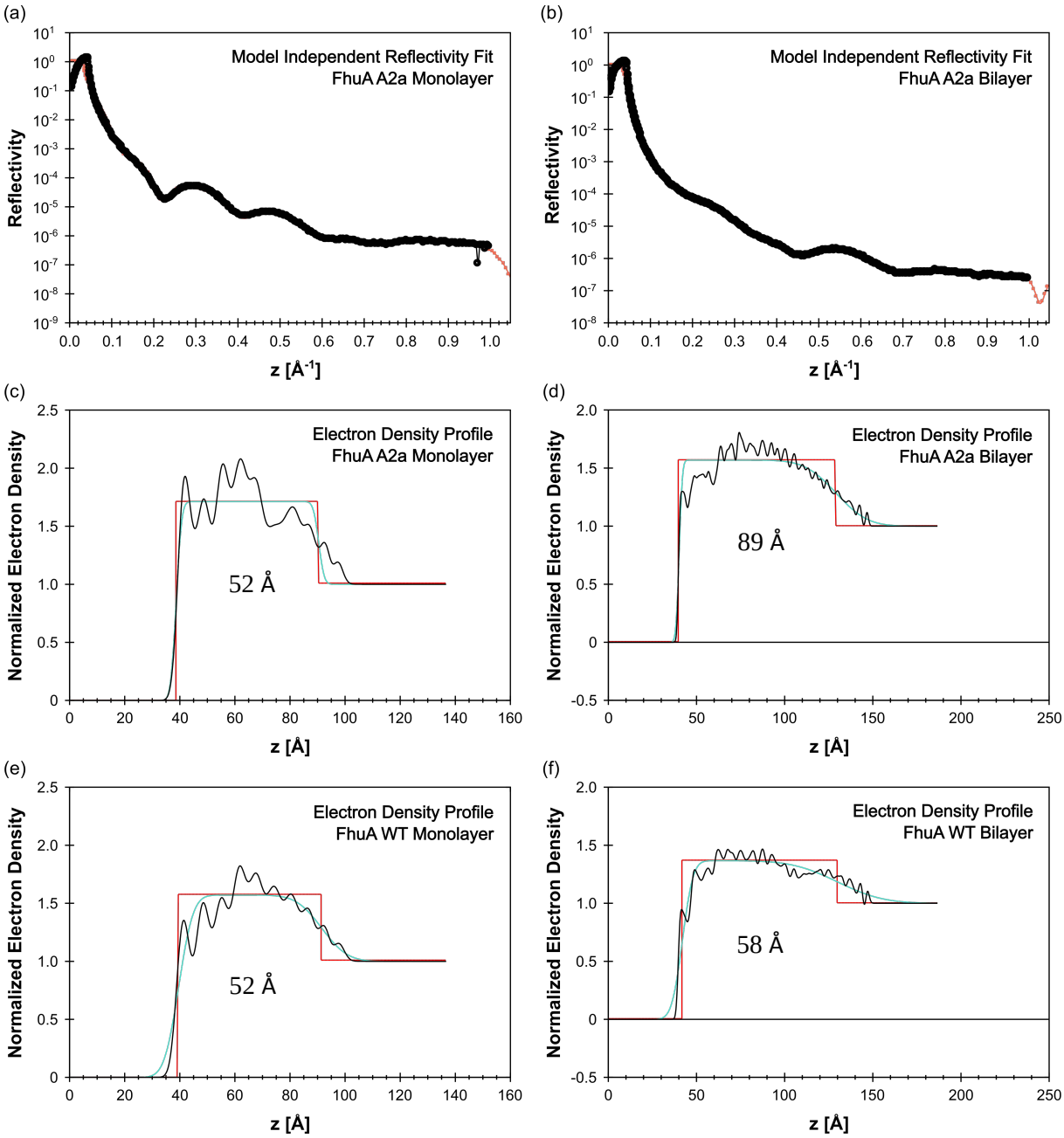


Figure 5.17: Specular XRR of FhuA A2a and FhuA WT mono- and bilayer prepared by Langmuir-Schaefer approach after assembly, compression and crosslinking with glutaraldehyde in a Langmuir trough. Reflectivity curves were analyzed using the software StochFit and scattering length density of FhuA variants estimated using the provided SLD calculator of StochFit.[315]

Afterwards, the protein films (not conjugates) were analyzed by GISAXS to determine if the films are highly ordered. However, regardless of surface pressure in the Langmuir trough, subphase, FhuA variant and crosslinking, no diffraction pattern indicating an order in the FhuA film was observed with the chosen set-up. Either the film is – contrary to the expectations – not highly ordered or the difference between the scattering length densities (SLDs) of sample and water/buffer is too close resulting in a weak contrast. As sum frequency generation (SFG) spectroscopy later demonstrated a high ordering in FhuA WT films assembled at the air/water interface with upright orientation,[291] the contrast was probably too low during GISAXS measurements.

For asymmetric membranes of protein-polymer conjugates on top of a porous PES support, permeability using different amounts of conjugate was analyzed to evaluate the minimum amount of conjugate needed to induce a significant reduction of flux. The measurements were performed at room temperature defined here as 22 °C, meaning that water can pass the small channel of FhuA WT as well as the hydrophilic polymer matrix surrounding the proteins. Experiments were performed with calculated amounts of conjugate, considering the assumptions mentioned above, to reach films composed of 1, 17.5, 35 and 78.5 layer equivalents of conjugate solution. For 1 and 17.5 layer equivalents, no reduction in flux was observed and values near the blank PES support were obtained. At 35 and 78.5 layer equivalents, the flux was significantly decreased to 91 % and 58 %, respectively, compared to the unaltered PES support (Figure 5.18 a) indicating a successful and homogeneous crosslinking at least over the majority of the support. For further analysis with SFM, XRR and GISAXS, membranes prepared with at least 35 equiv. were used.

In contrast to directly crosslinked protein films, electron density profiles for conjugates were not in accordance with SFM data (Figure 5.18 c). For a membrane prepared using 35 layer equivalents of protein-polymer conjugate, a theoretical thickness of 200–245 nm is expected considering the dimensions of FhuA in upright position (6.9 nm length). SFM determined a thickness of ~ 250 nm for a FhuA WT-PNIPAm-co-PDMMIBA film prepared on a silicon wafer (Figure 5.18 b), which is well in accordance with the theoretical expected value. However, specular XRR data suggest a much smaller film thickness (Figure 5.18 c). For high membrane thicknesses, a high periodicity of Bragg peaks or in other words small spacing between the periodic peaks in the diffraction pattern is assumed in specular XRR. For a conjugate membrane based on FhuA A2a (100 layer equiv.), a shorter spacing hence a higher periodicity of Bragg peaks was observed (Figure 5.18 c, yellow curve). Still, spacing between Bragg peaks are more relatable to a thickness below 60 nm, estimated by the inverse spacing between peaks of ~ 0.01825 $Å^{-1}$. When the same sample was measured at a different spot, reflectivity curves more comparable to protein monolayers shown in Figure 5.17 a and b were observed. Same results were obtained for FhuA WT-polymer conjugate membranes. Furthermore, GISAXS measurements as shown in Figure 5.18 d did not show a proper diffraction pattern indicating no measurable order in the FhuA-

polymer conjugate films. The apparent lack of correlation between SFM and XRR data can be attributed to a not ideal performance of the measurement, arising from the complex state of such kind of biohybrid membranes. Penetration depth of the beam to hit the interface between membrane and support may not be optimal chosen, and estimation of scattering length density of heterogeneous samples and complex data analysis with advanced software were not considered adequately prior to the experiment. Additionally, contrast between sample and interface might be too low for appropriate signal acquisition in GISAXS measurements. Although performance was not ideal, information obtained for directly crosslinked protein films are of great value on the way to protein-derived membrane materials.

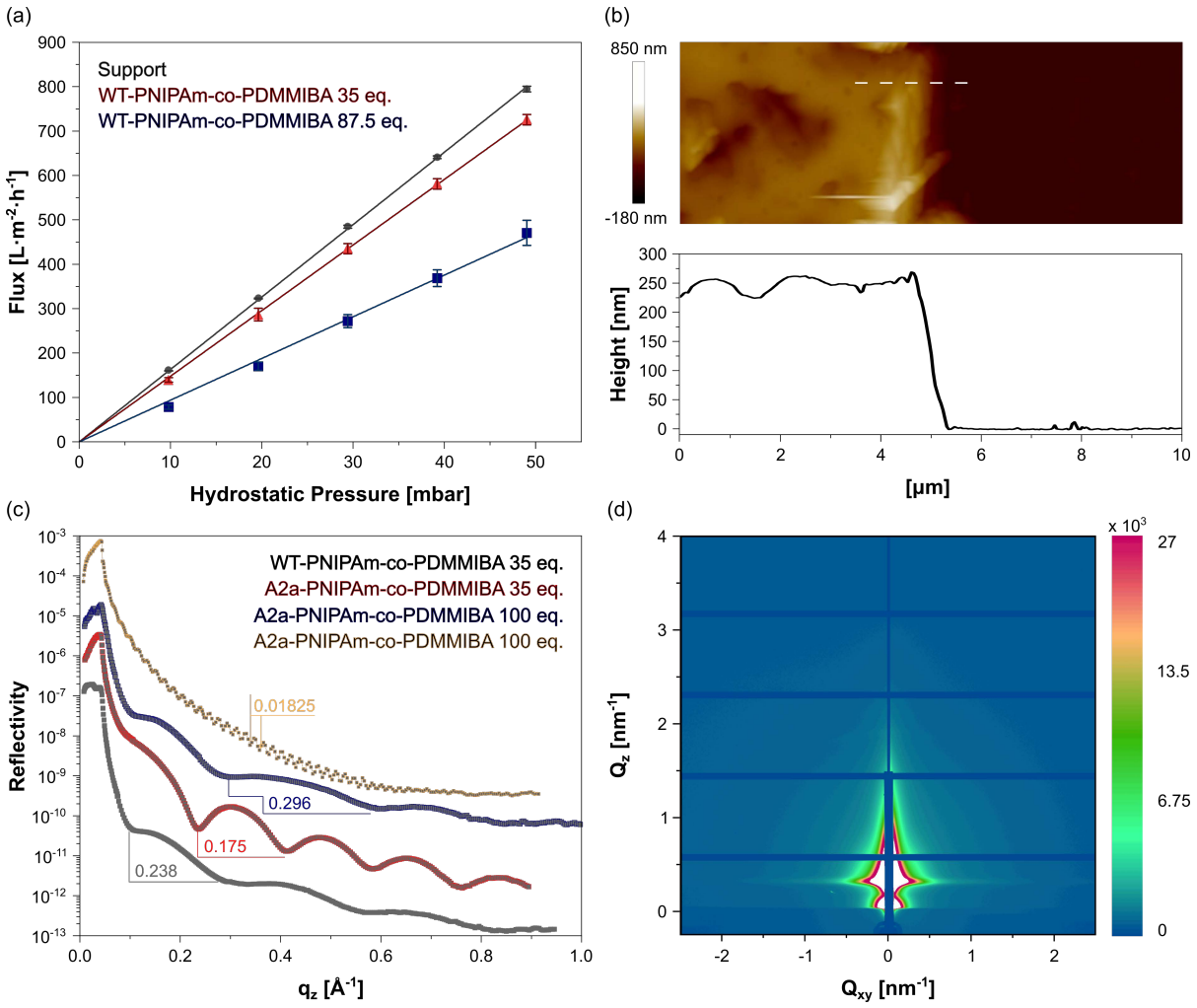


Figure 5.18: Flux measured at different hydrostatic pressures through FhuA WT-PNIPAm-co-PDMMIBA membranes on top of a porous support (a). Membrane thickness of protein-polymer conjugate membrane (35 layer equiv.) measured by SFM. A scratch was made to measure the height profile in tapping mode (b). Specular XRR curves of protein-polymer conjugates and determined distances between Bragg peaks in $Å^{-1}$. FhuA A2a membrane with 100 layer equiv. was measured at two different spots on the same sample (c). GISAXS signal of FhuA A2a-PNIPAm-co-PDMMIBA film on top of a silicon wafer (100 layer equivalents) measured with a 2D pixel detector (d).

**Flux measurements at higher temperatures:** The incorporation of stimuli-responsiveness in a membrane material can be used to modulate permeability by an external trigger.[252] PNIPAm as thermo-responsive polymer undergoes a coil-globule transition at ~ 32 °C.[229] Consequently, the change from hydrophilic to hydrophobic state should be reflected by a decrease in the permeation because of increased resistance to flow of water. However, another effect of analyte temperature on membrane operation should be kept in mind. The flux is greatly affected by the analyte temperature as this in turn correlates with the analyte viscosity $\mu$. With increasing temperature, the viscosity of water increases resulting in an increase in flux.[243] Figure 5.19 illustrates this correlation and the resulting effect on the flux. These graphs are based on theoretical calculations taking the average flux obtained for a PES membrane as provided from the manufacturer and the mathematical correlation of temperature, viscosity and flux for water.[243,316]

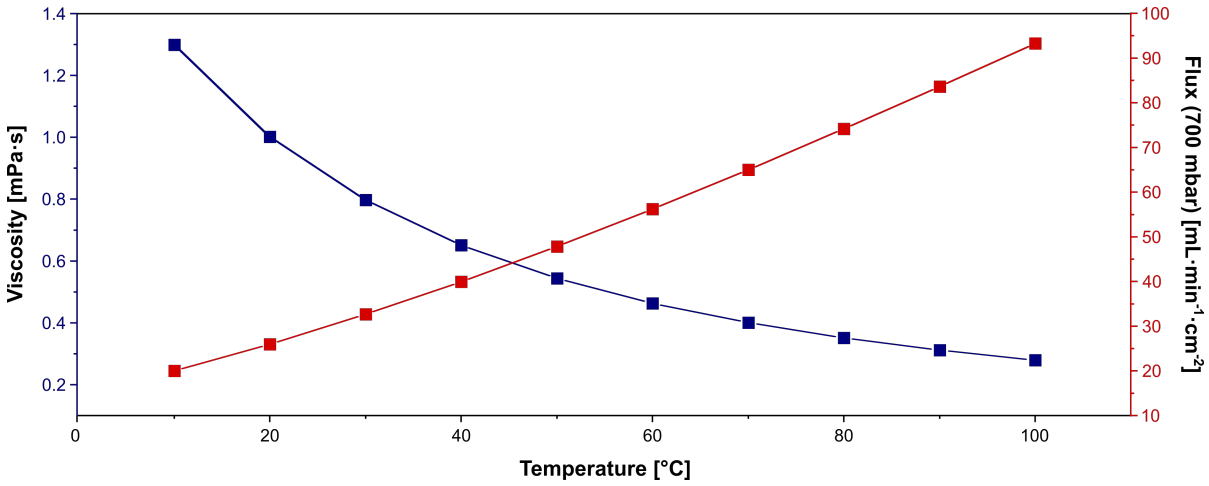


Figure 5.19: Correlation between temperature, water viscosity and flux of a commercial PES membrane, pore size 0.2 µm from PALL. Permeability data provided from the manufacturer were used for the generation of this graph. The water flux typically increases by 3% with each degree of analyte temperature.

This means that, at higher temperature, the flux already increases because of the changed viscosity which has to be considered additionally to any change in flux caused by altered properties or permeability of the membrane material. For practical purposes, a reference temperature is defined in membrane sciences to correct the flux for changes caused by viscosity.[243] Therefore, data can be compared based on membrane performance rather than physical changes in analyte viscosity. Within this thesis, this reference temperature is defined as 22 °C, correlating to the room temperature of the lab where the measurement set-up was installed. A temperature correction factor can be applied for each measurement defined as the quotient of viscosity of analyte solution at applied temperature and viscosity at reference temperature of 22 °C. The normalized flux can therefore be calculated by the use of Equation (5.2). Here, $J_{22}$ is the normalized flux at 22 °C, $J_T$ the measured flux at water or permeate temperature T, $\mu_{22}$ the permeate viscosity at 22 °C and $\mu_T$ the permeate viscosity at experimentally used temperature T.

$$J_{22} = J_T \cdot TCF = J_T \cdot \frac{\mu_T}{\mu_{22}} \quad (5.2)$$

It has to be noted that the density is not significantly affected by the temperature (0.998 g·mL$^{-1}$ at 21 °C compared to 0.983 g·mL$^{-1}$ at 60 °C).[316] Therefore, within the practical setup of the in-house device, simply measuring the increase of weight on a balance is still applicable and change in density was neglected.

Initial experiments at higher temperature were already performed by CHARAN in the scope of his thesis.[134] In the previously used set-up, measurements were performed in a tempered hood guaranteeing a uniform temperature in each part of the device. In these experiments, a lower flux at higher temperatures was observed indicating the anticipated function of the polymeric matrix to switch from hydrophilic to hydrophobic.[134] The results obtained during this thesis differ significantly. In the own measurements, a thermostat was connected to the device as conceptualized by Murat Tutuş, membrane scientist at Fraunhofer IAP (see again Figure 5.16). The thermostat heats the analyte solution to a specific temperature and the solution then passes over tubes through the membrane clamped in a measurement chamber. As the system was not constructed to be completely isolated, the temperature of the analyte solution was tested at different points of the setup, namely in the reservoir, above the membrane and in the catch tank. Depending on the resistance of the membrane, the water passes the membrane with different velocity. As a result, measurements are not consistent. In other words, the same reservoir temperature can lead to different analyte temperatures above the membrane and in the catch tank.

First, membranes derived from FhuA WT-PNIPAm-co-PDMMIBA prepared by grafting-from and a reference membrane solely composed of the respective polymer matrix were tested at room temperature and at elevated temperature above the cloud point of PNIPAm and the respective copolymers (Figure 5.20). The cloud points of the polymers in solution are listed in the Experimental Section of this Chapter. At 22 °C, the conjugate membrane decreased the flux to 91 % whereas the polymer membrane reduced the flux to 63% compared to the support material. Hence, the reference polymer membrane had a lower flux than the protein-polymer membrane although both should have the same amount of polymer incorporated in the active layer. One possible explanation could be the disruption of packing density after incorporation of proteins in the polymer layer. Another possibility is a lack in grafting density or polymerization yield in grafting-from the protein surface and therefore a lower amount of polymer attached to the protein as expected. As a result, amount of polymer representing the polymer matrix surrounding the protein would be overestimated in the reference membrane. Furthermore, although most of the channel of FhuA WT is blocked with a cork domain, it still has a small water channel.[317,318] When switching the analyte temperature above the cloud point temperature of the polymer (~ 32 °C), an increase in permeability is observed. Considering the decrease in viscosity of water and using

Equation (5.2) to refer the flux to room temperature, no significant change in performance of the tested membranes is concluded. The reasons for this result are not yet entirely understood. An increase in porosity of the polymer matrix as a result of the coil-globule transition could be one possible explanation. Moreover, competing events between polymer hydrophobicity and decreased water viscosity should be also kept in mind. It is mentioned that the effects are completely reversible with permeate being close to the initial values when switching back to room temperature.

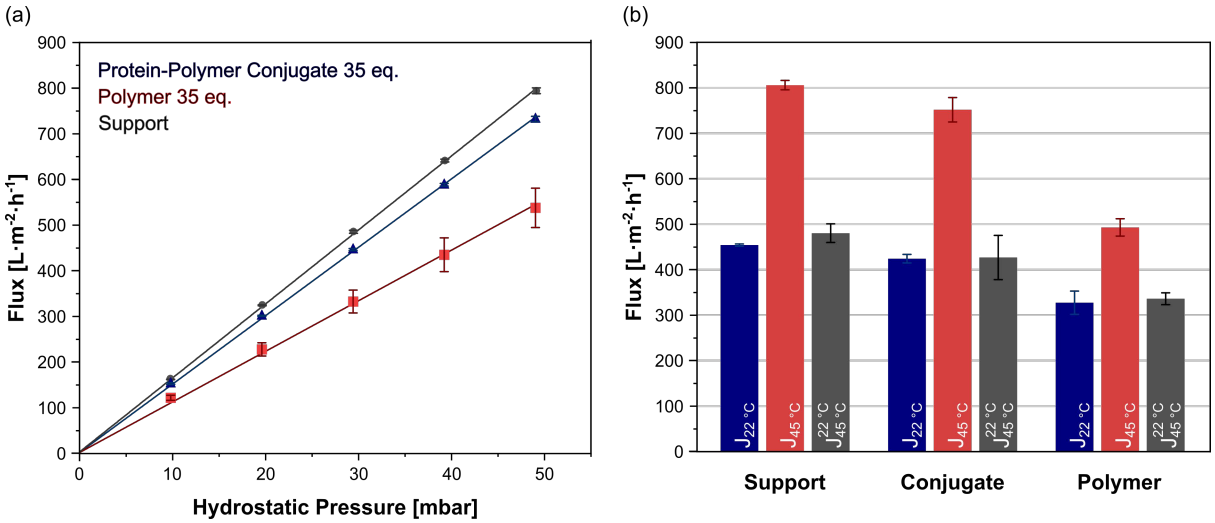


Figure 5.20: Water flux of a FhuA WT-PNIPAm-co-PDMMIBA membrane, polymer membrane and support at room temperature at different hydrostatic pressures (a) and at elevated temperature at a fixed hydrostatic pressure of 25 mbar (b). The flux measured at room temperature (22 °C) is shown in blue, the measured value at elevated temperature in red and the values referenced to room temperature in grey as calculated by Equation (5.2).

Second, membranes prepared using the protein-polymer blends – mixture of unbound polymer with proteins as a result of unsuccessful grafting-to approach – were tested for their water permeability. To increase the chance of protein entrapment and performance, a higher amount of material was deposited on the PES support. For FhuA WT/PNIPAm-co-PDMIAm blends, different layer equivalents corresponding to higher film thicknesses of the active layers were tested and a decrease in flux observed with increasing amount of material deposited on the PES support (Figure 5.21 a). The same trend was already observed for membranes derived from protein-polymer conjugates synthesized by grafting-from (Figure 5.18 a). In general, the flux of the blend material is lower compared to the respective protein-polymer conjugate material. This might be explained by the higher packing density of polymer material as already shown above for membranes derived solely from polymer. Interestingly, even though the protein is not covalently attached within the membrane material, no protein bleeding was observed which would be noticeable as an increase in permeability after a certain amount of time. Additionally, different copolymers were used in the blend mixtures (Figure 5.21 b & c) for FhuA WT and FhuA A2a. The flux for FhuA WT/blend membranes seems to depend on the copolymer while no influence could be found for FhuA A2a/blend membranes. Unfortunately, neither a significant deviation

in performance of the different copolymers nor both protein variants was observed in these experiments. It was assumed that the more hydrophobic polymer (PNIPAm-co-PcoumAAm and PNIPAm-co-PDMMIBA) would display a lower flux compared to the more hydrophilic polymers (PNIPAm-co-PDMIAm and PNIPAm-co-PDMMIBAAm) as a result of the unfavored interaction of water with the polymer membrane material. Additionally, a significantly higher flux was expected for FhuA A2a compared to FhuA WT because of the open channel.

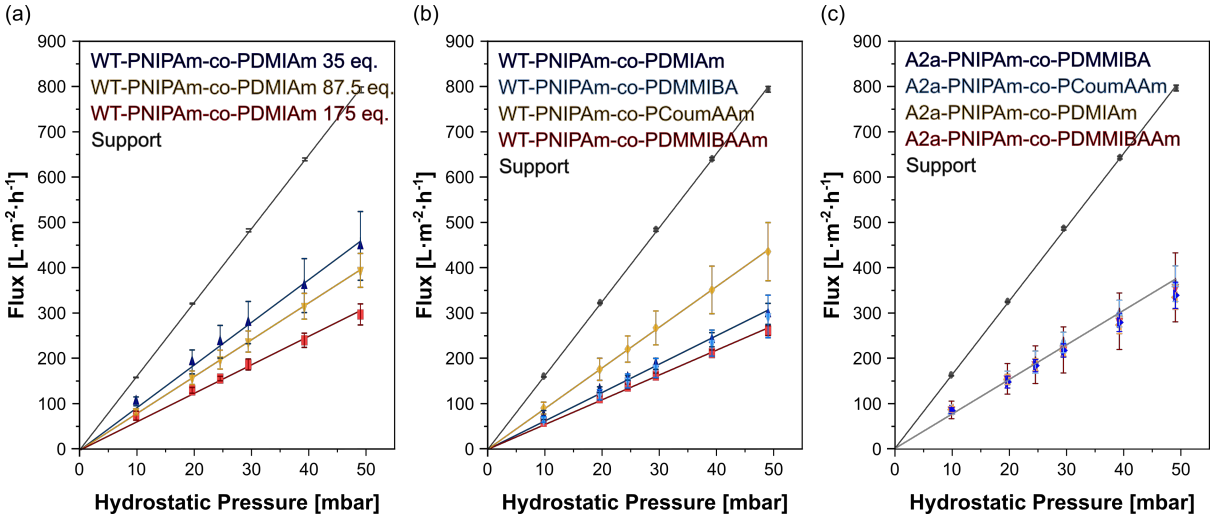


Figure 5.21: Protein/polymer blends of FhuA WT and FhuA A2a with different copolymers. Hydrostatic pressure was varied and performance of wild type membranes at different thicknesses (a) and with different polymers (b) were tested. A2a/copolymer blends were tested as well (c). For b and c, active layer thickness was set to 175 layer equivalents. For all samples, degree of polymerization was 100 repeating units and distance to UV source and crosslinking time was set to 15 cm and 120 min, respectively. All measurements shown here were performed at 22 °C.

Whereas for protein-polymer conjugates a membrane thickness of 35 layer equivalents was used for characterization at room and elevated temperature, for measurements with protein/polymer blends the layer thickness was set to 175 layer equivalents. Correspondingly, a thicker membrane on top of the PES support of approximately 1.25 µm was observed as determined by SFM measurements (Figure 5.23). All membranes were tested at room temperature as discussed in the section above and at elevated temperature. Nevertheless, despite the higher layer thickness no change in flux at elevated temperature was observed for those membranes neither (data not shown).

**Reference systems:** To fully accredit a specific functionality to be caused by one component in the system, one must consider respective reference systems. Therefore, different references were tested including the performance of the polymer without protein, membrane formation in the absence of UV light and non-covalent interactions of the protein in the absence of polymer with the support material.

The first reference system tested was the performance of polymer material in the absence of protein. Fluxes measured at different hydrostatic pressures, varied film thickness (Figure 5.22 a) and from different polymers (Figure 5.22 b) are shown below. Again, the more material was deposited on the support material, the lower the flux. However, in this case, the effect was not as pronounced as seen for protein-polymer conjugates and blend materials. It has to be noted, that, here, the amount of material was further increased ranging from 175–525 layer equiv. compared to 35–175 layer equiv. used for conjugates and blends. Using such high amount of material, the flux decreased not as much as assumed from the experience with the other membranes. It could be that the membrane is at some point "saturated" and an increase in equivalents is not directly correlated with a decrease in permeability or vice versa an increase in resistance.

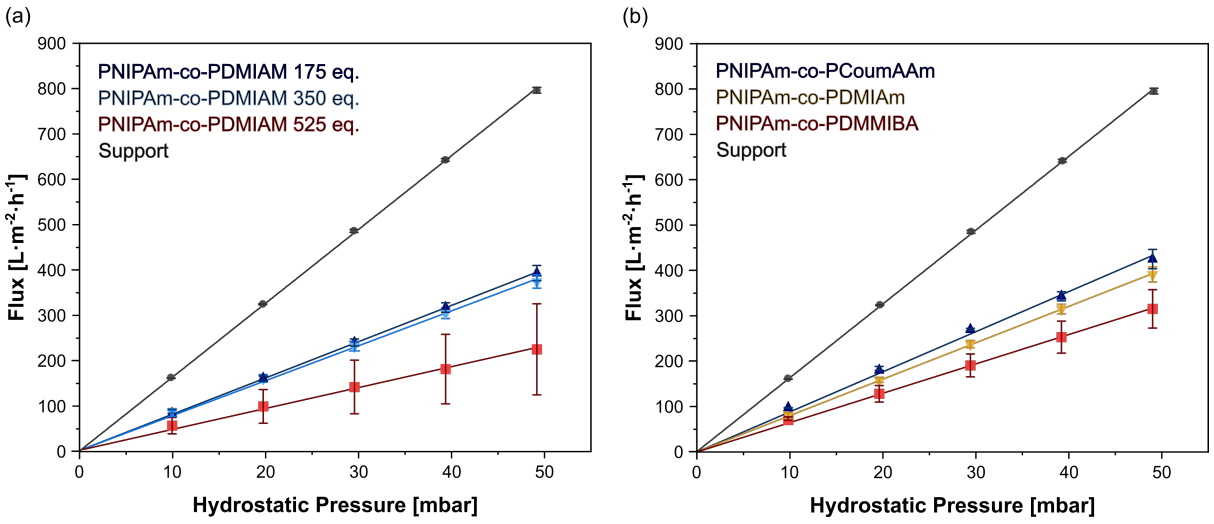


Figure 5.22: Flux determined for crosslinked polymers at different hydrostatic pressures ranging from 10 up to 50 mbar. Active layer thickness for membranes prepared from PNIPAm-co-PDMIAm was varied from 175 to 525 layer equivalents (a). For comparison of polymer membranes prepared from PNIPAm-co-PcoumAAm (blue), PNIPAm-co-PDMIAm (yellow) and PNIPAm-co-PDMMIBA (red) the active layer thickness was set to 175 layer equivalents. For all samples, degree of polymerization was 100 repeating units and distance to UV source and crosslinking time was set to 15 cm and 120 min, respectively.

However, visual observation and surface analysis with SFM showed, that membranes composed solely from polymer are much more homogeneous compared to protein-polymer conjugate membranes (Figure 5.23). This correlates nicely with the theory of packing density of polymer material in presence and absence of protein used as explanation for the variation in flux (see again Figure 5.20).

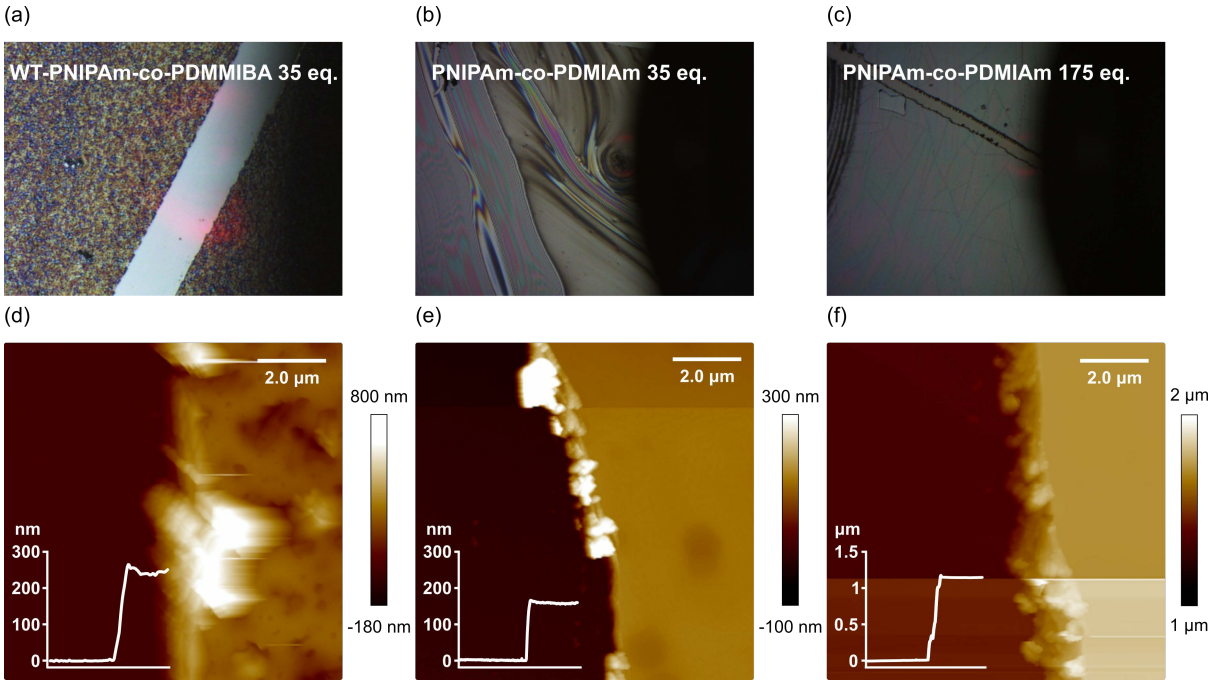


Figure 5.23: Optical and SFM images of generated membranes. Scratches were made in order to determine the SFM height profiles.

Lastly, performance of membranes derived in the absence of UV irradiation was investigated. CHARAN already showed the impact of irradiation on generation of a homogenous membrane material.[134] Nevertheless, the impact on permeability of the material was not tested yet. It is assumed that, without UV irradiation, no membrane and therefore no alteration of permeability should be obtained. Interestingly, a reduction in flux was observed in the same order of magnitude with and without UV treatment of the membrane system (Figure 5.24). Additionally, protein – in the chosen reference system BSA – also leads to a significant reduction in flux in the absence of polymer and without UV irradiation. Surprisingly, this phenomenon, namely deposition of material through non-covalent interactions of polymer and protein with the bare PES support, is consistent throughout the course of the measurement with a linear increase in flux in correlation to applied hydrostatic pressure. In general, for weak non-covalent interactions between polymer or protein with support membrane material, an increase in permeability would be assumed after a certain amount of time as the material is washed off to leave the unfunctionalized support membrane. All observations indicate a strong adsorption of protein to the support material although a weak interaction of PES supports with proteins is claimed by the manufacturer (PALL). It should be mentioned that error bars for triplicate measurements of BSA in the absence of polymer and without UV irradiation are more pronounced compared to the other measurements. Therefore, it can be assumed that the observed effect is highly unpredictable.

Even though it was shown that, in the chosen set-up, the crosslinking efficiency is increased with longer irradiation time, no difference in membrane performance was found when irradiated for 15 min (Figure 5.24 b, BSA-PNIPAm-co-PDMMIBA I) or 90 min (Figure 5.24 b, BSA-PNIPAm-co-PDMMIBA II).

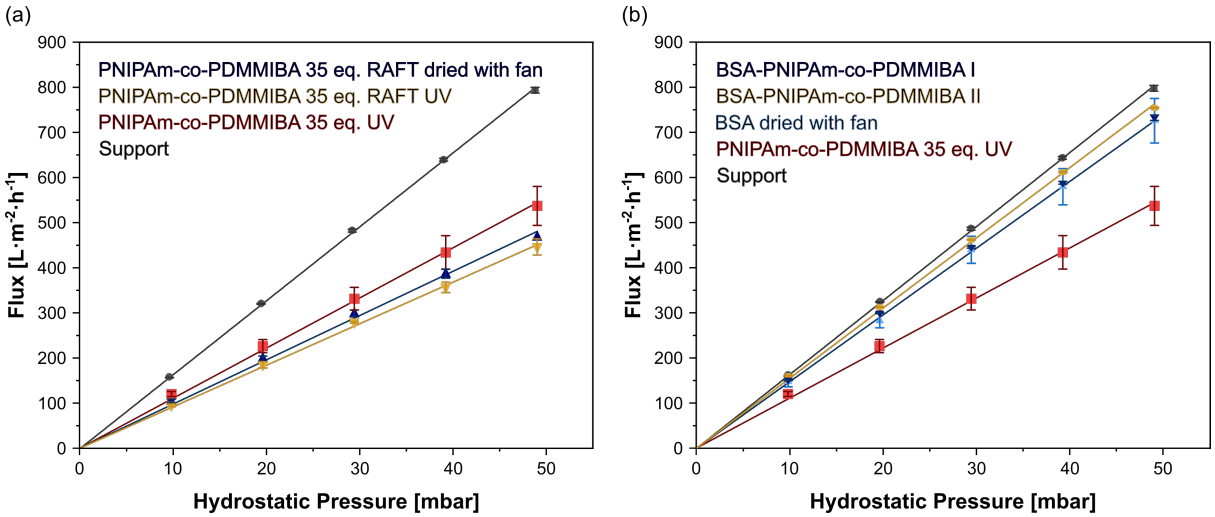


Figure 5.24: Reference set of different membrane systems based on polymers and protein-polymer conjugates. Flux was measured at different hydrostatic pressures for membranes composed of PNIPAm-co-PDMMIBA (a) and BSA-PNIPAm-co-PDMMIBA (b). Thickness of active layer on top of the PES support was set to 35 layer equivalents for all measurements. Samples were either cross-linked with UV light or dried using the fan function of an UV nail lamp. Polymers (in a) were either synthesized by RAFT polymerization (blue and yellow) or Cu(0)-mediated radical polymerization in water (red) and the degree of polymerization set to 100 repeating units. Protein-polymer conjugates were prepared by grafting-from. The sample BSA-PNIPAm-co-PDMMIBA I (blue) was irradiated with UV for 15 min whereas BSA-PNIPAm-co-PDMMIBA II (yellow) was irradiated for 90 min.

**Size exclusion experiments:** Despite the lack of temperature responsiveness, further characterizations in terms of size exclusion experiments were performed. First, suited analytes were selected and tested for non-covalent interactions with support material. An overview of chosen analytes is provided in Table 5.2. Those analytes were already used in different reported studies for the characterization of protein-polymer hybrid membranes.[62,319,320]

**Table 5.2: Analytes for size exclusion experiments and their key parameters.[320]**

| Name | Molar mass [g·mol$^{-1}$] | Size [nm] | Charge |
|---|---|---|---|
| **BSA** | ~ 66 400 | 14 x 4 | - |
| **Rhodamine B** | 479.09 | 1.70 x 1.33 | + |
| **Methylene blue** | 319.85 | 1.51 x 0.63 | + |
| **Methyl blue** | 799.80 | 2.43 x 1.10 | - |
| **Methyl orange** | 327.33 | 1.60 x 0.54 | - |

First, possible non-covalent interactions of dye molecules with unmodified PES support were investigated. Beforehand, the pH dependency of the analyte absorption was investigated. In particular, methyl blue, methyl orange and methylene blue are used as pH indicators. Thus, 1 mL of 1 µM dye solution in Milli-Q water was mixed with 10 µL aq. HCl or NaOH to lower or increase the pH, respectively. UV–Vis spectra of dye solutions with adjusted pH are shown in Figure 5.25 a. Methylene blue, methyl blue and methyl orange showed a pH dependent absorption maximum and intensity as

expected from their use as redox and pH indicators.[321] As those reactions are commonly reversible, the original dye intensity and absorption maximum is regained under appropriate conditions. When passed through the PES support, permeated dye solutions were measured unaltered and treated with HCl to adjust the pH (Figure 5.25 b). For methylene blue and rhodamine b, unspecific binding on the PES support was observed. For methyl orange, no change in absorption maximum and intensity was observed when passed through the support material. Addition of aq. HCl to lower the pH to acidic regime resulted in the same spectral changes for both, feed and permeate solution. For methyl blue, a decrease in absorption intensity is observed when feed and analyte were measured prior to the addition of aq. HCl. Initial absorbance was regained when aq. HCl was added to the solution revealing no decrease of analyte concentration in the permeate solution. A non-covalent interaction between methyl blue and PES can be assumed where the original form of the dye is recovered when aq. HCl is added to the solution. As a consequence of these experiments, methyl blue and BSA were chosen as analytes for size exclusion experiments with asymmetric polymer membranes on top of PES as support material. Both molecules should be larger than the molecular-size cut-off of polymer membranes defined by the dimensions of the FhuA pore (2.5 x 3.0 nm for open channel variant, 1.2 x 0.8 nm for closed WT). Methyl orange was not chosen, because of its smaller molecule size able to pass the wild type channel.

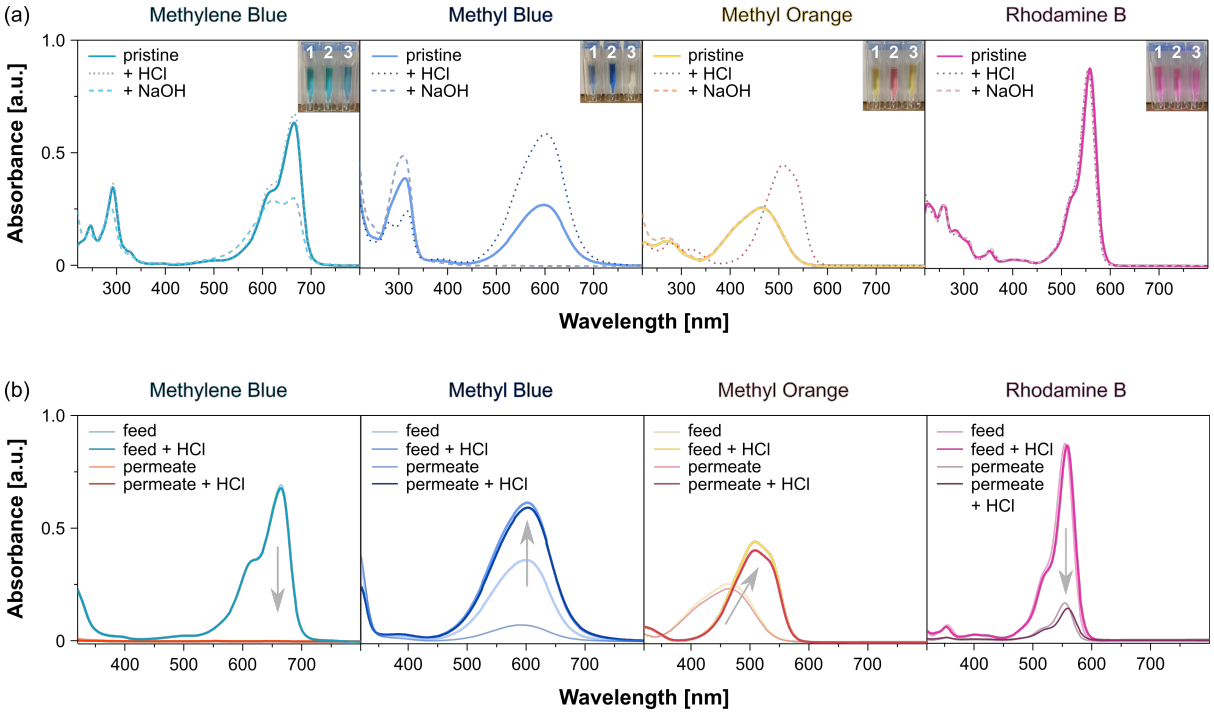


Figure 5.25: UV–Vis spectra of methylene blue, methyl blue, methyl orange and rhodamine b in dependence on the pH value (a). Feed and permeate absorbance of the different dye solutions when passed through a blank PES support (b). The pH value of permeate was adjusted with aq. HCl (10 µL HCl per mL permeate solution) to account for pH dependency of dye solutions.

To test the extreme case and evaluate the suitability of the concept, size exclusion experiments with micrometer-thick membranes composed of solely the polymer were tested at room temperature and 45 °C, referred to as elevated temperature or abbreviated ET in the Figure below. In theory, these membranes should be completely tight above the cloud point of the polymer and show the highest rejection of analytes, as no functional pores should be present. To additionally reduce stress on the membrane, measurements were not performed in the flux device used for evaluation of permeability. As an alternative, Merck Swinnex™ filter holders connected to a syringe were used. A defined volume of analyte was placed in the syringe where the plunger was removed. The analyte solution then passed the membrane clamped in the filter holder (Figure 5.26 a). Representative results are provided in Figure 5.26 b for a PNIPAm-co-PDMMIBA membrane with a thickness of ~ 1.2 µm as derived by SFM. As can be seen, the analyte passes the membrane unhindered at both temperatures. For BSA, a slight reduction of concentration is observed, but is still not in a sufficient range to justify further experiments with this membrane material. Membrane materials from the other copolymers and protein/polymer blends were also tested at 22 °C and 45 °C, but did not show an improved performance either.

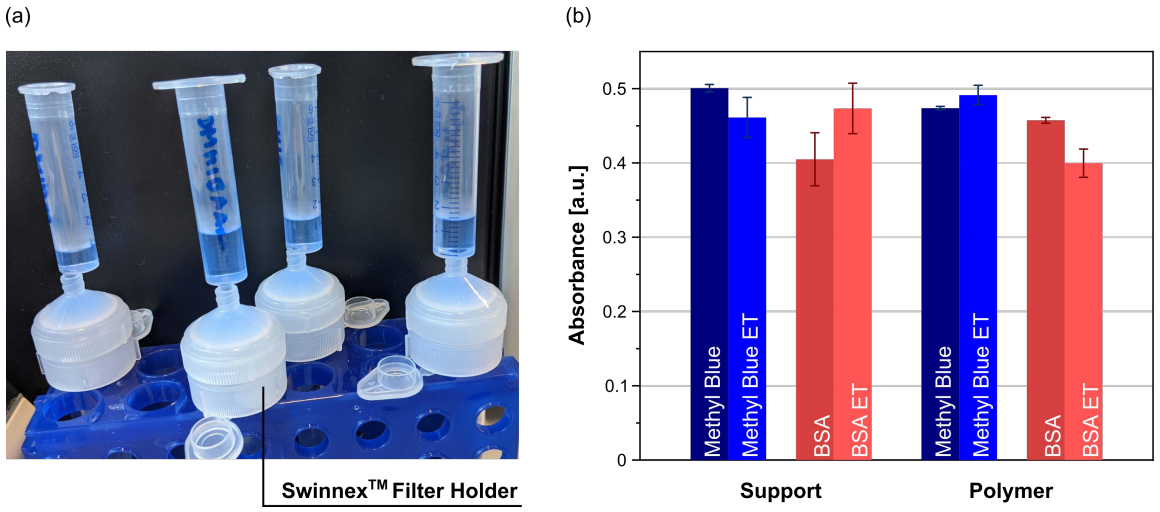


Figure 5.26: Set-up for size exclusion experiments taking use of Swinnex™ filter holders and syringes as reservoirs (a). Absorbance of a methyl blue and BSA solution when passed through the PES support membrane as reference or a PNIPAm-co-PDMMIBA membrane (175 layer equivalents) on top of the porous support (b). Measurements were performed at room temperature and elevated temperature denoted as ET (22 °C and 45 °C, respectively). Absorbances at room temperature and elevated temperature are in the same order of magnitude taking into account the measurement uncertainty represented as error bars of triplicate measurements for each sample.

It is likely that immobilization and UV irradiation in the course of membrane formation results in intrachain rather than interchain crosslinking. The latter is crucial to obtain a densely packed polymer mash surrounding the protein and membrane formation on top of the porous PES support. A hint could be the absence of gel formation in crosslinking experiments presented the beginning of this chapter. Furthermore, membranes prepared on top of a silicon wafer were found to easily wash off, which would be unlikely for covalent interchain crosslinked membrane materials. Intrachain crosslinking would

result in a loop formation in the polymer chain which further reduces interchain entanglement. This effect was already described by ZHAO and coworkers, who investigated the effect of polymer concentration in aqueous solutions on crosslinking efficiency and cloud point temperature. The polymer used was a copolymer of PDMAEMA-co-PCMA, with CMA being a comonomer bearing a photo-crosslinkable coumarin moiety, comparable to the monomer CoumAAm used in this thesis.[311] To sum up this study, a polymer concentration higher than 5 mM corresponding to a coumarin concentration of 50 mM was needed to induce interchain crosslinking. Furthermore, at low polymer concentration and preferred intrachain crosslinking, an increase in cloud point temperature with increasing crosslinking efficiency was observed.[311] It is mentioned, that those experiments were performed as well in the time scope of this thesis, but no correlation of degree of photodimerization and cloud point temperature was observed. This could be explained by the lower number of comonomers incorporated in the polymer (~ 5) compared to the studies by ZHAO (~ 12). Nevertheless, detailed studies have to be performed to tackle the observed lack in membrane formation. The amount of crosslinkable groups incorporated in the polymer material needs to be increased to give the polymers the chance to encounter other polymers in the solution and be part of photodimerization that occurs in an interchain fashion. One possibility could be the preparation of block copolymers which self-assemble into higher order structures with proximity of hydrophobic and hydrophilic parts of the polymer. This technique was frequently used by APPELHANS, MEIER or SUMERLIN and co-workers.[30,42,301,322,323] Nevertheless, in these approaches the protein is most of the time incorporated after the assembly of the copolymers in solution and not covalently attached to the system. This might result in a lack of stability of membranes in operation. An alternative could be, for example, the assembly of block copolymers and proteins functionalized with UV-crosslinkers at the air/water interface in a Langmuir trough. After UV-crosslinking, generated stable membranes could be transferred to a solid support by Langmuir-Schaefer or Langmuir-Blodgett technique and subsequently tested.

### 5.4 Conclusion and Outlook

Even though results in the project Chiral Membranes I seemed promising, the membranes generated during this thesis did not show the anticipated performance. CD spectroscopy and SANS measurements led to the assumption of incomplete refolding of the protein sample prior to modification. The appearance and amount of correctly refolded protein in the sample was not accessible by the chosen analytical methods. Furthermore, the crosslinking efficiency of the polymer matrix seems to be not sufficient under the chosen conditions to obtain a tightly packed mesh of matrix surrounding the protein. Lastly, the temperature-dependent behavior of polymer material in aqueous solution was not transferrable to membrane-scale. Within the completion time of this thesis, other promising membrane approaches utilizing proteins as pores have been presented in the literature, as already shown in the introduction of this thesis. Nevertheless, the use of customizable protein pores is still unique and worth investigating. In following approaches, more detailed look in protein performance and alternative

immobilization procedures is recommended. Reference systems to test protein performance after each modification step, protein refolding, conjugate synthesis and immobilization, would be needed. A polymer matrix based on block copolymers analogous to systems presented by VOIT et al. and MEIER et al. seems more promising as higher local concentration of crosslinker molecules would lead to a denser matrix material.[58,300,324,325] Nevertheless, these systems are as complex as the approach used for this thesis and should also be handled with care.

Even though the route to protein-polymer membranes using protein-polymer conjugates seems not to be promising, a great step towards protein-based membranes was accomplished by my colleague Magnus SCHWIETERS.[291] The direct immobilization of proteins at an interface with a homo-bifunctional crosslinker has shown to yield uniform nano-thin membranes with unique properties. Water permeability and size exclusion experiments using FhuA WT and open channel variant FhuA $\Delta$CVF$^{tev}$ showed sufficient performance. In ongoing experiments, this concept shall be transferred to other biopores like tobacco-mosaic virus-based particles which could be additionally used to vary the membrane thickness by utilizing variants of different length ranging from 20 nm up to 300 nm.[326]

## 5.5 Experimental Part

**Materials:** All materials were received as stated and used as received unless otherwise noted. Ethylenediamine ($\geq$ 99.5 %) and methylene blue were purchased from Roth. 2,3-Dimethyl maleic anhydride (> 98 %) was purchased from TCI. 1,4-Diaminobutane (99 %), 2-bromoethylamine hydrobromide (99 %) and 4-amino-1-butanol (98 %) were purchased from Sigma-Aldrich. Rhodamine B, methyl blue, methyl orange and 7-hydroxy-4-methylcoumarin (97 %) were purchased from Alfa Aesar. Acryloyl chloride (97 %) was used as received from Merck. 2-Methyl-2,4-pentane-$d_{12}$-diol (deuterated MPD) was purchased from Sigma-Aldrich via the stable isotopes customer service. Silicon wafers (p-type, 625 µm thickness, front side polished) were purchased from CrysTec. Circular PES membranes with diameter of 47 or 25 mm and pore size 0.2 µm were purchased from PALL Life Sciences (New York, USA). Glass fiber filters, type MN 85/70 BF with a diameter of 45 mm, were purchased from Carl Roth GmbH (Karlsruhe, Germany). MPD buffer refers to a buffer containing 10 mM sodium phosphate, 10 mM NaCl and 50 mM MPD, pH 7.4, unless otherwise noted. For protein storage, 1 mM $NaN_3$ was added to prevent bacteria growth. All other components are as listed in the other sections of this thesis.

**Instrumentation:**

**Scanning force microscopy** (SFM) was performed on a Bruker Dimension FastScan instrument (Bruker, Bremen, Germany). Silicon tips on a Silicon Nitride cantilever [Fastscan-A probe with a force constant of 18 N/m ($f_0$ = 1400 kHz)] were used for tapping mode measurements in air at a scan rate of 0.506 Hz and 512 samples/line. A scratch was made using a needle at multiple places on the dried sample to measure the thickness of the membrane. **Grazing-incidence small-angle X-ray scattering** (GISAXS) and **x-ray reflectivity** (XRR) experiments were performed on SIRIUS (Soft Interfaces and Resonant Investigation on Undulator Source) station at the SOLEIL synchrotron in Gif-sur-Yvette (France), beamtime 29.05.–03.06.2019.[267] The incident beam energy was 8 keV ($\lambda$ = 0.155 nm). GISAXS 2D scattering patterns were collected with a PILATUS 1 M Dectris detector with a vertical beam stop in front of the detector's window. For films at the air/water interface, a Langmuir trough enclosed in a temperature-controlled sealed chamber was used and flushed with helium during data collection. Spectra analysis of XRR data was performed with StochFit.[315] SLD of wild type and mutant FhuA was estimated using the comprised calculating tool of StochFit based on elemental composition and density of the material. The density of the FhuA variants was estimated by relating the respective molecular volume to the molar mass. To do so, the volume of FhuA was assumed as elliptical tube (height: 5 nm; outer diameters: 4.6 nm, 3.9 nm; inner diameters: 2.3 nm, 1.95 nm), fully hollow in case of FhuA A2a, and filled up to 2/3 in case of FhuA WT accounting for the cork domain. On this basis, StochFit calculated the following SLDs: FhuA WT 18.464 $10^{-6}$ Å$^{-2}$, FhuA A2a 18.048 $10^{-6}$ Å$^{-2}$, and silicon dioxide 22.453 $10^{-6}$ Å$^{-2}$. Small-angle neutron scattering (SANS) experiments were carried out at the D22 beamline at Institute Laue-Langevin, beamtime 15.03.–16.03.2021. Transfer of membrane protein FhuA into deuterated detergent was performed using a Superdex 200 Increase 10/300 GL column system (bead size 8.6 µm, column dimensions 10 x 300 mm) with an initial flow rate of 0.5 mL·min$^{-1}$. The flow-through from the column was collected, measured and used for background subtraction. The flow rate was adjusted during measurement to increase resolution of protein separation. Buffer used contained 50 mM deuterated MPD, 10 mM phosphate pH 7.4 in $D_2O$.

**Methods:**

**Refolding of FhuA variants:** Engineering, expression and extraction of the FhuA variants used in this study were performed by the group of Prof. SCHWANEBERG, RWTH Aachen, according to previously published procedures.[132] The lyophilized powders of denatured proteins, containing approx. 66 wt% SDS, were stored at -20 °C until used for protein refolding. The powder of the respective FhuA variant was dissolved in MPD buffer to a concentration of approximately 2 mg/ml and passed through a sterile PVDF syringe filter to get rid of larger aggregates, cell fragments and bacteria. Controlled refolding was achieved by dialysis against MPD buffer using 12-14 kDa MWCO dialysis membranes (Sigma-Aldrich, USA) at 4 °C. Ratio between sample and dialysis solution was set to 1:200 and buffer changed

every 24 h for three days. Protein concentration was determined by measuring the absorption of protein at 280 nm by UV–Vis absorption spectroscopy. Respective absorption coefficients were obtained using the ProtParam tool and provided amino acid composition of the variants.

**RAFT CTA BTMP, protein-reactive PFP-BTMP and NHS-activated functional CRP initiator** were synthesized as already described in Chapter 2 of this thesis.

**Synthesis of 3,4-dimethyl maleic imidobutyl acrylate (DMMIBA)**

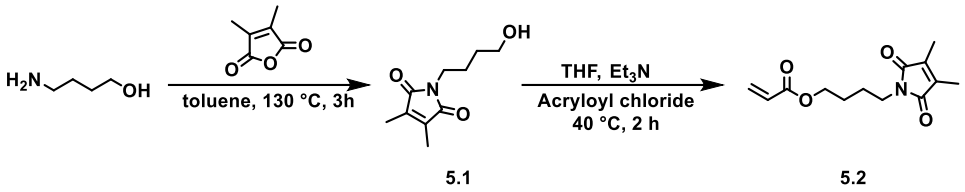


Scheme 5.2: Synthesis of DMMIBA starting from aminobutanol.

2,3-dimethyl maleic anhydride (5 g, 39.6 mmol) was dissolved in a round-bottom flask in 100 mL toluene. Aminobutanol (3.65 mL, 3.53 g, 39.6 mmol) was added in one portion and the flask equipped with a steam separator. The reaction mixture was heated to 130 °C and stirred for 3 h. Solvent was removed under reduced pressure to obtain the crude product as orange oil. After column chromatography (silica gel, *n*-hexane/ethyl acetate, 1:1), the solvent was removed under reduced pressure to yield the product **5.1** as colorless oil (7.8 g, 95 %).

4.68 g of the precursor (23.7 mmol, 1 equiv.) were placed in a Schlenk flask and degassed by three freeze-pump thaw cycles and flushed with inert gas $N_2$. THF (40 mL), acryloyl chloride (3 mL, 3.33 g, 36.8 mmol, 1.55 equiv.) and triethylamine (5 mL, 3.65 g, 36 mmol, 1.8 equiv.) were added under $N_2$ stream and the reaction mixture heated to 40 °C and stirred for 2 h. The mixture was poured in water, extracted 3-times with ethyl acetate (in total 300 mL), organic phase washed 2-times with water, dried with sodium sulfate, filtered and solvent removed under reduced pressure. The crude product was purified by column chromatography (silica gel, *n*-hexane/ethyl acetate, 9:1). The second fraction was collected, solvent removed under reduced pressure, dried in vacuo and the product **5.2** obtained as slightly yellow oil (684 mg, 25 %).

**$^1$H NMR** (300 MHz, chloroform-$d_1$) δ = 6.39 (dd, *J* = 17.3, 1.5 Hz, 1H, C*H*$_2$=), 6.10 (dd, *J* = 17.3, 10.4 Hz, 1H, -C*H*=), 5.81 (dd, *J* = 10.4, 1.5 Hz, 1H, C*H*$_2$=), 4.22 – 4.08 (m, 2H, -OC*H*$_2$), 3.61 – 3.42 (m, 2H, -OC*H*$_2$), 1.95 (s, 6H, 2 -C*H*$_3$), 1.73 – 1.60 (m, 4H, -C*H*$_2$-C*H*$_2$-) ppm.

The $^1$H NMR spectrum was in accordance with literature data.[300]

**Synthesis of *N*-[2-(3,4-dimethyl-2,5-dioxo-2,5-dihydro-pyrrol-1-yl)-ethyl]-acrylamide (DMIAm)**

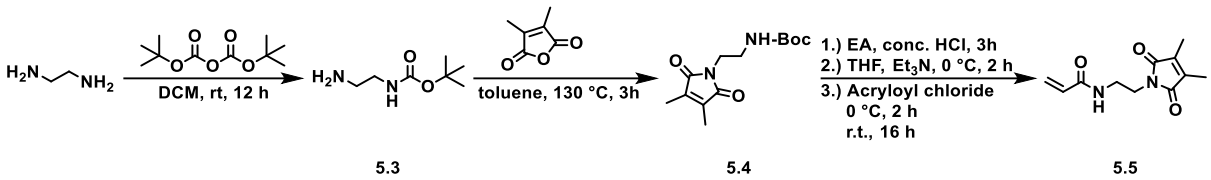


Scheme 5.3: Synthesis of DMIAm starting from ethylenediamine.

To a solution of ethylenediamine (30.05 g, 33.4 mL, 0.5 mol, 7.4 equiv.) dissolved in 200 mL $CH_2Cl_2$, di-*tert*-butyldicarbonate (di-Boc, 14.7 g, 67.8 mmol, 1 equiv.) pre-dissolved in 400 mL $CH_2Cl_2$ was added dropwise under vigorous stirring. Stirring was continued for 3 h at 22 °C. $CH_2Cl_2$ was removed in vacuo, the residual oil dissolved in water and the immediately formed precipitate filtered off. The aqueous phase was saturated with sodium chloride, extracted with $CH_2Cl_2$, organic phase dried with sodium sulphate, filtered and the solvent removed under reduced pressure to yield the product **5.3** as slightly yellow oil (8.74 g, 54.5 mmol, 80 %).

To a solution of mono *N*-Boc-protected ethylenediamine **5.3** (3.71 g, 23 mmol, 1 equiv.) in 100 mL toluene placed in a round-bottomed flask equipped with a water trap and a reflux condenser, 2,3-dimethyl maleic anhydride (2.92 g, 23 mmol, 1 equiv.) was added and the mixture heated to reflux (130 °C) for 3 h. Afterwards, the solvent was removed in vacuo to provide the product **5.4** as yellowish solid (5.85 g, 21.8 mmol, 95 %).

To a suspension of N-[2-(3,4-Dimethyl-2,5-dioxo-2,5-dihydro-pyrrol-1-yl)-aminoethyl]-tert-butyl-carbonate **5.4** (5.85 g, 21.8 mmol) in 45 mL ethyl acetate, 4.5 mL concentrated hydrochloric acid was added under vigorous stirring and stirring continued for 20 h at 22 °C. The precipitate was collected, washed with ethyl acetate and dried in vacuo to yield **unprotected 5.4** as colorless solid (quantitatively).

The HCl-precursor **unprotected 5.4** (3.5 g, 17.1 mmol, 1 equiv.) was dissolved in 160 mL THF, the flask sealed with a septum and degassed by bubbling $N_2$ through the solution. Triethylamine (6.33 g, 9 mL, 62.5 mmol, 3.7 equiv.) was added dropwise followed by the dropwise addition of acryloyl chloride (3.86 g, 3.5 mL, 42.6 mmol, 2.5 equiv.). The reaction mixture was stirred for 3 h under nitrogen atmosphere at 22 °C. The solvent was removed, and the crude product purified by column chromatography (silica gel, $CH_2Cl_2$/EtOH, 97:3). The product **5.5** was obtained as an off-white powder (3.11, 82 %)

**$^1$H NMR** (300 MHz, chloroform-$d_1$) δ = 6.27 – 6.13 (m, 2H, C$H_2$=, N*H*), 6.06 (dd, *J* = 17.0, 10.2 Hz, 1H, -C*H*=), 5.62 (dd, *J* = 10.2, 1.5 Hz, 1H, C$H_2$=), 3.70 (dd, *J* = 6.5, 4.2 Hz, 2H, -C$H_2$N), 3.55 – 3.45 (m, 2H, -NHC$H_2$), 1.96 (s, *J* = 9.0 Hz, 6H, 2 -C$H_3$) ppm.

The $^1$H NMR spectrum was in accordance with literature data.[300]

***N*-[2-(3,4-dimethyl-2,5-dioxo-2,5-dihydro-pyrrol-1-yl)-butyl]-acrylamide (DMMIBAAm)** was prepared using the same procedure described for DMIAm. As starting material, 1,4-diaminobutane instead of ethylene diamine was used. Yields: 1$^{st}$ step: 12.4351 g, 66 mmol, 97 %; 2$^{nd}$ step: 11.6 g, 39.1 mmol, 74 %; 3$^{rd}$ step: 4.7 g, 20.6 mmol, quantitatively; 4$^{th}$ step: 600 mg, 2.4 mmol, 28 %.

**$^1$H NMR** (300 MHz, chloroform-$d_1$) δ = 6.26 (dd, *J* = 17.0, 1.6 Hz, 1H, C*H*$_2$=), 6.08 (dd, J = 17.0, 10.2 Hz, 1H, -C*H*=), 5.79 (s, 1H, N*H*), 5.62 (dd, *J* = 10.2, 1.6 Hz, 1H, C*H*$_2$=), 3.50 (t, *J* = 6.8 Hz, 2H, -C*H*$_2$N), 3.35 (dd, *J* = 12.8, 6.7 Hz, 2H, -NHC*H*$_2$), 1.95 (s, 6H, 2 -C*H*$_3$), 1.68 – 1.46 (m, 4H, -C*H*$_2$-C*H*$_2$-) ppm.

**Synthesis of 7-(2-acrylamidoethoxy)-4-methylcoumarin (CoumAAm):**

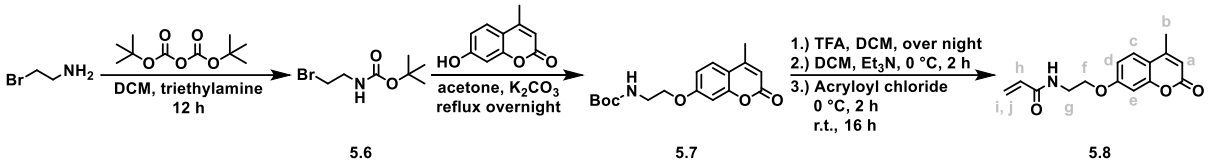


Scheme 5.4: Synthesis of CoumAAm monomer starting from 2-bromoethylamine hydrobromide. Proton assignment as used in NMR spectrum interpretation given in the final step.

To a solution of 2-bromoethylamine hydrobromide (7.45 g, 36.3 mmol, 1 equiv.) and di-Boc (7.55 g, 34.6 mmol, 1 equiv.) in 200 mL $CH_2Cl_2$ placed in a round bottom flask, triethylamine (3.65 g, 5 mL, 36 mmol, 1.04 eq) was added dropwise and the mixture stirred overnight at 22 °C. The reaction mixture was diluted with $CH_2Cl_2$ (100 mL), washed with brine, the organic phase dried with sodium sulfate, filtered and the solvent evaporated under reduced pressure. The product **5.6** was obtained as colorless oil (5.66 g, 25.3 mmol, 70 %).

7-Hydroxy-4-methylcoumarin (1.44 g, 8.18 mmol, 1 equiv.) and potassium carbonate (1.23 g, 8.9 mmol, 1.1 equiv.) were suspended in 100 mL acetone and the solution refluxed for 1 h. Then, *N*-Boc-protected 2-bromoethylamine (2 g, 8.9 mmol, 1.1 equiv.) was added and the reflux was continued for further 18 h. After overnight reflux, the reaction was stopped and filtered after cooling to room temperature. After column chromatography (silica gel, $CH_2Cl_2$/MeOH, 200:1), the product **5.7** was obtained as a colorless solid (1 g, 3.13 mmol, 38%).

*N*-Boc-protected 7-(2-aminoethoxy)-4-methylcoumarin (1 g, 3.13 mmol, 1 equiv.) was dissolved in 25 mL $CH_2Cl_2$. To this solution, trifluoroacetic acid (TFA, 4.075 mL, 6.1 g, 53.3 mmol, 17 equiv.) was added and the solution stirred overnight at 22 °C. The solvent was removed and the residual solid dried in vacuo to yield **TFA-salt of 5.7** as colorless solid (quantitatively).

**TFA-salt of 5.7** (1 g, 3 mmol, 1 equiv.) and triethylamine (2.27 mL, 1.65 g, 16.4 mmol, 5.5 equiv.) were dissolved in 12 mL $CH_2Cl_2$ and degassed by nitrogen flushing. Acryloyl chloride (0.5 mL, 6 mmol, 2 equiv.) was added under ice bath cooling and the reaction mixture stirred overnight, initially under ice bath cooling and later at 22 °C, as the ice melted. The resultant clear brown solution was diluted with 300 mL $CH_2Cl_2$ and washed 3-times each with 0.1 M HCl, saturated sodium bicarbonate and brine. The organic phase was dried with sodium sulphate, filtered and the solvent removed under reduced pressure. The crude product was purified by column chromatography (silica gel, gradient $CH_2Cl_2$/EtOH, 200:1 to 9:1). The 3rd fraction was collected, the solvent removed under reduced pressure and the obtained brownish solid recrystallized in diethyl ether to yield the final product **5.8** as off-white solid (500 mg, 1.82 mmol, 61 %).

**$^1$H NMR** (400 MHz, $D_1$-chloroform) δ = 7.47 (d, *J* = 8.8 Hz, 1H, **c**), 6.84 (dd, *J* = 8.8, 2.4 Hz, 1H, **e**), 6.77 (d, *J* = 2.4 Hz, 1H, **d**), 6.33 (d, *J* = 16.9 Hz, 1H, h), 6.21 – 6.09 (m, 2H, **a** & i), 5.67 (d, *J* = 10.3 Hz, 1H, j), 4.14 (t, *J* = 5.1 Hz, 2H**, g**), 3.79 (dd, *J* = 10.8, 5.4 Hz, 2H, f), 2.38 (s, 3H, **b**) ppm.

The $^1$H NMR spectrum was in accordance with literature data.[301]

**RAFT polymerization of NIPAm with crosslinkable monomers** was performed analogous to the procedure described for the synthesis of PNIPAm homopolymer. Either BTMP or functionalized PFP-BTMP was used for RAFT copolymerization of NIPAm and crosslinkable monomers (CLM) in unstabilized dioxane (monomer concentration 2 M) at 90 °C using ABCVA as initiator. Ratios of [NIPAm]:[CLM]:[CTA]:[AIBN] of [95]:[5]:[1]:[0.1] were used in all cases. Components were introduced to a Schlenk tube, deoxygenated by three freeze-pump-thaw cycles, and transferred to a preheated oil bath at 90 °C. The polymerization was stopped after 3 h by immersing the flask in an ice bath. The polymer was precipitated in cold diethyl ether. The final (protein-reactive) polymer and was dried in vacuo and characterized by NMR spectroscopy, SEC and turbidimetry (Table 5.2).

**Table 5.2: Overview of synthesized copolymers of PNIPAm with crosslinkable co-monomers.**

| PNIPAm-co- | Conversion[1] | $M_{n,theor.}$[a] [g·mol$^{-1}$] | $M_{n,SEC}$ [g·mol$^{-1}$] | $M_{w,SEC}$ [g·mol$^{-1}$] | Đ | $T_{CP}$ [°C] |
|---|---|---|---|---|---|---|
| **PDMMIBA** | 80 % | 9 858 | 11 492 | 13 122 | 1.14 | 25.3 |
| **PDMIAm** | 75 % | 9 148 | 10 771 | 12 745 | 1.18 | 30.2 |
| **PDMMIBAAm** | 83 % | 10 454 | 11 520 | 13 650 | 1.18 | 27.2 |
| **PCoumAAm** | 88 % | 10 915 | 10 038 | 13 116 | 1.31 | 25.5 |

[a] According to NMR spectra of the crude reaction mixtures and based on NIPAm vinylic and polymeric peaks.

**Synthesis of FhuA-polymer conjugates by grafting-from or grafting-to** was performed according to the procedures described in Chapter 2 and Chapter 3 in this thesis. In a typical experiment, CuBr (8.0 mg, 55.8 µmol, 7.0 equiv.) was placed in a syringe along with a magnetic stirring bar. A solution of $Me_6$TREN (22.0 µL, 80.0 µmol, 10.0 equiv.) in 2.5 mL MPD buffer was added and headspace eliminated. The solution was left for disproportionation at 4 °C under rapid stirring for 15 min. Then, a solution containing FhuA-MI (17.0 mg, 0.22 µmol, 8.0 µmol attached initiating units, 1 equiv.), NIPAm (172 mg, 1515 µmol, 190 equiv.) and DMMIBA (20 mg, 80 µmol, 10 equiv.) in 15 mL MPD buffer was added to the syringe and polymerized for 1 h at 4 °C under rapid stirring. Afterwards, the solution was filtered through a 0.2 µm sterile PVDF syringe filter, transferred to a 14 kDa MWCO dialysis membrane and purified by 3x dialysis with buffer exchange every 24 h. The degree of polymerization was adjusted by varying the ratio of monomer to initiator to obtain FhuA-PNIPAm$_{50}$ and FhuA-PNIPAm$_{100}$.

**Membranes on silicon wafers:** Silicon wafers of respective size varying between 1–2 cm$^2$ were cleaned with absolute ethanol and dried using pressurized air. To impart hydrophilicity, the wafers were etched with air plasma for 5 min at a pressure of 0.2 mbar. For UV crosslinked samples, the wafer was put on a teflon block placed on an ice bath. The respective amount of protein-polymer conjugate solution was spread on top of the silicon wafer, equilibrated for 15 min and irradiated with UV light for 15–120 min.

**Membranes on PES support:** PES support was soaked in water, the excess water wiped off and the support placed on a teflon block put atop an ice bath. The respective amount of protein-polymer conjugate in a total volume of 500 µL for 17.349 cm$^2$ supports or 145 µL for 4.908 cm$^2$ supports was spread on top of the porous support, equilibrated for 15 min and then exposed to UV light for 15–120 min. After that, the dry membrane on top of the PES support was used for water flux and permeation experiments.

**UV-crosslinking:** UV-crosslinking was carried out with a Panacol UV-F 400F device, operating at 450 W. Different distances to the source and crosslinking times were evaluated to obtain optimal crosslinking efficiency. For membranes prepared for permeation and size exclusion experiments, 15 cm distance and 120 min of irradiation were used. Values for radiant flux density and dose at different detector–source distances are provided in Table 5.3.

**Table 5.3: Radiant flux density and dose at different distances to the used UV source equipped with a blue filter unit measured with a Dymax ACCU-CAL™ 50-LED radiometer.**

| Distance [cm] | Radiant Flux Density [mW·cm$^{-2}$] | Dose [mJ·cm$^{-2}$·min$^{-1}$] |
|---|---|---|
| **5** | 46 | 2 796 |
| **10** | 26 | 1 604 |
| **15** | 19 | 1 188 |
| **20** | 15 | 888 |
| **25** | 11 | 695 |
| **30** | 8 | 492 |

**Flux and permeation measurements:** The flux and permeation measurements were conducted on a custom-made in-house device. The scheme for the device is shown in Figure 5.16. The flow rate was calculated by recording the rate of increase in mass on the balance. An equilibration time of 3 min was used for each membrane and increase in mass over the balance measured for at least 3 min at a given transmembrane pressure with data acquisition every second. The transmembrane pressure correlates in the setup with the hydrostatic pressure defined by the height difference between reservoir and measurement chamber. For measurements at higher temperature, a thermostat connected to the device was used to heat up the analyte solution in the reservoir. The tempered solution was passed through the measurement chamber and the temperature checked on the permeate site until steady. Increase in mass on the balance was recorded for 30 min or until a linear increase in mass over time at a specific temperature was achieved. The flux at different temperatures was viscosity-corrected using temperatures in the reservoir, above the membrane and on the permeate side.

**Amino acid composition of FhuA WT, FhuA ΔCVF$^{tev}$ and FhuA ΔCVF$^{tev}$K$_{11}^{up}$** were used as reported by Julia KINZEL.[293] The amino acids belonging to the cork domain in FhuA WT are highlighted in red and blue. Removal of the cork domain, three point mutations and the incorporation of a cleavage site for the TEV protease leads to the generation of FhuA ΔCVF$^{tev}$. Exchange of lysine residues with arginine residues by point mutations to adjust the number and position of anchoring points for modification with small CRP initiators results in FhuA ΔCVF$^{tev}$K$_{11}^{up}$.

**Sequence FhuA WT**

**AVEPKEDTIT VTAAPAPQES AWGPAATIAA RQSATGTKTD TPIQKVPQSI SVVTAEEMAL HQPKSVKEAL SYTPGVSVGT RGASNTYDHL IIRGFAAEGQ SQNNYLNGLK LQGNFYNDAV IDPYMLERAE IMRGPVSVLY GKSSPGGLLN MVSKRPTTEP** LKEVQFKAGT DSLFQTGFDF SDSLDDDGVY SYRLTGLARS ANAQQKGSEE QRYAIAPAFT WRPDDKTNFT FLSYFQNEPE TGYYGWLPKE GTVEPLPNGK RLPTDFNEGA KNNTYSRNEK MVGYSFDHEF NDTFTVRQNL RFAENKTSQN SVYGYGVCSD PANAYSKQCA ALAPADKGHY LARKYVVDDE KLQNFSVDTQ LQSKFATGDI DHTLLTGVDF MRMRNDINAW FGYDDSVPLL NLYNPVNTDF DFNAKDPANS GPYRILNKQK QTGVYVQDQA QWDKVLVTLG GRYDWADQES LNRVAGTTDK RDDKQFTWRG GVNYLFDNGV TPYFSYSESF EPSSQVGKDG NIFAPSKGKQ YEVGVKYVPE DRPIVVTGAV YNLTKTNNLM ADPEGSFFSV EGGEIRARGV EIEAKRPLSA SVNVVGSYTY TDAEYTTDTT YKGNTPAQVP KHMASLWADY TFFDGPLSGL TLGTGGRYTG SSYGDPANSF KVGSYTVVDA LVRYDLARVG MAGSNVALHV NNLFDREYVA SCFNTYGCFW GAERQVVATA TFRF

### Sequence FhuA ΔCVF$^{tev}$

LKEVQFKAGT DSLFQTGFDF SDSLDDDGVY SYRLTGLARS ANAQQKGSEE QRYAIAPAFT WRPDDKTNFT
FLSYFQNEPE TGYYGWLPKE GTVEPLPNGK RLPTDFNEGA KNNTYSRNEK MVGYSFDHEF NDTFTVRQNL
RFAENKTSQN SVYGYGVCSD PANAYSKQCA ALAPADKGHY LARKYVVDDE KLQNFSVDTQ LQSKFATGDI
DHTLLTGVDF MRMRNDINAW FGYDDSVPLL NLYNPVNTDF DFNAKDPANS GPYRILNKQK QTGVYVQDQA
QWDKVLVTLG GRYDWADQES LNRVAGTTDK RDDKQFTWRG GVNYLFDNGV TPYFSYSESF FPSSQVGKEN
LYFQGDGNIF APSKGKQYEV GVKYVPEDRP IVVTGAVYNL TCTNVLMADP EGENLYFQGS FFSVEGGEIR
ARGVEIEAKR PLSASVNVVG SYTYTDAEYT TDTTYKGNTP AQVPKHMASL WADYTFFDGP LSGLTLGTGG
RYTGSSYGDP ANSFKVGSYT VVDALVRYDL ARVGMAGSNV ALHVNNLFDR EYVASCFNTY GCFWGAERQV
VATATFRF

### FhuA ΔCVF$^{tev}$K$_{11}^{up}$

LREVQFRAGT DSLFQTGFDF SDSLDDDGVY SYRLTGLARS ANAQQKGSEE QRYAIAPAFT WRPDDRTNFT
FLSYFQNEPE TGYYGWLPLE GTVEPLPNGR RLPTDFNEGA KNNKYSRNER MVGYSFDHEF NDTFTVRQNL
RFAENKTSQN SVYGYGVCSD PANAYSRQCA ALAPADRGHY LARRYVVDDE RLQNFSVDTQ LQSRFATGDI
DHTLLTGVDF MRMRNDINAW FGYDDSVPLL NLYNPVNTDF DFNARDPANS GPYRILNKQR QTGVYVQDQA
QWDRVLVTLG GRYDWADQES LNRVAGTTDK RDDRQFTWRG GVNYLFDNGV TPYFSYSESF FPSSQVGREN
LYFQGDGNIF APSKGRQYEV GVRYVPEDRP IVVTGAVYNL TCTNVLMADP EGENLYFQGS FFSVKGGEIR
ARGVEIEARR PLSASVNVVG SYTYTDAEYT TDTTYKGNTP AQVPRHMASL WADYTFFDGP LSGLTLGTGG
RYTGSSYGDP ANSFKVGSYT VVDALVRYDL ARVGMAGSNV ALHVNNLFDR KYVASCFNTY GCFWGAERQV
VATATFRF

# 6 Contributions

This thesis is the teamwork of several cooperations and I would like to thank all my cooperation partners and clarify their respective contributions.

Marcus Michaelis (University of Potsdam, group of Prof. Dr. Heiko Möller) helped with the **protein NMR** experiments, provided the protein samples and performed sample purification and measurements. Evaluation and interpretation of the data was a joint process. Conjugate synthesis, data illustration and discussion as part of this thesis was done by me.

Dr. Jasmin Preis (PSS GmbH, Mainz with Prof. Dr. Thorsten Hofe as additional supervisor) was the main counterpart for the **SEC-MALS** experiments. Dr. Jasmis Preis suggested respective column and eluent systems and performed measurements at PSS. Evaluation and interpretation of the data was a joint process. Conjugate synthesis, data illustration and discussion as part of this thesis was done by me.

Dr. Ivo Nischang (University of Jena) performed **SV-AUC** experiments and provided respective plots of the measurements. Evaluation and interpretation of the data was a joint process. Conjugate synthesis, data illustration and discussion as part of this thesis was done by me.

**FhuA** protein samples were designed, produced and provided by co-workers in the group of Prof. Dr. Ulrich Schwaneberg (RWTH Aachen) in denatured and lyophilized form. Refolding, conjugate synthesis and characterization was performed by me. Analysis of samples by **CD spectroscopy** was performed under supervision from Dr. Anja Thalhammer (University of Potsdam). Measurement of **MALDI** data was performed by Dr. Ulrich Glebe, Fraunhofer IAP. GISAXS and XRR measurements at Synchrotron SOLEIL were done with kind help of Dr. Stephanie Taßler. Measurements of protein samples by SANS, data evaluation and interpretation were performed by Dr. Anne Martel, Dr. Andrea Lassenberger and Dr. Andrea Tummino (Institute Laue-Langevin, Grenoble, France).

# 7 Bibliography


[1] N. Teramoto, *Polymers* **2020**, *12*, 2386.

[2] C. Brigham in *Green Chemistry* (Eds.: B. Török, T. Dransfield), Elsevier, Amsterdam, **2018**, pp. 753–770.

[3] G. Löffler, *Basiswissen Biochemie. Mit Pathobiochemie*, Springer, Berlin Heidelberg, **2005**.

[4] J. M. Berg, J. L. Tymoczko, L. Stryer, N. D. Clarke, *Biochemistry*, W. H. Freeman, New York, **2002**.

[5] S. Kapoor, A. Rafiq, S. Sharma, *Crit. Rev. Food. Sci. Nutr.* **2017**, *57*, 2321–2329.

[6] S. Nagarajan, S. Radhakrishnan, S. N. Kalkura, S. Balme, P. Miele, M. Bechelany, *Macromol. Chem. Phys.* **2019**, *220*, 1900126.

[7] D. A. Ferreira-Filipe, A. Paço, A. C. Duarte, T. Rocha-Santos, A. L. Patrício Silva, *Int. J. Environ. Res. Public Health* **2021**, *18*, 7729.

[8] B. Erickson, Nelson, P. Winters, *Biotechnol. J.* **2012**, *7*, 176–185.

[9] B. Mattiasson, *Biotechnol. Rep.* **2016**, *11*, 1.

[10] J. A. Himmelberger, K. E. Cole, D. P. Dowling in *Green Chemistry* (Eds.: B. Török, T. Dransfield), Elsevier, Amsterdam, **2018**, pp. 471–512.

[11] F. Rigoldi, S. Donini, A. Redaelli, E. Parisini, A. Gautieri, *APL Bioeng.* **2018**, *2*, 11501.

[12] L. A. de Graaf, P. Kolster, *Macromol. Symp.* **1998**, *127*, 51–58.

[13] N. C. Abascal, L. Regan, *Open Biol.* **2018**, *8*, 180113.

[14] R. Singh, M. Kumar, A. Mittal, P. K. Mehta, *3 Biotech* **2016**, *6*, 174.

[15] H. M. Berman, J. Westbrook, Z. Feng, G. Gilliland, T. N. Bhat, H. Weissig, I. N. Shindyalov, P. E. Bourne, *Nucleic Acids Res.* **2000**, *28*, 235–242.

[16] R. Berisio, L. Vitagliano, L. Mazzarella, A. Zagari, *Protein Sci.* **2002**, *11*, 262–270.

[17] N. Ramasubbu, V. Paloth, Y. Luo, G. D. Brayer, M. J. Levine, *Acta Cryst.* **1996**, *D52*, 435–446.

[18] J. Sakon, D. Irwin, D. B. Wilson, P. A. Karplus, *Nat. Struct. Mol. Biol.* **1997**, *4*, 810–818.

[19] H. Sakuraba, K. Yoneda, K. Yoshihara, K. Satoh, R. Kawakami, Y. Uto, H. Tsuge, K. Takahashi, H. Hori, T. Ohshima, *Appl. Environ. Microbiol.* **2007**, *73*, 7427–7434.

[20] D. F. Savage, P. F. Egea, Y. Robles-Colmenares, J. D. O'Connell, R. M. Stroud, *PLoS Biol.* **2003**, *1*, E72.

[21] M. Saur, M. J. Hartshorn, J. Dong, J. Reeks, G. Bunkoczi, H. Jhoti, P. A. Williams, *Drug Discov. Today* **2020**, *25*, 485–490.

[22] G. L. Gilliland, E. L. Winborne, J. Nachman, A. Wlodawer, *Proteins* **1990**, *8*, 82–101.

[23] D. Sehnal, S. Bittrich, M. Deshpande, R. Svobodová, K. Berka, V. Bazgier, S. Velankar, S. K. Burley, J. Koča, A. S. Rose, *Nucleic Acids Res.* **2021**, *49*, W431-W437.

[24] D. Gaddes, H. Jung, A. Pena-Francesch, G. Dion, S. Tadigadapa, W. J. Dressick, M. C. Demirel, *ACS Appl. Mater. Interfaces* **2016**, *8*, 20371–20378.

[25] V. Tournier, C. M. Topham, A. Gilles, B. David, C. Folgoas, E. Moya-Leclair, E. Kamionka, M.-L. Desrousseaux, H. Texier, S. Gavalda et al., *Nature* **2020**, *580*, 216–219.

[26] L.-T. Lim in *Improving and Tailoring Enzymes for Food Quality and Functionality* (Ed.: R. Y. Yada), Woodhead Publishing, Cambridge, **2015**, pp. 161–178.

[27] M. Mohammadi, S. Mirabzadeh, R. Shahvalizadeh, H. Hamishehkar, *Int. J. Biol. Macromol.* **2020**, *149*, 11–20.

[28] K. Jakab, F. Marga, R. Kaesser, T.-H. Chuang, H. Varadaraju, D. Cassingham, S. Lee, A. Forgacs, G. Forgacs, *Mater. Today Sustain.* **2019**, *5*, 100018.

[29] J. Lane, O. Selifonova, T. Beardslee, D. Demirjian, A. Forgacs, *Ind. Biotechnol.* **2015**, *11*, 259–265.

[30] H. Wang, T.-S. Chung, Y. W. Tong, K. Jeyaseelan, A. Armugam, Z. Chen, M. Hong, W. Meier, *Small* **2012**, *8*, 1185-1190.

[31] A. Woolfson, *Science* **2019**, *364*, 340.1-340.

[32] Y. Chun, L. Qing, G. Sun, M. R. Bilad, A. G. Fane, T. H. Chong, *Desalination* **2018**, *445*, 75–84.

[33] E. Abaie, L. Xu, Y.-X. Shen, *Front. Environ. Sci. Eng.* **2021**, *15*, 124.

[34] L. Xia, M. F. Andersen, C. Hélix-Nielsen, J. R. McCutcheon, *Ind. Eng. Chem. Res.* **2017**, *56*, 11919–11925.

[35] M. Garni, R. Wehr, S. Y. Avsar, C. John, C. Palivan, W. Meier, *Eur. Polym. J.* **2019**, *112*, 346–364.

[36] M. Garni, S. Thamboo, C.-A. Schoenenberger, C. G. Palivan, *Biochim. Biophys. Acta Biomembr.* **2017**, *1859*, 619–638.

[37] C. Xu, S. Hu, X. Chen, *Mater. Today* **2016**, *19*, 516–532.

[38] V. Chimisso, V. Maffeis, D. Hürlimann, C. G. Palivan, W. Meier, *Macromol. Biosci.* **2020**, *20*, e1900257.

[39] X. Zhang, P. Tanner, A. Graff, C. G. Palivan, W. Meier, *J. Polym. Sci. A Polym. Chem.* **2012**, *50*, 2293–2318.

[40] N. Abdullah, M. A. Rahman, M. H. Dzarfan Othman, J. Jaafar, A. F. Ismail in *Current Trends and Future Developments on (Bio-) Membranes* (Eds.: A. Basile, S. Mozia, R. Molinari), Elsevier, Amsterdam, **2018**, pp. 45–70.

[41] P. van Rijn, M. Tutus, C. Kathrein, L. Zhu, M. Wessling, U. Schwaneberg, A. Böker, *Chem. Soc. Rev.* **2013**, *42*, 6578–6592.

[42] J. Kowal, D. Wu, V. Mikhalevich, C. G. Palivan, W. Meier, *Langmuir* **2015**, *31*, 4868–4877.

[43] P. van Rijn, A. Böker, *J. Mater. Chem.* **2011**, *21*, 16735.

[44] N. Muhammad, T. Dworeck, M. Fioroni, U. Schwaneberg, *J. Nanobiotechnol.* **2011**, *9*, 8.

[45] F. Itel, A. Najer, C. G. Palivan, W. Meier, *Nano Lett.* **2015**, *15*, 3871–3878.

[46] C. G. Palivan, R. Goers, A. Najer, X. Zhang, A. Car, W. Meier, *Chem. Soc. Rev.* **2016**, *45*, 377–411.

[47] K. P. Locher, B. Rees, R. Koebnik, A. Mitschler, L. Moulinier, J. P. Rosenbusch, D. Moras, *Cell* **1998**, *95*, 771–778.

[48] C. Dong, K. Beis, J. Nesper, A. L. Brunkan-LaMontagne, B. R. Clarke, C. Whitfield, J. H. Naismith, *Nature* **2006**, *444*, 226–229.

[49] E. C. McCusker, C. Bagnéris, C. E. Naylor, A. R. Cole, N. D'Avanzo, C. G. Nichols, B. A. Wallace, *Nat. Commun.* **2012**, *3*, 1102.

[50] C. A. Stevens, K. Kaur, H.-A. Klok, *Adv. Drug Deliv. Rev.* **2021**, *174*, 447–460.

[51] A. Huang, B. D. Olsen, *Macromol. Rapid. Commun.* **2016**, *37*, 1268–1274.

[52] N. Misawa, T. Osaki, S. Takeuchi, *J. R. Soc. Interface.* **2018**, *15*, 20170952.

[53] H. Ryu, A. Fuwad, S. Yoon, H. Jang, J. C. Lee, S. M. Kim, T.-J. Jeon, *Int. J. Mol. Sci.* **2019**, *20*, 1437.

[54] X. Peng, J. Jin, Y. Nakamura, T. Ohno, I. Ichinose, *Nat. Nanotechnol.* **2009**, *4*, 353–357.

[55] S. Reinicke, H. C. Rees, P. Espeel, N. Vanparijs, C. Bisterfeld, M. Dick, R. R. Rosencrantz, G. Brezesinski, B. G. de Geest, F. E. Du Prez et al., *ACS Appl. Mater. Interfaces* **2017**, *9*, 8317–8326.

[56] Y.-K. Cen, Y.-X. Liu, Y.-P. Xue, Y.-G. Zheng, *Adv. Synth. Catal.* **2019**, *361*, 5500–5515.

[57] R. Sarma, M. S. Islam, A.-F. Miller, D. Bhattacharyya, *ACS Appl. Mater. Interfaces* **2017**, *9*, 14858–14867.

[58] C. Draghici, V. Mikhalevich, G. Gunkel-Grabole, J. Kowal, W. Meier, C. G. Palivan, *Langmuir* **2018**, *34*, 9015–9024.

[59] U. Schwaneberg, A. Böker, *Basistechnologien für die nächste Generation biotechnologischer Verfahren: Chirale Membranen*. *Veröffentlichung der Ergebnisse vom Forschungsvorhaben im BMBF-Programm*, Fraunhofer IAP, Potsdam-Golm, Projektlaufzeit: 01.11.2012-31.01.2018, **2018**.

[60] R. Sinha, P. Shukla, *Curr. Protein Pept. Sci.* **2019**, *20*, 398–407.

[61] Z. Liu, I. Ghai, M. Winterhalter, U. Schwaneberg, *ACS Sens.* **2017**, *2*, 1619–1626.

[62] Y.-M. Tu, W. Song, T. Ren, Y.-X. Shen, R. Chowdhury, P. Rajapaksha, T. E. Culp, L. Samineni, C. Lang, A. Thokkadam et al., *Nat. Mater.* **2020**, *19*, 347–354.

[63] D. Anand, G. V. Dhoke, J. Gehrmann, T. M. Garakani, M. D. Davari, M. Bocola, L. Zhu, U. Schwaneberg, *Chem. Commun.* **2019**, *55*, 5431–5434.

[64] T. Mirzaei Garakani, D. F. Sauer, M. A. S. Mertens, J. Lazar, J. Gehrmann, M. Arlt, J. Schiffels, U. Schnakenberg, J. Okuda, U. Schwaneberg, *ACS Catal.* **2020**, *10*, 10946–10953.

[65] A. D. Ferguson, E. Hofmann, J. W. Coulton, K. Diederichs, W. Welte, *Science* **1998**, *282*, 2215–2220.

[66] M. Bonhivers, M. Desmadril, G. S. Moeck, P. Boulanger, A. Colomer-Pallas, L. Letellier, *Biochemistry* **2001**, *40*, 2606–2613.

[67] L. Plançon, C. Janmot, M. Le Maire, M. Desmadril, M. Bonhivers, L. Letellier, P. Boulanger, *J. Mol. Biol.* **2002**, *318*, 557–569.

[68] V. Braun, *J. Bacteriol.* **2009**, *191*, 3431–3436.

[69] T. Dworeck, A.-K. Petri, N. Muhammad, M. Fioroni, U. Schwaneberg, *Protein Expr. Purif.* **2011**, *77*, 75–79.

[70] M. Krewinkel, T. Dworeck, M. Fioroni, *J. Nanobiotechnol.* **2011**, *9*, 33.

[71] A. Dennig, A. V. Shivange, J. Marienhagen, U. Schwaneberg, *PLoS ONE* **2011**, *6*, e26222.

[72] D. F. Sauer, M. Bocola, C. Broglia, M. Arlt, L.-L. Zhu, M. Brocker, U. Schwaneberg, J. Okuda, *Chem. Asian J.* **2015**, *10*, 177–182.

[73] J. Kinzel, D. F. Sauer, M. Bocola, M. Arlt, T. Mirzaei Garakani, A. Thiel, K. Beckerle, T. Polen, J. Okuda, U. Schwaneberg, *Beilstein J. Org. Chem.* **2017**, *13*, 1498–1506.

[74] D. F. Sauer, Y. Qu, M. A. S. Mertens, J. Schiffels, T. Polen, U. Schwaneberg, J. Okuda, *Catal. Sci. Technol.* **2019**, *9*, 942–946.

[75] H. Osseili, D. F. Sauer, K. Beckerle, M. Arlt, T. Himiyama, T. Polen, A. Onoda, U. Schwaneberg, T. Hayashi, J. Okuda, *Beilstein J. Org. Chem.* **2016**, *12*, 1314–1321.

[76] A. Thiel, D. F. Sauer, U. Markel, M. A. S. Mertens, T. Polen, U. Schwaneberg, J. Okuda, *Org. Biomol. Chem.* **2021**, *19*, 2912–2916.

[77] M. Kovaliov, T. A. Wright, B. Cheng, R. T. Mathers, X. Zhang, D. Meng, K. Szcześniak, J. Jenczyk, S. Jurga, D. Cohen-Karni et al., *Bioconjugate Chem.* **2020**, *31*, 939–947.

[78] A. K. Thakur, L. Movileanu, *ACS Sens.* **2019**, *4*, 2320–2326.

[79] I. Gutiérrez-del-Río, L. Marín, J. Fernández, M. Álvarez San Millán, F. J. Ferrero, M. Valledor, J. C. Campo, N. Cobián, I. Méndez, F. Lombó, *PLoS ONE* **2018**, *13*, e0184277.

[80] T. A. Wright, R. C. Page, D. Konkolewicz, *Polym. Chem.* **2019**, *10*, 434–454.

[81] A. J. Russell, S. L. Baker, C. M. Colina, C. A. Figg, J. L. Kaar, K. Matyjaszewski, A. Simakova, B. S. Sumerlin, *AIChE J.* **2018**, *64*, 3230–3245.

[82] C. Chen, D. Y. W. Ng, T. Weil, *Prog. Polym. Sci.* **2020**, *105*, 101241.

[83] A. Bujacz, *Acta Cryst.* **2012**, *D68*, 1278–1289.

[84] K. M. Burridge, T. A. Wright, R. C. Page, D. Konkolewicz, *Macromol. Rapid. Commun.* **2018**, *39*, e1800093.

[85] J. Phommalysack-Lovan, Y. Chu, C. Boyer, J. Xu, *Chem. Commun.* **2018**, *54*, 6591–6606.

[86] D. Konkolewicz, Y. Wang, P. Krys, M. Zhong, A. A. Isse, A. Gennaro, K. Matyjaszewski, *Polym. Chem.* **2014**, *5*, 4409.

[87] A. Theodorou, P. Mandriotis, A. Anastasaki, K. Velonia, *Polym. Chem.* **2021**, *12*, 2228–2235.

[88] A. Theodorou, E. Liarou, D. M. Haddleton, I. G. Stavrakaki, P. Skordalidis, R. Whitfield, A. Anastasaki, K. Velonia, *Nat. Commun.* **2020**, *11*, 1486.

[89] G. Szczepaniak, M. Łagodzińska, S. Dadashi-Silab, A. Gorczyński, K. Matyjaszewski, *Chem. Sci.* **2020**, *11*, 8809–8816.

[90] E. Liarou, Y. Han, A. M. Sanchez, M. Walker, D. M. Haddleton, *Chem. Sci.* **2020**, *11*, 5257–5266.

[91] J. Xu, K. Jung, N. A. Corrigan, C. Boyer, *Chem. Sci.* **2014**, *5*, 3568–3575.

[92] B. S. Tucker, M. L. Coughlin, C. A. Figg, B. S. Sumerlin, *ACS Macro Lett.* **2017**, *6*, 452–457.

[93] A. Bagheri, C. W. A. Bainbridge, K. E. Engel, G. G. Qiao, J. Xu, C. Boyer, J. Jin, *ACS Appl. Polym. Mater.* **2020**, *2*, 782–790.

[94] J. Yeow, R. Chapman, J. Xu, C. Boyer, *Polym. Chem.* **2017**, *8*, 5012–5022.

[95] N. Corrigan, J. Yeow, P. Judzewitsch, J. Xu, C. Boyer, *Angew. Chem.* **2019**, *131*, 5224–5243.

[96] G. R. Jones, A. Anastasaki, R. Whitfield, N. Engelis, E. Liarou, D. M. Haddleton, *Angew. Chem. Int. Ed.* **2018**, *57*, 10468–10482.

[97] A. Simakova, S. E. Averick, D. Konkolewicz, K. Matyjaszewski, *Macromolecules* **2012**, *45*, 6371–6379.

[98] S. Averick, A. Simakova, S. Park, D. Konkolewicz, A. J. D. Magenau, R. A. Mehl, K. Matyjaszewski, *ACS Macro Lett.* **2012**, *1*, 6–10.

[99] D. Cohen-Karni, M. Kovaliov, T. Ramelot, D. Konkolewicz, S. Graner, S. Averick, *Polym. Chem.* **2017**, *8*, 3992–3998.

[100] Q. Zhang, M. Li, C. Zhu, G. Nurumbetov, Z. Li, P. Wilson, K. Kempe, D. M. Haddleton, *J. Am. Chem. Soc.* **2015**, *137*, 9344–9353.

[101] M. Li, H. Li, P. De, B. S. Sumerlin, *Macromol. Rapid. Commun.* **2011**, *32*, 354–359.

[102] C. Boyer, V. Bulmus, J. Liu, T. P. Davis, M. H. Stenzel, C. Barner-Kowollik, *J. Am. Chem. Soc.* **2007**, *129*, 7145–7154.

[103] M. Kovaliov, M. L. Allegrezza, B. Richter, D. Konkolewicz, S. Averick, *Polymer* **2018**, *137*, 338–345.

[104] X. Li, L. Wang, G. Chen, D. M. Haddleton, H. Chen, *Chem. Commun.* **2014**, *50*, 6506–6508.

[105] N. Vanparijs, S. Maji, B. Louage, L. Voorhaar, D. Laplace, Q. Zhang, Y. Shi, W. E. Hennink, R. Hoogenboom, B. G. de Geest, *Polym. Chem.* **2015**, *6*, 5602–5614.

[106] R. M. Broyer, G. N. Grover, H. D. Maynard, *Chem. Commun.* **2011**, *47*, 2212–2226.

[107] M. S. Messina, K. M. M. Messina, A. Bhattacharya, H. R. Montgomery, H. D. Maynard, *Prog. Polym. Sci.* **2020**, *100*, 101186.

[108] W. Zhao, F. Liu, Y. Chen, J. Bai, W. Gao, *Polymer* **2015**, *66*, A1-A10.

[109] Y. Qi, A. Chilkoti, *Polym. Chem.* **2014**, *5*, 266–276.

[110] J. D. Wallat, K. A. Rose, J. K. Pokorski, *Polym. Chem.* **2014**, *5*, 1545–1558.

[111] P. Wilson, *Macromol. Chem. Phys.* **2017**, *218*, 1600595.

[112] S. Averick, R. A. Mehl, S. R. Das, K. Matyjaszewski, *J. Control. Release* **2015**, *205*, 45–57.

[113] Nathaniel Corrigan, Kenward Jung, Graeme Moad, Craig J. Hawker, Krzysztof Matyjaszewski, Cyrille Boyer, *Prog. Polym. Sci.* **2020**, *111*, 101311.

[114] Y. Wang, C. Wu, *Biomacromolecules* **2018**, *19*, 1804–1825.

[115] W. Yang, L. Zhu, Y. Cui, H. Wang, Y. Wang, L. Yuan, H. Chen, *ACS Appl. Mater. Interfaces* **2016**, *8*, 15967–15974.

[116] B. S. Sumerlin, *ACS Macro Lett.* **2012**, *1*, 141–145.

[117] S. Carmali, H. Murata, K. Matyjaszewski, A. J. Russell, *Biomacromolecules* **2018**, *19*, 4044–4051.

[118] C. M. Riccardi, K. S. Cole, K. R. Benson, J. R. Ward, K. M. Bassett, Y. Zhang, O. V. Zore, B. Stromer, R. M. Kasi, C. V. Kumar, *Bioconjugate Chem.* **2014**, *25*, 1501–1510.

[119] N. J. Greenfield, *Nat. Protoc.* **2006**, *1*, 2876–2890.

[120] B. A. Wallace, J. G. Lees, A. J. W. Orry, A. Lobley, R. W. Janes, *Protein Sci.* **2003**, *12*, 875–884.

[121] J. T. Pelton, L. R. McLean, *Anal. Biochem.* **2000**, *277*, 167–176.

[122] B. S. Moorthy, L. K. Iyer, E. M. Topp, *Curr. Pharm. Des.* **2015**, *21*, 5845–5853.

[123] A. Ausili, M. Sánchez, J. C. Gómez-Fernández, *Biomed. Spectrosc. Imaging* **2015**, *4*, 159–170.

[124] H. Amartely, O. Avraham, A. Friedler, O. Livnah, M. Lebendiker, *Sci. Rep.* **2018**, *8*, 6907.

[125] S. Unzai, *Biophys. Rev.* **2018**, *10*, 229–233.

[126] J. K. Pokorski, M. J. Hore, *Curr. Opin. Colloid Interface Sci.* **2019**, *42*, 157–168.

[127] A. Miller, J. Tanner, *Essentials of Chemical Biology: Structure and Dynamics of Biological Macromolecules*, Wiley, Chichester, **2009**.

[128] D. Marion, *Mol. Cell. Proteom.* **2013**, *12*, 3006–3025.

[129] A. Giwa, S. W. Hasan, A. Yousuf, S. Chakraborty, D. J. Johnson, N. Hilal, *Desalination* **2017**, *420*, 403–424.

[130] A. A. Vorobieva, P. White, B. Liang, J. E. Horne, A. K. Bera, C. M. Chow, S. Gerben, S. Marx, A. Kang, A. Q. Stiving et al., *Science* **2021**, *371*.

[131] P. van Rijn, M. Tutus, C. Kathrein, N. C. Mougin, H. Park, C. Hein, M. P. Schürings, A. Böker, *Adv. Funct. Mater.* **2014**, *24*, 6762–6770.

[132] H. Charan, J. Kinzel, U. Glebe, D. Anand, T. M. Garakani, L. Zhu, M. Bocola, U. Schwaneberg, A. Böker, *Biomaterials* **2016**, *107*, 115–123.

[133] H. Charan, U. Glebe, D. Anand, J. Kinzel, L. Zhu, M. Bocola, T. M. Garakani, U. Schwaneberg, A. Böker, *Soft Matter* **2017**, *13*, 2866–2875.

[134] H. Charan, *Self-Assembled Transmembrane Protein-Polymer Conjugates for the Generation of Nano-Thin Membranes and Micro-Compartments(Doctoral Thesis)*, University of Potsdam, Potsdam, Germany, Retrieved from: urn:nbn:de:kobv:517-opus4-402060, **2017**.

[135] T. Sugiki, N. Kobayashi, T. Fujiwara, *Comput. Struct. Biotechnol. J.* **2017**, *15*, 328–339.

[136] G. B. Edwards, U. M. Muthurajan, S. Bowerman, K. Luger, *Curr. Protoc. Mol. Biol.* **2020**, *133*, e131.

[137] H.-S. Kang, M. Sattler, *Emerg. Top. Life Sci.* **2018**, *2*, 107–119.

[138] W. Jahnke, H. Widmer, *Cell. Mol. Life Sci.* **2004**, *61*, 580–599.

[139] J. A. Purslow, B. Khatiwada, M. J. Bayro, V. Venditti, *Front. Mol. Biosci.* **2020**, *7*, 9.

[140] M. P. Williamson, *Prog. Nucl. Magn. Reson. Spectrosc.* **2013**, *73*, 1–16.

[141] D. J. Hodgson, Y. Aubin, *J. Pharm. Biomed. Anal.* **2017**, *138*, 351–356.

[142] K. O. Ramberg, P. M. Antonik, D. L. Cheung, P. B. Crowley, *Bioconjugate Chem.* **2019**, *30*, 1162–1168.

[143] G. Digilio, L. Barbero, C. Bracco, D. Corpillo, P. Esposito, G. Piquet, S. Traversa, S. Aime, *J. Am. Chem. Soc.* **2003**, *125*, 3458–3470.

[144] C. Dhalluin, A. Ross, L.-A. Leuthold, S. Foser, B. Gsell, F. Müller, H. Senn, *Bioconjugate Chem.* **2005**, *16*, 504–517.

[145] A. Zaghmi, A. A. Greschner, E. Mendez-Villuendas, J. Y. Liu, H. W. de Haan, M. A. Gauthier, *Data in Brief* **2019**, *25*, 104037.

[146] G. Cattani, L. Vogeley, P. B. Crowley, *Nat. Chem.* **2015**, *7*, 823–828.

[147] E. Ravera, S. Ciambellotti, L. Cerofolini, T. Martelli, T. Kozyreva, C. Bernacchioni, S. Giuntini, M. Fragai, P. Turano, C. Luchinat, *Angew. Chem. Int. Ed.* **2016**, *55*, 2446–2449.

[148] A. Zaghmi, E. Mendez-Villuendas, A. A. Greschner, J. Y. Liu, H. W. de Haan, M. A. Gauthier, *Mater. Today Chem.* **2019**, *12*, 121–131.

[149] Z. Evgrafova, B. Voigt, M. Baumann, M. Stephani, W. H. Binder, J. Balbach, *ChemPhysChem* **2019**, *20*, 236–240.

[150] K. M. Burridge, B. A. Shurina, C. T. Kozuszek, R. F. Parnell, J. S. Montgomery, J. L. VanPelt, N. M. Daman, R. M. McCarrick, T. A. Ramelot, D. Konkolewicz et al., *Chem. Sci.* **2020**, *11*, 6160–6166.

[151] O. Yaniv, S. Petkun, L. J. W. Shimon, E. A. Bayer, R. Lamed, F. Frolow, *Acta Cryst.* **2012**, *D68*, 819–828.

[152] S. Jindou, Q. Xu, R. Kenig, M. Shulman, Y. Shoham, E. A. Bayer, R. Lamed, *FEMS Microbiology Letters* **2006**, *254*, 308–316.

[153] H. Li, M. Li, X. Yu, A. P. Bapat, B. S. Sumerlin, *Polym. Chem.* **2011**, *2*, 1531.

[154] Y. Cui, F. Liu, X. Li, L. Wang, H. Wang, G. Chen, L. Yuan, J. L. Brash, H. Chen, *ACS Appl. Mater. Interfaces* **2015**, *7*, 21913–21918.

[155] D. Chang, C. N. Lam, S. Tang, B. D. Olsen, *Polym. Chem.* **2014**, *5*, 4884–4895.

[156] P. J. Roth, K. T. Wiss, R. Zentel, P. Theato, *Macromolecules* **2008**, *41*, 8513–8519.

[157] K. Skrabania, A. Miasnikova, A. M. Bivigou-Koumba, D. Zehm, A. Laschewsky, *Polym. Chem.* **2011**, *2*, 2074–2083.

[158] C. Bao, J. Chen, D. Li, A. Zhang, Q. Zhang, *Polym. Chem.* **2020**, *11*, 1386–1392.

[159] S. Bhattacharjee, W. Liu, W.-H. Wang, I. Weitzhandler, X. Li, Y. Qi, Y. Pang, D. F. Hunt, A. Chilkoti, *ChemBioChem* **2015**, 2451–2455.

[160] S. Carmali, H. Murata, E. Amemiya, K. Matyjaszewski, A. J. Russell, *ACS Biomater. Sci. Eng.* **2017**, *3*, 2086–2097.

[161] L. Fu, A. Simakova, M. Fantin, Y. Wang, K. Matyjaszewski, *ACS Macro Lett.* **2018**, *7*, 26–30.

[162] Nathalie Céline Mougin, *Self-Assembled Bionanoparticle-Polymer-Conjugates for Building Soft Composite Membranes (Doctoral Thesis)*, Rheinisch-Westfaelische Technische Hochschule, Aachen, Germany, Retrieved from: urn:nbn:de:hbz:82-opus-32899, **2010**.

[163] F. Alsubaie, A. Anastasaki, V. Nikolaou, A. Simula, G. Nurumbetov, P. Wilson, K. Kempe, D. M. Haddleton, *Macromolecules* **2015**, *48*, 6421–6432.

[164] D. Konkolewicz, Y. Wang, M. Zhong, P. Krys, A. A. Isse, A. Gennaro, K. Matyjaszewski, *Macromolecules* **2013**, *46*, 8749–8772.

[165] Q. Zhang, P. Wilson, Z. Li, R. McHale, J. Godfrey, A. Anastasaki, C. Waldron, D. M. Haddleton, *J. Am. Chem. Soc.* **2013**, *135*, 7355–7363.

[166] J. Zhang, E. Liarou, J. Town, Y. Li, A. M. Wemyss, D. M. Haddleton, *Polym. Chem.* **2020**, *11*, 5534–5541.

[167] S. R. Samanta, V. Nikolaou, S. Keller, M. J. Monteiro, D. A. Wilson, D. M. Haddleton, V. Percec, *Polym. Chem.* **2015**, *6*, 2084–2097.

[168] A. Simula, V. Nikolaou, A. Anastasaki, F. Alsubaie, G. Nurumbetov, P. Wilson, K. Kempe, D. M. Haddleton, *Polym. Chem.* **2015**, *6*, 2226–2233.

[169] A. Simula, V. Nikolaou, F. Alsubaie, A. Anastasaki, D. M. Haddleton, *Polym. Chem.* **2015**, *6*, 5940–5950.

[170] R. Falatach, C. McGlone, M. S. Al-Abdul-Wahid, S. Averick, R. C. Page, J. A. Berberich, D. Konkolewicz, *Chem. Commun.* **2015**, *51*, 5343–5346.

[171] C. Fu, B. Demir, S. Alcantara, V. Kumar, F. Han, H. G. Kelly, X. Tan, Y. Yu, W. Xu, J. Zhao et al., *Angew. Chem. Int. Ed.* **2020**, *59*, 4729–4735.

[172] X. Dong, Z. Gong, Y.-B. Lu, K. Liu, L.-Y. Qin, M.-L. Ran, C.-L. Zhang, Z. Liu, W.-P. Zhang, C. Tang, *Proc. Natl. Acad. Sci. U.S.A.* **2017**, *114*, 6770–6775.

[173] S. Gupta, S. Bhattacharjya, *PLoS ONE* **2014**, *9*, e90557.

[174] C. S. Le Duff, S. B.-M. Whittaker, S. E. Radford, G. R. Moore, *J. Mol. Biol.* **2006**, *364*, 824–835.

[175] H. Murata, C. S. Cummings, R. R. Koepsel, A. J. Russell, *Biomacromolecules* **2013**, *14*, 1919–1926.

[176] S. Jindou, S. Petkun, L. Shimon, E. A. Bayer, R. Lamed, F. Frolow, *Acta Cryst.* **2007**, *F63*, 1044–1047.

[177] M. D. Hossain, D. Valade, Z. Jia, M. J. Monteiro, *Polym. Chem.* **2012**, *3*, 2986.

[178] A. W. Snow, E. E. Foos, *ChemInform* **2003**, *34*, 509–512.
[179] E. Lubomirsky, A. Khodabandeh, J. Preis, M. Susewind, T. Hofe, E. F. Hilder, R. D. Arrua, *Anal. Chim. Acta* **2021**, *1151*, 338244.
[180] P. Hong, S. Koza, E. S. P. Bouvier, *J. Liq. Chromatogr. Relat. Technol.* **2012**, *35*, 2923–2950.
[181] E. Sahin, C. J. Roberts in *Therapeutic Proteins* (Eds.: V. Voynov, J. A. Caravella), Humana Press, Totowa, **2012**, pp. 403–423.
[182] D. Some, H. Amartely, A. Tsadok, M. Lebendiker, *J. Vis. Exp.* **2019**, e59615.
[183] T. Ogawa, N. Hirokawa, *Biophys. Rev.* **2018**, *10*, 299–306.
[184] D. J. Slotboom, R. H. Duurkens, K. Olieman, G. B. Erkens, *Methods* **2008**, *46*, 73–82.
[185] R. Xu, *Particuology* **2015**, *18*, 11–21.
[186] P. J. Wyatt, *Anal. Chim. Acta* **1993**, *272*, 1–40.
[187] T. O. C. Kwan, R. Reis, G. Siligardi, R. Hussain, H. Cheruvara, I. Moraes, *Int. J. Mol. Sci.* **2019**, *20*.
[188] P. Weiland, F. Altegoer, *Front. Plant Sci.* **2021**, *12*, 669835.
[189] M. R. Dorwart, R. Wray, C. A. Brautigam, Y. Jiang, P. Blount, *PLoS Biol.* **2010**, *8*, e1000555.
[190] A. Pabbathi, S. Patra, A. Samanta, *ChemPhysChem* **2013**, *14*, 2441–2449.
[191] J.-F. Lutz, A. Hoth, K. Schade, *Des. Monomers Polym.* **2009**, *12*, 343–353.
[192] M. Mertoglu, S. Garnier, A. Laschewsky, K. Skrabania, J. Storsberg, *Polymer* **2005**, *46*, 7726–7740.
[193] G. Vancoillie, D. Frank, R. Hoogenboom, *Prog. Polym. Sci.* **2014**, *39*, 1074–1095.
[194] M. Zhang, M. F. Cunningham, R. A. Hutchinson, *Polym. Chem.* **2015**, *6*, 6509–6518.
[195] L. Medda, M. Monduzzi, A. Salis, *Chem. Commun.* **2015**, *51*, 6663–6666.
[196] P. C. Nauka, J. Lee, H. D. Maynard, *Polym. Chem.* **2016**, *7*, 2352–2357.
[197] S. N. Crooke, J. Zheng, M. S. Ganewatta, S. M. Guldberg, T. M. Reineke, M. G. Finn, *ACS Appl. Bio Mater.* **2019**, *2*, 93–103.
[198] A. J. Miles, B. A. Wallace, *Chem. Soc. Rev.* **2016**, *45*, 4859–4872.
[199] S. M. Kelly, T. J. Jess, N. C. Price, *Biochim. Biophys. Acta* **2005**, *1751*, 119–139.
[200] J. Liu, S. Yadav, J. Andya, B. Demeule, S. J. Shire, *Meth. Enzymol.* **2015**, *562*, 441–476.
[201] P. Schuck, *Biophys. Rev.* **2013**, *5*, 159–171.
[202] S. E. Harding, *Eur. Biophys. J.* **2018**, *47*, 697–707.
[203] K. S. Sharma, G. Durand, F. Giusti, B. Olivier, A.-S. Fabiano, P. Bazzacco, T. Dahmane, C. Ebel, J.-L. Popot, B. Pucci, *Langmuir* **2008**, *24*, 13581–13590.
[204] A. Sverzhinsky, S. Qian, L. Yang, M. Allaire, I. Moraes, D. Ma, J. W. Chung, M. Zoonens, J.-L. Popot, J. W. Coulton, *J. Membr. Biol.* **2014**, *247*, 1005–1018.
[205] K. S. Sharma, G. Durand, F. Gabel, P. Bazzacco, C. Le Bon, E. Billon-Denis, L. J. Catoire, J.-L. Popot, C. Ebel, B. Pucci, *Langmuir* **2012**, *28*, 4625–4639.

[206] S. C. Lee, T. J. Knowles, V. L. G. Postis, M. Jamshad, R. A. Parslow, Y.-P. Lin, A. Goldman, P. Sridhar, M. Overduin, S. P. Muench et al., *Nat. Protoc.* **2016**, *11*, 1149–1162.

[207] S. Uchiyama, M. Noda, E. Krayukhina, *Biophys. Rev.* **2018**, *10*, 259–269.

[208] B. Monterroso, C. Alfonso, S. Zorrilla, G. Rivas, *Methods* **2013**, *59*, 349–362.

[209] R. Khan, S. Ray in *Phytochemistry: An in-silico and in-vitro Update* (Eds.: S. Kumar, C. Egbuna), Springer, Singapore, **2019**, pp. 109–132.

[210] F. Krieg, Q. K. Ong, M. Burian, G. Rainò, D. Naumenko, H. Amenitsch, A. Süess, M. J. Grotevent, F. Krumeich, M. I. Bodnarchuk et al., *J. Am. Chem. Soc.* **2019**, *141*, 19839–19849.

[211] P. Klemm, S. Huschke, M. Rodewald, N. Ehteshamzad, M. Behnke, X. Wang, G. Cinar, I. Nischang, S. Hoeppener, C. Weber et al., *Polym. Chem.* **2021**, *12*, 911–925.

[212] G. Cinar, C. Englert, U. S. Schubert, I. Nischang, *Nanoscale* **2020**, *12*, 22462–22466.

[213] I. Nischang, I. Perevyazko, T. Majdanski, J. Vitz, G. Festag, U. S. Schubert, *Anal. Chem.* **2017**, *89*, 1185–1193.

[214] I. Muljajew, S. Huschke, A. Ramoji, Z. Cseresnyés, S. Hoeppener, I. Nischang, W. Foo, J. Popp, M. T. Figge, C. Weber et al., *ACS Nano* **2021**, *7*, 12298–12313.

[215] M. E. Mikhailova, A. S. Senchukova, A. A. Lezov, A. S. Gubarev, A.-K. Trützschler, U. S. Schubert, N. V. Tsvetkov, *Polymers* **2019**, *11*, 1647.

[216] X. Ye, J. Yang, J. Ambreen, *RSC Adv.* **2013**, *3*, 15108.

[217] J. Sun, P. Černoch, A. Völkel, Y. Wei, J. Ruokolainen, H. Schlaad, *Macromolecules* **2016**, *49*, 5494–5501.

[218] M. Grube, G. Cinar, U. S. Schubert, I. Nischang, *Polymers* **2020**, *12*, 277.

[219] S. E. Wawra, M. Thoma, J. Walter, C. Lübbert, T. Thajudeen, C. Damm, W. Peukert, *Eur. Biophys. J.* **2018**, *47*, 777–787.

[220] M. Grube, I. Perevyazko, T. Heinze, U. S. Schubert, I. Nischang, *Carbohydr. Polym.* **2020**, *229*, 115452.

[221] E. M. Pelegri-O'Day, E.-W. Lin, H. D. Maynard, *J. Am. Chem. Soc.* **2014**, *136*, 14323–14332.

[222] Y. Hou, H. Lu, *Bioconjugate Chem.* **2019**, *30*, 1604–1616.

[223] J. Y. Shu, C. Tan, W. F. DeGrado, T. Xu, *Biomacromolecules* **2008**, *9*, 2111–2117.

[224] T. Lühmann, M. Schmidt, M. N. Leiske, V. Spieler, T. C. Majdanski, M. Grube, M. Hartlieb, I. Nischang, S. Schubert, U. S. Schubert et al., *ACS Biomater. Sci. Eng.* **2017**, *3*, 304–312.

[225] B. I. Kurganov, I. N. Topchieva, N. V. Efremova, *Bioconjugate Chem.* **1997**, *8*, 637–642.

[226] K. D. Webster, D. Dahhan, A. M. Otto, C. L. Frosti, W. L. Dean, J. B. Chaires, K. W. Olsen, *Artif. Organs* **2017**, *41*, 351–358.

[227] Y. Lu, S. E. Harding, A. Turner, B. Smith, D. S. Athwal, J. G. Grossmann, K. G. Davis, A. J. Rowe, *J. Pharm. Sci.* **2008**, *97*, 2062–2079.

[228] Y. R. Gokarn, M. McLean, T. M. Laue, *Mol. Pharm.* **2012**, *9*, 762–773.

[229] M. Heskins, J. E. Guillet, *J. Macromol. Sci. A* **1968**, *2*, 1441–1455.

[230] Y. Qiao, J. Wan, L. Zhou, W. Ma, Y. Yang, W. Luo, Z. Yu, H. Wang, *Wiley Interdiscip. Rev. Nanomed. Nanobiotechnol.* **2019**, *11*, e1527.

[231] T. Svedberg, J. B. Nichols, *J. Am. Chem. Soc.* **1923**, *45*, 2910–2917.

[232] T. Svedberg, R. Fåhraeus, *J. Am. Chem. Soc.* **1926**, *48*, 430–438.

[233] X. Xu, H. Cölfen, *Nanomaterials* **2021**, *11*, 333.

[234] G. J. Howlett, A. P. Minton, G. Rivas, *Curr. Opin. Chem. Biol.* **2006**, *10*, 430–436.

[235] J. Lebowitz, M. S. Lewis, P. Schuck, *Protein Sci.* **2002**, *11*, 2067–2079.

[236] Z. Liu, Q. Liao, D. Yang, Y. Gao, X. Luo, Z. Lei, H. Li, *Des. Monomers Polym.* **2013**, *16*, 465–474.

[237] R. Umapathi, K. Kumar, G. M. Rani, P. Venkatesu, *J. Colloid. Interface Sci.* **2019**, *541*, 1–11.

[238] P. H. Brown, A. Balbo, H. Zhao, C. Ebel, P. Schuck, *PLoS ONE* **2011**, *6*, e26221.

[239] P. Kujawa, F. M. Winnik, *Macromolecules* **2001**, *34*, 4130–4135.

[240] M. Grube, M. N. Leiske, U. S. Schubert, I. Nischang, *Macromolecules* **2018**, *51*, 1905–1916.

[241] P. van Rijn, H. Park, K. Özlem Nazli, N. C. Mougin, A. Böker, *Langmuir* **2013**, *29*, 276–284.

[242] H. B. Park, J. Kamcev, L. M. Robeson, M. Elimelech, B. D. Freeman, *Science* **2017**, *356*, eaab0530.

[243] L. S. Hager, *Membrane Systems For Wastewater Treatment*, McGraw-Hill, New York, **2006**.

[244] D. He, H. Susanto, M. Ulbricht, *Prog. Polym. Sci.* **2009**, *34*, 62–98.

[245] X. Hu, E. McIntosh, M. G. Simon, C. Staii, S. W. Thomas, *Adv. Mater.* **2016**, *28*, 715–721.

[246] B.-Y. Lee, S. Hyun, G. Jeon, E. Y. Kim, J. Kim, W. J. Kim, J. K. Kim, *ACS Appl. Mater. Interfaces* **2016**, *8*, 11758–11764.

[247] Z. Liu, W. Wang, R. Xie, X.-J. Ju, L.-Y. Chu, *Chem. Soc. Rev.* **2016**, *45*, 460–475.

[248] M. Wei, Y. Gao, X. Li, M. J. Serpe, *Polym. Chem.* **2017**, *8*, 127–143.

[249] D. Wandera, S. R. Wickramasinghe, S. M. Husson, *J. Membr. Sci.* **2010**, *357*, 6–35.

[250] R. Ghosh in *Polymers and Polymeric Composites* (Eds.: M. A. Jafar Mazumder, H. Sheardown, A. Al-Ahmed), Springer International Publishing, Cham, **2019**, pp. 491–508.

[251] T. Still, P. J. Yunker, K. Hanson, Z. S. Davidson, M. A. Lohr, K. B. Aptowicz, A. G. Yodh, *Adv. Mater. Interfaces* **2015**, *2*, 1500371.

[252] L.-Y. Chu, *Smart Membrane Materials and Systems: From Flat Membranes to Microcapsule Membranes*, Springer, Berlin Heidelberg, **2011**.

[253] J. Elbert, F. Krohm, C. Rüttiger, S. Kienle, H. Didzoleit, B. N. Balzer, T. Hugel, B. Stühn, M. Gallei, A. Brunsen, *Adv. Funct. Mater.* **2014**, *24*, 1591–1601.

[254] D. J. Bell, S. Ludwanowski, A. Lüken, B. Sarikaya, A. Walther, M. Wessling, *J. Membr. Sci.* **2021**, *620*, 118912.

[255] D. Alsteens, H. E. Gaub, R. Newton, M. Pfreundschuh, C. Gerber, D. J. Müller, *Nat. Rev. Mater.* **2017**, *2*.

[256] I. Tessmer, P. Kaur, J. Lin, H. Wang, *J. Nanobiotechnol.* **2013**, *11*, 25.

[257] G. Binnig, C. F. Quate, C. Gerber, *Phys. Rev. Lett.* **1986**, *56*, 930–933.

[258] E. F. Semeraro, L. Marx, M. P. K. Frewein, G. Pabst, *Soft Matter* **2021**, *17*, 222–232.

[259] E. Mahieu, F. Gabel, *Acta Cryst.* **2018**, *D74*, 715–726.

[260] A. Hexemer, P. Müller-Buschbaum, *IUCrJ* **2015**, *2*, 106–125.

[261] T. Li, A. J. Senesi, B. Lee, *Chem. Rev.* **2016**, *116*, 11128–11180.

[262] D. Dwivedi, K. Lepková in *Application and Characterization of Surfactants* (Ed.: R. Najjar), InTech, London, **2017**, DOI: 10.5772/intechopen.69290.

[263] D. K. Clare, E. V. Orlova, *J. Struct. Biol.* **2010**, *171*, 303–308.

[264] M. Pflüger, V. Soltwisch, J. Probst, F. Scholze, M. Krumrey, *IUCrJ* **2017**, *4*, 431–438.

[265] Andreas Meyer, "Grazing Incidence Small Angle X-ray Scattering", can be found under http://www.gisaxs.de, **2018**.

[266] J. K. Basu, *Resonance* **2014**, 1158–1176.

[267] G. Ciatto, M. H. Chu, P. Fontaine, N. Aubert, H. Renevier, J. L. Deschanvres, *Thin Solid Films* **2016**, *617*, 48–54.

[268] C. Mocuta, S. Stanescu, M. Gallard, A. Barbier, A. Dawiec, B. Kedjar, N. Leclercq, D. Thiaudiere, *J. Synchrotron Rad.* **2018**, *25*, 204–213.

[269] M. Yasaka, *Rigaku J.* **2010**, *26*, 1–9.

[270] A. Huang, H. Yao, B. D. Olsen, *Soft Matter* **2019**, *15*, 7350–7359.

[271] D. I. Svergun, F. Ekström, K. D. Vandegriff, A. Malavalli, D. A. Baker, C. Nilsson, R. M. Winslow, *Biophys. J.* **2008**, *94*, 173–181.

[272] C. N. Lam, H. Yao, B. D. Olsen, *Biomacromolecules* **2016**, *17*, 2820–2829.

[273] D. Chang, B. D. Olsen, *Polym. Chem.* **2016**, *7*, 2410–2418.

[274] J. M. Paloni, X.-H. Dong, B. D. Olsen, *ACS Sens.* **2019**, *4*, 2869–2878.

[275] A. Huang, J. M. Paloni, A. Wang, A. C. Obermeyer, H. V. Sureka, H. Yao, B. D. Olsen, *Biomacromolecules* **2019**, *20*, 3713–3723.

[276] G. Walsh in *Proteins: Biochemistry and Biotechnology* (Ed.: G. Walsh), John Wiley & Sons Inc, Chichester, West Sussex, **2014**, pp. 141–176.

[277] S. Mahalik, A. K. Sharma, K. J. Mukherjee, *Microb. Cell Fact.* **2014**, *13*, 177.

[278] K. Khambhati, G. Bhattacharjee, N. Gohil, D. Braddick, V. Kulkarni, V. Singh, *Front. Bioeng. Biotechnol.* **2019**, *7*, 248.

[279] G. L. Rosano, E. A. Ceccarelli, *Front. Microbiol.* **2014**, *5*, 172.

[280] K. Tsumoto, D. Ejima, I. Kumagai, T. Arakawa, *Protein Expr. Purif.* **2003**, *28*, 1–8.

[281] A. Singh, V. Upadhyay, A. K. Upadhyay, S. M. Singh, A. K. Panda, *Microb. Cell Fact.* **2015**, *14*, 41.

[282] H. Lilie, E. Schwarz, R. Rudolph, *Curr. Opin. Biotechnol.* **1998**, *9*, 497–501.

[283] E. D. B. Clark, *Curr. Opin. Biotechnol.* **2001**, *12*, 202–207.

[284] E. de Bernardez Clark, *Curr. Opin. Biotechnol.* **1998**, *9*, 157–163.

[285] H. Yamaguchi, M. Miyazaki, *Biomolecules* **2014**, *4*, 235–251.

[286] L. D. Cabrita, S. P. Bottomley, *Biotechnol. Annu. Rev.* **2004**, 31–50.

[287] K. S. Hingorani, L. M. Gierasch, *Curr. Opin. Struct. Biol.* **2014**, *24*, 81–90.

[288] C. Michaux, N. C. Pomroy, G. G. Privé, *J. Mol. Biol.* **2008**, *375*, 1477–1488.

[289] G. Roussel, E. A. Perpète, A. Matagne, E. Tinti, C. Michaux, *Biotechnol. Bioeng.* **2013**, *110*, 417–423.

[290] M. Schwieters, *Protein nanopore membranes prepared by a simple Langmuir approach (unpublished Doctoral Thesis)*, Technische Universität Berlin, Berlin, Germany, **2021**.

[291] M. Schwieters, M. Mathieu-Gaedke, M. Westphal, R. Dalpke, M. Dirksen, D. Qi, M. Grull, T. Bick, S. Taßler, D. F. Sauer et al., *Small* **2021**, doi: 10.1002/smll.202102975.

[292] Schrödinger LLC, *The PyMOL Molecular Graphics System*.

[293] J. Kinzel, *Towards chiral nanopores based on tailor-made FhuA β-barrel proteins (Doctoral Thesis)*, Rheinisch-Westfaelische Technische Hochschule, Aachen, Germany, DOI: 10.18154/RWTH-2017-06488, **2017**.

[294] L. Whitmore, A. J. Miles, L. Mavridis, R. W. Janes, B. A. Wallace, *Nucleic Acids Res.* **2017**, *45*, D303-D307.

[295] A. Abdul-Gader, A. J. Miles, B. A. Wallace, *Bioinformatics* **2011**, *27*, 1630–1636.

[296] S. Deep, J. C. Ahluwalia, *Phys. Chem. Chem. Phys.* **2001**, *3*, 4583–4591.

[297] J. G. Lees, A. J. Miles, F. Wien, B. A. Wallace, *Bioinformatics* **2006**, *22*, 1955–1962.

[298] S. E. Lietzke, R. D. Scavetta, M. D. Yoder, F. Jurnak, *Plant Physiology* **1996**, *111*, 73–92.

[299] D. P. Chimento, A. K. Mohanty, R. J. Kadner, M. C. Wiener, *Nat. Struct. Mol. Biol.* **2003**, *10*, 394–401.

[300] J. Gaitzsch, D. Appelhans, L. Wang, G. Battaglia, B. Voit, *Angew. Chem. Int. Ed.* **2012**, *51*, 4448–4451.

[301] C. P. Kabb, C. S. O'Bryan, C. C. Deng, T. E. Angelini, B. S. Sumerlin, *ACS Appl. Mater. Interfaces* **2018**, *10*, 16793–16801.

[302] S. Seiffert, W. Oppermann, K. Saalwächter, *Polymer* **2007**, *48*, 5599–5611.

[303] C. D. Vo, D. Kuckling, H.-J. P. Adler, M. Schnhoff, *Colloid Polym. Sci.* **2002**, *280*, 400–409.

[304] J. Jiang, B. Qi, M. Lepage, Y. Zhao, *Macromolecules* **2007**, *40*, 790–792.

[305] D. Roy, B. S. Sumerlin, *Macromol. Rapid. Commun.* **2014**, *35*, 174–179.

[306] C. C. Corten, *Synthese und Charakterisierung dünner Hydrogelschichten mit modulierbaren Eigenschaften (Doctoral Thesis)*, Technische Universität Dresden, Dresden, Germany, Retrieved from: urn:nbn:de:bsz:14-ds-1209463829168-95283, **2008**.

[307] B. A. Kerwin, R. L. Remmele, *J. Pharm. Sci.* **2007**, *96*, 1468–1479.

[308] C. Schöneich, *Pharm. Res.* **2020**, *37*, 45.

[309] E. Yousif, R. Haddad, *SpringerPlus* **2013**, *2*, 398.

[310] H.-L. Chan, P. R. Gaffney, M. D. Waterfield, H. Anderle, H. Peter Matthiessen, H.-P. Schwarz, P. L. Turecek, J. F. Timms, *FEBS Lett.* **2006**, *580*, 3229–3236.

[311] Y. Zhao, L. Tremblay, Y. Zhao, *Macromolecules* **2011**, *44*, 4007–4011.

[312] W. F. Yong, H. Zhang, *Prog. Mater. Sci.* **2021**, *116*, 100713.

[313] G. Sudre, E. Siband, B. Gallas, F. Cousin, D. Hourdet, Y. Tran, *Polymers* **2020**, *12*, 153.

[314] K.-V. Peinemann, S. Pereira Nunes, *Membrane Technology: Volume 4: Membranes For Water Treatment*, Wiley-VCH, Weinheim, **2010**.

[315] S. M. Danauskas, D. Li, M. Meron, B. Lin, K. Y. C. Lee, *J. Appl. Crystallogr.* **2008**, *41*, 1187–1193.

[316] W. M. Haynes, *CRC Handbook of Chemistry and Physics, 95th Edition*, CRC Press, Hoboken, **2015**.

[317] H. Killmann, R. Benz, V. Braun, *EMBO J.* **1993**, *12*, 3007–3016.

[318] J. D. Faraldo-Gómez, G. R. Smith, M. S. Sansom, *Biophys. J.* **2003**, *85*, 1406–1420.

[319] X. Feng, Q. Imran, Y. Zhang, L. Sixdenier, X. Lu, G. Kaufman, U. Gabinet, K. Kawabata, M. Elimelech, C. O. Osuji, *Sci. Adv.* **2019**, *5*, eaav9308.

[320] T. Chen, M. Duan, P. Shi, S. Fang, *J. Mater. Chem. A* **2017**, *5*, 20208–20216.

[321] D. Harvey, *Modern Analytical Chemistry*, McGraw-Hill Professional, Boston, **2000**.

[322] D. Gräfe, J. Gaitzsch, D. Appelhans, B. Voit, *Nanoscale* **2014**, *6*, 10752–10761.

[323] H. Gumz, S. Boye, B. Iyisan, V. Krönert, P. Formanek, B. Voit, A. Lederer, D. Appelhans, *Adv. Sci.* **2019**, *6*, 1801299.

[324] J. Gaitzsch, D. Appelhans, D. Gräfe, P. Schwille, B. Voit, *Chem. Commun.* **2011**, *47*, 3466–3468.

[325] A. Mecke, C. Dittrich, W. Meier, *Soft Matter* **2006**, *2*, 751–759.

[326] S. Zhang, J. Zhang, W. Fang, Y. Zhang, Q. Wang, J. Jin, *Nano Lett.* **2018**, *18*, 6563–6569.